



SYNTHESIS OF ACID MESOPOROUS SAPONITES AND ITS APPLICATION IN CATALYTIC GLYCIDOL HYDROGENOLYSIS

Fiseha Bogale Gebretsadik

ADVERTIMENT. L'accés als continguts d'aquesta tesi doctoral i la seva utilització ha de respectar els drets de la persona autora. Pot ser utilitzada per a consulta o estudi personal, així com en activitats o materials d'investigació i docència en els termes establerts a l'art. 32 del Text Refós de la Llei de Propietat Intel·lectual (RDL 1/1996). Per altres utilitzacions es requereix l'autorització prèvia i expressa de la persona autora. En qualsevol cas, en la utilització dels seus continguts caldrà indicar de forma clara el nom i cognoms de la persona autora i el títol de la tesi doctoral. No s'autoritza la seva reproducció o altres formes d'explotació efectuades amb finalitats de lucre ni la seva comunicació pública des d'un lloc aliè al servei TDX. Tampoc s'autoritza la presentació del seu contingut en una finestra o marc aliè a TDX (framing). Aquesta reserva de drets afecta tant als continguts de la tesi com als seus resums i índexs.

ADVERTENCIA. El acceso a los contenidos de esta tesis doctoral y su utilización debe respetar los derechos de la persona autora. Puede ser utilizada para consulta o estudio personal, así como en actividades o materiales de investigación y docencia en los términos establecidos en el art. 32 del Texto Refundido de la Ley de Propiedad Intelectual (RDL 1/1996). Para otros usos se requiere la autorización previa y expresa de la persona autora. En cualquier caso, en la utilización de sus contenidos se deberá indicar de forma clara el nombre y apellidos de la persona autora y el título de la tesis doctoral. No se autoriza su reproducción u otras formas de explotación efectuadas con fines lucrativos ni su comunicación pública desde un sitio ajeno al servicio TDR. Tampoco se autoriza la presentación de su contenido en una ventana o marco ajeno a TDR (framing). Esta reserva de derechos afecta tanto al contenido de la tesis como a sus resúmenes e índices.

WARNING. Access to the contents of this doctoral thesis and its use must respect the rights of the author. It can be used for reference or private study, as well as research and learning activities or materials in the terms established by the 32nd article of the Spanish Consolidated Copyright Act (RDL 1/1996). Express and previous authorization of the author is required for any other uses. In any case, when using its content, full name of the author and title of the thesis must be clearly indicated. Reproduction or other forms of for profit use or public communication from outside TDX service is not allowed. Presentation of its content in a window or frame external to TDX (framing) is not authorized either. These rights affect both the content of the thesis and its abstracts and indexes.

Fiseha Bogale Gebretsadik

Synthesis of Acid Mesoporous Saponite and Its
Application In Catalytic Glycidol Hydrogenolysis

Doctoral Thesis

Supervised by:

Dr. Pilar Salagre Carnero
Prof. Yolanda Cesteros Fernández

Department of Physical and Inorganic Chemistry



UNIVERSITAT ROVIRA I VIRGILI

Tarragona
2015

UNIVERSITAT ROVIRA I VIRGILI

SYNTHESIS OF ACID MESOPOROUS SAPONITES AND ITS APPLICATION IN CATALYTIC GLYCIDOL HYDROGENOLYSIS

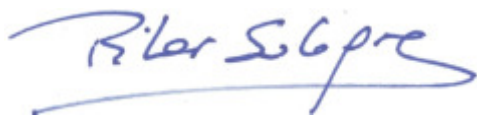
Fiseha Bogale Gebretsadik



We STATE that the present study, entitled “*Synthesis of acid mesoporous saponite and its application in catalytic glycidol hydrogenolysis*”, presented by Fiseha Bogale Gebretsadik for the award of the degree of Doctor, has been carried out under our supervision at the Department of Physical and Inorganic Chemistry of this university, and that it fulfills all the requirements to be eligible for the International Doctorate Award.

Tarragona, 1st Sept., 2015

Doctoral Thesis Supervisor/s



Dr. Pilar Salagre



Prof. Yolanda Cesteros

UNIVERSITAT ROVIRA I VIRGILI

SYNTHESIS OF ACID MESOPOROUS SAPONITES AND ITS APPLICATION IN CATALYTIC GLYCIDOL HYDROGENOLYSIS

Fiseha Bogale Gebretsadik

Acknowledgments

First and foremost, I praise and honor the almighty God, the son of the Virgin Mary, for his good paternity, care and blessing. My heart felt gratitude goes to my directors, Dr. Pilar Salagre and Dr. Yolanda Cesteros, for their unreserved help and for offering me everything with no limit, in the course of the thesis. Your irreplaceable effort and contribution was instrumental for the completion of the thesis; I thank you very much for your generosity. Pilar, you were more than a director. You are like a kind mother for me. It is not enough to say thank you, I wish you long live and may happiness and health abound in your life.

Mekelle University, department of chemistry was where I started my professional life as an assistant graduate. I have grown both as a man and professionally in those golden years of my life. I was like a brother or son to the university community and the department members. You are grateful for me for the love and the confidence you have on me. I am also indebted to the chemistry department of Addis Ababa University for the fruitful time that I spent as a graduate student. My special appreciation goes to Prof. Wendemagegn Mamo for being my role model for a hardworking man and helping me develop a sense of confidence in science and perseverance.

I am highly indebted to the University of Rovira I Virgili for the financial assistance and for the chance I was offered to perform this PhD thesis. I would like to extend my appreciation for the people of Tarragona, the university community and students, staffs and professors of the Inorganic and Physical Chemistry Department for making my stay lovely and making me feel home. Nanosensor group members in the Analytical and Organic Chemistry Department and my former classmates in Nanoscience and Nanotechnology and Synthesis and Catalysis masters programs, you really deserve my gratitude for the best time that we shared. I am especially indebted to Prof. Xavier Rius and Dr. Francisco Andrade (Pancho) for their condolence and assistance in those pity days.

Many people have given me a helping hand and have been there for me whenever I needed them. I would like to mention the names of some of them: Raquel, Agustin, Susana and people in the Servei de Recursos Científics i Tècnics: Francesec, Ramon,

Toni, Rita, Merce, Mariana, Lucas and Nuria. It would not be possible to succeed without you, may your kindness pay you back. The habesha @ Tarragona community, the Friday football group, the habeshas in Barcelona and my lab mates: Dolores, Tatiana, Elena, Xavi, Judith, Alex, Beatriz, Ester and Melanie, I thank you very much for your great friendship, for being patient in times I was crazy and for everything that we shared together. I will treasure the good memories of our friendship and wish you the best.

I was supposed to spend three months in another research laboratory out of Spain in order to apply for the European mention. My destination was the inorganic chemistry and catalysis group in Utrecht University, The Netherlands. I thank you very much Prof. Bert Weckhuysen for your good will to accept me in your group. I am grateful for Dr. Javier Ruiz-Martinez, who was my good friend, mentor and scientific advisor throughout my stay. I also appreciate the help of Ramon, Carlo, Marjan and Fuad for their training on some characterization techniques and Tom and Arjan for running H₂ chemisorption analysis of my samples. I met the finest and caring compatriots in Utrecht who make my stay easy and pleasant. I thank you, Miku, Keni, Kdrae, Nebi, Bini and Hannico and their angles Yanit and Amen and the congregation in Debre Mewi St. Gabriel Ethiopian Orthodox Church in Rotterdam.

I am blessed with a good family. My father had rentlessly worked to shape me and he is the most important part of my life. Dad, I love and respect you for what you did to me and pardon me for not being on your side in those nasty days. Dad, I wish you were alive to see me achieving what you have dreamt. I know that your spirit is looking after and helping me. I keep you deep in my heart. In tribute to your good paternity and selfless love, I have dedicated the thesis to you. Dear Biyn, you are not only a mom, you have been a best friend to me and my brother and sisters and without exaggeration you have lived for us. I will not find the right word to thank you. I would like to let you know that you are my precious blessing from God. Dear Habtu, you have scarified your life for me and our family. You are my great teacher of love and generosity. I know that I owe you what I cannot pay you back in this life. I can only tell you that this is the fruit of your scarification. It is not me who succeed, all is yours; congratulations brother. Brukeye, you are the one who listen to my cry, understand me the best and

make me laugh. You are the best sister overall. You taught me patience, hard work and more importantly purpose in life. I say hats off to you for your priceless gifts. My younger sisters, Eskesh and Leleena and my brother in law Henisho and my nephew Yabets, your love was an impetus to keep me going, thank you for being the reason to live. Messiti, you have accepted me unconditionally and showed me love like I never know before. You are such wise and caring girl, I am blessed with, I thank you very much for being with me.

I grew up in a neighborhood where life was typically communal. Everyone in the community was like father, mother, sister and brother for me. I was looked after prudently and they were there for me whenever I needed them. I thank you very much Kumae, Natan, Asmetae, Merdae, Marta, Frae, Mefin Bekelle, Mesfin Dagn, Birtukan, Weizero Almaz, Etye Brukae, Etye Nunush, Umerae, Etalem, Aguye, Haile, Ahmed, Jimi, Muler and Meazi for stretching out your hands when I was in need. My childhood and school friends, Faso, Sami, Jimi, Jossi, Besri, Desu, Efuye, Bini, Essie, Yasino and Yoni, I am longing to see your bright faces-“*Ubuntu*”.

UNIVERSITAT ROVIRA I VIRGILI

SYNTHESIS OF ACID MESOPOROUS SAPONITES AND ITS APPLICATION IN CATALYTIC GLYCIDOL HYDROGENOLYSIS

Fiseha Bogale Gebretsadik

This work has been funded by:

- Ministerio de Economía y Competitividad of Spain and FEDER funds (CTQ2011-24610).
- Universitat Rovira i Virgili grant URV-PDI-2011



UNIVERSITAT ROVIRA I VIRGILI

UNIVERSITAT ROVIRA I VIRGILI

SYNTHESIS OF ACID MESOPOROUS SAPONITES AND ITS APPLICATION IN CATALYTIC GLYCIDOL HYDROGENOLYSIS

Fiseha Bogale Gebretsadik

Thou wilt keep him in perfect peace, whose mind is stayed on thee.

Isaiah 26:3

UNIVERSITAT ROVIRA I VIRGILI

SYNTHESIS OF ACID MESOPOROUS SAPONITES AND ITS APPLICATION IN CATALYTIC GLYCIDOL HYDROGENOLYSIS

Fiseha Bogale Gebretsadik

UNIVERSITAT ROVIRA I VIRGILI
SYNTHESIS OF ACID MESOPOROUS SAPONITES AND ITS APPLICATION IN CATALYTIC GLYCIDOL HYDROGENOLYSIS
Fiseha Bogale Gebretsadik

To my Dad Bogale Gebretsadik

UNIVERSITAT ROVIRA I VIRGILI

SYNTHESIS OF ACID MESOPOROUS SAPONITES AND ITS APPLICATION IN CATALYTIC GLYCIDOL HYDROGENOLYSIS

Fiseha Bogale Gebretsadik

Table of Contents

1. General Introduction.....	1
1.1. Saponite.....	3
1.2. Glycidol.....	9
1.3. 1,2- and 1,3-propanediols (PDs)	11
2. Objective.....	13
3. Experimental Section.....	17
3.1. Microwaves Technology	19
3.2. Sonochemistry.....	21
3.3. Saponite preparation.....	22
3.4. Characterization techniques	24
3.4.1. X-ray diffraction (XRD).....	24
3.4.2. Fourier transform infrared (FT-IR)	25
3.4.3. N ₂ - physisorption.....	26
3.4.4. Magic angle spinning-nuclear magnetic resonance spectroscopy (MAS-NMR)	29
3.4.5. Cation exchange capacity (C.E.C).....	30
3.4.6. UV-Vis spectroscopy	30
3.4.7. Inductively coupled plasma (ICP).....	31
3.4.8. Scanning electron microscopy (SEM), energy dispersive x-ray (EDX)	32
3.4.9. Transmission electron microscopy (TEM).....	33
3.4.10. Thermogravimetric analysis (TGA).....	33
3.4.11. Temperature-programmed reduction (TPR)	34
3.4.12. H ₂ -chemisorption	35
3.4.13. X-ray photoelectron spectroscopy (XPS)	36
3.5. Catalytic activity test.....	37
4. Preparation of mesoporous acid saponite	39
4.1. Background on the preparation of mesoporous clay	41

4.1.1. Acid treatment	42
4.1.2. Pillared clays.....	43
4.1.3. Use of polymer or surfactant as a template.....	45
4.2. Use of polymer as template in microwaves synthesis of saponite. Study of several factors of influence.....	47
Introduction	49
Experimental	50
Results and discussion.....	54
Conclusions	67
Acknowledgments	68
4.3. Microwave synthesis of delaminated acid saponites using quaternary ammonium salt or polymer as template. Study of pH influence.	69
Introduction	71
Experimental	72
Results and discussion.....	75
Conclusions	94
Acknowledgments	94
5. Application of acid saponite in glycidol hydrogenolysis	95
5.1. Background on the selective hydrogenolysis of glycerol to propanediols and potential of glycidol as an alternative substrate.....	97
5.2. Selective hydrogenolysis of glycidol to propanediols using Ni supported on various mesoporous acid saponites as bi-functional catalysts.....	103
Introduction	105
Experimental	107
Results and discussion.....	111
Conclusions	126
Acknowledgments	127
5.3. Liquid phase hydrogenolysis of glycidol over Ni-Cu bimetallic catalysts supported on acid saponite	129
Introduction	131

Experimental	133
Results and discussion.....	136
Conclusions	150
Acknowledgements	151
5.4. Hydrogenolysis of glycidol to 1,3-propanediol using MO _x modified Ni, Cu mono and bimetallic catalysts supported on acid mesoporous saponite. ...	153
Introduction.....	155
Experimental	157
Results and discussion.....	161
Conclusions	179
Acknowledgments.....	180
6. General conclusions.....	181
7. References	187

Glossary of Terms and Abbreviations

1,2-PD	1,2-Propanediol
1,3-PD	1,3-Propanediol
CEC	Cation exchange capacity
CHA	Cyclohexylamine
EDX	Energy dispersive X-ray
FID	Flame ionization detector
FT-IR	Fourier transformed infrared spectroscopy
FWHM	Full width at half maximum
GC	Gas chromatography
HOMO	Highest occupied molecular orbital
ICP	Inductively coupled plasma
IUPAC	International union of pure and applied chemistry
JCPDS	Joint commite on powder diffraction standards
LDH	Layered double hydroxides
LUMO	Lowest unoccupied molecular orbital
MAS	Magic angle spinning
MPa	Megapascal
MS	Mass spectroscopy
NMR	Nuclear magnetic resonance
O	Octahedral
ppm	parts per million
rpm	revolution per minute
SEM	Scanning electron microscope
T	Tetrahedral
TCD	Thermal conductivity detector
TEM	Transmission electron microscope
TGA	Thermogravimetric analysis
THFA	Tetrahydrofurfuryl Alcohol
TPR	Temperature programmed reduction

UV	Ultraviolet
Vis	Visible
wt	Weight
XPS	X-ray photoelectron spectroscopy
XRD	X-ray diffraction

UNIVERSITAT ROVIRA I VIRGILI

SYNTHESIS OF ACID MESOPOROUS SAPONITES AND ITS APPLICATION IN CATALYTIC GLYCIDOL HYDROGENOLYSIS

Fiseha Bogale Gebretsadik

1. General Introduction



CHAPTER 1

1.1. Saponite

Clays are naturally occurring materials composed of fine grained minerals formed as a result of chemical weathering of other silicate minerals. It contains mainly phyllosilicates that are plastic at appropriate water content and will harden when dried or fired (Guggenheim and Martin, 1995). However, it is frequent in the literature to talk about clay mineral instead of clay. Clay mineral is the terminology used when we are referring, specifically, to the phyllosilicate part of clays. As different to clays, clay minerals can be natural and synthetic. The layers of the lamellar structure of the mineral clays are composed of octahedrally coordinated sheets, $M(O, OH)_6$ where $M = Mg^{2+}$, Al^{3+} , Fe^{2+} or Fe^{3+} and tetrahedrally coordinated sheets of mainly silicon $Si(O, OH)_4$ and sometimes Al^{3+} . Isomorphic substitution can occur in both tetrahedral and octahedral sheets generating clay minerals with negative layer charge. Hydrated exchangeable cations are incorporated in the interlayer space to neutralize the layer charge. Layered double hydroxide (LDH) are a family of layered materials that present positive layer charge with anions in the interlayer space neutralizing the lamella charge. Many properties of these minerals are similar to those of clay minerals. For this reason, they are named anionic clays. In nature, cationic clays are more common than anionic ones (Vaccari, 1998).

The number of octahedral and tetrahedral sheets per layer could vary depending on the type of clay minerals. Some clay minerals contain two tetrahedral and one octahedral sheet per unit cell resulting in 2:1 (TOT) structure and others have one tetrahedral and one octahedral sheet per layer giving 1:1 type layer. The octahedral sheet may consist of either divalent cations with full occupancy or trivalent cations with 1/3 vacancies, giving trioctahedral or dioctahedral clay, respectively. Based on the amount of layer charge, the number of octahedral and tetrahedral sheets per unit cell and occupancy of the octahedral sheet, planar clay minerals can be classified into 6 major types. The characteristics of each of them are summarized in Table 1.1-1.

CHAPTER 1

Table 1.1-1: Classification scheme of planar phyllosilicate clay minerals.

Layer type	Charge per unit cell (x)	Group	Mineral examples	Ideal composition	Remarks
1:1(TO)	x = 0	Kaolin-Serpentine	Kaolinite, dickite,	$Al_4Si_4O_{10}(OH)_8$	Kaolin subgroup, dioctahedral nonswelling Kaolin subgroup, dioctahedral, swelling Serpentine subgroup, trioctahedral nonswelling
			Halloysite	$Al_4Si_4O_{10}(OH)_8 \cdot 4H_2O$	
			Chrysotile, antigorite, lizardite	$Mg_6Si_4O_{10}(OH)_8$	
2:1 (TOT)	x = 0	Pyrophyllite-talc	Pyrophyllite	$Al_4Si_8O_{20}(OH)_4$	Dioctahedral nonswelling trioctahedral nonswelling
			Talc	$Mg_6Si_8O_{20}(OH)_4$	
	x = 0.5-1.2	Smectite	Beidellite	$Al_4Si_{8-x}Al_x(OH)_4Ex_x$	Dioctahedral, swelling Trioctahedral, swelling
			Montmorillonite	$Al_{4-x}Mg_xSi_8O_{20}(OH)_4Ex_x$	
			Nontronite	$Fe_{4-x}Si_{8-x}Al_xO_{20}(OH)_4Ex_x$	
			Saponite	$Mg_6Si_{8-x}Al_x(O)_{20}(OH)_4Ex_x$	
			Hectorite	$Mg_{6-x}Li_xSi_8(O)_{20}(OH)_4Ex_x$	
	x = 1.2-1.8	Vermiculite	Vermiculite	$Al_4Si_{8-x}Al_xO_{20}(OH)_4Ex_x$	Dioctahedral, swelling Trioctahedral, swelling Trioctahedral, nonswelling
			Vermiculite	$Mg_6Si_{8-x}Al_x(O)_{20}(OH)_4Ex_x$	
			Illite, glauconite	$Al_4Si_{8-x}Al_xO_{20}(OH)_4K_x$	
	x = 2	Mica	Muscovite,	$[(Al_4)(Si_6Al_2)O_{20}(OH,F)_4]K_2$	Dioctahedral, nonswelling Trioctahedral, nonswelling Trioctahedral, lithium mica Dioctahedral, nonswelling
			Celadonite	$[(Fe_2Mg_2)(Si_8)O_{20}(OH,F)_4]K_2$	
Phlogopite			$[(Mg_6)(Si_6Al_2)O_{20}(OH,F)_4]K_2$		
Taenolite			$[(Li_4Mg_4)(Si_8)O_{20}(OH,F)_4]K_2$		
Brittle mica			Margarite	$[(Al_4)(Si_4Al_4)O_{20}(OH,F)_4]Ca_2$	

x is the layer charge per unit cell and Ex is the number of equivalents of the exchangeable cations.

Clays were used by mankind as early as prehistoric times for curing wounds, soothing irritation, mummification of cadavers and creating pottery and other decorative items and as a skin cleansing and anti-inflammatory agent, (Bech, 1987; Robertson, 1996; Veniale, 1997). More recently, the surface area, ion exchange capacity or hydration properties of the clay minerals, makes them important materials for more technological applications such as in building, paper industries, oil drilling, foundry mould, adsorbents, catalysts and catalyst supports, ion exchangers and decolorizing agents (Konta, 1995; Murray, 2000; Ding et al., 2001; Carretero, 2002; Babel and Kurniawan, 2003; Bergaya and Lagaly, 2006; Brigatti et al., 2006; Choy et al., 2007; Barwood et al., 2014). Smectites, palygorskite, kaolinite and talc are used in modern pharmaceutical formulations as active principle or excipients owing to their specific surface area, adsorption capacity, rheological properties, chemical inertness and low or null toxicity (Veniale, 1997; Viseras and López-Galindo, 1999; López Galindo and Viseras, 2000). Na-4 mica was used as super selective cation exchanger in the decontamination of drinking water and soils from radioactive wastes (Komarneni et al., 2001).

In the emerging field of nanoscience and nanotechnology, clay minerals serve as naturally occurring nanomaterials or nano-reactors for the fabrication of nanoparticles, nanospecies and nanodevices (Zhou et al., 2006). Nanoparticles, nanotubes and other various types of nano-species were incorporated in the interlayer space of clay minerals or clay minerals based nano-films were synthesized to give various types of functional materials (Yariv and Cross, 2002; Zhou et al., 2004; Tong et al., 2009) applicable in catalysis, adsorption, environmental remediation, polymers, electronics and fuel cells (Adoor et al., 2006; Bergaya and Lagaly, 2006; Brigatti et al., 2006; Kim et al., 2006 ; Villaluenga et al., 2007; Lin et al., 2009).

Though clays are the most abundant minerals on the surface of the earth and other planets, for example Mars (McKeown et al., 2009), naturally occurring clays have limitations for various applications. They invariably contain impurities and their mineralogical composition differs depending on the genesis process and on the provenance site (Utracki, 2007). In order to get clay minerals in pure and homogeneous phase and with known composition, they need to be synthesized

CHAPTER 1

through controllable preparation procedures (Kloprogge et al., 1999). Additionally, the knowledge obtained during the synthesis will give an insight on the mechanism of formation, modification of composition and properties and allows foreseeing new applications (Zhang *et al.*, 2010). Among clay minerals, the synthesis of smectites was widely studied due to high purity and homogeneity of synthetic samples, and the ease to control and fine tune their composition and structure (Kloprogge, 1998; Kloprogge et al., 1999; Andrieux and Petit, 2010).

Saponites are trioctahedral smectites. Figure 1.1-1 shows a general distribution of the tetrahedral and octahedral sheets in clay minerals of type 2:1. The general formula of saponites is $M^{n+}_{x/n}[(Mg_6)(Al_xSi_{8-x})^T O_{20}(OH)_4].nH_2O$ (Figure 1.1-1), where M is a neutralizing interlayer cation: Mg^{2+} , Na^+ , K^+ , Ca^{2+} , NH_4^+ (Kloprogge et al., 1994b), n is its charge and T and O, represents the tetrahedral and octahedral sheet, respectively. An isomorphous substitution of Si^{4+} by Al^{3+} occurs in the tetrahedral sheet with the subsequent generation of a negative layer charge. Certain substitution of the octahedral Mg^{2+} by Al^{3+} can also occur resulting in a positive layer charge that partially neutralizes the negative layer charge generated in the tetrahedral sheet. When the interlayer cation is H^+ the saponite presents Brønsted acid properties.

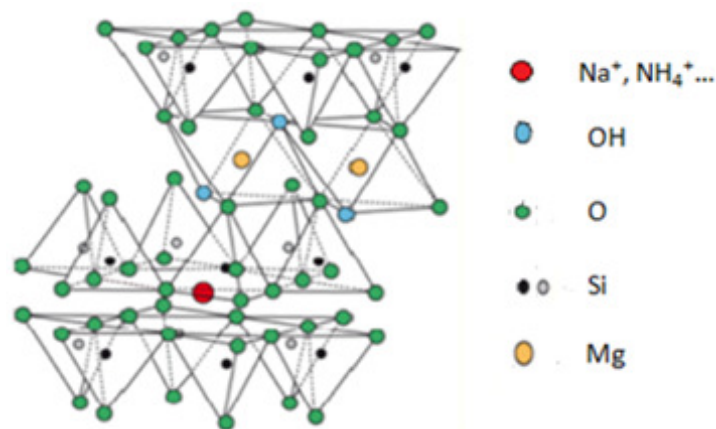


Figure 1.1-1: Structure of TOT clay mineral.

Saponites have been synthesized by non-hydrothermal approaches at 373 K and atmospheric pressure (Decarreau, 1981; Farmer et al., 1991, 1994), and by hydrothermal treatment of a gel containing stoichiometric mixtures of the precursors and the interlayer cation at temperatures ranging from 453 K to 723 K using conventional ovens or

microwaves during the ageing treatment (Kloprogge et al., 1993, 1994 a,b; Vogels et al., 1997; Kawi and Yao, 1999; Yao et al., 2005; Higashi et al., 2007; Bisio et al., 2008; Vicente et al., 2010; Xue and Pinnavaia, 2010). The hydrothermal synthesis gave a better result in terms of both purity and crystallinity of the resulting saponite (Kloprogge et al., 1999).

The influence of chemical composition, crystallization time, temperature, pH, gel dilution, heat source and etc. on the growth of saponite material, its morphology, textural and surface properties has been investigated (Kloprogge et al., 1994a and Bisio et al., 2008). The use of higher temperature during hydrothermal crystallization increased the rate of hydrolysis and improved nucleation and growth of the saponite mineral (Kloprogge et al., 1993). Samples prepared from higher initial pH of the synthesis gels and using concentrated slurries showed higher Al incorporation in the tetrahedral sheet and higher crystallinity (Bisio et al., 2010) whereas those prepared from more diluted slurries displayed disordered morphology with higher contribution of mesoporosity (Vicente et al., 2010). The use microwaves for saponite preparation decreased temperature and synthesis time with subsequent energy saving in addition to affording unique characteristics to the synthesized saponite (Trujillano et al, 2010; 2011; Vicente et al., 2011).

Saponites has been also investigated as catalyst supports for several reactions. For instance, Cs/saponite catalysts were studied for the synthesis of N-alkyl pyrazoles (Velasco et al., 2011), Fe/saponites catalysts for Fenton reaction (Herney-Ramirez et al., 2007), Co/saponite catalysts for air oxidation of polyvinyl alcohol (Garade et al., 2011) and Ni/saponite catalysts for the hydrogenation of styrene oxide (Vicente et al., 2011). Saponites containing Mg^{2+} , Ni^{2+} , or Fe^{2+} in their octahedral sheets and Al^{3+} and Fe^{3+} substituting Si^{4+} in the tetrahedral positions were prepared and tested for the epoxidation of (Z)-cyclooctene by hydrogen peroxide (Trujillano et al. 2011). The polymerization of ethylene was carried out with iron and nickel complexes immobilized in saponite interlayers (Kurokawa et al., 2014). However, most synthetic unmodified saponites prepared by conventional hydrothermal or non-hydrothermal procedures are microporous and are not useful for catalysis involving bulky molecules.

CHAPTER 1

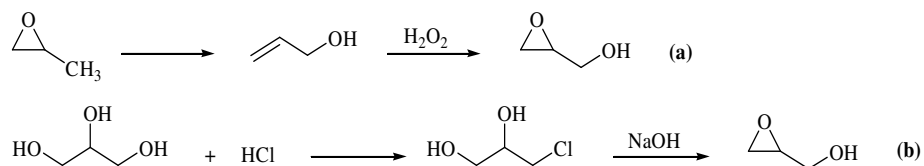
Surface area and porosity of layered solids are crucial criteria in adsorption and catalysis since they are the main factors that determine accessibility and activity of the sites. The pore architecture of a porous solid also controls transport phenomena and governs shape selectivity. The use of materials with bigger pore structures (mesoporous) is necessary for the production of chemicals involving bigger molecules (Corma, 1997). Saponites have been proposed as raw materials in the preparation of mesoporous acid catalysts owing to their high thermal stability and layer charge density (Liu and Pinnavaia, 2003).

In the literature, different strategies have been proposed for the preparation of layered mesoporous materials. One was by exchanging the interlayer cations of various layered materials with polyoxocations and subsequent calcination. This results in the formation of bulky oxide clusters in the interlayer space serving as pillars with a generation of mesoporosity (Pinnavia, 1983; Burch, 1988; Figuras, 1988; Butruille and Pinnavaia, 1996). Other alternative was delamination. Delaminated mesoporous hectorites has been prepared by in-situ hydrothermal crystallization of a gel containing polyvinylpyrrolidone (Carrado & Xu, 1999) or quaternary ammonium salt (Iwasaki et al., 1998; Sánchez et al., 2012) followed by removal of the template from the organo-clay composite by calcination.

Delamination of saponites with important inter-particle mesoporosity was reported by Vicente et al. (2010) during the preparation of saponites using microwaves and for saponites prepared from highly diluted slurries (H_2O/Si molar ratio > 150) (Costenaro et al., 2012). There are not literature report about the preparation of mesoporous saponite using templates. In this thesis, we propose the use of templates for the preparation of mesoporous acid saponites from slurries of different degrees of dilution and initial pH of 8 and 13 using conventional heat source or microwaves during the aging treatment to investigate its effect on the porosity and other physico-chemical properties of the resulting saponite.

1.2. Glycidol

Glycidol, IUPAC name 2,3-epoxypropan-1-ol, is a colorless, odorless organic liquid soluble in water and other polar organic solvents. It is a bi-functional compound with epoxide and alcohol functional groups, which makes it very special material for different kind of industrial applications (Tarnacka et al., 2014). Glycidol is widely used in pharmaceuticals, cosmetics, detergents, demulsifiers, dye leveling agents, etc (Wu and Tatsumi, 2003; Konaka et al., 2014). It is also an important feedstock in the preparation of polyglycerols, glycidol ethers, polyurethanes and pharmaceuticals (Pagliaro et al., 2007). Currently, glycidol is produced commercially by two major non-environmentally friendly routes (Hanson, 1991). The first one is by epoxidation of allyl alcohol in the presence of tungsten or vanadium homogeneous catalyst (Scheme 1.2-1a). The other route involves reaction of 3-chloro-1,2-propanediol with bases (Scheme 1.2-1b). (Hanson, 1991; Wu and Tatsumi, 2003; Palomo et al., 2005; Pagliaro et al, 2007). These industrial processes are not attractive because they are expensive, due to corrosion of reactors, involve multiple steps, are not sustainable as they use petrochemical based feed stocks and large amount of liquid and solid wastes are produced in the process (Bai et al., 2013; Zhou et al., 2015).

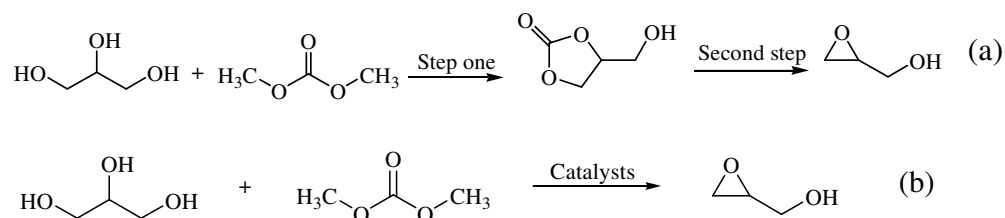


Scheme 1.2-1: Industrial preparation of glycidol by (a) epoxidation of allyl alcohol and (b) reaction of 3-chloro-1,2-propanediol with bases.

A research effort was underway to replace the non-environmentally friendly industrial glycidol production route with a green and sustainable process. The most interesting approach has been the one based on dimethyl carbonate (DMC) and a renewable glycerol substrate. DMC is an environmentally friendly, less toxic, highly biodegradable compound with low bio-accumulation (Tundo et al., 2008). Glycidol was synthesized from glycerol and DMC in two steps (Scheme 1.2-2 (a)) first by formation of glycerol carbonate followed by decarboxylation to glycidol using metal

CHAPTER 1

salts (Malkemus, 1958), [BMIm]-based ionic liquids (Choi et al., 2013) and metal oxide modified zeolite (Bolivar-Diaz et al., 2013) as catalysts. In recent years, direct one pot synthesis of glycidol from glycerol and DMC (Scheme 1.2-2 (b)) has been attempted by using tetramethylammonium hydroxide (Munshi et al., 2014) and NaAlO₂ (Bai et al., 2013) as catalysts. The former gave 78% and the latter afforded 76% yield to glycidol. However, the use of both catalysts was limited by problems related to low thermal stability and reusability in the former and hydrolysis in the latter catalysts (Zhou et al., 2015). The use of tetraethylammonium amino acid based ionic liquids was reported by Zhou et al. (2015). The reaction gave 79% yield of glycidol with 96% conversion at 403 K and after 2 h of reaction with good stability and reusability.



Scheme 1.2-2: (a) two step and (b) one pot synthesis of glycidol from glycerol and dimethyl carbonate.

Glycidol, which contains a highly strained epoxide ring, is a very reactive molecule. The ring opening isomerization, dimerization and oligomerization reactions of various substituted epoxides in the presence of several solid acid (Fási et al., 1999; 2000; 2001) and base catalysts (Fási et al., 2004) has been reported. Other epoxides, such as 1,2-epoxyoctane (van Grieken et al., 2004) and styreneoxide (Ruiz-Hitzky and Casal, 1985; Salla et al., 2005; González et al., 2009) were isomerized, specifically, to octanal and acetaldehyde using solid acid catalysts. The hydrogenolysis reaction of different substituted epoxides to alcohol was reported using supported metal catalysts (Pálinkó et al., 2002; Bartók1 et al., 1998a, b). However, some supported metals, for example Cu catalyze deoxygenation of epoxides to alkenes in addition to hydrogenolysis (Bartók1 et al., 1998b). The high reactivity of epoxides, make glycidol a potential alternative substrate to glycerol for the catalytic 1,3-PD production.

1.3. 1,2- and 1,3-propanediols (PDs)

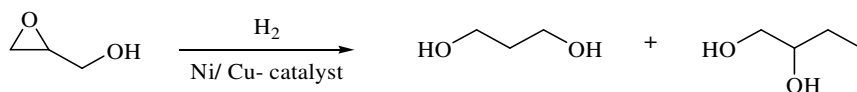
As a result of biodiesel production, the supply of glycerol has increased enormously in recent years and several ways have been proposed for its valorization to added-value products (Ruppert et al., 2012). One attractive approach to transform glycerol to useful chemicals is its selective hydrogenolysis, which is a clean and competitive process, that allows the formation of 1,2- and 1,3-propanediol (1,2- and 1,3-PD) (Nakagawa et al., 2011). 1,2-PD (propylene glycol) has interesting applications as anti-freeze or cooling agent, a monomer for polyester resins and in paints, humectant in tobacco industry, in pharmaceutical industry, costumer care products, food among others. (Pagliaro and Rossi, 2008). The current industrial process for the production of 1,2-PD involves selective hydrogenolysis of propylene oxide obtained either from chlorohydrin process or by epoxidation of petroleum derived propylene. (Trent, 1996).

1,3-propanediol (1,3-PD) is commercially the most interesting hydrogenolysis product of glycerol. It is used in resins, engine coolants, dry-set mortars, water based inks, solvents, adhesives, detergents and cosmetics (Lam et al., 1997; Arhancet et al., 2000). Much of 1,3-PD produced industrially is used in the production of a specialized polypropylene terephthalate (PPT) polymer, a polyester synthesized from 1,3-PD and terephthalic acid. It is traded with a brand name CORTERRA by Shell and SORONA by DuPont (Dam and Hanefeld, 2011). The fibers, films and coatings obtained from this polymer have excellent properties in their chemical resistance, light stability, elastic recovery, and dyeability (Zeng and Biebl, 2002, Haas et al., 2005). Currently, 1,3-PD is industrially produced by hydration of petroleum derived acrolein to 3-hydroxypropanal followed by hydrogenation (Dugassa-DuPont process) (Arntz et al., 1991a, b; Haas et al., 1998, 2005) or hydroformylation of ethylene oxide to 3-hydroxypropanal with subsequent hydrogenation (Shell process) (Lam et al., 1997; 2000; 2003).

The main problems of these classic processes of 1,2- and 1,3-PD synthesis are: the starting materials for both diols synthesis are petrochemical derivatives, the high pressure applied to hydroformylation and hydrogenation steps together with the use

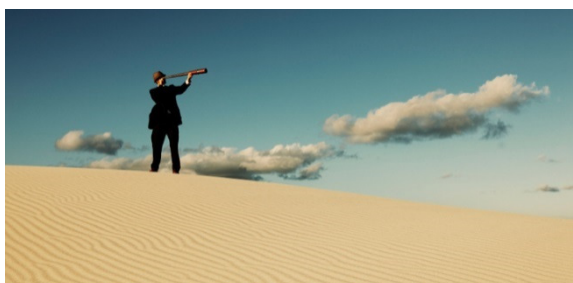
CHAPTER 1

of aromatic solvents or the hazardous nature of acrolein (Behr et al., 2008). Therefore, considerable efforts have been made for replacing the petroleum derived starting materials in the production of diols by green and renewable resources, such as glycerol (Bozell and Petersen, 2010). The direct hydrogenolysis of glycerol to 1,2-propanediol with high selectivity and conversion values has been reported using various types of catalysts. (Chaminand et al., 2004; Akiyama et al., 2009; Gandarias et al., 2010; Gong et al., 2010; Nakagawa et al., 2010; Qin et al., 2010; Sánchez et al., 2012; Nakagawa et al., 2014). However, the synthesis of 1,3-propanediol from glycerol was more challenging (Chaminand et al., 2004; Gandarias et al., 2010; Qin et al., 2010; Nakagawa et al., 2014). Hence, in this thesis we propose the use of glycidol as an alternative renewable resource for the synthesis of 1,3-PD using cheap heterogeneous catalysts (Scheme 1.2-3) and moderate reaction conditions. The justification for the use of glycidol will be discussed later in the thesis.



Scheme 1.2-3: Hydrogenolysis of glycidol to propanediols using heterogeneous Ni/ or Cu catalysts.

2. Objective



The transformation of glycerol to 1,3-propanediol (1,3-PD), which is an important high added-value derivative of glycerol, is at the forefront of current scientific research. The direct glycerol hydrogenolysis to 1,3-propanediol has been attempted by many researchers and the limitations are multifaceted. In one hand, the current protocols are based on expensive noble metals, elevated pressure, high temperature and/ or long reaction time. On the other hand, the conversion and selectivity of these systems is low. Therefore, in order to improve the existing protocol, it is important to develop a procedure based on cheap non-noble metal based catalysts.

The aim of this thesis was to synthesize acid mesoporous saponites and study their use as acid supports of Ni, Cu and Ni-Cu catalysts, for the hydrogenolysis of glycidol to 1,2- and 1,3-PD, with a view to find the catalysts characteristics that favor a higher selectivity to 1,3-PD. In order to achieve the main objective, the following specific objectives were drawn:

- To vary different parameters in the synthesis of saponites and study their influence on the physicochemical properties of the resulting materials, especially, specific BET area, porosity and surface acidity. The parameters modified were initial pH of the synthesis gel, type of heat source (microwave or conventional oven) during the aging treatment, degree of dilution of the slurry and the use of polymer or surfactant as a template. The effect of surfactant during in-situ hydrothermal crystallization or post-synthesis modification was compared.
- To evaluate the catalytic activity of Ni supported on various saponites for the selective hydrogenolysis of glycidol and the role of the acidity of the support in the catalytic pathway. To optimize the amount of metal loading, reaction time and reaction temperature.
- To compare the activity of acid saponite-supported Ni and Cu and Ni-Cu bimetallic catalysts, with different relative wt % Ni and Cu loading, in the hydrogenolysis of glycidol and to study the effect of the reaction temperature.
- To assess the influence of several metal oxides (MO_x , M = V, Mo, W, Re) used as catalyst modifiers in promoting the selective formation of 1,3-PD. To

CHAPTER 2

compare the effect of the amount of ReO_x , with respect to the metal phase (Ni or Ni-Cu) used.

- To characterize saponites, catalyst precursors and catalysts with X-ray diffraction (XRD), Fourier transform infrared spectroscopy (FT-IR), N_2 adsorption-desorption analysis, energy dispersive X-ray (EDX), aluminum magic angle spinning nuclear magnetic resonance spectroscopy (^{27}Al -MAS-NMR), transmission electron microscopy (TEM), cation exchange capacity (CEC), thermogravimetric analysis (TG), X-ray photoelectron spectroscopy (XPS), NH_3 temperature programmed desorption (TPD), H_2 chemisorption, temperature programmed reduction (TPR).

3. Experimental Section



Experimental section

This chapter gives an overview on the theoretical background behind various experimental techniques, which were employed in the thesis for preparation and characterization of saponite, catalyst precursor and catalyst samples. The experimental details of each characterization techniques is described in the respective sections, in the results and discussion part of the thesis.

3.1. Microwaves Technology

Microwaves are electromagnetic waves with frequencies ranging from 0.3 to 300 GHz and with wavelengths between 1 mm to 1 m, which are between infrared and radio frequency waves in the electromagnetic spectrum (Figure 3.1-1). Microwaves are used in telecommunication, radar and heating applications. Radar equipment uses microwaves of lower wavelength (0.01–0.25 m) and much of the microwave band is applied for telecommunication. In order to avoid interference with these applications, the frequency of the microwaves heating equipment is regulated at 2.45 GHz (with a wavelength of about 12.24 cm) (Ying-Jie and Feng, 2014).

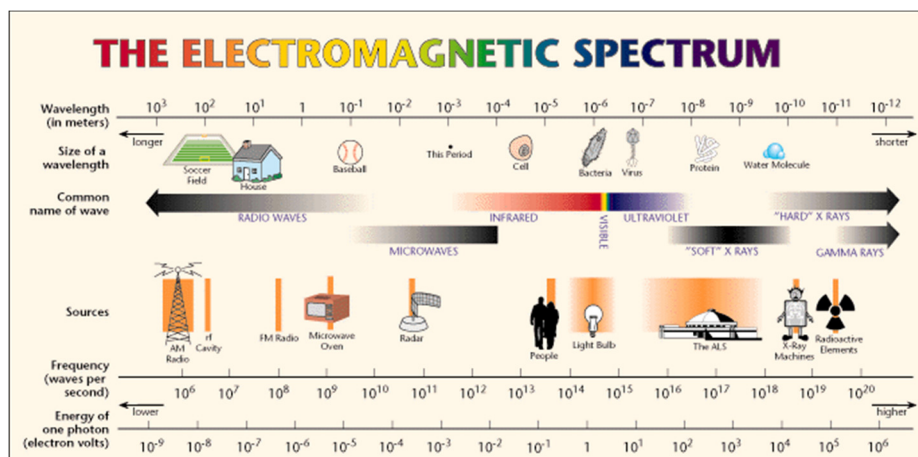


Figure 3.1-1: The electromagnetic spectrum

One of the twelve principles of green chemistry is “design of energy efficiency” (Anastas and Warner, 1998). Microwave dielectric heating uses the ability of some liquids and solids to transform electromagnetic radiation into heat to drive chemical reactions. Microwave heating involves two main mechanisms: dipolar polarization

CHAPTER 3

and ionic conduction. In dipolar polarization mechanism, polar molecules try to orientate themselves with the rapidly alternating electric field (4.9×10^9) as shown in Figure 3.1-2. In the latter case, ions move under the influence of the rapidly fluctuating electric field. This rapid oscillation of the electric field direction causes friction and collision of molecules or ions with an ultimate effect of local temperature rise (Collins, 2010).

In microwaves heating, the energy is directly supplied to molecules and there is no energy loss due to indirect heating unlike in conventional heating where heat is first transferred from the heat source (oil bath or electric furnace) to the walls of the reactor and then to the reactants by convection or conduction. In conventional heating, the core of the sample takes much longer to achieve the target temperature. Such a pathway typically leads to thermal gradients throughout the bulk media, and to inefficient and non-uniform reactions. Microwaves have been extensively used in organic synthesis and material preparation. Microwaves, as an energy source, offers many advantages over the conventional heat sources. The great potential of this technique applied to the preparation of materials is the decrease of the synthesis time or temperature, introduction of structural modifications in the synthesized compounds and improving yield and purity of product by reducing unwanted side reactions compared to conventional heating (Dahl et al. 2004; Patete et al., 2011).

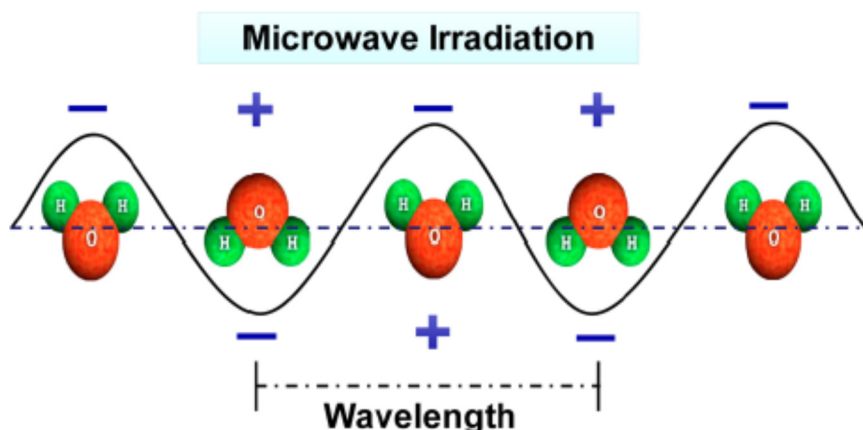


Figure 3.1-2: Microwave heating of water molecules by dipolar polarization mechanism.

In the thesis, a 6-positions rotor Milestone Ethos Touch control laboratory microwaves (Figure 3.1-3) was used for the hydrothermal aging treatment in the preparation of saponite. Each of the autoclaves with capacity 85 mL was filled with 50 mL of slurry and sealed. The temperature of the autoclaves was controlled by a thermowell placed in one of the reactors. The power of the microwaves heating was maintained below 400 W and the homogeneity of the heating was assured by maintaining the rotor on and magnetically stirring the autoclaves during aging.

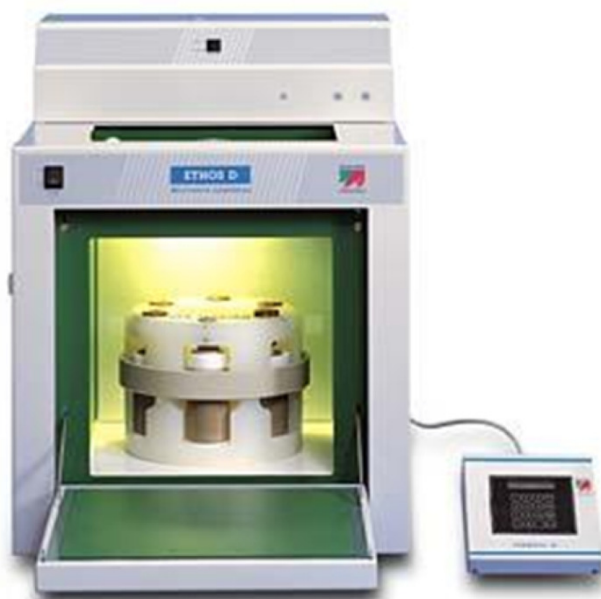


Figure 3.1-3: Milestone Ethos Touch control laboratory Microwave

3.2. Sonochemistry

Sound is a form of energy which is characterized by its wave length and amplitude. The speed of sound in a medium is determined by the density (ρ) and compressibility of the medium through which it travels. A typical speed of sound in gases and liquids is in the order of 300-400 and 100-1500 m/s, respectively. Based on their frequency, sound waves can be classified into three groups: infrasound ($f < 20$ Hz), audible sound ($20 \text{ Hz} < f < 20 \text{ kHz}$), and ultrasound ($f > 20 \text{ kHz}$) (Cheeke, 2002). Ultrasound has technological applications in cutting brittle material and surface treatment and used in medicine for diagnostics and treatment. Ultrasound is also best known as a means of communication in some animals.

CHAPTER 3

The use of ultrasound in chemical processes is called sonochemistry. The application of ultrasound in various fields of chemistry and material preparation has been scrutinized over the last few decades (Suslick, 1988; Crum et al., 1994). Ultrasound was successfully employed in the fabrication of nanomaterials (Suslick and Price, 1999; Gedanken and Mastai, 2004; Gedanken, 2007), synthesis of polymers (Kruus, 1991) and their controlled degradation (Singla et al. 2004), for promoting supramolecular aggregates (Price, 1990), activate metal catalysts (Davidson et al., 1987) etc. In the liquid phase, the frequency of ultrasound spans from 20 kHz to 10 MHz (wavelengths 100-0.15 mm) and is not on the scale of molecular dimension to have direct interaction with molecules. The chemical effect of ultrasound is derived from non-linear acoustic phenomenon of which cavitation is the most important. In acoustic cavitation, when ultrasound propagates through a liquid it causes the formation, growth and impulsive collapse of micrometric sized bubbles. Such a collapse is actually a quasiadiabatic process resulting in the generation of high temperatures and pressures within the nanosecond scale and with extreme cooling rates ($>10^{10} \text{ Ks}^{-1}$). Due to this phenomena, ultrasound provides a non-invasive means for enhancing mass and heat transfer and successfully increases conversion, changes reaction pathways, initiates reactions, and accelerates mixing (Thompson et al., 1999).

In this thesis, BRANSON SONIFIER 450 ultrasound was used at an output control of 5, duty cycle of 70% and for 30 min for reactant mixing during the slurry preparation stage of the saponite synthesis.

3.3. Saponite preparation

The effects of various synthesis conditions in the preparation of acid mesoporous saponite were investigated. Several saponite samples were prepared at pH 8 and 13, different degree of slurry dilution (250, 125 and 50) expressed as molar ratio of $\text{H}_2\text{O}/\text{Si}$, without and with template, surfactant (dodecyltrimethyl ammonium chloride, As) or polymer (polyvinyl pyrrolidone, PVP) and using microwaves or conventional oven as a heat source during the aging treatment. In the case of saponite preparation in the presence of polymer, one of the two types of polymers at molecular weights of 40,000 g/mol (P1) and 360,000 g/mol (P2) was added during slurry preparation in order to

understand the effect of the molecular weight of the polymer on the property of the resulting saponite.

Table 3.3-2: Preparation conditions and nomenclature of the saponites studied in the thesis.

Nomenclature	H ₂ O/ Si molar ratio	Template	Template loading (%) ^a	Mode of template addition	Aging
SC250	250	—	—	—	Conventional
SM250	250	—	—	—	Microwaves
SM250P1	250	P1	20	In-situ	Microwaves
SM250P2	250	P2	20	In-situ	Microwaves
SC250P1	250	P1	20	In-situ	Conventional
SC125	125	—	—	—	Conventional
SM125	125	—	—	—	Microwaves
SM125P1	125	P1	20	In-situ	Microwaves
SM125P2	125	P2	20	In-situ	Microwaves
SC50	50	—	—	—	Conventional
SM50	50	—	—	—	Microwaves
SM50P1	50	P1	20	In-situ	Microwaves
SM50P2	50	P2	20	In-situ	Microwaves
SM13	125	—	—	—	Microwaves
SM13P	125	P1	20	In-situ	Microwaves
SM13AS	125	As	20	In-situ	Microwaves
SC13	125	—	—	—	Conventional
SM8(250)AS	250	As	20	In-situ	Conventional
SM8(125)AS	125	As	20	In-situ	Microwaves
SM8(50)AS	50	As	20	In-situ	Microwaves
SM13AS _{PSM}	125	As	40	Post synthesis	Microwaves
SC13AS _{PSM}	125	As	40	Post synthesis	Conventional
SM13AS _{PSM} R	125	As	40	Post synthesis	Microwaves
SC13AS _{PSM} R	125	As	40	Post synthesis	Conventional

^a The amount of template was calculated with the respect to the mass of other solid reactants.

CHAPTER 3

Some samples were modified after synthesis by exchanging their interlayer cations with surfactant (As) either at room temperature or by refluxing in order to compare the relative delamination and other structural and compositional effects of the in-situ hydrothermal synthesis and post synthesis modification. The saponites that were synthesized in the thesis work, their synthesis conditions and their nomenclature are summarized above (Table 3.3-2). The outcome of each of the synthesis conditions and the specific samples that were compared to draw important conclusions on the influence of each factor will be presented in detail in the corresponding result and discussion part of the thesis.

3.4. Characterization techniques

3.4.1. X-ray diffraction (XRD)

When samples are irradiated with an X-ray, a highly energetic beam with wave length in the Å range that is capable of penetrating the internal structure of a substance, the oscillating field of the incident x-ray moves the atomic electrons and their acceleration generates outgoing waves. The waves generated in this way from each atom of the sample could undergo constructive or destructive interference depending on the long range periodicities of the atoms in the sample. Crystalline sample with precise periodicities have their outgoing waves interfering constructively comprising diffraction peak. Samples with defects are less precisely periodic in their atomic arrangement but still have distinct diffraction peaks. X-ray powder diffraction (XRD) is a technique used for phase identification of a crystalline material and can provide information on unit cell dimensions (Cohen and Schwartz, 1977). X-ray diffraction pattern of a pure substance is like its finger print. Each phase presents characteristics peaks (hkl), characterized by the value of the diffraction angle, 2θ and its relative intensity, that can be useful for phase identification.

XRD measurements of synthesized clays, catalyst precursors and catalysts were made using a Siemens D5000 diffractometer fitted with a curved graphite diffracted-beam monochromator and diffracted-beam Soller slits, a 0.06° receiving slit, and scintillation counter as a detector. $\text{Cu}_{k\alpha}$ radiation was obtained from a copper X-ray tube operated at 40 kV and 30 mA. Sample was dusted on to a low background Si

(510) sample holder. The data were collected with an angular step of 0.05° at 3 s per step and sample rotation. Measurement was done in 2θ diffraction range between 5° and 70° . Crystalline phases were identified by comparing the diffractogram of the sample with the Joint Committee on Powder Diffraction Standard (JCPDS). The peak width, β_i , was estimated by fitting the characteristics reflections of each of the phases by applying TOPAS 4.1 program which takes the contribution of the specific instrument configuration into account. The crystallite size was calculated according to the formula, $\beta_i = \lambda/\varepsilon\cos\theta$, that was derived from the Scherrer equation, where, λ is the X-ray wavelength, ε is the crystallite size and θ is the Bragg's angle.

In-situ XRD was conducted for some supported NiO catalyst precursors was performed in order to understand the differences in the reducibility of the samples resulted from different degree of dispersion and support NiO interaction. The samples were heated in an Anton Paar XRK900 X-ray reactor chamber mounted on the diffractometer, from room temperature to 573 K at a heating rate of 50 K/min under a flow of 25% H_2 in He. Subsequently, the catalyst was heated in 30 K steps until reaching 773 K. At each step, the sample was kept for 30 min and the XRD pattern was recorded in the 2θ range of 40 - 60° , where the most intense reflections of Ni and NiO appear. The measurements were done at a step size of 0.05° and a rate of 2 s per scan using a Bruker-AXS D8 Advance powder X-ray diffractometer equipped with a $Co_{K\alpha}$ radiation ($\lambda = 1.79 \text{ \AA}$) source.

3.4.2. *Fourier transform infrared (FT-IR)*

Infrared (IR) spectroscopy is commonly employed in conjunction with XRD and other techniques for the characterization of clay minerals (McKelvy et al., 1996; Stuart, 1996). It is a cheap and rapid technique whereby spectra can be acquired within minutes. When structural units and groups absorb infrared radiation, they experience a variation in their dipolar moment, which is a consequence of their vibration and rotation movements. The frequency of vibration depends on the shape of the molecular potential energy surface, the masses of the atoms and the associated vibronic coupling. The resulting spectrum is a unique finger print and is used in its identification. In addition, IR spectra gives valuable information about mineral

CHAPTER 3

structure, degree of regularity in the structure, the family of minerals to which a specimen belongs, the nature of isomorphous substitution and the presence of crystalline and non-crystalline impurities (Madejova and Komadel, 2001).

Transmission Infrared spectra of pellets of clay samples were recorded on a Bruker-Equinox-55 FT-IR spectrometer. The spectra were acquired by accumulating 32 scans at 4 cm^{-1} resolution in the range of $4000\text{-}400\text{cm}^{-1}$. Pellets were prepared by pressing powder obtained by mixing 10 mg of clay sample with 250 mg IR grade KBr. The pellets were dried overnight in an oven before measurement.

3.4.3. N_2 - physisorption

The term physisorption refers to the phenomenon of gas molecules adsorbed to a surface at a pressure less than the vapor pressure. The adsorption isotherm is the measurement of amount adsorbed versus adsorptive pressure at constant temperature. Nitrogen physisorption at 77 K is widely used for the determination of surface area and pore size distribution of various porous materials. The first stage in the interpretation of a nitrogen isotherm is the identification of the physisorption mechanism(s): monolayer-multilayer adsorption, capillary condensation or micropore filling. According to Brunauer, Deming, and Teller, shortly BET, there are five major types of adsorption isotherms which are elicited in Figure 3.4-1 and described below.

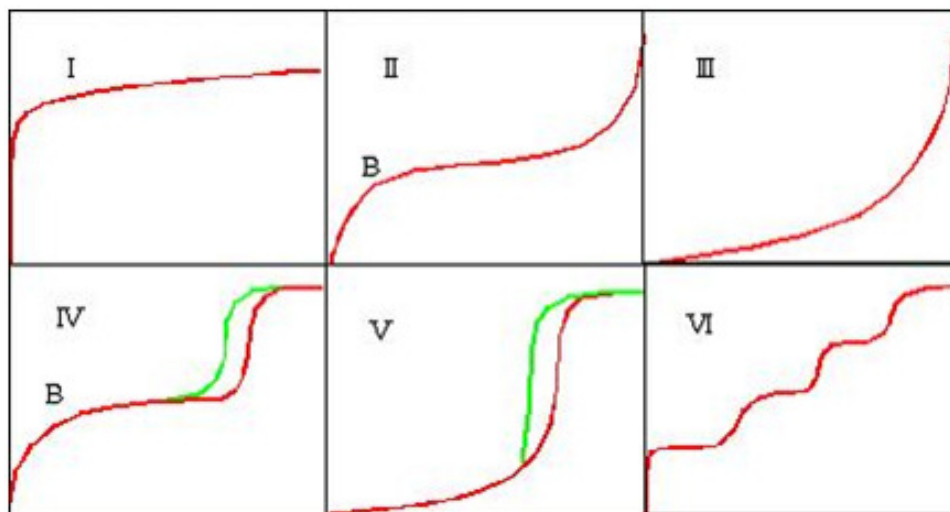


Figure 3.4-1: The six types of adsorption isotherms according to the IUPAC classification.

- Isotherm type I is reversible and concave to the P/P° axis and approach its limiting value as P/P° approaches to 1. It is characteristic to microporous solids with low external surface area, such as molecular sieves and activated carbons. The limiting uptake is governed by the accessible micropore volume rather than the internal surface area.
- Isotherm type II denotes unrestricted monolayer-multilayer adsorption and is common to non-porous or macroporous solids.
- Isotherm III is concave to the P/P° and is characteristic to weak gas solid interaction.
- Isotherm IV is characterized by its hysteresis loop, which is associated with capillary condensation and a limiting uptake over a range of high P/P° . This initial part of this isotherm can be taught to be identical to Type II isotherm as it involves monolayer-multilayer adsorption of non-porous materials. Type IV isotherms are typical of common industrial mesoporous adsorbents.
- Isotherm V is similar to that of isotherm III in that both of them denote weak adsorbent-adsorbate interaction. Type V isotherm is associated with certain types of porous adsorbents.
- Type VI Isotherm shows a step wise multilayer adsorption of gas on a uniform non-porous surface. Each step represents a monolayer adsorption and the sharpness of the steps depends on the temperature of adsorption. The step height is proportional to the monolayer capacity.

Point B in the type II and IV adsorption isotherms is located at the beginning of an almost linear middle section of the isotherm. It often indicates a stage at which the monolayer coverage are complete and multilayer adsorption is about to begin.

The physisorption isotherms of non-reactive gases on a microporous and non-porous surface is completely reversible and its adsorption and desorption wings are completely identical (Gregg and Sing, 1982). On the other hand, physisorption isotherms of many mesoporous materials are not reversible over certain ranges of P/P° due to capillary condensation. This phenomenon is called adsorption hysteresis and its shape is dependent on the shape of the pore structure. According to de Boer (1958),

CHAPTER 3

five major types of hysteresis loops were identified based on a combination between the steep or sloping character of the adsorption and desorption branches of the isotherm. The five types hysteresis loops are presented in figure 3.4-2 and their brief description is given below.

- Hysteresis A is related to tubular pores open at both ends.
- Hysteresis B represents parallel lamellas that are separated by small particles or defects.
- Hysteresis C and D are not common and come from type A and B isotherms, respectively. Type C is related to conic pores and type D for pores formed by non-parallel layers.
- Hysteresis E corresponds to wide pores with a bottle neck.

The surface area of samples can be estimated from the monolayer volume (V_m) based on Brunauer, Emmett and Teller (BET) theory by applying the following formula.

$$V/V_m = c(p/p^\circ) / [(1-(p/p^\circ))(1-(1-c))(p/p^\circ)]$$

Where, V is the volume of gas adsorbed, V_m is the volume of the gas adsorbed in the monolayer and P° is the vapor pressure above the macroscopically thick layer of the pure liquid on the surface. The c value approximates to $\exp -(\Delta H_d - H_{vap})/RT$, in which the ΔH_d is the enthalpy of adsorption on the first adsorbed layer and H_{vap} is the heat of vaporization.

Quadrasorb SI surface analyzer was used to measure BET and external surface area, pore volume and estimate the pore size distribution of saponite and saponite supported catalyst precursor, catalyst and some spent catalyst samples. Samples, which amount corresponded to $\geq 10 \text{ m}^2$ absolute BET area, were degassed under vacuum at 353 K overnight prior to N_2 physisorption measurement.

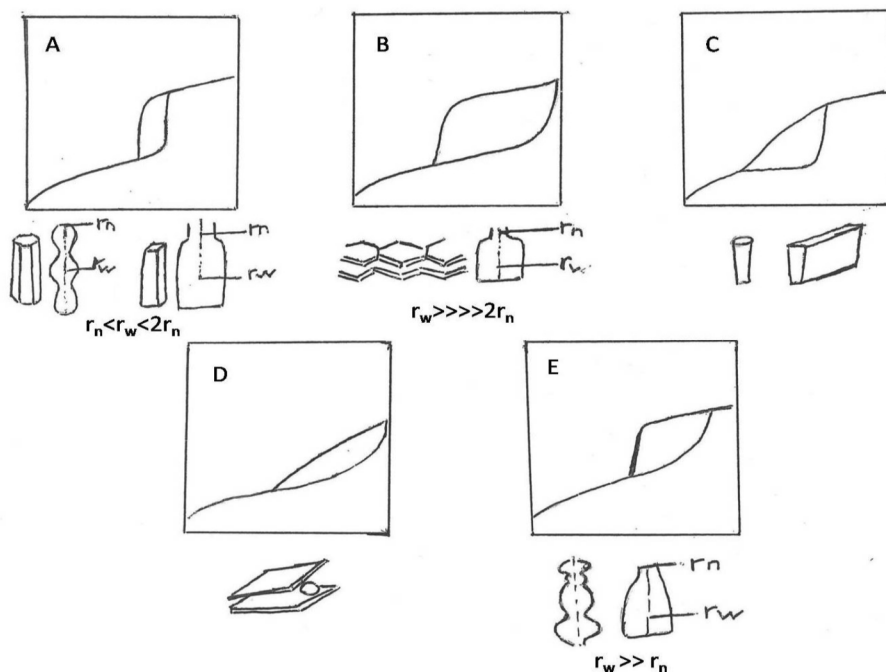


Figure 3.4-2: The five types of hysteresis according to de Boer's classification.

3.4.4. Magic angle spinning-nuclear magnetic resonance spectroscopy (MAS-NMR)

Nuclear magnetic resonance (NMR) spectroscopy has proved its crucial importance as a tool to study molecular structure. When placed in a magnetic field, a nuclei with a non-zero angular momentum, absorbs an electromagnetic radiation characteristic to the nuclei which resonates. The resonance frequency of the absorption is proportional to the applied magnetic field strength and the electronic environment of the nuclei. In solution, high resolution NMR spectra consist of sharp transitions due to averaging of anisotropic interactions by fast isotopic molecular tumbling. In solid samples, however, these types of motions are usually restricted and results in resonance broadening due to dipolar coupling and chemical shift anisotropy. In high resolution solid state NMR, the unfavorable anisotropic effects can be removed or reduced by high speed rotation of the sample at a "magic angle", 54.74° , introduced by Andrew et al. (1959) and Lowe (1959).

^{27}Al -MAS-NMR provides direct information about the chemical environment (co-ordination state) of the Al in a given clay sample. Hence, Al with tetrahedral

CHAPTER 3

coordination appeared at about 60 ppm and octahedrally coordinated Al in the clay structure or in the interlayer space will display its peak at 0 ppm (Sanz, 2006).

^{27}Al -MAS-NMR spectra were obtained on a 400 MHz wide-bore spectrometer (Bruker Biospin) using a 3.2 mm double-channel magic angle spinning probe. Experiments were conducted at an MAS rate of 12 kHz. Single pulse experiments involved $\pi/12$ excitations using radio-frequency field strength of 42 kHz. Repetition rate and acquisition time were set to 1 s and 5 ms, respectively. Signal averaging was done for a total of 10 k scans. Chemical shifts were given in ppm relative to high purity $\text{Al}(\text{NO}_3)_3 \cdot 9\text{H}_2\text{O}$ (Sigma-Aldrich) as reference.

3.4.5. *Cation exchange capacity (C.E.C)*

Cation exchange capacity (CEC) of a clay sample gives valuable information about the amount of its interlayer cations available for exchange. It was determined based on the method proposed by Bergaya and Vasager (1997). A saponite (200 mg) sample, dried at 473 K overnight prior to the CEC measurement, was put into 25 ml, 0.01 M $[\text{Cu}(\text{ethylenediamine})_2]^{2+}$ solution and stirred for 2 h. The mixture was separated by centrifugation and the absorbance of the supernatant was measured at $\lambda=547$ nm using UV-Vis spectrophotometer. The absorbance was correlated to the concentration of the Cu remaining in the solution by fitting to standard calibration curve. The CEC value was equivalent to the change in concentration of the Cu solution and it was reported as milliequivalents exchangeable cations per 1g of dried sample.

3.4.6. *UV-Vis spectroscopy*

UV-Vis spectroscopy is one of the most commonly used analytical techniques for qualitative and quantitative determination of transition metal ions, highly conjugated compounds and biological macromolecules. It is based on the fact that molecules containing Π or non-bonding electrons absorb visible or near UV-radiation and undergo electronic excitation. The amount of radiation absorbed or transmitted as a function of wavelength is recorded, giving spectra characteristic of each ion, molecule or compound.

Most transition metals compounds with a configuration different from d^0 or d^{10} have color and appear colorless in its un-complexed form. This is because the energy difference between its highest occupied molecular orbital (HOMO) and lowest unoccupied molecular orbital (LUMO) is too short to be in the visible range. When copper forms a complex, its 3d orbitals, which are degenerate in the un-complexed form, split and the energy difference (d-d transition) is in the visible light or near UV wave length range. The amount of splitting and hence the stability of the complex depends on the type of ligand around the transition metal cation. Copper forms a blue colored complex with ethylenediamine ($\lambda_{\max} = 547 \text{ nm}$).

According to Beer's law, in dilute solution, absorption is proportional to the number (concentration) of absorbing molecules. Lambert's law states that the fraction of the radiation absorbed is independent of the intensity of the incident radiation. The combination of the two laws, Beer-Lambert law, gives the basis for deriving a mathematical relationship between concentration and absorbance.

$$A = \epsilon lc$$

Where, A is absorbance, ϵ is the molar absorption coefficient of the molecule, l is the path length and c is the concentration.

Shimadzu spectrophotometer was used to measure absorbance of $[\text{Cu}(\text{ethylenediamine})_2]^{2+}$ solution at 547 nm.

3.4.7. Inductively coupled plasma (ICP)

Inductively coupled plasma (ICP) is one of the most powerful techniques for the determination of trace elements in liquid and gaseous samples. In case of solids, acid digestion or extraction is carried out to transform them to solutions. Liquid samples are transformed into aerosol and subjected to a plasma source where its core attains a temperature as high as 10,000 K. Hence, the aerosol is quickly vaporized into a gas with subsequent liberation of free atoms. The atoms undergo collision with the plasma source generating enough energy to undergo ionization and promotion to an excited state. The relaxations of the atomic and ionic excited states to the ground states emit photons, which have characteristic energy determined by the quantized energy level of structure of atoms or ions. Thus, the wavelength of the emitted photos gives the

CHAPTER 3

basis for identifying the atoms or the ions from which it was originated and the total number of photons is directly proportional to the concentration of the atoms or ions undergoing relaxation.

Inductively coupled plasma (ICP) measurement was conducted with a Perkin Elmer Optima 4300 D analyser to determine the Mg, Si, Al content of saponite samples. Measurement was done in triplicate for each sample and average values were reported.

3.4.8. Scanning electron microscopy (SEM), energy dispersive x-ray (EDX)

The scanning electron microscope (SEM) is primarily designed for producing electron images but can also be used for element mapping if an X-ray spectrometer is added. EDX makes use of the X-ray spectrum emitted by a solid sample bombarded with a focused beam of electrons to obtain a localized chemical analysis. When a sample is irradiated with a focused beam of x-ray, core shell electrons of an atom absorb energy and excite to higher energy state creating a hole. An electron from an outer, high energy state moves to fill the hole releasing energy in the form of X-ray which can be collected and analyzed by the X-ray spectrometer. The energy of the emitted radiation is characteristic of the specimen atomic number and the intensity of the radiation is proportional to the concentration. All elements from atomic number 4 (Be) can be detected in principle, though not all instruments are equipped for 'light' elements ($Z < 10$). Qualitative analysis involves the identification of the lines in the spectrum and is fairly straightforward owing to the simplicity of X-ray spectra. Quantitative analysis (determination of the concentrations of the elements present) entails measuring line intensities for each element in the sample and for the same elements in calibration standards of known composition. By scanning the beam in a raster and displaying the intensity of a selected X-ray line, element distribution images or 'maps' can be produced.

The surface Si, Mg, Na and Al composition contents of the synthesized saponite samples were quantified by energy dispersive X-ray experiments. EDX was performed on a scanning electron microscope, JEOL JSM6400, operating at accelerating voltage of 15 kV and work distances of 15 mm. All samples were covered

with a graphite layer before analysis and EDX signals were obtained with an accumulation time of 120 seconds.

3.4.9. Transmission electron microscopy (TEM)

Transmission electron microscope (TEM) uses highly energetic electrons, wave length typically between 0.1-1 nm, to see atomic details. A high intensity primary electrons passes through the condenser impinging the sample. Electrons may transverse the sample cross-section or be absorbed gradually losing their energy. Another possible phenomenon is a portion of the incident electron beam be back scattered. In TEM, an objective diaphragm is inserted in the back focal plane to select the transmitted beam and filters out most of the scattered electrons so that only transmitted electrons are imaged. At the bottom of the microscope, the transmitted electrons hit a fluorescent screen, which gives rise to a "shadow image" of the specimen with its different parts displayed in varied darkness according to their density. Therefore, materials composed of lighter atoms that give less impedance to the transmission of electrons appear brighter than the heavier ones.

Transmission electron micrographs of saponite, saponite supported Ni and Cu catalyst precursors and catalyst samples were obtained using JEOL 1011 transmission electron microscope operated at an accelerating voltage of 80 kV. Samples were dispersed in ethanol, and a drop of resultant suspensions were poured on carbon coated-copper grids and air dried before analysis.

3.4.10. Thermogravimetric analysis (TGA)

Thermogravimetric analysis is a technique in which the change in mass of a substance is studied as a function of temperature or time as the sample is subjected to a controlled temperature program in a controlled atmosphere. Measurements are used primarily to determine the composition of materials and to predict their thermal stability. The technique can characterize materials that exhibit weight loss or gain due to decomposition, oxidation, dehydration and etc. The decomposition or other processes happening in the samples can be observed from the graphic representation

CHAPTER 3

of weight variation vs. temperature called a thermogram. The first derivative of this curve permits to better differentiate these steps.

Thermogravimetric analyses were carried out in a Labsy Setaram TGA microbalance equipped with a programmable temperature furnace. The dehydroxylation temperature of the saponites was studied by heating the sample from room temperature to 1173 K at a rate of 10 K/ min under N₂ atmosphere. The % template loading of organo-clay samples was predicted from their thermograms obtained by heating the samples under O₂ atmosphere and in the same conditions as the previous TG experiments. In all analysis, the amount of sample used was about 50 mg. The acidity values of cyclohexylamine treated saponite and saponite supported Ni, Cu and modified and unmodified Ni-Cu bimetallic catalyst precursor samples were obtained by heating the samples under N₂ in the same conditions as in the dehydroxylation experiment. The % template loading and the total surface acidity values were determined from the mass loss occurring between 523-923 K.

The total surface acidity value was determined from the amount of cyclohexylamine lost during the TG analysis by applying a formula:

$$\text{Acidity (mmol. CHA/g sample)} = \frac{(M1 - M2)}{M2} * \frac{1000}{99.18}$$

Where, M1 is the mass % of cyclohexylamine treated sample at 523 K and M2 is its mass % at 923 K. 1000 is the factor to get the acidity in unit of mmol/g and 99.18 is the molecular weight of cyclohexylamine.

3.4.11. Temperature programmed reduction (TPR)

Temperature programmed reduction (TPR) of Ni and Ni-Cu catalyst precursors was first reported by Robertson et al. (1975). Since then, TPR has developed as one of the most common method of characterization in catalysis research. In a TPR technique, an oxide catalyst precursor is subjected to a programmed temperature rise under a flow of reducing gas or gas mixture. The reduction of the sample is continuously monitored as a function of time or temperature by measuring the composition of the reductive gas using a thermal conductivity detector (TCD). The decrease in the hydrogen concentration at the gas outlet with respect to its initial

concentration at the gas inlet monitors the reaction progress. An important application of this technique is that it may be used to obtain useful information about the interaction of atoms or formation of alloy in bimetallic catalytic systems (Robertson et al., 1975; Bernardo et al., 1985). It also serves as a basis to evaluate the reducibility and surface properties of catalysts (Van Santen et al., 2000).

TPR study of several Ni, Cu, Ni-Cu and modified Ni-Cu catalyst precursors were carried out using an Autochem AC2920 Micrometric apparatus. Sample calcined (100 mg) prior to the TPR analysis was placed in a tubular reactor and heated from room temperature to 1173 K at a rate of 10 K/min under a flow of 5 vol. % H₂ in argon (50 mL/min). A TCD detector monitored the amount of hydrogen consumed.

3.4.12. H₂-chemisorption

Chemisorption techniques are well established analytical tools to determine metal specific surface area and dispersion. It is a technique used to evaluate the number of active sites of a catalytic material that can be reached or interact with a fluid phase. The method is based on the chemical reaction between suitable gas, H₂ in case of hydrogen chemisorption, and metallic atoms on the surface reactive site. The process involves pretreatment procedure to clean the catalyst surface. This first step of surface cleaning involves degassing the sample at suitable temperature under vacuum or helium to remove water or other vapor. After the preliminary cleaning, the sample activation is done by reduction treatment and removal of the chemisorbed H₂ by flowing an inert gas. At this stage, the surface is ready for the actual reactive hydrogen chemisorption treatment.

Metallic area was determined from H₂ chemisorption experiment using an Autochem AC2920 Micrometric apparatus. In a typical experiment, 0.3 g of pre-reduced sample was re-activated by reduction under hydrogen flow at 623 K for 1 h and flushed with helium (40 mL/ min) for 30 min and cooled down to 313 K. Pulses of hydrogen were injected until saturation. The sample was purged with helium to remove the excess hydrogen. The number of metal active sites was proportional to the number of hydrogen atoms irreversibly chemisorbed.

CHAPTER 3

3.4.13. X-ray photoelectron spectroscopy (XPS)

X-ray photoelectron spectroscopy, also called Electron Spectroscopy for Chemical Analysis (ESCA), is a surface sensitive analysis technique based on the photoelectric effect. When a specimen is irradiated with a low energy (1.5 keV) X-ray of a fixed wave length, electrons absorb energy and will be ejected from the sample-photoelectrons. According to the law of conservation of energy, the kinetic energy (K.E) of the electrons will be,

$$\text{K.E} = h\nu - \text{B.E} - \phi_{\text{spectrometer}}$$

Where, B.E is the binding energy and ϕ is the work function of the spectrometer detector.

Given that the binding energies of each element's orbitals are unique and are dependent on the bonding environment, the technique is a "figure print" for elements and chemical states. Hence, the technique is a semi-quantitative analysis method for obtaining composition and chemical information. The XPS works by collecting photoelectrons into the concentric hemispherical analyzer of the spectrometer. The common mode of collection of photoelectrons is "the constant energy analyzer mode" where by the photoelectrons will be retarded to the same kinetic energy before they enter into the spectrometer. By varying the retardation potential, the spectrometer collects photoelectrons of different retarded K.E and the result is displayed as a plot of photoelectron intensity as a function B.E. According to "the universal curve", the typical inelastic mean free path (IMFP or λ) of photoelectrons with kinetic energy between 10 to 100 eV, only ranges from about 1 to 3 nm of the surface of the specimen. The analysis is carried out in high vacuum ($\approx 10^{-10}$ torr) in order to facilitate the transmission of the photoelectrons and minimizes the recombination rate of a freshly cleaned sample.

XPS analysis of some of ReO_x modified fresh and used bimetallic catalysts was performed to determine the oxidation state of the modifier and estimate the surface composition of Ni and Cu on the catalyst. The spectra were acquired in a VG Escalab 200R electron spectrometer equipped with a hemispherical electron analyzer, operating in a constant pass energy mode. A non-monochromatic Mg-K operated at

10 mA and 1.2 kV was used as an X-ray ($h\nu=1253.6$) source. The irradiation of the X-ray was made 45° to the normal of the sample surface and the pressure of the chamber was maintained at 7×10^{-9} torr during data acquisition. The binding energy (BE C1s = 284.9 eV) of adventitious C1 was used as reference. A Shirley background subtraction was applied and Gaussian–Lorentzian product functions were used to approximate the line shapes of the fitting components.

3.5. Catalytic activity test

Hydrogenolysis of glycidol was tested in a 50 ml stainless steel autoclave equipped with an electronic temperature controller and a mechanical stirrer as shown in figure 3.5-1. Glycidol (3.77 mL) was dissolved in sulfolane (30 mL) and purged with nitrogen. A freshly reduced catalyst (1 g) was carefully transferred to the reactor under a positive nitrogen pressure to avoid contact with atmosphere. The reactor was sealed and purged three times with 2 MPa N₂ pressure and three times with 1 MPa H₂ pressure. After performing a leakage test, the temperature of the reaction was set and the mixture was stirred at 600 rpm while 1 MPa of H₂ was introduced. When the temperature in the electronic control reached the reaction temperature, the hydrogen pressure was adjusted at 5 MPa and the reaction time was started (t_0).



Figure 3.5-1: Catalytic activity test setup used for the hydrogenolysis of glycidol.

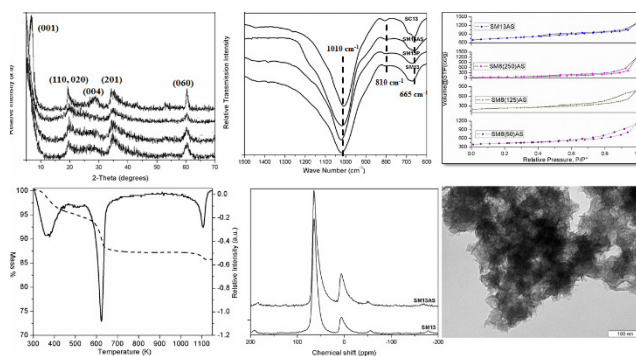
CHAPTER 3

The reaction was run for some period of time (1, 2 or 4 h) while feeding hydrogen on demand. At the end of the reaction, the reaction mixture was cooled down and gaseous products were collected in a gas sample bag. The reaction products were separated from the catalyst by centrifugation and liquid products were analyzed on a Shimadzu GC-2010 chromatograph using SupraWAX-280 capillary column, 1-butanol as internal standard and a FID detector. Some of the liquid samples were submitted for GC-MS analysis to identify formed products. Conversion and selectivity of the reactions were calculated according to the following equations:

$$\text{Conversion} = \frac{(\text{moles of glycidol } t_o - \text{moles of glycidol } t_f)}{\text{moles of glycidol } t_o} * 100\%$$

$$\text{Selectivity to } x (\%) = \frac{\text{moles of analyte } x}{\text{moles of glycidol converted}} * 100\%$$

4. Preparation of Mesoporous Acid Saponite



4.1. Background on the preparation of mesoporous clays

Strict economic and environmental policies are deriving the chemical industries to redesign their processes in a way that the use of harmful chemical and generation of wastes could be avoided or at least minimized. Heterogeneous catalysis is attractive in order to develop more environmentally friendly chemical processes (Frost et al. 1998; Kloprogge 1998; Ding et al. 2001; Taguchi and Schüth, 2005). For example, the use of zeolites as a solid acid catalyst solved many of the problems related to the use of liquid mineral acid catalysts. However, zeolites present severe limitations when large reactant molecules are involved, especially in liquid-phase systems as is frequently the case in the synthesis of fine chemicals, due to the fact that mass transfer limitations are very severe for microporous solids. An important line of research has focused on the enlargement of the pore sizes into the mesopore range, allowing larger molecules to enter the pore system, to be processed there and to leave the pore system again.

Mesoporous materials are very attractive due to their higher accessibility and high specific surface areas. They are widely applied in adsorption, chromatography, catalysis, sensor technology, gas adsorption and etc. (Tanev et al., 1994; Corma, 1997; Sen et al., 2006; Slowing et al., 2007; Vallet-Regí et al., 2007; Shi, 2012). Natural clays and clay minerals are microporous in nature and are interesting raw materials in the preparation of mesoporous materials owing to their abundance, low cost and environmental friendliness (Cifredo et al., 2010). The 2:1 type smectites such as montmorillonite, hectorite, saponite and beidellite are commonly modified to prepare mesoporous clays (Bergaya and Lagaly, 2013). This is because these types of materials have high negative layer charge that allows intercalation of bulky organic and inorganic cations in the interlayer space substituting the charge neutralizing exchangeable cations. This generates galleries in the interlayer space allowing molecular access inside the resulting materials (Ruiz-Hitzky and Aranda, 2014). Different strategies, such as acid activation, the use of structure directing agents or templates and pillaring, have been reported in the literature for the preparation of

CHAPTER 4

mesoporous materials from clay minerals (Kosuge et al., 1995; Vicente-Rodriguez et al., 1995; Shinoda et al., 1995; Okada et al., 2006).

4.1.1. Acid treatment of clay minerals

Acid activation of clay minerals with strong mineral acids, such as sulfuric or hydrochloric acid, is one of the strategies to increase surface area, porosity and surface acidity (Komadel, 2003; Pushpalettha et al., 2005) and to remove mineral impurities such as Fe_2O_3 (Folletto et al., 2001; Pushpletha et al., 2005). It is based on differences in solubility and dissolution rates of the various components of the clay mineral in acid solution (Okada and MacKenzie, 2006). In the process of acid activation, the acid dissolves Mg^{2+} , Al^{3+} and Fe^{2+} from the crystal structure or substitutes the interlayer cations with H^+ with an effect of increasing specific surface area, porosity and surface acidity (Theocharis et al., 1988; Komadel, 2003). For example, acid activation of ferrous saponite using different concentrations (0.62, 1.25 and 2.5%, w/w) of HCl for 2, 6, 24 and 48 h increased the surface area of the material by almost a factor of ten (Vicente-Rodriguez et al., 1995).

It was observed that the resistance of a given clay mineral for acid activation was dependent on the mineralogical composition (with smectites being more susceptible and kaolinite more resistant) (Nguetnkam et al., 2011). The operational parameters of the acid activation was another factor of influence. The concentration and time of acid treatment (Christidis et al., 1997; Didi et al., 2009), temperature of activation (Christidis et al., 1997) and type of acid (Komadel, 2003; Pushpletha et al., 2005) played an important role in the degree of acid activation. Higher temperature, use of H_2SO_4 and higher acid concentration and longer treatment resulted in greater leaching (Christidis et al., 1997; Didi et al., 2009). The acid activation of saponite in a concentrated HCl (5-10 M) led to complete amorphization of the sample (Linszen et al., 2003). Milder acid treatment using 0.05-1 M HCl at 70°C and for 0.5 h on the other hand afforded the desired result with an important improvement in specific area and porosity. The surface area was 5 times higher when the saponite was treated with 0.5 M HCl solution (Okada et al., 2007).

4.1.2. Pillared clays

Pillaring is a process by which a clay mineral is transformed into a thermally stable mesoporous material with retention of its layered structure. This was achieved by exchanging the interlayer cation with hydrated inorganic polyhydroxy cations which after heating forms an oxide cluster intercalated in the interlayer space. The resulting two-dimensional zeolite-like materials with an inter-layer space of molecular dimensions and a well-defined pore system is called pillared clay (PILCs). Pillaring increases the thermal and hydrothermal stability, specific surface area and porosity and generates Brønsted and Lewis acid sites (Tang et al., 1995).

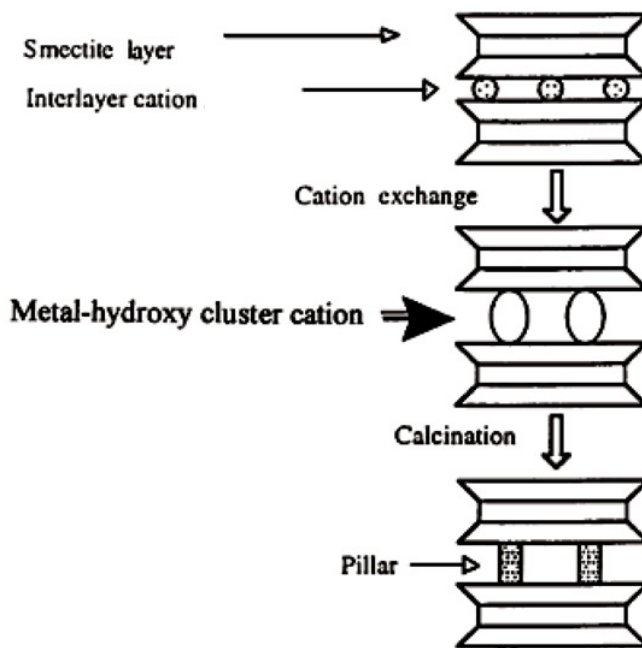


Figure 4.1-1: Scheme for the preparation of pillared clays. (Moore and Reynolds, 1997)

Pillared clay preparation involves different steps as show in figure 4.1-1. The first step involves the swelling of clay mineral in water to make the interlayer accessible for cation exchange or intercalation of the polycation. The pillaring agent is prepared by mixing the aqueous solution of polycation precursor with an excess of a base. For example, in case of Al pillared clays, the Al source, AlCl_3 or $\text{Al}(\text{NO}_3)_3$, is mixed with a basic solution at OH/Al^{3+} ratio up to 2.5. The Al^{3+} forms what is taught to be the

CHAPTER 4

Keggin-like ion, tridecameric polyhydroxy aluminium cation (Kloprogge et al., 1992; Kloprogge, 1998; Kloprogge and Frost, 1999). The clay is then suspended in the polyoxocation solution to allow cation exchange reaction or intercalation of the polyoxocation (Gil and Gandia, 2000). Eventually, the clay is filtered, washed and calcined to give the pillared clay. Molecular modelling studies showed that Al/ Si-substituted smectites, such as saponites, gave homogenously distributed pillars (Pruissen et al., 1997), and the pillars are strongly anchored to the clay layer by Al-O-Al covalent anchoring (Chevalier, 1995; Bergaoui et al., 1995; Lambert and Poncelet, 1997).

Al has been extensively studied in the literature as a pillaring agent and various types of other cations, such as Ce, Cr, Ga, La, Si, Ti and Zr has been also used as pillar or added as a co-pillaring agent in order to give specific properties to the resulting pillared clay (Kloprogge et al., 2005). The presence of small amounts of Ga³⁺ resulted in the formation GaAl₁₂ Keggin like species where the Ga³⁺ occupies the central position of the Keggin structure (Bradley et al., 1992; 1993). The presence of Ga in the pillar improved thermal stability and increased Brønsted acidity (Bradley et al., 1993). Bentonite clays were initially intercalated with Al pillars and later modified with Ce and La. The result showed a pillared clay with similar structure and acidity properties to Al pillared clays but with higher specific surface area and higher thermal and hydrothermal stability (Valverde et al., 2000). The higher thermal and hydrothermal stability was explained in terms of delayed dehydroxylation in the presence of Ce and La which could either block the hexagonal cavities in the tetrahedral layer or strengthen the bonding of the Al pillars. Various authors (Sterte and Shabtai, 1987; Zhao et al., 1992; Fetter et al., 1995) reported the use of Si-Al polyoxocation as pillaring agent. These pillars gave more Brønsted acid sites compared to Al pillared species and lower Lewis/ Brønsted acid ratio which was attributed to the presence of acidic silanol groups in the pillars (Sterte and Shabtai 1987).

4.1.3. Use of polymer or surfactant as a template

The use of surfactant in the preparation of mesoporous silica and aluminosilicate sieves was first reported in 1992 (Krsege et al., 1992). In this approach, surfactant forms a well ordered micelle, micellar rod or hexagonal lamellar liquid crystal mesostructure depending on its concentration in aqueous solution and serves as an organized template around which the silicate condensed. When the surfactant is removed by calcination, uniform network of pores that mimic the size and shape of the template are created. The method gave uniform large mesopores where the size of the pore was controlled by the molecular weight of the template. In this way, a family of ordered mesoporous materials based on silica, called M41S, were prepared by Mobil researchers using liquid crystal templating mechanism (Beck et al., 1992).

Another approach involves an in-situ hydrothermal crystallization of a gel containing an organic template and the clay precursor salts. The hydrothermal crystallization initially afforded an organo-clay composite in which small organic intercalated stacks of clay layers were dispersed in the remaining organic matrix. Calcination of the polymer-clay composite removed the polymer leaving behind a void space of narrow mesoporous range within the inorganic network (Carrado and Xu, 1999), as shown in figure 4.1-2. Delaminated hectorite was synthesized by hydrothermal treatment of a gel containing a quaternary ammonium surfactant salt (Torii and Iwasaki, 1988; Sánchez et al., 2012). The interparticle space generated by edge to face bonded disc shaped crystallite aggregates increases the pore volume, surface area and pore size of the resulting hectorite (Torii and Iwasaki, 1988). Carrado and Xu (1999) prepared a mesoporous hectorite by in-situ hydrothermal crystallization of a gel containing a polyvinylpyrrolidone (PVP). The authors demonstrated that the average pore size of the resulting mesopore could be controlled by either the molecular weight or the amount of polymer loading.

CHAPTER 4

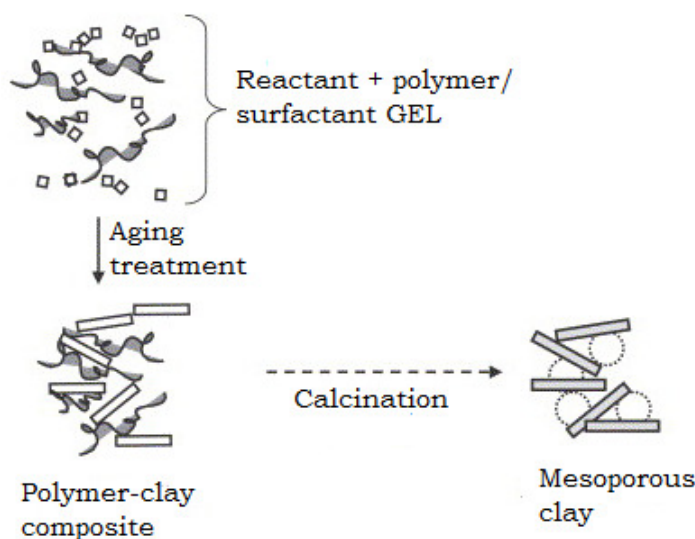
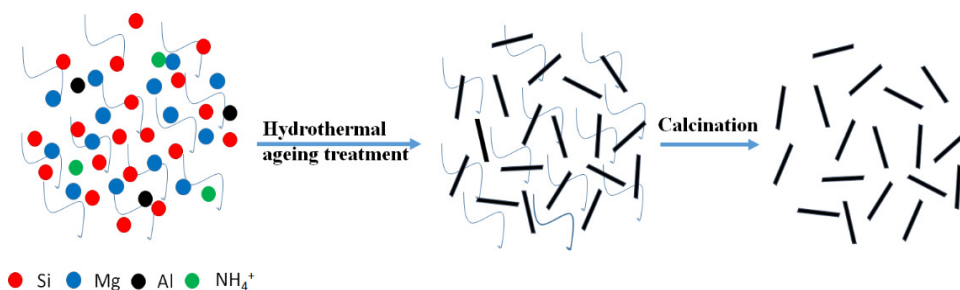


Figure 4.1-2: Template assisted synthesis of mesoporous clay

Other strategies for the introduction of mesoporosity in clay structures consist of the manipulation of the synthetic procedures during the preparation of a gel or hydrothermal crystallization. Delaminated saponites with high mesoporous size, high pore volume and specific surface area was obtained by hydrothermal crystallization of diluted slurries with dilution of H_2O/Si molar ratio > 150 (Vicente et al., 2010; Costenaro et al., 2012). Sánchez et al., (2013) reported the synthesis of delaminated, high specific surface area mesoporous hectorite ($536-603 \text{ m}^2/\text{g}$) in short times (1-2 h) by hydrothermal crystallization of a gel with initial pH 7 and 10. The authors claimed that the high surface area was the result of magnesium vacancies generated in the octahedral sheet as a result of short hydrothermal treatment in microwaves.

In this thesis, the preparation of mesoporous saponite using polymer (section 4.2) and surfactant (section 4.3) as template during the synthesis was presented. The influence of several preparation parameters such as pH, slurry dilution and heat source (microwaves or conventional oven) were studied and optimized. The effect of surfactant addition during hydrothermal aging treatment or after synthesis on the delamination and other physicochemical properties of the resulting saponite was explored.

4.2. Use of polymer as template in microwave synthesis of saponite. Study of several factors of influence.



Abstract

Several saponites were synthesized at pH = 8 by microwaves or conventional hydrothermal aging with different slurry dilutions (H₂O/Si molar ratios of 250, 125 and 50) at 453 K under autogenic pressure. The influence of using a polymer as template, during the synthesis, and its molecular mass was investigated. The saponite prepared with medium dilution slurry by microwaves had the highest incorporation of Al³⁺ in tetrahedral positions (Al^T/Al^O = 2.6) in agreement with its highest C.E.C (0.87 mEq./g). Additionally, this sample showed the highest surface area (461 m²/g). In general, the increase of the slurry concentration and the presence of polymer improved the order in the tetrahedral sheet and decreased the amorphous silica content. The effect of polymer, on the stacking, was low but depended on the dilution and heat source (microwaves or conventional). The use of polymer and its molecular mass modified the saponite porosity and the incorporation of Al³⁺ in the tetrahedral sheet.

CHAPTER 4

Introduction

Saponites are trioctahedral 2:1 layer phyllosilicates of the smectite group with general formula $M_x[Mg_6Al_xSi_{8-x}O_{20}(OH)_4]$ ($M = Na, Li, NH_4$). The layer consists of an octahedral sheet sandwiched between two tetrahedral ones (TOT type clay mineral). In the tetrahedral sheet, Si^{4+} and Al^{3+} are four-fold coordinated with oxygen. The octahedral sheets are composed of Mg^{2+} cations six-fold coordinated with oxygen and/or hydroxyl groups.

An isomorphous substitution of Si^{4+} in the tetrahedral position by Al^{3+} results in a negative layer charge in the sheet. However, substitution can also occur in the octahedral position whereby Al^{3+} substitutes Mg^{2+} with an atomic ratio of 2:3 without affecting the layer charge (Suquet et al., 1981) or in a 1:1 ratio with the generation of a positive layer charge, which compensates the negative charge of the tetrahedral sheet. Additional negative charge in the layer could appear due to the presence of octahedral vacancies, as detected during the synthesis of hectorites in short reaction times (Iwasaki et al., 1989 and Sánchez et al., 2013). The resulting negative charge is compensated by interlayer hydrated exchangeable cations such as Na^+ , K^+ , Ca^{2+} , or even NH_4^+ , obtaining, in the latter case, a Brønsted acid material after decomposition.

Smectites are currently used for composite preparation (Ishimaru et al., 2003, Liu and Breen, 2005 and Xue and Pinnavaia, 2008). Additionally, acidity of smectites combined with the possibility of modulating composition makes this material attractive for heterogeneous catalysis (Varma, 2002, Casagrande et al., 2005, Gandía et al., 2005, Mata et al., 2007, Trujillano et al., 2011, and Velasco et al., 2011). Nevertheless, the natural porosity of smectites is limited to microporosity. This gives restricted access to their interlayer space for bulky reactants in catalytic applications. The swelling capacity of smectites could solve this problem for reactions performed in the liquid phase, but one more general solution could be the generation of mesopores by pillar formation in their interlayer space (Yao et al., 2004; Carniato et al., 2011) or by delamination (Iwasaki et al., 1998). Smectites and composites with modified properties have been prepared (Auerbach et al., 2004; Bisio et al., 2011) by

CHAPTER 4

the intercalation of bulky organic and inorganic cationic species and neutral polar compounds (Yui et al., 2002) taking advantage of the swelling capacity of smectites.

Delamination of clays has been widely used for the synthesis of composites. However, there are only few reports in the literature about the synthesis of delaminated mesoporous smectites. Thus, delaminated mesoporous hectorites were prepared by in-situ hydrothermal aging of a gel containing polyvinylpyrrolidone (Carrado and Xu, 1999) or quaternary ammonium salt (Iwasaki et al., 1998 and Sánchez et al., 2012) followed by removal of the template by calcinations. Delamination of saponites was noticed by Vicente et al. (2010) during the preparation of saponites using microwaves for the aging treatment, and by Costenaro et al. (2012) for saponites prepared from highly diluted slurries (H_2O/Si molar ratio > 150). In these two references, low C.E.C. values (<60 mEq/g) and the presence of some residual amorphous silica were reported. These low values can be related to the presence of Al^{3+} in the octahedral sheet, by compensation of the tetrahedral sheet charge, and in the interlamellar space, thus making more difficult the exchange.

The aim of this work was to study the influence of several parameters in the characteristics of ammonium saponites synthesized at $pH = 8$ using ultrasounds for reagent mixing and microwave irradiation or conventional heating during the aging treatment. The parameters studied were: slurry dilution by preparing three blocks of samples with H_2O/Si molar ratios of 250, 125, and 50, influence of using a polymer (polyvinylpyrrolidone) as template during the saponite synthesis and its molecular mass. The comparative effect of these parameters when applying microwaves or conventional heating during aging was also investigated. Samples were characterized by XRD, EDX, TEM, FT-IR, C.E.C determination, N_2 physisorption and ^{27}Al -MAS-NMR techniques.

Experimental

For the saponite preparation, the synthetic protocol previously reported by our research group (Vicente et al., 2010) was adopted with some modifications: incorporation of template, sequence of reagent addition and the use of tip probe ultrasound for reagent mixing. Two blocks of ammonium saponites, with and without

Preparation of acid mesoporous saponite

template, were prepared at pH = 8 with different dilution slurries and using microwave irradiation or conventional heating for the aging treatment. The preparation condition and nomenclature of the synthesized samples are summarized in Table 4.2-1.

Fumed silica (Sigma Aldrich), $Mg(CH_3CO_2)_2$ (Sigma Aldrich) and $Al(OH)(CH_3COO)_2$ (Panreac) were used in the synthesis as a source of silicon, magnesium and aluminum sources, respectively. Saponites targeted have theoretical formula, $(NH_4)_{1.2}Si_{6.8}Al_{1.2}Mg_6O_{20}(OH)_4.nH_2O$. Slurry was prepared in 150 mL aqueous ammonia solution with excess of ammonia to that required from the theoretical formula. The reagent amounts were varied to make slurries with H_2O/Si molar ratios of 250, 125 and 50. Stoichiometric amounts of aluminum, silicon and magnesium sources were gradually dispersed one after the other in the same order while the slurry was mechanically stirred for half an hour between each addition.

Table 4.2-1: The nomenclature and preparation conditions of the synthesized samples.

Nomenclature	H_2O/Si molar ratio	Template	Aging
SC250	250	–	Conventional
SM250	250	–	Microwaves
SM250P1	250	P1	Microwaves
SM250P2	250	P2	Microwaves
SC250P1	250	P1	Conventional
SC125	125	–	Conventional
SM125	125	–	Microwaves
SM125P1	125	P1	Microwaves
SM125P2	125	P2	Microwaves
SC50	50	–	Conventional
SM50	50	–	Microwaves
SM50P1	50	P1	Microwaves
SM50P2	50	P2	Microwaves

P1: polyvinylpyrrolidone (40,000 g/mol); P2: polyvinylpyrrolidone (360,000 g/mol).

CHAPTER 4

For the synthesis of samples with template (Table 1), polyvinylpyrrolidone (Sigma) was the first added to the aqueous ammonia solution at 20% loading with respect to the mass of the other solid reagents. Polymer was used with two different molecular masses of 40,000 g/mol (P1) and 360,000 g/mol (P2) to investigate the effect of this parameter. After addition of the template, the procedure of addition of the rest of the reagents was the same as for the samples synthesized without template. For all samples (with and without template), the final mixing of the gel was carried out with a tip probe ultrasound for 30 min and the pH of the resulting slurry was 8. Then, the resulting gel was distributed in 3 Teflon reactors of 100 ml and finally the reactors were sealed previous to the hydrothermal treatment. The treatment was performed at 453 K and autogenic pressure by conventional heating for 72 h or by microwaves (Milestone Ethos Touch Control) at the same temperature for 6 h. Samples were washed by centrifugation to neutrality with double distilled water and dried overnight at 363 K. For the samples prepared with polymer, the template was removed by calcination in a quartz tube reactor first at 773 K in an air flow of 2 mL/s for 12 h followed by a second step at 823 K under an oxygen flow of 2 mL/s for 12 more hours.

Characterization techniques

XRD measurements of samples were made in Siemens D5000 diffractometer equipped with a CuK α radiation ($\lambda = 1.54 \text{ \AA}$) source. Sample was dusted onto a low background Si (510) sample holder and data were collected with an angular step of 0.05° and at rate of 3s per step. Measurement was done in 2θ diffraction angle between 5 and 70° . Integral breadth estimated from the (060) reflection by applying TOPAS 3.1 was used to calculate the crystallite sizes (Stokes and Wilson, 1942) using the Scherrer equation. Additionally, the position in the pattern of (060) reflection was employed to determine the preferential occupation of Mg $^{2+}$ in the octahedral positions (trioctahedral character) comparing with the theoretical value of 1.53 \AA . Reflection (001) was selected to compare the relative degree of delamination between the samples.

Transmission infrared spectra of pellets (1 mg of sample with 250 mg IR grade KBr, Sigma Aldrich) dried at 353K for 2 h before measurement were recorded on a Bruker-Equinox-55 FT-IR spectrometer. The spectra were acquired by accumulating 32 scans at 4 cm⁻¹ resolution in the range of 400–4000 cm⁻¹.

Surface Si, Mg and Al contents of samples were quantified by energy dispersive X-ray experiments (EDX). EDX was performed on a scanning electron microscope, JEOL JSM6400, operating at accelerating voltage of 15 kV and working distances of 15 mm. All samples were covered with a graphite layer and accumulation time was 120 s.

Micromeritics ASAP 2000 apparatus was used for measurement of Nitrogen adsorption-desorption isotherms. Samples were degassed under vacuum at 383 K over night before measurement. Specific surface areas and external surface area were determined from the BET and t-plot methods, respectively. Pore size distribution was calculated by applying the BJH method.

²⁷Al-MAS-NMR spectra were obtained on Varian Mercury Vx 400 Mhz spectrometer. A 7 mm CPMAS probe was used with the samples spun at 4 kHz at the magic angle, using pulses at a duration of 2 μs with a time between pulses of 5 s and accumulation times of 3 h. Chemical shifts are given in ppm relative to [Al(H₂O)₆]³⁺ (0 ppm) using high purity Al(NO₃)₃·9H₂O (Sigma-Aldrich) as reference.

Transmission electron micrographs of the samples were obtained with a JEOL 1011 transmission electron microscope operating at an accelerating voltage of 100 kV and magnification of 200 k. Samples were prepared by dispersing 0.1 mg of clay in 50 μL ethanol and applying a drop of the resulting suspension onto a carbon coated-copper grid followed by air drying to remove the solvent.

The cation exchange capacity (C.E.C) values were determined as reported by Bergaya and Vayer (1997). Samples were dried overnight at 473 K before measurement. For the samples prepared with template, since the calcination procedure used for removing the template involves decomposition of the interlamellar NH₄⁺ cation, samples were submitted to an exchange step in saturated NaCl solution for 36 h, washed several times with deionised water and dried, before C.E.C. measurement.

CHAPTER 4

Thermogravimetric analysis was carried out in a Labsy Setaram TGA microbalance equipped with programmable temperature furnace. Each sample was heated under an N₂ or air flow (80 cm³/min) from room temperature to 353 K at a rate of 5 K/ min. An isotherm was maintained at 353 K for 30 minutes and ramp was acquired between 353K - 1473K at a rate of 5 K/ minute. In all experiments, the amount of sample used was about 50mg.

Results and discussion

Effect of the slurry dilution

The effect of the slurry dilution (H₂O/Si molar ratio) was studied in the samples aged under microwaves (SM250, SM125, SM50) and in the samples aged by conventional heating (SC250, SC125 and SC50), all of them without template (Table 4.2-1).

XRD patterns of these samples showed the reflections (110) and (060), at 2 θ of 19.4° (4.57 Å), and 60.5° (1.53 Å), respectively (Fig. 4.2-1A and B). The presence of these reflections together with the (001) reflection is characteristic of trioctahedral smectite phase (Srodon, 2006), confirming the saponite structure of the synthesized samples. The (001) and (004) reflections, related to the clay stacking, appeared as a shoulder at about 8° (11 Å) and 28°, respectively only for SC50 (Fig. 4.2-1B). These reflections were weak or absent for the rest of the samples, indicating low periodicity in the c-direction. An increase of the stacking by increasing the slurry concentration has been previously reported for the synthesis of saponites aged by conventional heating (Bisio et al., 2008).

No other crystalline phases, than saponite, were detected in any case. Nevertheless, a broader peak related to the presence of amorphous silica appeared at about 22–23° for SM250. All the smectite reflections were sharper and more intense for the samples aged by conventional heating for 72 h than their corresponding microwave aged samples prepared at the same slurry dilution for 6 h. This suggests some higher crystallinity for the conventional samples in agreement with Trujillano et al. (2011). However, the particle sizes, calculated from the (060) reflection, were

fairly comparable for all samples with values between 10.8 nm (SC50) and 7.7 nm (SM250).

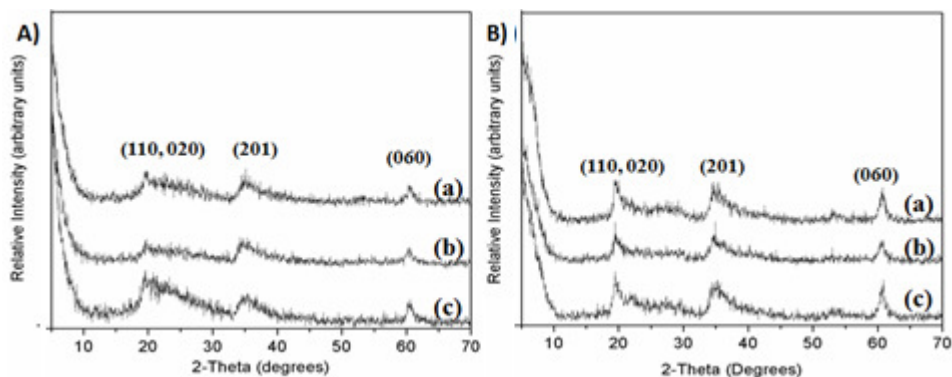


Figure 4.2-1: XRD patterns of the samples A) (a) SM50 (b) SM125 (c) SM250 B) (a) SC50 (b) SC125 (c).SC250.

FT-IR spectra of all the samples were recorded in the range from 4000 to 400 cm^{-1} (Figure 4.2-2). The band assignment was done according to previous literature reports (Russell and Fraser, 1994, Klopogge et al., 1999a, Klopogge et al., 1999b and Klopogge and Frost, 2000). Thus, bands at 3675 and 666 cm^{-1} , observed in all samples, could be assigned to the stretching and liberation vibration modes of Mg–OH, respectively and denoted trioctahedric character of the synthetic saponites. A shoulder at 3630 cm^{-1} and an intense band around 1020 cm^{-1} could be attributed to Al–OH stretch and ordered O–Si–O stretch in the tetrahedral sheet, respectively.

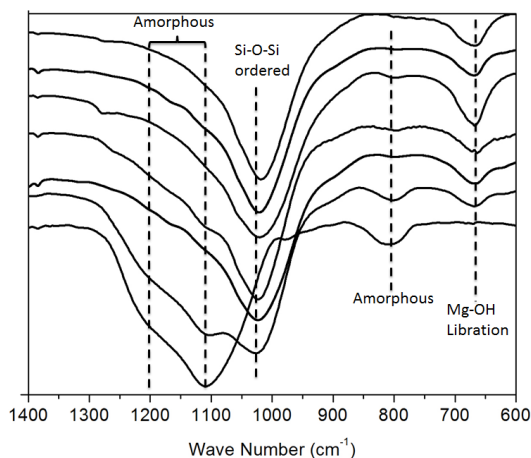


Figure 4.2-2: FT-IR spectra of the samples (a) fumed SiO_2 (b) SM250 (c) SM125 (d) SM50 (e) SC250 (f) SC125 and (g) SC50.

CHAPTER 4

FT-IR spectra of the samples in the 1400 to 600 cm^{-1} range, together with the spectrum of commercial fumed silica, were used to compare the order of the tetrahedral sheet and to detect the presence of amorphous material (Fig. 4.2-2). The band corresponding to the ordered O-Si-O shifted from 1027 cm^{-1} for SM250 to 1023 cm^{-1} for SM125 and SM50 indicating a better ordering of the tetrahedral sheet in the saponite structure obtained from lower dilution slurries (Klopogge and Frost, 2000). The same tendency, but less marked, was observed for the samples aged by conventional heating (from 1025 cm^{-1} for SC250 to 1023 cm^{-1} for SC125 and SC50). The appearance of an intense band for SM250 at 1105 cm^{-1} together with a shoulder at 1200 cm^{-1} and a weak band at 800 cm^{-1} confirmed the presence of amorphous silica for this sample, according to its XRD pattern (Fig. 4.2-1A). Moreover, the weak band observable at 800 cm^{-1} for samples SM125, SM50 and SC250 but not for SC125 and SC50 suggested the presence of residual amorphous material in the former samples. In general, the amount of amorphous material decreased by decreasing the slurry dilution, and using conventional heating during aging.

Typical TEM images of the saponites showed lamellar morphology characteristic of clay minerals (Fig. 4.2-3A–F). SC50 presented a higher layer orientation that could be related to its higher stacking detected by XRD (Fig. 4.2-1B). In contrast, for sample SM250, randomly oriented layers were observed in accordance with the poor definition or total absence of the (001) reflection in its XRD pattern (Fig. 4.2-1A). Additionally, TEM images allowed us to see that delamination was higher for the saponites prepared by microwaves, in agreement with Trujillano et al. (2010). This could be justified by the use of stirring during the microwave synthesis. However, all saponites showed a certain increase of layer orientation at lower slurry dilutions (Fig. 4.2-3B and C). Thus, the stacking was higher for SC50 whereas delamination was higher for SM250, as previously commented.

Fig. 4.2-4 and Fig. 4.2-5 and Table 4.2-2 depict the N_2 physisorption analysis results. All samples showed an important contribution of type IV adsorption isotherm according to the IUPAC classification. This isotherm is characterized by capillary condensation in the mesopores. Nevertheless, significant and interesting differences in shape of the hysteresis loop were observed among the samples (Fig. 4.2-4A and B).

The shape of the hysteresis loops, according to de Boer's classification, were mainly type B for SM125, SC125 and SC50, and type D for SM250, corresponding to parallel and non-parallel platelets, respectively. This agreed with the XRD and TEM results, which showed a higher degree of delamination for sample SM250. The shape of the hysteresis loop for samples SC250 and SM50 was a mixture of B and D types (Fig. 4.2-4A and B) involving the presence of oriented and randomly oriented layers.

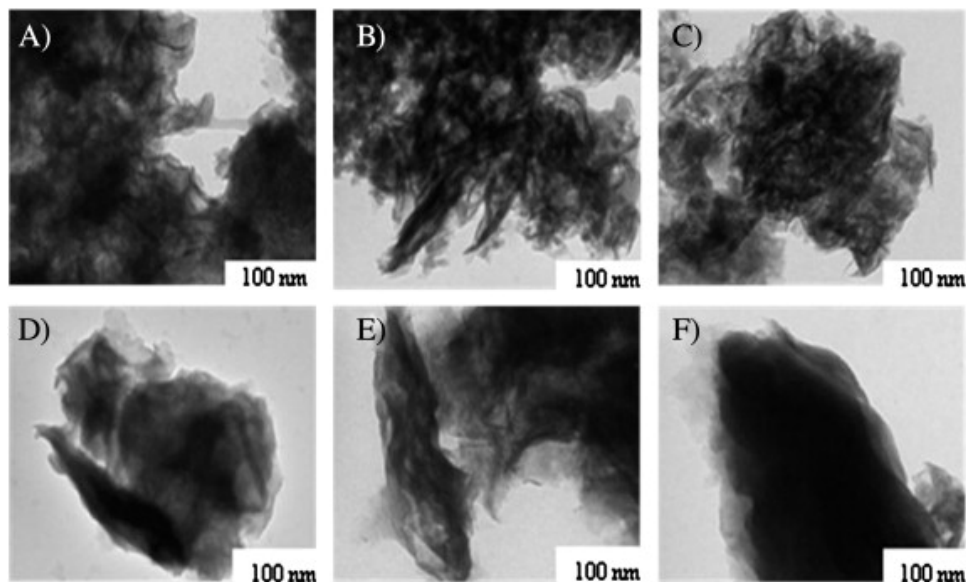


Figure 4.2-3: TEM micrographies of A) SM250 B) SM125 C) SM50 D) SC250 E) SC125 and F) SC50 all at ($\times 200k$).

The average pore radius values were in the mesoporous range in all samples (Table 4.2-2). This could be related to the inter-layer porosity resulting mainly from the delamination contribution. Fig. 4.2-5 showed the pore size distribution graphics of the samples. The average pore size and the pore size distribution were comparable and no appreciable differences were observed for all samples except for SM250 and SM50 (Fig. 4.2-5, Table 4.2-2). The highest average pore radius of SM250 (70 Å) was a consequence of its broader pore size distribution (Fig. 4.2-5A), which could be probably associated with the porosity of amorphous silica, since this reagent presented a similar broader pore size distribution. In contrast, the higher average pore radius observed for sample SM50 (39 Å), was a result of its bimodal pore size distribution (Fig. 4.2-5A). This could be attributed to a higher heterogeneity of the particle sizes

CHAPTER 4

due to some diffusion problems generated by the higher viscosity of the slurry for this sample.

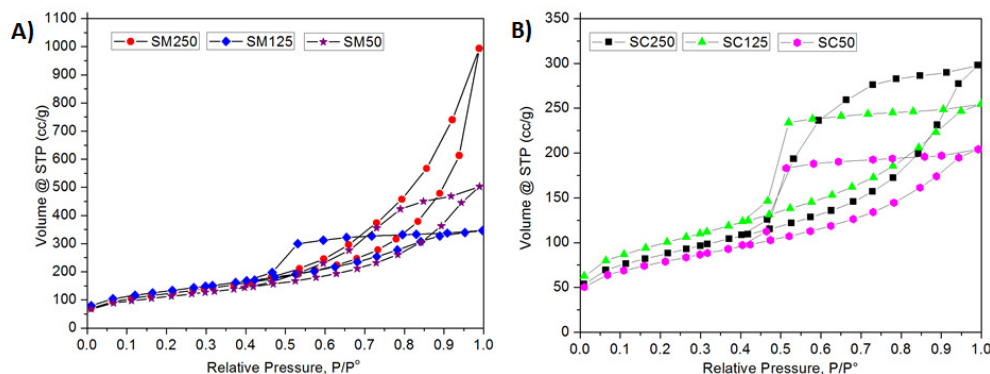


Figure 4.2-4: N₂ adsorption–desorption isotherms of A) microwave aged and B) conventional aged samples.

The highest surface area of SM125 (461 m²/g) could be related to its delamination and the absence of amorphous silica, as previously discussed. The surface area of SM250 was also high (438 m²/g), but a higher value should be expected since higher delamination and smaller particles were observed for this sample by TEM (Fig. 4.2-3B). The presence of amorphous silica blocking a part of the pores could explain this value. The lower surface area values of SM50, SC250, SC125 and SC50 (394, 257, 340 and 254 m²/g, respectively) with respect to the microwave aged samples at dilutions 125 and 250 should be a consequence of their higher crystallinity and improved ordering in the stacking direction. In contrast, the higher area of SC125 compared to SC250 can be explained by the presence of amorphous silica in this later sample, as observed by FT-IR (Fig. 4.2-2). In fact, the pore size distribution of SC250 showed some contribution of mesoporosity with higher pore size (Fig. 4.2-5B), which could be related to the presence of amorphous silica.

Surface composition analysis results, obtained by EDX, are summarized as Si/Al and Si/Mg ratios in Table 4.2-2. All samples had lower Mg and Al and higher Si content than those corresponding to the theoretical formula of the targeted saponite. In comparison, the amount of Mg was lower than that of Al. This behavior could be explained by the pH of slurry during the hydrothermal treatment (initial pH = 8, final

pH = 6). As previously reported in the literature (Jaber and Miéché-Brendlé, 2005), at pH values between 5 and 9 the solubility of Mg^{2+} was higher than for Al^{3+} . Therefore, the incorporation of Mg into the saponite structure became more difficult.

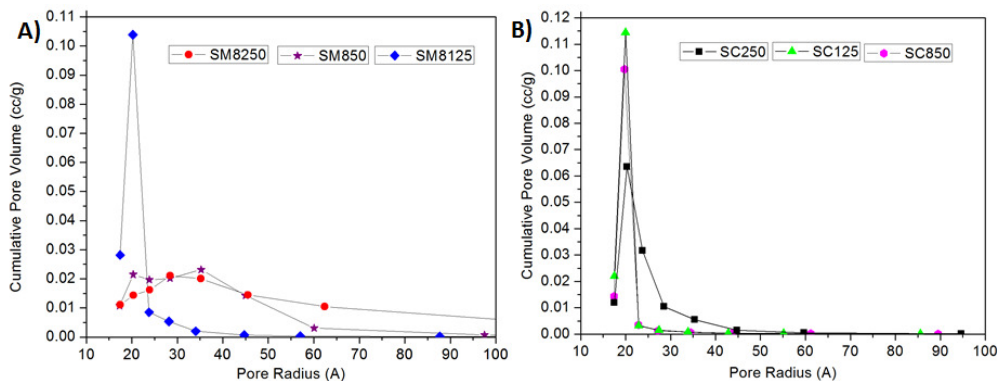


Figure 4.2-5: Pore size distribution graphs of A) microwave aged and B) conventional aged samples.

With respect to the Si/Mg ratio, the highest value was obtained for SM250 (3.55) (Table 4.2-2). This could be related to its high amorphous silica content, although higher defects of Mg could be present at higher dilution slurry due to increase of its solubility. The Si/Mg ratio of SM125 (1.66) was lower than that of SM50 (2.02) indicating higher incorporation of magnesium in SM125. An increase of cation incorporation with the increase of slurry concentration could be expected. However, the increase of viscosity in the slurry dilution at $H_2O/Si = 50$ could make the cation mobility difficult. This could explain the lower amount of Mg in sample SM50. For conventional aged samples, the Si/Mg ratio varied in the order $SC50 < SC125 < SC250$. The change of order with respect to the samples aged using microwaves could be attributed to a better magnesium incorporation in SC50, after longer time of synthesis (72 h) compared to SM50 (6 h).

The Si/Al ratio of samples SM250, SC250, SM50 and SC50 (7.3–7.1) was higher than that of SM125 and SC125 (6.4 and 6.5, respectively). The presence of amorphous silica observed for SM250 and SC250 by FT-IR (Fig. 4.2-2), and a lower incorporation of Al due to diffusion problems of highly viscous slurries for SM50 and SC50, could justify these values. Taking into account the low amount of amorphous

CHAPTER 4

silica in samples SM125 and SC125, their lower Si/Al ratio could be attributed to a better construction of the structure with higher Al incorporation.

The C.E.C values of all samples were lower than the theoretical value (1.60 mEq/g). The presence of amorphous silica, without exchange capacity, and aluminum in the octahedral positions, which could be distributed between octahedral sheet and interlamellar space, could justify these lower values. The highest C.E.C. value was obtained for SM125 (0.87 mEq/g, Table 4.2-2). This could be related to its high Al^T/Al^O ratio (2.6), which was determined from ^{27}Al -MAS-NMR. The higher amorphous silica content combined with its lower Al^T/Al^O (2.2) ratio should lead to a lower C.E.C. However, the presence of Mg^{2+} vacancy is expected in SM250 which could lead to an increase of the negative charge of the octahedral sheet and offsets the effect of amorphous silica content. For SM50 (0.58 mEq/g), its lower C.E.C value should be the result of its lower Al^T/Al^O ratio (1.8). For the conventional aged samples, the C.E.C values were in direct agreement with the corresponding Al^T/Al^O ratios (Table 4.2-2). For high and low slurry dilutions, the Al^T/Al^O ratios of conventional aged samples were lower than those of their corresponding microwave aged samples whereas at medium slurry dilution, the values were comparable (Table 4.2-2).

Effect of template

In order to study the effect of using a polymer as template, several saponites were prepared at the same conditions as those synthesized without template using three different H_2O/Si molar ratios of 250, 125 and 50 (Table 4.2-1) but in the presence of polyvinylpyrrolidone at two different molecular masses (P1 and P2). For this study, we compared samples SM250P1, SM250P2, SM125P1, SM125P2, SM50P1, SM50P2 and SC250P1, synthesized with polymer with those synthesized without polymer, SM250, SM125, SM50 and SC250 (Table 4.2-1).

Regarding the XRD patterns of the samples prepared with polymer (Fig. 4.2-6A, B), we could state that the presence of polymer as a template in the microwave aged samples at high dilution (SM250P1, SM250P2) favored the ordering in the stacking direction as it could be deduced from the observation of the (001) reflection as a small

Preparation of acid mesoporous saponite

and very small shoulder, for SM250P1 and SM250P2, respectively (Fig. 4.2-6A and B). However for the saponites prepared at the other dilutions and the conventional aged sample, SC250P1, the presence of polymer did not affect the delamination degree sufficiently to be detected by XRD. With respect to the other reflections, on the whole, a lesser intensity was observed for the samples prepared with polymer (Fig. 4.2-6A and B) indicating a lower crystallinity of these samples. For example, the crystallite size of sample SM125P1, calculated from the (060) reflection, was lower (7.5 nm) than that of sample SM125 (8.4 nm).

Table 4.2-2: Physico-chemical properties characterization results of the samples.

Sample	C.E.C. (mEq./g)	BET area (m ² /g)	External surface area (m ² /g)	Average pore radius (Å)	Si/Al (EDX) (5.6) ^a	Si/Mg (EDX) (1.13) ^b	Al ^{IV} /Al ^{VI} (²⁷ Al- NMR)
SC250	0.38	298	257	31	7.3	1.88	1.1
SM250	0.58	438	438	70	7.1	3.55	2.2
SM250P1	0.61	353	353	44	–	–	2.4
SM250P2	0.56	330	327	49	–	–	2.6
SC250P1	0.55	259	237	22	–	–	1.4
SC125	0.72	340	285	23	6.5	1.62	2.3
SM125	0.87	461	425	26	6.4	1.66	2.6
SM125P1	0.63	396	396	25	–	–	1.6
SM125P2	0.59	354	354	32	–	–	1.2
SC50	0.57	254	202	24	7.1	1.47	1.3
SM50	0.55	394	364	39	7.1	2.02	1.8
SM50P1	0.52	334	334	33	–	–	1.6
SM50P2	0.57	323	323	35	–	–	1.4

^a Theoretical Si/Al value. ^b theoretical Si/Mg value.

The FT-IR spectra of the samples prepared with polymer, by microwaves or conventional heating and at all slurry dilutions (Fig. 4.2-7) showed some differences compared to the samples prepared without polymer (Fig. 4.2-2). For the samples

CHAPTER 4

prepared with polymer at higher dilution (Fig. 4.2-7), we observed a decrease in the intensity of the shoulder at 1105 cm^{-1} and in the weak band at 800 cm^{-1} . These peaks were characteristic of the amorphous silica presence with respect to the samples prepared at the same conditions without polymer (Fig. 4.2-2) whereas for the samples prepared with polymer at medium and lower dilution slurries, the bands characteristic of amorphous silica were absent. Another effect observed in the saponites prepared with polymer was an increase of order in the tetrahedral sheet, since the band corresponding to O-Si-O shifted to a lower wave number (Klopprogge and Frost, 2000). This shift was higher for the samples prepared with microwaves at higher slurry dilution, varying from 1027 cm^{-1} for SM250 (Fig. 4.2-2) to 1017 cm^{-1} for SM250P1 and SM250P2 (Fig. 4.2-7). For the sample aged by conventional heating and for the samples synthesized with microwaves at lower dilution slurries, the shift was lower from 1023 cm^{-1} (SC250, SM50, SM125) to 1015 cm^{-1} (SC250P1, SM50P1, SM50P2, SM125P1, SM125P2).

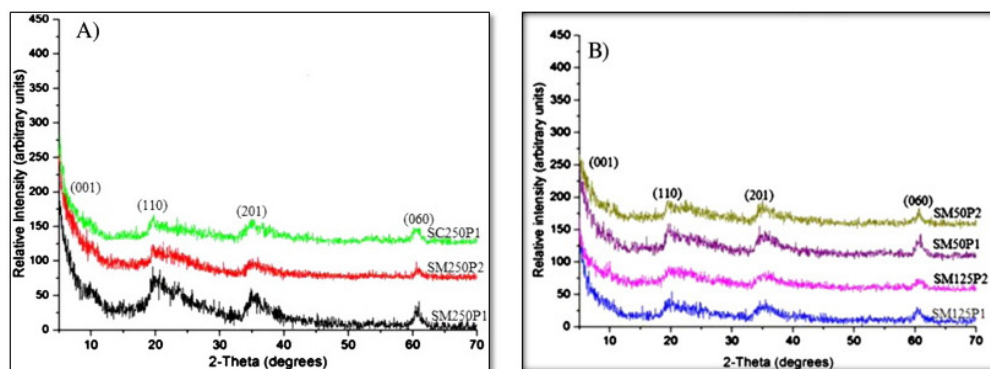


Figure 4.2-6: XRD patterns of the samples prepared with template at H₂O/Si molar ratios of A) 250 and B) 125 and 50.

Fig. 4.2-8A–F shows the TEM images of the samples prepared with template at different H₂O/Si molar ratios. All samples presented the expected lamellar morphology with an important contribution of delamination. Comparing the micrographies of samples SM250, SM250P1 and SM250P2 (Figs. 4.2-3A, 4.2-8A and B) it was not possible to see the increase of the stacking detected by XRD for the samples prepared with polymer. However, we observed a higher aggregation

accompanied with a loss of layer definition when using the higher molecular mass polymer (P2). The TEM images of the other samples (SC250P1, SM125P1, SM125P2, SM50P1 and SM50P2) showed a better delamination compared to the corresponding samples without template, suggesting that at higher slurry dilution in the conventional synthesis and using a lower dilution with microwaves, the presence of polymer favored delamination, fact that was not well observed by XRD.

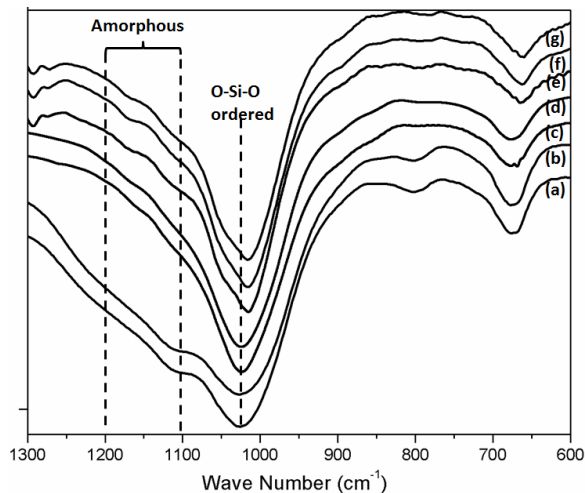


Figure 4.2-7: FT-IR spectra of the samples (a) SM250P1 (b) SM250P2 (c) SC250P1 (d) SM125P1 (e) SM125P2 (f) SM50P1 and (g) SM50P2.

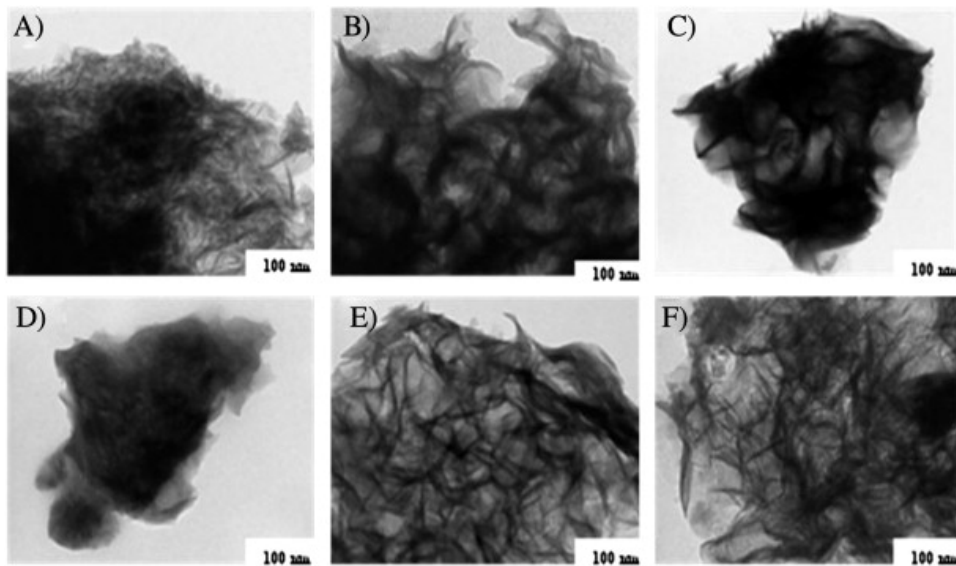


Figure 4.2-8: TEM images of samples A) SM250P1 B) SM250P2 C) SC250P1 D) SM125P1 E) SM50P1 and F) SM50P2 all at ($\times 200k$).

CHAPTER 4

The effect of using the polymer during the synthesis was also noted in the hysteresis loop of the N₂ adsorption–desorption isotherms and depended on the dilution and type of heating. In the presence of polymer, the shape of the hysteresis loop changed from type D in sample SM250 to one with some contribution of type B for SM250P1 and SM250P2 (Fig. 4.2-9A). This corresponded to the presence of lamellae with parallel disposition, according to the higher layer stacking observed by XRD (Fig. 4.2-6). The nature of the hysteresis loop in the other samples was a mixture of B and D types with different contributions of both. Higher contribution of type B was observed in SC250, SM125 (Fig. 4.2-4A) and SM125P1 (Fig. 4.2-9B), attributed to the presence of parallel platelets. In contrast, an increase of type D was observed for SC250P1 and SM125P2. This suggested some higher degree of lamellae disorder upon addition of the polymer during conventional synthesis at high slurry dilution and also when the higher molecular mass polymer was used at medium dilution. Finally, at low dilution slurry, the shape of the hysteresis loop was a mixture of types B and D for both SM50P1 and SM50P2 (Fig. 4.2-9B) as for SM50 (Fig. 4.2-4A).

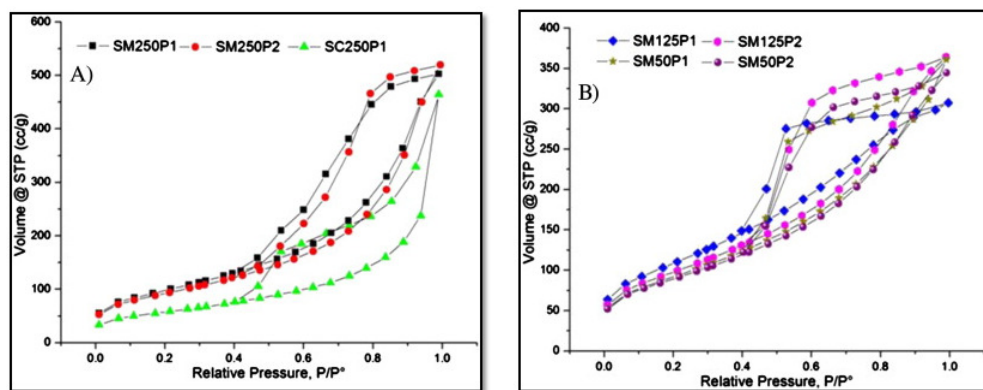


Figure 4.2-9: N₂ adsorption–desorption isotherms for the samples prepared with template at H₂O/Si molar ratios of A) 250 and B) 125 and 50.

The pore size distribution graphics of the samples prepared with and without polymer at medium dilution slurry (SM125, SM125P1 and SM125P2) were similar (Fig. 4.2-5 and Fig. 4.2-10), presenting a narrow peak around 20 Å. In fact, the average pore size was also similar for all of them (25–32 Å, Table 4.2.2). However, at high and low dilution slurries (Fig. 4.2-10A), the samples with polymer (SM250P1,

SM250P2, SC250P1, SM50P1 and SM50P2) showed a narrower pore size distribution in comparison to the corresponding samples prepared at the same conditions without polymer (SM250, SC250 and SM50) (Fig. 4.2-5A). These differences could be related to the lower amount of amorphous silica content of the samples prepared with polymer at high dilution slurry, as confirmed by IR and by the decrease of the average pore radius observed (Table 4.2-2). For the samples prepared at low dilution slurry, the differences can be attributed to a directing effect of the polymer in the generation of mesoporosity. On the whole, when the polymer P2 was used in the synthesis, the contribution of the number of pores with higher size increased. This was in agreement with the certain increase of the average pore radius obtained in these samples.

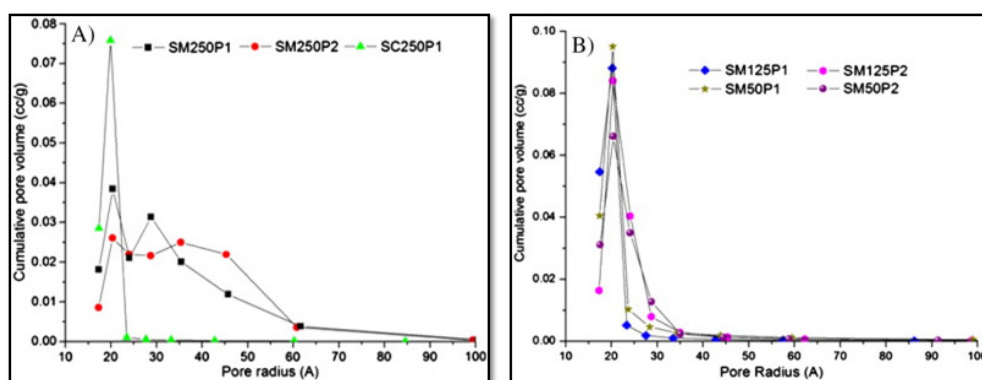


Figure 4.2-10: Pore size distribution graphs for the samples prepared with template at H₂O/Si molar ratios of A) 250 and B) 125 and 50.

Samples prepared with polymer had lower surface areas than the corresponding samples prepared without polymer (Table 4.2-2). This was not the result expected for the samples prepared at high dilution slurry, since the samples prepared with template presented low amorphous silica content blocking pores. The BET area decrease could be explained mainly by some blocking of smaller pores due to residual organic material from the incomplete removal of the polymer. This also could explain the decrease of surface area observed for the samples prepared at the other dilutions. Comparing the BET areas of the samples prepared with polymers P1 and P2 (Table 4.2-2), the higher values were obtained for the samples with P1. For example, the area decrease with respect to SM125 (461 m²/g), was higher for SM125P2 with an area

CHAPTER 4

value of 354 m²/g than for SM125P1 with a value of 396 m²/g. This could be justified by the presence of lower amounts of residual organic material since the polymer with lower molecular mass was easily removed. Significant information for all samples prepared with polymers was that BET and external surface areas were similar (Table 4.2-2). This behavior could be related not only to an increase of delamination but also with the blocking of the smaller pore by residual organic material. This residual amount was determined by thermogravimetric analysis. The results revealed that all samples had between 3.5 and 4.5% residual material. Samples prepared with the highest molecular mass polymer (P2) gave slightly higher amount of residual products. This was in agreement with the higher decrease of BET area observed for these samples.

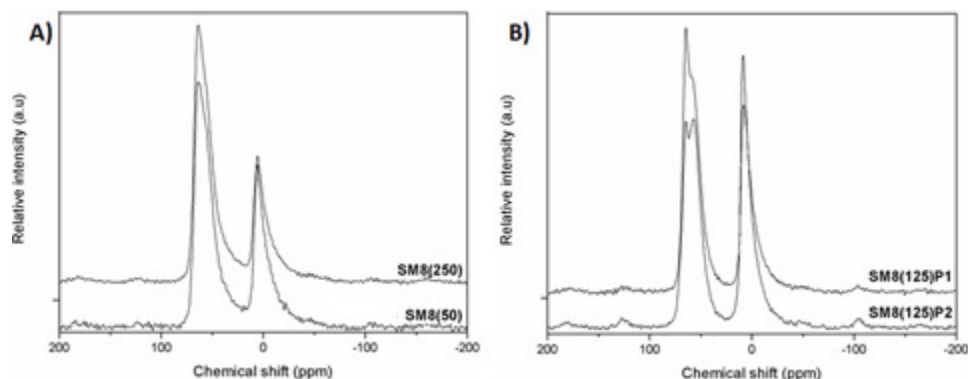


Figure 4.2-10: Typical Al-MAS-NMR of some of the synthesized samples.

The Al^T/Al^O ratios calculated from the ²⁷Al-MAS-NMR spectra are shown in Table 4.2-2. At high dilution slurry, the Al^T/Al^O ratio increased for the samples prepared with template by microwaves or conventional heating compared with their corresponding samples prepared without template. The highest Al^T/Al^O value was obtained for SM250P2 with a ratio of 2.6. These results mean that polymer had a directing effect for preferential incorporation of aluminum to the tetrahedral position. On the other hand, the presence of polymer, during the synthesis at medium dilution slurry, supposes a decrease of Al³⁺ incorporation in tetrahedral position, with a decrease of Al^T/Al^O ratio from 2.6 for SM125 to 1.6 for SM125P1 and 1.2 for

SM125P2. Samples SM50, SM50P1 and SM50P2 had comparable Al^T/Al^O ratio (1.6–1.4).

The C.E.C. values for all samples are shown in Table 4.2-2. Samples, SM250P1 and SM250P2 had comparable C.E.C to SM250. Taking into account the higher amorphous silica content and the lower Al^T/Al^O ratio of sample SM250 (Table 4.2-2), the C.E.C value should be lower. However, the presence of higher Mg vacancies, as commented above, could explain this higher value. For the conventional aged sample prepared with template (SC250P1), the higher C.E.C. value could be related to the combined effect of the higher incorporation of Al^{3+} in the tetrahedral position (higher Al^T/Al^O ratio, 1.4) and the decrease in the amount of amorphous material by the effect of the polymer. Among the samples prepared with polymer, SM125P1 had the highest C.E.C. value (0.63 mEq./g), in agreement with its medium Al^T/Al^O ratio (1.6) and lower amorphous siliceous material content. The decrease of C.E.C for this sample compared to SM125 and its increase with respect to SM125P2 could be correlated with the Al^T/Al^O ratio values. Samples prepared at lower dilution slurry (SM50, SM50P1 and SM50P2) had similar C.E.C values in agreement with their similar Al^T/Al ratios (1.6–1.4).

Conclusions

Several saponites were synthesized by hydrothermal treatment at pH = 8, at 453 K for 6 h with microwaves and for 72 h by conventional heating, from slurries of different H_2O/Si molar ratios (250, 125 and 50). The effect of the presence in the synthesis medium of polyvinylpyrrolidone with different molecular masses was studied. The layered structure and the order of lamellae of the synthesized samples were corroborated by XRD, TEM and N_2 physisorption techniques. Using FT-IR and ^{27}Al -MAS-NMR, we obtained information about the order of the tetrahedral sheet and the Al^T/Al^O ratio. C.E.C were also calculated for all the synthesized saponites.

The sample prepared at medium slurry dilution with microwaves presented the best incorporation of Al in tetrahedral positions, with an Al^T/Al^O ratio of 2.6, in agreement with its highest C.E.C (0.87 mEq./g). Additionally, this sample presented the highest surface area (461 m^2/g). In general, the increase of the slurry concentration

CHAPTER 4

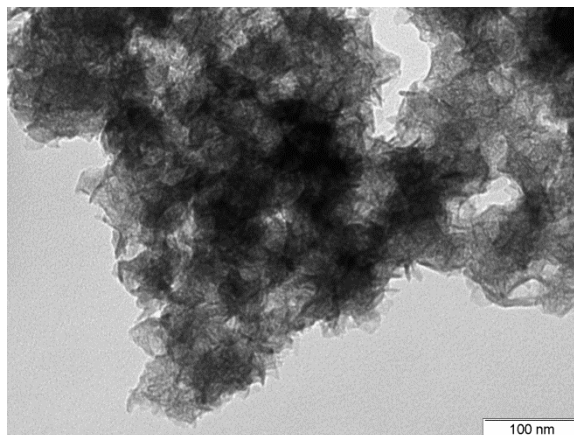
tended to give a more ordered tetrahedral sheet, measured by the shifts of the O-Si-O FT-IR band to lower wavenumber, together with a decrease of the amount of amorphous silica.

The polymer template showed a dilution and heat source (microwaves or conventional heating) dependent effect. The presence of polymer favored stacking in microwave synthesis and improved disorder in conventional preparation at high slurry dilution conditions. Additionally, the use of polymer at these dilutions improved the Al^T/Al^O ratio, especially using microwaves, with ratios of 2.4 for SM250P1 and 2.6 for SM250P2. In contrast, for medium and low slurry dilution, polymer assisted a certain lamellae disorder and supposed a decrease of the Al^T/Al^O ratio for medium dilution and a similar Al^T/Al^O ratio for low dilution with respect to the corresponding samples without polymer. The C.E.C values were in general correlated with the Al^T/Al^O ratio. This correlation was clear for the samples prepared at medium and low dilution slurries. At higher dilution conditions, it was necessary to consider a lower incorporation of magnesium in the structure and the presence of higher amounts of amorphous silica. A general effect related to the presence of polymers was to improve order in the tetrahedral sheet. We also observed a certain directing effect of the polymer in the control of mesoporosity, with a slight increase of the average pore radius when the polymer with higher molecular mass was used. However, the surface area was lower for the samples prepared with polymers. The presence of residual amounts of organic material in these samples could justify this decrease.

Acknowledgments

The authors are grateful for the financial support of the Ministerio de Ciencia i Innovación of Spain and FEDER funds (CTQ2011-24610).

4.3. Microwave Synthesis of Delaminated Acid Saponites Using Quaternary Ammonium Salt or Polymer as Template. Study of pH Influence.



Abstract

Mesoporous saponites were prepared at pH 8 and 13 without and with template (surfactant or polymer) at 453 K and autogenic pressure using microwaves or conventional oven during the hydrothermal aging treatment. Acidity was obtained by calcination of the NH_4 -form. The effect of dilution ($\text{H}_2\text{O}/\text{Si}$ molar ratios of 250, 125 and 50) was studied for the samples prepared at pH 8 with surfactant. In order to compare the effect of introducing surfactant during or after saponite synthesis, several samples prepared at pH 13 were modified after synthesis by refluxing or by stirring at room temperature in a surfactant solution. Preparation of samples at pH 13 favoured the ordering in the stacking direction, improved $\text{Al}^{\text{T}}/\text{Al}^{\text{O}}$ ratio and led to samples with lower amorphous siliceous material content. The use of microwaves and surfactant for the synthesis at pH 13 afforded a saponite with the highest surface area ($603 \text{ m}^2/\text{g}$) and the smallest lamellae crystallite size (about 4 nm). The properties of the samples synthesized at pH 8 with surfactant depended on the dilution. Thus, the degree of delamination, the BET area and the $\text{Al}^{\text{T}}/\text{Al}^{\text{O}}$ ratio increased whereas the amorphous siliceous material content decreased at lower slurry dilution. The incorporation of the surfactant by post-synthesis resulted in some degree of delamination especially when using refluxing. However, the degree of delamination was higher for the saponites prepared with the addition of the surfactant during the hydrothermal synthesis.

Introduction

Some reactions and processes in the industry are catalysed by corrosive and polluting solution acid catalysts (Taguchi and Schüth, 2005). Their use is posing safety, health, environmental, economic and etc. concerns due to problems related to catalyst loss, separation and disposal (Busca, 2007). Important efforts were made to find benign and recoverable acid catalysts (Gładysz, 2002). The emergence of zeolite as solid acid catalyst brought a lot of benefits (Corma, 1997). However, many reagents in the fine and petrochemical industries were excluded by the microporous structures of zeolites (Occelli et al., 2002).

Solid acid catalysts with wider pore structure and high thermal stability were reported (Beck et al., 1992; Kresge et al., 1992). Researchers at Mobil came up with a family of mesoporous aluminosilicates called M41S exhibiting large and uniform pores, high specific surface area and pore volume (Karge et al., 1994; Vartuli et al., 1994). Subsequently, attempts were made to modify and control the pore geometry, acidity and thermal stability of mesoporous materials (Selvam et al., 2001). Preparation methods based on incorporation of bulky polyoxocations of Al, Ce, Cr, Ga, La, Si, Ti, and Zr (Klopogge et al., 2005) and silicate (Torii et al., 1988) as pillars were developed to prepare stable clays with accessible pores. The use of transition metal oxides as pillars also increased Lewis acid or redox characteristics (Yuan et al., 1988).

Clay minerals are cheap, easily available materials widely used in catalysis and adsorption (Busca, 2007). Surface area and acidity of natural clays are low and acid treatment and delamination was used to increase surface area (Vaccari, 1999). Among clay minerals, smectites have comparatively high surface area, acidity and swelling capacities making, them good adsorption and catalytic materials (Dentel et al., 1995; Breen, 1997; He et al., 2001 Alther, 2003).

Saponites are trioctahedral clays of the smectite family with TOT structure (Griffen, 1992). The isomorphous substitution of Si^{4+} by Al^{3+} occurs in the tetrahedral sheets causing a negative layer charge. Hence, hydrated exchangeable cations are incorporated in the interlamellar space to maintain electrical neutrality. The possibility

CHAPTER 4

of exchanging the interlamellar cations with others gave clays with modified properties (Mortland et al., 1986; Boyd et al., 1988; Jaynes and Boyd, 1991). The exchange by H^+ could provide acid properties. When cations were exchanged by organic cations of long alkyl chains, hydrophobic composites with high adsorption capacity for organic contaminants could be obtained (Ray and Okamoto, 2003).

One way of preparation of mesoporous clay minerals involved the use of bulky organic polymers and surfactants as void fillers or galleries, which upon calcination left porous structure behind. For example, mesoporous hectorite was prepared by in-situ hydrothermal crystallization of gel containing cationic surfactant (Iwasaki, et al., 1989) or neutral polymer (Carrado and Xu, 1999). Moreover, the use of different technologies and manipulation of the synthesis conditions allowed some degree of control over the pore structure of materials (Costenaro et al., 2012). Saponites with large pores were prepared by microwaves from gels of high slurry dilution (H_2O/Si molar ratio 250) (Gebretsadik et al., 2014). The use of microwaves in preparation also afforded samples with higher delamination and reduced reaction time with subsequent energy saving (Bergadà et al., 2007). Ultrasound technology resulted in highly dispersed particles with homogeneous morphology and high surface area (Suslick and Price, 1999).

In this work, we report the use of microwaves, ultrasounds and template (polymer or surfactant) in the preparation of high surface area acid mesoporous saponites. Various preparation parameters such as pH, effect of template, type of template and use of surfactant during or after saponites synthesis were investigated in order to establish their effect.

Experimental

Two groups of saponites with theoretical formula, $(M)_{1.2}Si_{6.8}Al_{1.2}Mg_6O_{20}(OH)_4 \cdot nH_2O$ ($M = Na^+, NH_4^+$), determined from the masses of the precursors compounds added in the slurry preparation, were prepared at pH=8 and 13, with and without template (Table 1). The preparation of the slurry for the synthesis of sodium saponites at pH=13 (4 samples) was carried out following the method described by Trujillano et al. (2011) with some modifications. A CO_3^{2-}/HCO_3^- buffer, pH 13, was prepared

Preparation of acid mesoporous saponite

by dissolving 3.63 g of NaOH and 6.56 g of NaHCO₃ in 50 mL double distilled water. Solution A was prepared in the buffer by adding 5.6 mL sodium silicate solution (SiO₂.NaOH, SiO₂ 27 wt %, density 1.39 g/mL, Aldrich) and stirring the mixture mechanically for 10 min. Some samples were prepared in the presence of template, dodecyl trimethylammonium chloride surfactant (AS) (Acros) or polyvinylpyrrolidone polymer (P) (Sigma-Aldrich) with molar mass 40,000g/mol. For these samples, the surfactant or the polymer (AS or P) was added before the silicate solution at 20 wt. % loading with respect to the mass of the other solid reagents. In another beaker, solution B was prepared by dissolving 2.31 g Al(NO₃)₃.9H₂O (Aldrich) and 7.91 g Mg(NO₃)₃.6H₂O (Aldrich) in 5 mL double distilled water. Solution B was added drop by drop into solution A while under mechanical stirring. The slurry was mixed for 30 min and submitted to a final mixing in a tip ultrasounds sonicator for 30 more min. All samples of pH 13 were prepared at slurry dilution (H₂O/ Si molar ratio) of 125.

Ammonium saponites (5 samples), with the same theoretical formula as pH 13 samples, were prepared from a slurry of initial pH = 8 with and without template by modifying the protocol previously reported by our research group (Gebretsadik et al. 2014). In 50 mL of a 3 wt % ammonia solution, for the samples prepared with template, this was added at 20 wt.% loading with respect to the mass of the other solid reagents. Then, stoichiometric amounts of Al(OH)(ac)₂ (Aldrich), fumed silica (Aldrich) and Mg(ac)₂.4H₂O (Panreac) were added one after the other in the same order while stirring the solution for 30 min between each addition. The amount of the precursor (Si, Mg and Al) salt was varied with respect to the amount of water so that slurries at H₂O/Si molar ratios of 250, 125 and 50 were prepared. These slurries were mechanically stirred for 30 min followed by sonication for 30 min more. The slurries of the samples prepared at pH 8 and 13 were then transferred into an autoclave, sealed and aged with microwaves (Milestone ETHOS-TOUCH CONTROL equipped with a temperature controller) at 453 K for 6 h or in a conventional oven at 453 K for 72 h. The resulting solution was filtered; the solid was washed with double distilled water until neutrality and dried overnight in an oven at 363 K. For the samples prepared with template, this was removed by calcination in air (1 mL/s) into a quartz tube reactor at

CHAPTER 4

773 K for 12 h. When the template removal was not complete (sample appeared black or grey), calcination was continued for another 12 h at 823 K under an oxygen flow (1 mL/s).

The sodium saponite synthesized at pH 13 was transformed to their NH_4 -form by exchanging the sodium interlamellar cation with saturated NH_4NO_3 solution at room temperature for 36 h (1 g of sample in 50 mL solution). The acid form was then obtained by calcination of the NH_4 -form in air at 723 K for 5 h.

Finally, two saponites prepared without template at pH 13 and aged with microwaves or by conventional heating were modified after synthesis by exchanging the sodium interlamellar cation of the precursor sodium saponite with a dodecyl trimethylammonium chloride (AS) solution. In a typical experiment, 1 g of sample was stirred in 50 mL of double distilled water to favour its swelling and 0.4 g of surfactant was added. The mixture was stirred at room temperature or refluxed for 24 h. The sample was filtered and washed rigorously with double distilled water, dried overnight in an oven at 363 K and calcined and transformed into their acid form as previously described.

The nomenclature of the samples appears in Table 4.3-1. The letter S means saponite, the letter M or C indicated the heating source used during aging, microwaves or conventional heating, respectively. The templates used were designated as P for the polymer and AS for the quaternary ammonium salt. The number 8 and 13 in the nomenclature indicated the pH of the initial slurry. For the samples prepared at pH 8, the numbers in bracket (250, 125 and 50) corresponded to the degree of slurry dilution given as $\text{H}_2\text{O}/\text{Si}$ molar ratio. Finally, the suffix-subscript PSM stands for the post synthesis modification with surfactant whereas the letter R at the end of the name refluxing was used during post-synthesis modification.

Extensive characterization of samples was performed using X-ray diffraction (XRD), Fourier transform infrared spectroscopy (FT-IR), N_2 adsorption-desorption analysis, inductively coupled plasma (ICP), aluminum magic angle spinning nuclear magnetic resonance spectroscopy (^{27}Al -MAS-NMR), transmission electron microscopy (TEM), cation exchange capacity (C.E.C) and thermogravimetric analysis

Preparation of acid mesoporous saponite

(TG). Details of the experimental procedures were described in section 3.4 of the experimental part.

Table 4.3-1: The nomenclature and preparation conditions of the synthesized samples

Nomenclature	H ₂ O/ Si molar ratio	Template	template Loading (%) ^a	Mode of template addition	Aging
SM13	125	—	—	—	Microwaves
SM13P	125	Polymer	20	During synthesis	Microwaves
SM13AS	125	Surfactant	20	During synthesis	Microwaves
SC13	125	—	—	—	Conventional
SM8(125)	125	—	—	—	Microwaves
SM8(125)P	125	Polymer	20	During synthesis	Microwaves
SM8(250)AS	250	Surfactant	20	During synthesis	Conventional
SM8(125)AS	125	Surfactant	20	During synthesis	Microwaves
SM8(50)AS	50	Surfactant	20	During synthesis	Microwaves
SM13AS _{PSM}	125	Surfactant	40	Post synthesis	Microwaves
SC13AS _{PSM}	125	Surfactant	40	Post synthesis	Conventional
SM13AS _{PSM} R	125	Surfactant	40	Post synthesis	Microwaves
SC13AS _{PSM} R	125	Surfactant	40	Post synthesis	Conventional

^a The amount of template was calculated with respect to the mass of the sample for the samples prepared by post-synthesis while for the samples in which the surfactant was added during synthesis, the amount of template was calculated with respect to the mass of the other solid reagents.

Results and discussion

Effect of type of template at pH 8 and 13

The effect of template was studied by preparing samples at the same slurry dilution (H₂O/ Si molar ratio of 125) with an initial slurry pH of 8 or 13, and using microwaves during the aging treatment. Samples prepared at pH=13 with template (SM13P and SM13AS) and without template (SM13) and at pH=8 with surfactant SM8(125)AS were compared with each other. Samples prepared previously by our

CHAPTER 4

group (Gebretsadik *et al.* 2014) at pH 8 with polymer (SM8(125)P) and without template (SM8(125)) were also compared. Finally, one reference sample was also synthesized at pH 13 at the same conditions than those employed for preparing SM13, but using conventional heating, instead of microwaves, during the aging treatment and longer time (72 h).

XRD patterns of all acid samples showed only one crystalline phase, identified as saponite, with some contribution of amorphous siliceous material, as evidenced from the broad reflection appeared at around 21-23°, especially for the saponites prepared at pH 8 (Figure 4.3-1). The characteristic reflections of saponites at 19.4° due to (110, 020) reflections, at about 35.6° for (201) reflection and at 60.5° for (060) reflection were observed for all samples (Figure 4.3-1). This later reflection, which corresponds to 1.53 Å, is characteristic for trioctahedral clays such as saponites (Prihod'ko *et al.*, 2004; Bisio *et al.* 2011).

The main difference between the XRD patterns of the samples lies in the (001) reflection. While this reflection was clearly observed for sample SC13, it was broader for SM13 and weak or absent for the rest of the samples (SM13P, SM13AS, SM8(125)P and SM8(125)AS) (Figure 4.3-1). The presence of this reflection involved an ordering in the c-direction (Carrado and Xu, 1998; Prieto *et al.*, 1999; Trujillano *et al.*, 2011). Hence, the sample aged by conventional heating at pH 13 (SC13) showed higher ordering than the other samples. Sample SM13, which was aged without template using microwaves, had a lower stacking order than SC13 but higher than SM13AS and SM13P. This could indicate that, at pH 13, there is a delamination effect due to the microwaves aging treatment, being higher when template was used. In contrast, the low stacking order of SM8(125)AS (Figure 4.3-1) was very similar to those of the samples prepared without template or with polymer at pH 8 (SM8(125), SM8(125)P) (Gebretsadik *et al.*, 2014).

The XRD reflection of the saponite phase that was not related to the stacking direction (001), appeared for all microwaved samples less intense and broader than in SC13, especially for the samples aged in the presence of surfactant (SM13AS and SM8(125)AS) (Figure 4.3-1). This confirmed the effect of using microwaves together with templates in preventing the growth of the clay mineral lamella,

especially when employing the surfactant. From all these results, we could conclude that microwaves in the presence of surfactant favoured the synthesis of saponites with smaller lamella and high delamination.

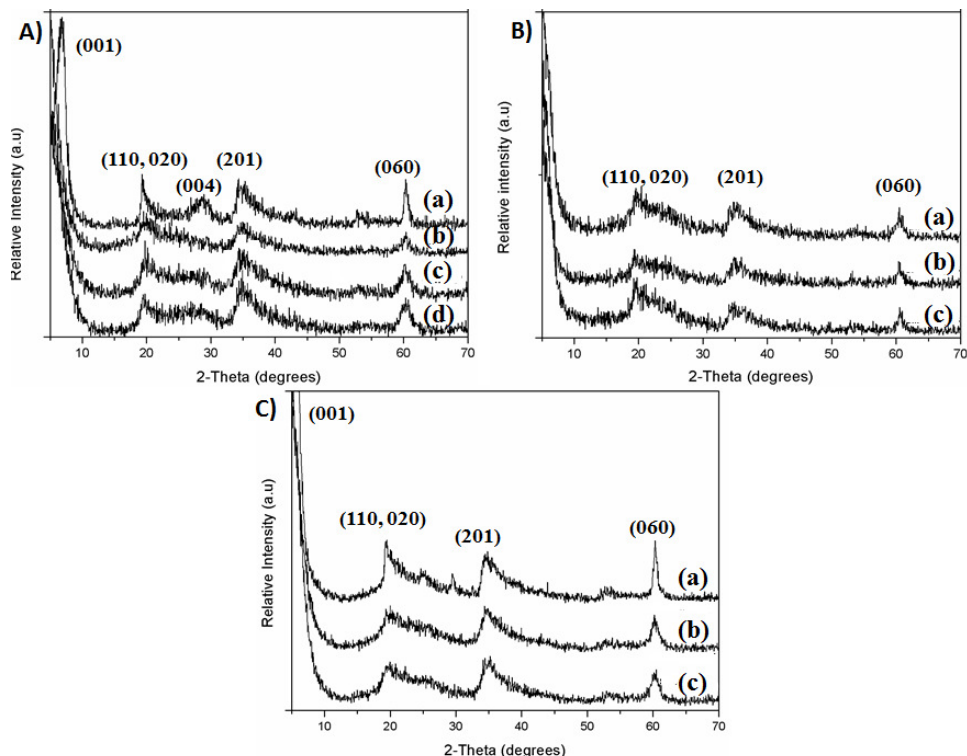


Figure 4.3-3: XRD patterns of the samples prepared A) (a) SC13 (b) SM13AS (c) SM13P (d) SM13 B) (a) SM8(50)AS (b) SM8(125)AS (c) SM8(250)AS C) a) SC13AS40_{PSMR} (b) SM13AS40_{PSMR} (c) SM13AS40_{PSM}.

FT-IR spectra of the samples were collected between 4000-400 cm^{-1} . Figure 2 showed the FT-IR spectra of the samples between 1500 and 600 cm^{-1} . A band at about 665 cm^{-1} , assignable to the Mg-OH stretching, and a weak peak around 810 cm^{-1} , attributed to apical Al-O bond of AlO_4 units, were observed for all samples. Additionally, an intense band, corresponding to O-Si-O band ordered in the clay mineral, appeared at 1022-1010 cm^{-1} . The position of this peak indicated the relative degree of order in the saponite structure (Kloprogge *et al.*, 1999a). The O-Si-O band for SC13 had lower wave number (1010 cm^{-1}) than for SM13 (1013 cm^{-1}) (Figure 4.3-2A). This confirmed better ordering of O-Si-O in the former sample,

CHAPTER 4

in agreement with the higher lamella size observed for this sample by XRD results. Bands that appeared outside the 1500-600 cm^{-1} interval and which were observed in all samples include: a band around 3680 cm^{-1} , due to O-H stretching in the octahedral sheet (Mg-OH) and a band around 3450 cm^{-1} corresponding to the stretching modes of water molecules whose bending mode appeared at 1664 cm^{-1} . The shoulder at 3220 cm^{-1} could be assigned O-H stretching mode of H-bridged groups whereas the bending vibration mode of Si-O-Mg was detected at about 465 cm^{-1} (Russell and Fraser, 1994; Trujillano *et al.*, 2011).

For the sample SM8(125)AS, synthesized at pH 8, the use of surfactant resulted in the presence of amorphous siliceous material identified by its characteristic band at 1105 cm^{-1} (Figure 4.3-2B) whereas the samples prepared without template, SM8(125), or with polymer, SM8(125)P did not show amorphous siliceous material, in a detectable level, in their FT-IR spectra (Gebretsadik *et al.*, 2014). Other effect observed was that the presence of surfactant and polymer had a positive effect on the order of the O-Si-O band in the saponite structure. This was confirmed by the shift of this band from 1023 cm^{-1} for SM8(125) to 1018 cm^{-1} and 1015 cm^{-1} for SM8(125)AS (Figure 4.3-2B) and SM8(125)P (Gebretsadik *et al.*, 2014), respectively. This means that at pH 8, in the presence of template, the lamella were smaller, but probably better crystallized.

The surface elemental composition analysis results obtained from ICP measurements are summarized in table 4.3-2 as wt % of SiO_2 , Al_2O_3 and MgO. For samples prepared at pH 13 had been showed also the wt % of Na_2O . The theoretical wt % values (Table 4.3-2) were calculated from amounts of Si, Al and Mg precursor compounds added during slurry preparation and assuming the anhydrous form of the saponite, $0.6\text{Na}_2\text{O} \cdot 0.8\text{SiO}_2 \cdot 0.6\text{Al}_2\text{O}_3 \cdot 6\text{MgO}$.

From the composition results, it seemed difficult to identify the presence of other solid phases than saponite or to know the distribution of Al in octahedral, tetrahedral sheets or its presence in the interlayer space of the saponite. However some information could be extracted. In SM13 sample, the values are slightly lower than the expected composition for Si and Mg, whereas for Al is higher and

lower for Na. Considering their XRD and FT-IR results we could say that probably only the saponite phase had been obtained. Additionally, we could conclude the loss of a small amount of Si and Mg species and the resulting stoichiometric excess of Al should suppose the presence of Al in Oh positions of the lamella and/or in the interlayer space of saponite, in addition to the expected Td positions.

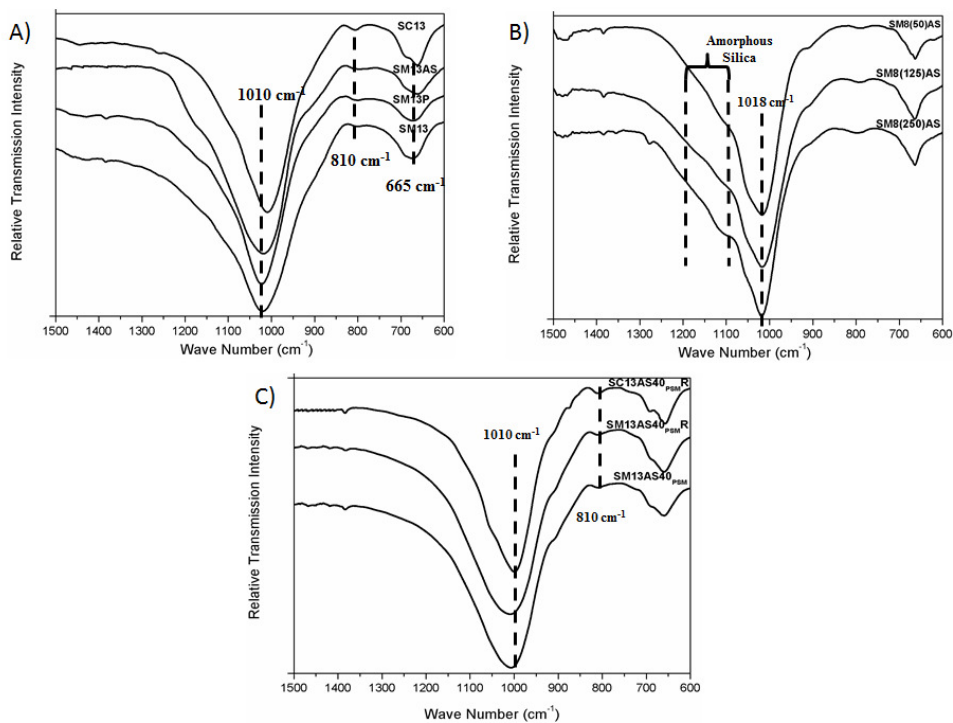


Figure 4.3-4: FT-IR spectra of the samples synthesized A) at pH 13, B) at pH 8 and C) by post-synthesis modification with surfactant.

The lower amount of Na₂O respect to the theoretical value (4.9) is in agreement with this hypothesis. However, the presence of a minor amount of amorphous phase rich in Al could not be discarded. Respect to the other samples, the use of conventional heating and templates in the saponite prepared at pH 13 led to an increase of the % of SiO₂ and a decrease in the % of MgO and Na₂O. Some contribution of siliceous amorphous species, observed by FT-IR (Figure 4.3-2A) and/or certain substitution of Mg by Al in the Oh sheet could justify this behaviour. The saponites prepared at pH 8 at slurry dilution 125 presented higher % SiO₂ and lower % of MgO and Al₂O₃ than those synthesized at pH 13. This

CHAPTER 4

agreed with the presence of amorphous silica observed by FT-IR for some pH 8 samples (Figure 4.3-2B). The effect of using polymer or surfactant, for synthesis at pH 8, on the % of amorphous silica was not relevant. However, the higher % of Al_2O_3 and lower % of MgO for the sample prepared with polymer (SM8(125)P) could be explained by a higher substitution of Mg by Al in the octahedral sheet when compared to the sample prepared with surfactant, SM8(125)AS.

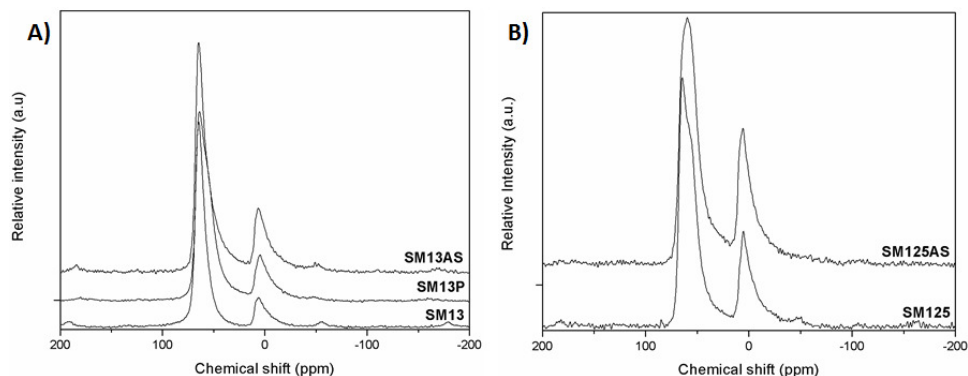


Figure 4.3-5: ^{27}Al NMR spectra of several samples prepared with and without surfactant at A) pH 8 and B) pH 13.

^{27}Al MAS NMR spectra of all samples showed peaks at about 0 and 60 ppm, with respect to the internal standard, which could be assigned to octahedrally and tetrahedrally coordinated Al, respectively (Figure 4.3-3). Additionally, a peak centred at about 54 ppm, corresponding to Al in distorted tetrahedral sites, was observed. It was important to consider that the octahedral Al in saponites corresponds to the Al present in the octahedral sheet and in the interlayer space. The possible presence of minor amount of an aluminium rich phase could introduce little modification in the $\text{Al}^{\text{T}}/\text{Al}^{\text{O}}$ ratio due to the saponite phase. The ratio of the amount of tetrahedral aluminium (ordered and distorted) (Al^{T}) to octahedral aluminium (Al^{O}) was calculated by integrating the area of the bands (Table 4.3-2).

Preparation of acid mesoporous saponite

Table4.3-2: Physico-chemical characterization results of the samples.

Sample	C.E.C. (mEq/ g)	BET area (m ² /g)	Pore radius (Å)	Elemental composition-ICP (wt. %)				Al ^T /Al ^O (²⁷ Al-NMR)	Total acidity (mEq CHA/g)	Template loading (wt %) (TGA)
				SiO ₂ (54.9) [#]	MgO (32.1) [#]	Al ₂ O ₃ (8.1) [#]	Na ₂ O (4.9)			
SM13	1.07	384	18	53.7	31.8	9.0	3.2	5.3	1.03	NA
SM13P	0.78	331	16	61.9	24.8	8.8	2.4	3.2	0.65	11.8
SM13AS	0.89	603	35	63.0	24.0	8.7	2.7	2.9	1.02	18.3 (14.2)
SC13	1.14	50	20	62.2	25.1	8.2	3.4	5.1	1.07	NA
SM8(125)*	0.87	461	26	65.5	21.9	8.2	—	2.6	0.87	NA
SM8(125)P*	0.63	396	25	68.5	22.9	8.6	—	2.2	0.60	18.9
SM8(250)AS	0.51	323	75	70.1	17.6	10.0	—	1.6	0.48	9.7
SM8(125)AS	0.68	339	58	66.0	23.8	7.6	—	2.0	0.62	18.1
SM8(50)AS	0.64	395	61	66.4	22.8	7.8	—	2.3	0.61	19.1
SM13AS _{PSM}	—	407	19	54.7	31.6	8.5	—	5.2	1.02	18.5 (3.1)
SC13AS _{PSM}	—	148	27	—	—	—	—	5.1	1.09	14.3(5.2)
SM13AS _{PSMR}	—	505	25	—	—	—	—	—	1.04	24.8 (9.9)
SC13AS _{PSMR}	—	236	22	—	—	—	—	—	1.11	19.6(8.7)

*These samples were reported in our previous work (Gebretsadik *et al.* 2014) in which the elemental composition results were obtained from EDS analysis and reported as Si/Al and Si/Mg ratio. [#]Theoretical values.

CHAPTER 4

In all samples compared in this section, the aluminium with tetrahedral coordination was higher than aluminium with octahedral coordination, ($Al^T/Al^O = 5.3-2.0$), this is agreement with the expected saponite phase. However, the octahedral Al amount was significant; even in the sample with highest amount of tetrahedral Al, about 20% of the Al is octahedral. Samples prepared at pH 13 without template and aged by microwaves (SM13) or conventional heating (SC13), had the highest Al^T/Al^O ratio values (5.3 and 5.1, respectively). The Al^T/Al^O ratio was lower for the samples prepared with surfactant, SM13AS (2.9) and polymer, SM13P (3.2). Moreover, samples prepared at lower pH (8) had lower Al^T/Al^O ratio than those prepared at high pH and the presence of template further lowered the value from 2.6 in SM8(125) to 1.6 in SM8(125)AS and 2.2 in SM8(125)P. The presence of polymer during the saponite synthesis, at both pH, favoured more Al incorporation in the tetrahedral positions than the use of surfactant.

Figure 4.3-4A showed a thermogram representative of the samples prepared without template. The thermogram displayed two mass losses with an inflection point at about 400 and 1035 K, which can be ascribed to loss of water of hydration and dehydroxylation, respectively. Otherwise, the thermogram was reasonably flat in the other regions and no significant mass loss was observed. Hence, we used the temperature range 523-923 K in the thermogram of samples prepared with template to determine the percentage template loading (e.g. Figure 4.3-4B). The relative amount of the template in the composite material was calculated as the percentage of the template relative to the dry mass of the pure saponite (Table 4.3-2). The same temperature range was also used to estimate the total acidity of the samples using cyclohexylamine as probe molecule. A representative thermogram is shown in Figure 4.3-4C.

For the samples synthesized at pH 13 with template, the percentage template loading was higher when using the surfactant (18.3) than when using the polymer (11.8) (Table 4.3-2). This higher surfactant incorporation combined with its relative easier removal during calcination could contribute to higher delamination and, subsequently, higher surface area for SM13AS compared to SM13P. The

Preparation of acid mesoporous saponite

surfactant loading in SM8(125)AS (14.1) was lower than the corresponding sample prepared at pH=13, SM13AS. This could be ascribed to the lower C.E.C of SM8(125)AS, which involved a lower exchange capacity to incorporate the quaternary ammonium salt (Table 4.3-2).

N₂ adsorption-desorption isotherms of all samples in figure 4.3-5 indicated type IV isotherm denoting the existence of mesoporosity. Samples SC13, SM13 and SM13P displayed higher contribution of hysteresis loop type B (Figure 4.3-5A) according to de Boer classification, which was characteristic of slit-pores between parallel lamellar particles. In contrast, for the samples prepared with surfactant at both pH, SM8(125)AS and SM13AS (Figure 4.3-5B), the hysteresis shape was mainly of type D. This hysteresis loop is due to the existence of disordered disposition of plate-like particles with more important contribution of inter-particle mesoporosity. This disorder could be consequence of the delamination produced by the presence of surfactant in the medium of synthesis.

Specific surface areas were calculated, from BET algorithm, for all samples (Table 4.3-2). The lowest surface area was observed for SC13 (50 m²/g). This could be related to its larger particle size and higher stacking, as observed by XRD. The BET area was higher for SM13 (384 m²/g) in agreement with the delamination and its smaller crystallite size. The area value was almost double for the sample prepared with surfactant at pH 13, SM13AS (603 m²/g). This could be attributed to its higher delamination. However, the BET area was lower for SM8(125)AS (332 m²/g) compared to SM(8)125 (461 m²/g) despite the higher delamination observed. This could be explained by the presence of amorphous siliceous material that blocks the pores and, subsequently, decreases the BET area. Finally, the surface areas slightly decreased for the samples prepared with polymer at both pH, SM13P (331 m²/g) and SM8(125)P (396 m²/g) with respect to the samples prepared without template. This was probably due to some pore blockage by carbonaceous materials from the incomplete oxidation of polymer in these samples. This had been estimated by combustion analysis to be about 3%.

CHAPTER 4

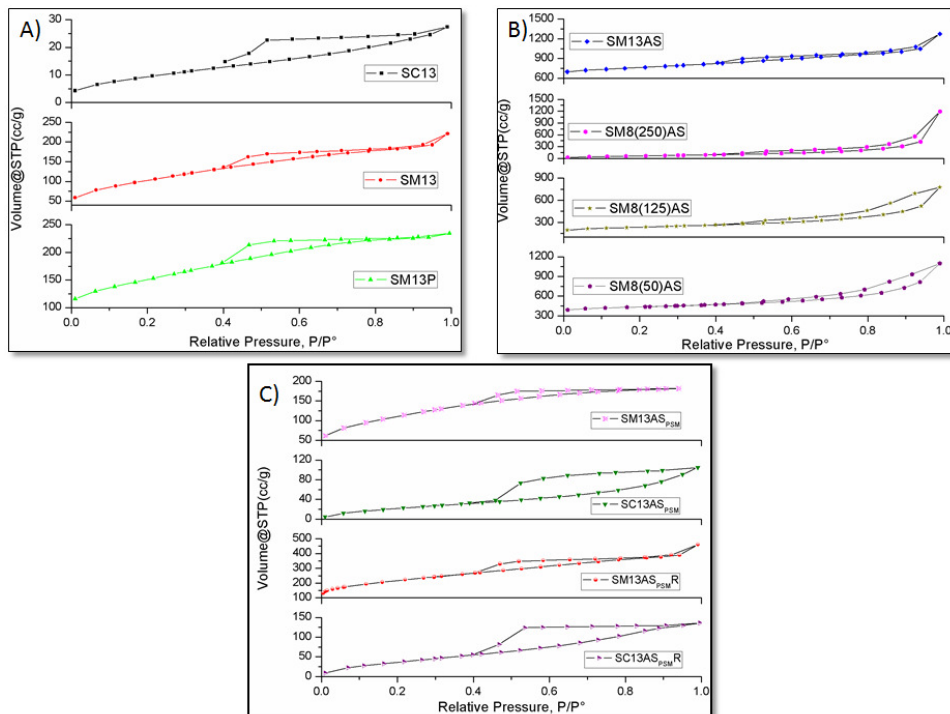


Figure 4.3-6: N₂ adsorption-desorption isotherms of the samples prepared A) at pH 13, B) with surfactant during synthesis C) modified with surfactant after synthesis.

Regarding pore size distribution graphics (Figure 4.3-6), samples SC13, SM13 and SM13P showed a narrow pore size distribution averaged around 20 Å. This could be related to the low degree of delamination and high aggregation of the stacked lamellae observed for these samples. In contrast, the sample prepared with surfactant (SM13AS) exhibited, in addition to the narrow porosity around 20 Å, a broad pore size distribution between 50-100 Å. This could be explained by the presence of different aggregates of randomly distributed lamella (Klopogge and Frost, 2000), according to the delamination observed for this sample by XRD. The effect of using surfactant or polymer during the saponites synthesis on the pore size distribution for the samples prepared at pH 8 was similar to that observed for the saponites prepared at pH 13. Only sample SM8(125)AS showed an additional mesoporosity, as evidenced from its bimodal pore size distribution (Figure 4.3-6B). Samples SM8(125) and SM8(125)P had a narrow monomodal pore size distribution (Gebretsadik *et al.*, 2014). From all these results, we could conclude

that the use of surfactant had a higher delaminating effect than the use of polymer.

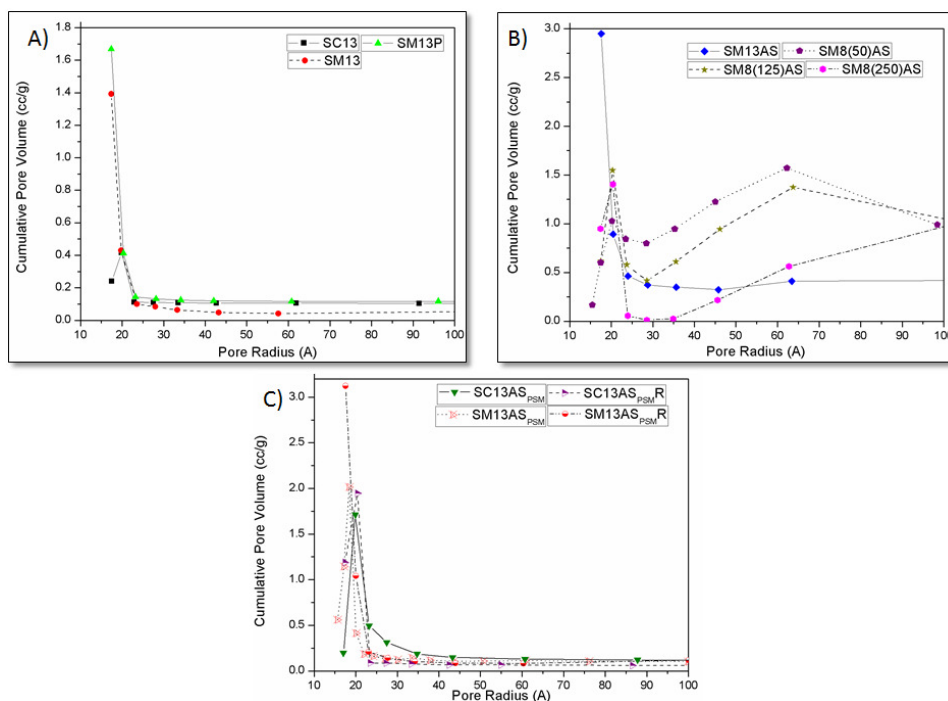


Figure 4.3-7: Pore size distribution graphics of the samples synthesized A) at pH 13 B) with surfactant during synthesis and C) modified with surfactant after synthesis.

The morphology of the synthesized samples was investigated by transmission electron microscopy (TEM). The images of all samples showed sheet like structure typical of clay minerals (Figure 4.3-7). SC13 exhibited well-defined stacked lamella with larger dimensions whereas SM13 and SM13P displayed some delamination. The samples prepared with surfactant, SM8(125)AS and SM13AS, exhibited higher delamination and smaller particle sizes compared to their non-templated counterparts. Additionally, the delamination effect of the surfactant was more effective than that observed for the polymer (Gebretsadik *et al.*, 2014).

The C.E.C. and surface acidity values (mEq. cyclohexylamine (CHA)/g) showed similar trend for almost all samples (Table 4.3-2). C.E.C. values could be related to the negative charge of the layers that in saponites should be obtained by the substitution of Si^{4+} by Al^{3+} in tetrahedral sites. The theoretical value calculated for a dehydrated samples should be 1.59 mEq./g for saponites with the

CHAPTER 4

stoichiometry used in this work ($(M)_{1.2}Si_{6.8}Al_{1.2}Mg_6O_{20}(OH)_4$). However, some substitution of Mg^{2+} by Al^{3+} in octahedral sites could be also expected resulting in a lower C.E.C. values. Additionally, the measured C.E.C. values could be lower due to the presence of hydrated Al^{3+} species in the interlayer space with low exchangeability, or presence of other solid phases without exchange capacity.

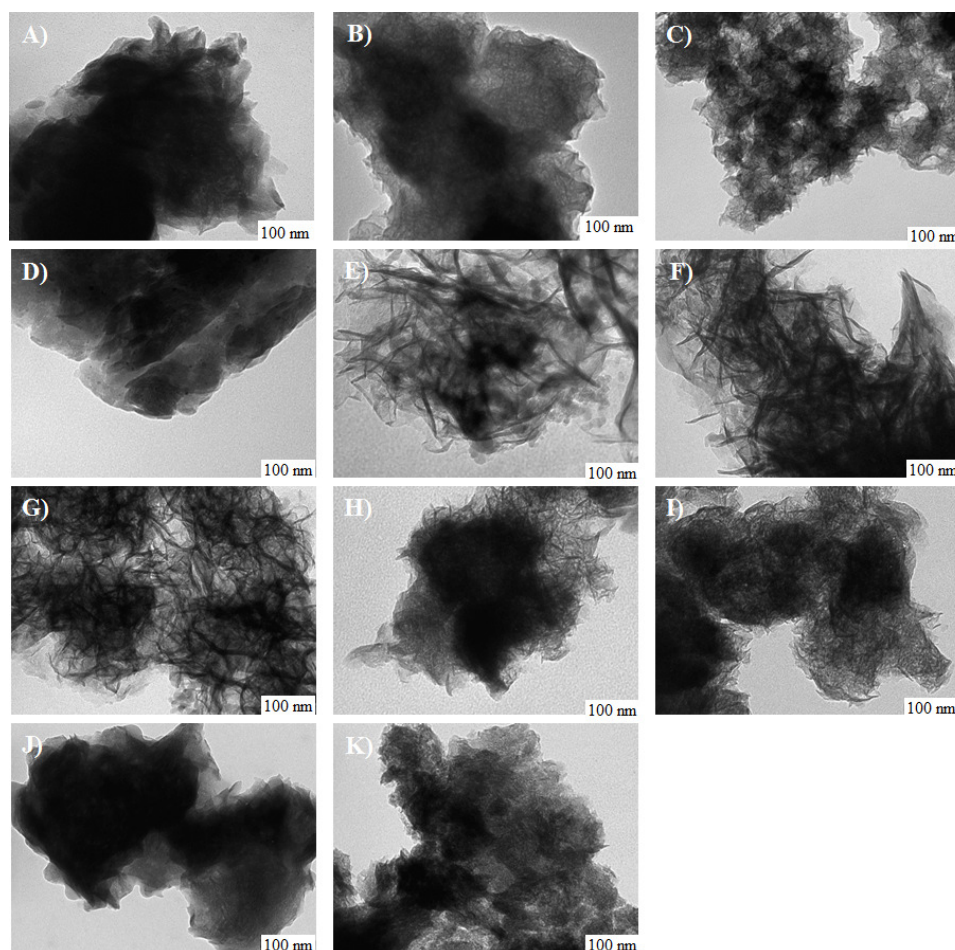


Figure 4.3-8: TEM micrographies of the samples A) SM13, B) SM13P, C) SM13AS, D) SC13, E) SM8(250)AS, F) SM8(125)AS, G) SM8(50)AS, H) SM13AS_{PSM}, I) SM13AS_{PSMR}, J) SC13AS_{PSM} and K) SC13AS_{PSMR} all at (x 200 k).

The highest C.E.C. values were obtained for SC13 (1.14 mEq/g) and SM13 (1.07 mEq/g). These values were in agreement with the highest Al^T/Al^O ratio of these samples (5.3 for SM13 and 5.1 for SC13). The differences between the

Preparation of acid mesoporous saponite

C.E.C. values of these two samples were considered to be not significant. The differences in C.E.C. values of samples prepared at pH 13 showed the same tendency as the Na₂O wt %, this confirmed the direct correlation between the C.E.C. values and the amount of Na. This cation was localized in the interlayer space of saponites and was easily exchangeable. In the samples prepared with template at both pH 8 and 13, the presence of template lowered the C.E.C. values (Table 4.3-2). The values of C.E.C. were higher for the samples prepared at pH 13 than for those prepared a pH 8 (SM13AS (0.87), SM13P (0.78), SM8(125)AS (0.65) and SM8(125)P (0.62)). This was in agreement with the lower Al^T/Al^O ratio obtained for the samples prepared at pH 8 and using surfactant during the synthesis.

The total surface acidity measurement gave, in general, lower values, than those expected considering C.E.C., since the acidity was mainly related to H⁺ that neutralize the negative charge of the layers. The difference between acidity and C.E.C. should be related to problems in the accessibility of the acid sites to the cyclohexylamine. For example, the lower area of SC13 than SM13 can justify the higher difference between C.E.C and acidity observed in sample SC13. In contrast, in sample SM13(AS), which was the sample with the highest BET area (603 m²/g), the acidity values were slightly higher than C.E.C. The good accessibility in this sample allowed the determination of some additional Lewis acidity present. For the rest of samples, similar tendency was established between C.E.C values and total surface acidity.

Effect of surfactant at different dilutions at pH 8

In our previous work (Gebretsadik *et al.*, 2014), we observed that the use of polymer as template in the synthesis of saponites at pH 8 had a slurry dilution dependent effect. Thus, the presence of polymer at high slurry dilution (H₂O/Si molar ratio of 250) favoured stacking, improved aluminium incorporation in the tetrahedral sheet and decreased the amorphous silica content. At medium and low slurry dilution, H₂O/Si molar ratio of 125 and 50, respectively, the presence of

CHAPTER 4

polymer favoured delamination. In addition, at medium slurry dilution, the use of polymer decreased incorporation of aluminium in the tetrahedral position whereas no significant differences were observed related to the presence of polymer at low slurry dilution. In order to investigate the effect of surfactant during the synthesis of saponite at pH 8 and different degrees of slurry dilution, we prepared samples SM8(250)AS, SM8(125)AS and SM8(50)AS.

XRD patterns of SM8(250)AS, SM8(125)AS and SM8(50)AS were similar (Figure 4.3-1B). The absence of the (001) reflection in these samples might indicate a lack of ordering in the stacking direction.

FT-IR spectra of these samples showed the presence of additional peaks when compared with the spectra described in the previous section for the sample prepared without surfactant (Figure 4.3-2B). Thus, a weak band appeared at 1105 cm^{-1} accompanied by a shoulder at 1200 cm^{-1} , with higher intensity for sample SM8(250)AS. This could be related to residual amorphous siliceous material. The O-Si-O band slightly shifted from 1018 cm^{-1} in SM8(250)AS to 1017 cm^{-1} in SM8(125)AS and SM8(50)AS. This might indicate a slight increase in the crystallinity of the tetrahedral sheet for the samples prepared with surfactant at medium and low slurry dilution.

Regarding elemental analysis results, SM8(250)AS had higher SiO_2 and Al_2O_3 and lower MgO % composition than the other two samples prepared at lower slurry dilutions (Table 4.3-2). The contribution of higher amounts of siliceous amorphous species, observed by FT-IR, together with some substitution of Mg by Al in the Oh positions and the presence of Al in the interlamellar space could justify this result.

The ^{27}Al MAS NMR results confirmed that aluminium incorporation in the tetrahedral position decreased when increasing the dilution of the synthesis gel (Table 4.3-2). This behaviour was different to that observed when polymer was used as template, since in that case, at higher concentration the viscosity was very high and the Al incorporation was more difficult (Gebretsadik *et al.*, 2014).

N_2 adsorption-desorption isotherms of SM8(250)AS, SM8(125)AS and SM8(50)AS were similar (Figure 4.3-5B). Hysteresis loop type D, related to

Preparation of acid mesoporous saponite

randomly oriented lamella and related to delamination, was observed for the three samples. The BET area values followed the same trend as the surfactant loading. When the surfactant loading is higher, higher delamination can be expected and, therefore, higher BET area, should be obtained. Hence SM8(50)AS with higher template loading (19.1 wt.%) gave higher BET area (395 m²/g) than SM8(125)AS which had 18.1 wt.% template loading. For SM8(250)AS, in addition to its lower template loading (9.7 wt.%), the presence of slightly higher amounts of residual siliceous material than the other two samples could also contribute to its lower BET area (323 m²/g).

The pore size distribution profile of sample SM8(50)AS showed an appreciable degree of mesoporosity contribution between 30 and 100 Å (Figure 4.3-6B) and higher average pore diameter of 61 Å (Table 4.3-2). The contribution of this mesoporosity was slightly lower for SM8(125)AS, in agreement with the presence of a lower degree of delamination. The highest average pore diameter (75 Å) observed for sample SM8(250)AS could be attributed to the contribution of the porosity corresponding to the amorphous siliceous material present in this saponite.

TEM images of these three samples showed disordered lamellar structure (Figure 4.3-7 G-I). SM8(250)AS had larger lamella than SM8(125)AS and SM8(50)AS. This could also contribute to its low BET area as discussed previously. TEM image of SM8(50)AS exhibited smaller particles with higher delamination than SM8(125)AS, in agreement with the results obtained with other characterization techniques.

SM8(250)AS had slightly lower C.E.C. value (0.51 mEq/g) than SM8(125)AS and SM8(50)AS (0.68 and 0.61 mEq./g, respectively) (Table 4.3-2). The higher amounts of amorphous siliceous material and the lower Al^T/Al^O ratio could explain the lower C.E.C. value of SM8(250)AS. The differences observed between the other two samples could be related to the higher amount of aluminium incorporated in the octahedral sheet for SM8(50)AS. The substitution of Mg²⁺ by Al³⁺ in the octahedral sheet neutralizes partially the negative charge produced by the substitution of Si⁴⁺ by Al³⁺.

CHAPTER 4

The values of total acidity (mEq CHA/g) for the three samples followed the same order as that obtained for the C.E.C values (Table 4.3-2), as expected. However, the values of C.E.C. were slightly higher than the corresponding acidity values might be due to restricted accessibility of the acid sites for the bulky cyclohexylamine (CHA) probe molecule.

Use of surfactant during synthesis Vs. Post synthesis modification

In order to compare the effect of incorporating the surfactant during saponites synthesis or by post synthesis, saponite SM13, synthesized at pH 13 without template, was modified after synthesis. The Na⁺ interlamellar cations were exchanged with surfactant solution at two conditions: stirring at room temperature and refluxing. Saponite SC13, which was more crystalline than SM13, was also modified by post-synthesis at the same conditions as SM13 in order to study the influence of saponite crystallinity on the degree of modification.

The post-synthesis modified samples (SM13AS_{PSM} SM13AS_{PSM}R, SC13AS_{PSM} and SC13AS_{PSM}R) did not show the reflection (001) in their XRD patterns (Figure 4.3-1C) as the corresponding saponite prepared with surfactant during synthesis (SM13AS) (Figure 4.3-1A). However, XRD patterns of the saponites prepared without template (SM13 and SC13) had a shoulder and a well-defined (001) reflection peak, respectively, as previously discussed (Figure 4.3-1A). This indicated that the surfactant induces delamination when used either during or in post-synthesis modification.

FT-IR spectra of the samples modified after synthesis (Figure 4.3-2C) did not show structural differences when compared with their corresponding precursors, SM13 and SC13 (Figure 4.3-2A), as expected.

Elemental analysis results of the post-synthesis modified samples (SM13AS_{PSM}) are presented in table 4.3-2. The compositions of the post-synthesis modified samples were almost similar to those of the unmodified samples. The slight higher wt. % of SiO₂ and the slight lower wt. % of MgO and Al₂O₃ could be explained by an exchange of Al and Mg in the interlamellar space by the

Preparation of acid mesoporous saponite

surfactant. Therefore, FT-IR and ICP results indicated that post-synthesis modification had very little effect on the structure or the composition of the sample with respect to the sample prepared without surfactant.

The overall surfactant loading was similar for the post-synthesis modified samples as for the samples prepared with surfactant during synthesis. However, some slight increase was observed for the refluxed samples (Table 4.3-2). An important difference between both methods was on the strength of the saponite-surfactant interaction. The wt. % loading of weakly interacting surfactant, which was easily removed from the sample in the temperature range 523-723 K, and can be assigned. The surfactant that was intercalated in interlamellar space and hence which was strongly interacting with the saponite was considered to be removed in the 723-923 K range. Figures 4.3-4B and 4.3-4D display the decomposition thermograms of samples SM13AS and SM13AS_{PSM} before the surfactant was removed, as example. For samples modified after synthesis, only small amounts of the overall surfactant loaded (the values in bracket, Table 4.3-2) was intercalated. For the samples modified by refluxing not only an increase in the total amount but also an increase in the wt. % of intercalated surfactant with respect to the samples modified at room temperature was observed. For the sample prepared with surfactant during synthesis, 77.6% of the surfactant incorporated into the saponite was intercalated.

The Al^T/ Al^O ratio of the samples modified after synthesis (Table 4.3-2) and the samples prepared without surfactant were similar. This agrees with our previous argument that surfactant does not affect structure and composition during post synthesis modification. However, the use of surfactant during synthesis resulted in lower Al^T/ Al^O ratio. A similar result was reported by Bisio *et al.*, (2011).

The N₂-physisorption isotherm of the microwaves sample modified after synthesis at room temperature (SM13AS_{PSM}) showed mainly an hysteresis loop type B (Figure 5C) similar to that of the unmodified sample (SM13) with low contribution of hysteresis type D. However, the sample modified by refluxing (SM13AS_{PSM}R) showed higher contribution of the hysteresis type D. The same

CHAPTER 4

trend was observed when comparing SC13AS_{PSM} and SC13AS_{PSMR} (Figure 4.3-5C). The increase of disorder in the disposition of the lamellar particles for the samples modified by refluxing could be probably related to higher incorporation of surfactant and especially of intercalated surfactant with. The sample prepared with surfactant during the synthesis (SM13AS) showed an isotherm with higher contribution of hysteresis type D compared with the samples modified after synthesis (SM13AS_{PSM} and SM13AS_{PSMR}). This was in agreement with the higher amount of intercalated surfactant observed for the sample prepared with surfactant during the synthesis.

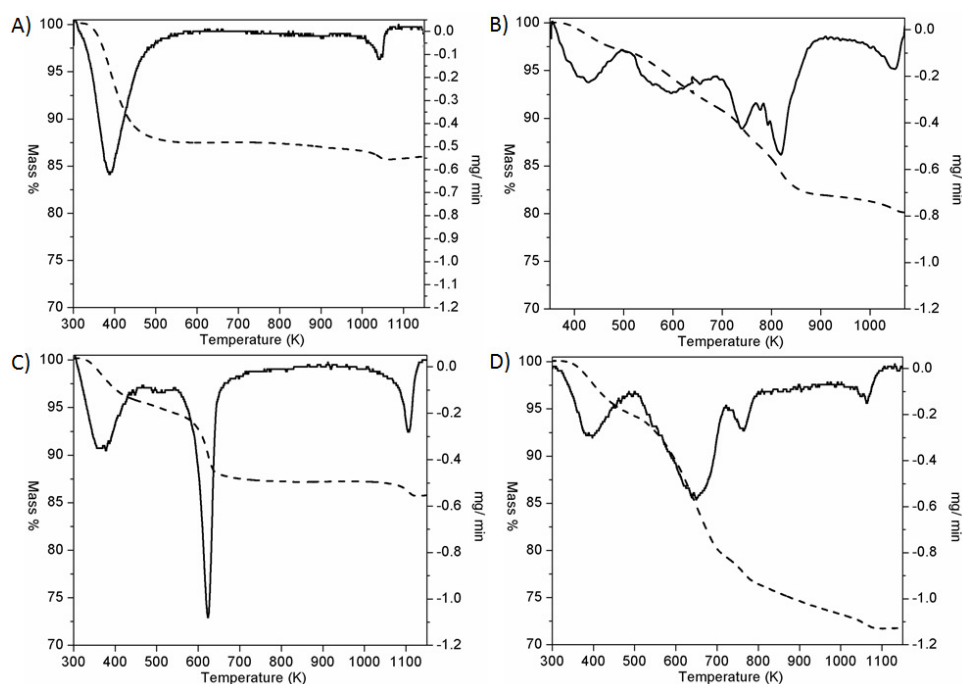


Figure 4.3-9: TGA curves of the samples A) SM13, B) SM13AS, C) cyclohexylamine treated H-form of SM13 and D) SM13 modified by post-synthesis stirring at room temperature (SM13AS_{PSM}).

The pore size distribution of the post-synthesis modified samples was similar (Figure 4.3-6C). When the precursor was prepared with microwaves (SM13), the average pore size of post-synthesis modified samples was slightly higher (25 Å), (Table 4.3-2) when refluxing was used, probably due to its higher delamination. In contrast, for samples SC13AS_{PSM} and SC13AS_{PSMR}, larger average pore radius

Preparation of acid mesoporous saponite

was obtained for the sample prepared at room temperature. However, the difference in the average pore diameter between all the post synthesis modified samples was not important (19-27 Å) with a certain tendency to increase with respect to the unmodified precursors.

BET areas of the post-synthesis modified samples were, in general, higher than those of the unmodified samples, SC13 and SM13 (Table 4.3-2). The BET area was three times higher for SC13AS_{PSM} (148 m²/g) and almost five times higher for SC13AS_{PSMR} (236 m²/g) than for the unmodified sample SC13 (50 m²/g). SM13AS_{PSM} and SM13AS_{PSMR} showed slightly higher (407 m²/g) and higher surface area (505 m²/g), respectively, than the unmodified sample, SM13 (384 m²/g). These BET area results were in agreement with the isotherms and the thermogravimetric analysis results discussed earlier. However, the BET area was higher for the sample prepared in the presence of surfactant during synthesis, SM13AS (603 m²/g) than for the samples modified after synthesis. This was in agreement with the higher delamination observed for SM13AS.

TEM images in figure 4.3-7 showed that the samples modified after synthesis at room temperature (SM13AS_{PSM} and SC13AS_{PSM}, Figures 4.3-7H and 4.3-7J) and by refluxing (SM13AS_{PSMR} and SC13AS_{PSMR}, Figures 4.3-7I and 4.3-7K) had more disorder than the unmodified samples, especially the refluxed samples. The samples prepared in the presence of surfactant during synthesis, SM13AS, showed higher delamination than those modified after synthesis. This was in agreement with the results obtained by other characterization techniques.

The acidity values of the post-synthesis modified samples were, in general, slightly higher than the corresponding values of the samples prepared without surfactant (SM13 and SC13) (Table 4.3-2). This could be probably related to the better accessibility of the acid centres to the probe molecule in the modified samples, which present higher surface areas because of their higher delamination. For example the surface acidity values of SM13AS_{PSM} (1.03 mEq/g) and SC13AS_{PSM} (1.09 mEq/g) were the same and slightly higher than that of the unmodified sample, respectively. The values further increased for SM13AS_{PSMR} (1.04 mEq/g) and SC13AS_{PSMR} (1.11 mEq/g) with an increase in the delamination

CHAPTER 4

degree.

Conclusions

The use of microwaves during the aging treatment for the synthesis at pH 13 (SM13) provided higher delamination with smaller lamella and higher BET area compared to SC13. SM13 and SC13 showed a higher incorporation of Al in the tetrahedral sheet (higher Al^T/Al^O ratio) and lower amorphous siliceous material content than SM8(125). SM13AS had higher specific BET area than SM13 due to its smaller and highly delaminated particles. The presence of polymer in pH 13 synthesis (SM13P) slightly improved the degree of delamination, as observed from TEM and XRD analysis. However, the BET area of SM13P was lower than that of SM13 due to pore blockage by carbonaceous material. Additionally, the presence of template (polymer or surfactant) at pH 13 decreased the Al^T/Al^O ratio, C.E.C and acidity values.

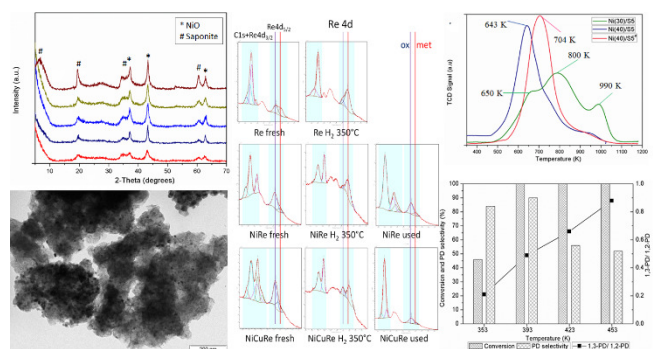
Samples prepared in the presence of surfactant at pH 8 showed dilution dependent effects. For the samples prepared at medium and low dilution, SM8(125)AS and SM8(50)AS), their FT-IR revealed the presence of lower amounts of amorphous siliceous material with higher crystallinity of their tetrahedral sheets compared to SM8(250)AS. Additionally, the Al^T/Al^O ratio increased with a decrease in the degree of dilution, leading to higher C.E.C and acidity values for SM8(125)AS and SM8(50)AS).

The post synthesis modified samples showed higher delamination from their XRD, N_2 - physisorption and TEM results with respect to SC13 and SM13, without any significant change in their composition. The post synthesis modified samples had lower amount of surfactant and lower specific surface BET area than the sample prepared with surfactant during synthesis.

Acknowledgment

The authors are grateful for the financial support of the Ministerio de Economía y Competitividad of Spain and FEDER funds (CTQ2011-24610).

5. Application of Acid Saponite in Glycidol Hydrogenolysis



5.1. Background on the selective hydrogenolysis of glycerol to propanediols and potential of glycidol as an alternative substrate

Glycerol, also called glycerin, with an IUPAC name 1,2,3-propanetriol is a renewable compound, mainly obtained as a byproduct (10 wt % yield) of a biodiesel industry, but also in the preparation of soap, fatty acid and fatty alcohol (Zhou et al., 2008). The expansion of bio-diesel industries over the past decades, as a source of renewable fuel, resulted in the over supply of glycerol (Zhou et al., 2008) which is projected to continue increasing (LMC International, 2013) in the coming years (Figure 5.1-1).

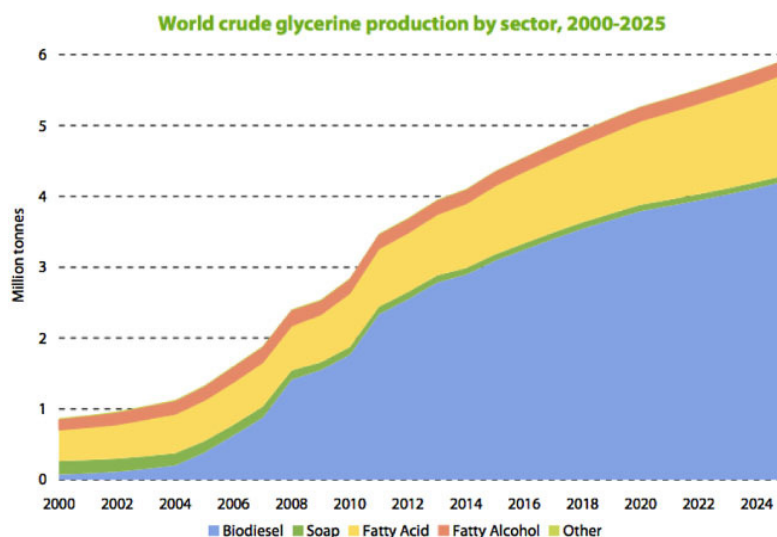


Figure 5.1-1: Projection of world glycerol supply. (LMC International, 2013)

Glycerol serves as an end use product in the pharmaceutical, cosmetic, tobacco and food industries (Tan et al., 2013). However, excessive supply has threatened its market value and it is very crucial to transform glycerol into other high-value added compounds in order to improve the economic competitiveness of the bio-diesel industry (Johnson and Taconi, 2007; Pagliaro et al., 2007; Behr et al., 2008; da Silva et al., 2009; Zhou et al., 2013). Various processes were proposed to transform glycerol into other useful chemicals (Behr et al., 2008; Zhou et al., 2013). Among them, direct hydrogenolysis of glycerol to 1,2-PD and 1,3-PD appears interesting. 1,3-PD is especially a high value derivative of glycerol because the current industrial processes for 1,3-PD production are expensive and involves hazardous intermediates (Kraus,

CHAPTER 5

2008). 1,3-PD is an important monomer in the production of polypropylene terphthalate (PPT) polymer that has good chemical, thermal and mechanical properties (Behr et al., 2008).

The hydrogenolysis of glycerol was extensively studied since the 1980's (Che, 1987; Montassier et al., 1988). The hydrogenolysis of an aqueous solution of glycerol at 30 MPa H₂ pressure and 473 K using Rh(CO)₂(acac) and tungstic acid was patented by Celanese corporation. The reaction gave 1,2-PD and 1,3-PD at 20 and 23 % yield, respectively (Che, 1987). Glycerol was hydrogenolyzed using supported Raney-Ni, Ru, Rh and Ir catalysts at 30 MPa H₂ pressure and 533 K giving mainly methane. When supported Raney-Cu was used as a catalyst, the main product was 1,2-PD (Montassier et al., 1988). The use of Pd complexes in glycerol hydrogenolysis was reported to afford 1-propanol as main product (Drent and Jager, 2000) while Ru complexes gave diols in low yield (5%) at lower (5.2 MPa) H₂ pressure (Schlaf et al., 2001).

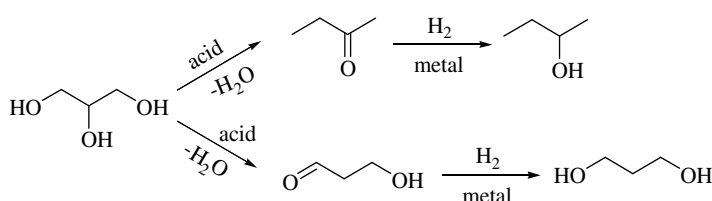
Starting from 2000, the number of publications on hydrogenolysis of polyols in general and glycerol, in particular, has greatly increased. Some of the work focused on mechanistic aspects of the reaction and other targeted the optimization of the reaction conditions and the development of new catalytic materials (Lahr et al., 2005). Several commercial Ni, Cu and noble metal catalysts were tested in a batch reactor using usually water as a solvent and at several MPa of H₂ pressure or in continuous flow reactors. The typical reaction temperature in most cases was 473 K (Chaminand et al., 2004; Perosa and Tundo, 2005; Dasari et al., 2005; Furikado et al., 2007; Schmidt et al., 2010). Most catalysts gave 1,2-PD as main product and higher 1,2-PD yield was obtained when Cu was used as catalyst (Dasari et al., 2005). The formation of C-C cracking products was observed in some catalysts, especially over Ru and Ni (Perosa and Tundo, 2005; Schmidt et al., 2010).

Hydrogenolysis occurred in these catalysts through mainly two mechanisms: dehydration, dehydrogenation and hydrogenation and dehydration and hydrogenation mechanisms (Nakagawa and Tomishige, 2011). 1,2-PD was the main product in both cases due to higher thermodynamic stability of acetol and hydroxylacrolein intermediates, respectively (Scheme 5.1-1). The addition of simple acid (Kusunoki et

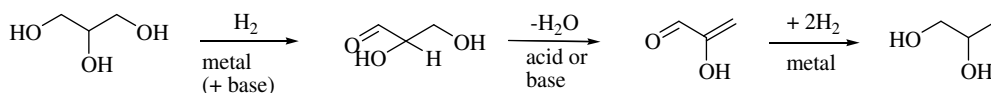
Application of Acid Saponite in Glycidol Hydrogenolysis

al., 2005; Miyazawa et al., 2006; 2007a, b) and base (Feng et al., 2007) catalysts has been proposed to improve activity and 1,2-PD selectivity by promoting dehydration and dehydrogenation pathways, correspondingly. For example, mixing acidic ion exchange resin with Ru/C catalyst significantly increases the activity and the 1,2-PD selectivity. (Kusunoki et al., 2005; Miyazawa et al., 2006; 2007a, b). Feng et al., (2007) reported that the activity and 1,2-PD selectivity of Ru/TiO₂ was improved by addition of an alkali hydroxide.

a) Two-step mechanism (Dehydration and hydrogenation)



b) Three-step mechanism (Dehydrogenation, dehydration and hydrogenation)



Scheme 5.1-1: Two and three steps, mechanisms of glycerol hydrogenolysis. (Nakagawa et al., 2014).

In order to improve the 1,3-PD selectivity in glycerol hydrogenolysis, the use of different types of tungsten compounds was interesting, since they can activate the glycerol by interaction with their hydroxyl groups. Dam et al. (2013) showed that the presence of various types of tungsten based additives (H₂WO₄, H₃PW₁₂O₄₀, H₄SiW₁₂O₄₀) in Pt/SiO₂ and Pt/Al₂O₃ catalysts improved the 1,3-PD selectivity (20-40%). Cu-H₄SiW₁₂O₄₀/SiO₂ catalyst was used in the vapour phase glycerol hydrogenolysis and at the optimized conditions gave 32.1% of 1,3-PD selectivity with 83.4% glycerol conversion (Huang et al., 2009). Some catalysts prepared using WO₃ as a support or modifier resulted in good selectivity to 1,3-PD. For example, mesoporous WO₃-supported Pt (Liu et al., 2012) and Pt-WO₃ co-catalysts supported on ZrO₂ (Qin et al., 2010) or boehmite (AlOOH) (Arundhathi et al., 2013), displayed higher 1,3-PD selectivity. A recent review by Nakagawa et al., (2014) described the

CHAPTER 5

activation of glycerol using tungsten compounds and other metal oxide as ReO_x or MoO_x as co-catalyst, and subsequently improving the 1,3-PD selectivity.

Rhenium oxide (ReO_x) was tested as modifier of supported Ir and Rh catalysts in glycerol hydrogenolysis, and afforded 1,3-PD in moderate to high yield, being higher (38%) for the Re modified Ir catalyst at 393 K, 8 MPa H_2 pressure after 36 h and in the presence of H_2SO_4 acid (Nakagawa et al., 2010). When the mineral acid was replaced by a solid acid such as Amberlyst 70 at the same reaction conditions, the yield to 1,3-PD was 31% but in 24 h (Nakagawa et al., 2012). Oxides of V, Cr, Mn, W, Ag and Mo were tested as modifiers of Ir catalysts showed some selectivity to 1,3-PD in glycerol hydrogenolysis although the selectivity was lower than that of Ir- ReO_x catalysts (Amada et al., 2011). Pt supported sulphated zirconia “superacid” was used in glycerol hydrogenolysis and gave an impressive 1,3-PD yield of 55.6% at 443 K, 7.3 MPa H_2 pressure, in 2,3-dimethyl-2-imidazolidinone after 24 h (Oh et al., 2011). The authors claimed that the presence of large amounts of Brønsted acid sites favour the removal of the hydroxyl group from the secondary carbon of the glycerol, leading to the formation of 1,3-PD.

In general, the selective hydrogenolysis of glycerol is very difficult and most catalytic systems gives 1,2-PD as main product. As it was described above, the most promising catalysts are those based on expensive noble metals (Nakagawa et al., 2014). Even with these kinds of catalysts, harsh reaction conditions and longer reaction times are required in order to achieve reasonable 1,3-PD selectivity. The area of glycerol hydrogenolysis is still a hot topic and many researchers are working to find better catalytic materials and understand the reaction mechanisms (Nakagawa et al., 2014). Other approaches based on protective group chemistry were reported giving high (72%) 1,3-PD overall yield (Zheng et al., 2013) although the number of steps and the formation of large amount of wastes were not desirable. It was discussed in section 1.3 that glycidol was readily obtained from glycerol (Yoo et al., 2001; Bai et al., 2013) and structurally similar compounds were hydrogenolyzed using various catalysts with selective cleavage of the most sterically hindered C-O bond (Pálinkó et al., 2002). In this thesis the use of glycidol as an alternative substrate to glycerol was proposed.

Application of Acid Saponite in Glycidol Hydrogenolysis

In the literature, the isomerization and hydrogenolysis of various substituted oxirane rings has been reported (Fási et al., 1999; 2000; 2001; Bartók1 et al., 1998a, b), as discussed in section 1.2. The presence of a solid acid catalyst favoured the breakage of the more substituted C-O bond. The hydrogenolysis of tetrahydrofurfuryl alcohol (THFA), a cyclic ether with similar substitution pattern as glycidol, using Ir–ReO_x/SiO₂ (Chen et al., 2012), and Rh–ReO_x/SiO₂ (Liu et al., 2014; Chia et al., 2011), Rh–MoO_x/SiO₂ (Koso et al., 2009; 2012) catalysts has been described. All catalysts afforded 1,5-pentanediol with very high selectivity (>90 %). Dumesic et al., (2011) reported the hydrogenolysis of secondary C-O bonds of several cyclic ethers. The authors claimed that these reactions require a bifunctional catalyst (metal + MO_x).

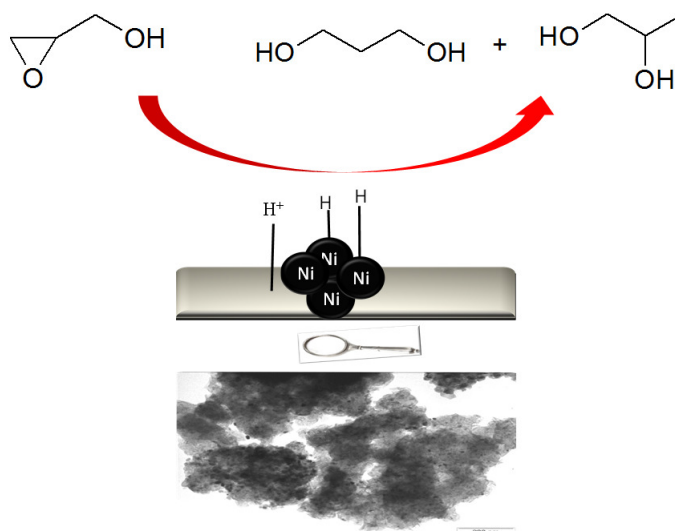
The mechanism of THFA hydrogenolysis with the above Mo modified Rh/SiO₂ or Re modified Ir/SiO₂ and Rh/SiO₂ catalysts involved adsorption of THFA on the surface of protonated ReO_x or MoO_x cluster at the –CH₂OH group to form alkoxide species followed by attack of the alkoxide at the C–O bond neighboring –CH₂ORE/MoO_x by the hydride activated on the active metal. The hydrolysis of the reduced alkoxide releases the 1,5-pentanediol (PeD) (Koso et al., 2009; Chen et al., 2012). Another mechanistic proposal on ReO_x-promoted Rh/C hydrogenolysis of THFA based on experimental results and density functional theory (DFT) calculations (Chia et al., 2011) suggested that hydroxyl groups on rhenium oxide are acidic, due to the rhenium high oxidation state, and these groups are likely responsible for proton donation leading to the formation of carbenium ion transition states. The presence of hydroxyl group on the carbon neighbouring the C-O bond undergoing scission stabilizes the resulting oxocarbenium ion intermediate.

In this chapter, the use of several acid saponites as supports and Brønsted acid source, for the selective hydrogenolysis of glycidol in shorter times and moderate reaction conditions was investigated. In the first section, Ni supported on several saponite samples was studied and in the second section the use of Ni-Cu bimetallic catalyst supported on a conventional saponite for glycidol hydrogenolysis was investigated. In the final section, the influence of various types of metal oxides as modifiers on the activity of Ni-Cu bimetallic catalysts was examined. Several reaction conditions such as; reaction temperature, reaction time, wt % of metal loading, metal

CHAPTER 5

composition, type of modifier and the relative wt % ratio between the modifier and active metal were varied and optimized with a view of improving the activity and selectivity to 1,3-PD.

5.2. Selective hydrogenolysis of glycidol to propanediols using Ni supported on various mesoporous acid saponites as bi-functional catalysts



Abstract

This study explores selective hydrogenolysis of glycidol to 1,3-propanediol using cheap Ni supported on several saponites catalysts. Catalysts prepared with 15 wt % Ni loading showed low conversion and low selectivity to 1,3-propanediol (1,3-PD) and 1,2-propanediol (1,2-PD) due to low metallic area. Conversion and selectivity to propanediols were improved by increasing Ni loading (30 and 40 wt %). The 1,3-PD/1,2-PD ratio increased when propanediols selectivity decreased. Acid activation of glycidol during reaction favored 1,3-PD formation. For catalyst prepared with 40 wt % Ni supported on high surface area (600 m²/g) saponite, an increase in the reaction temperature to 353 and 453 K resulted in higher 1,3-PD/1,2-PD ratio. The highest 1,3-PD yield (29%) and the highest 1,3-PD/1,2-PD ratio (0.97) at total conversion were obtained at 453 K and 1 h of reaction. The 1,3-PD yield was comparable or even higher than that obtained from glycerol using various modified noble metal catalysts.

CHAPTER 5

Introduction

Increased environmental awareness, the depletion and non-renewable nature of petroleum and geopolitical issues initiated the oil and petrochemical industry to look for other renewable options (Baños et al., 2011; Manzano-Agugliaro et al., 2012). Consequently, biodiesel production is interesting to supply renewable liquid fuel and raw materials (Bull, 1999). During biodiesel production, glycerol is co-produced in 10 wt % yield (Pagliaro et al., 2007; Zhou et al., 2008; Katryniok et al., 2010) and its over supply is decreasing its market value. Hence, in order to make the biodiesel production economically feasible, it is important to transform glycerol into added value chemicals. One of the most interesting approaches for glycerol valorization is its hydrogenolysis into 1,2- and 1,3-propanediol (PD). 1,2-PD is a precursor of polyethers, unsaturated polyester resins, hydraulic fluids and antifreeze products (Mane et al., 2011; Gandarias et al., 2012; Sánchez et al., 2012; Xiao et al., 2012). The synthesis of 1,3-PD is engaging since it is used in the production of polyester and polyurethane resins, but the current 1,3-PD conventional production processes are costly (Perosa and Tundo, 2005).

The direct hydrogenolysis of glycerol to 1,3-PD was extensively studied by academia and industries; the main products, in most cases, are the less valuable 1,2-PD and propanols (Jérmôe et al., 2008). Bacterial fermentation of glycerol was reported to give 1,3-PD with high selectivity (Gottschalk and Averhoff, 1992; Himmi et al., 1999; Nagarajan and Nakamura, 1998). Nevertheless, the reaction proceeds slowly in two steps with low product concentration (Kurosaka et al., 2008). Several homogeneous catalysts based on Pd, Rh, and Ru complexes and various acid co-catalysts have been patented or reported for this reaction (Che, 1987; Drent and Jager, 2000; Schlaf et al., 2001). Different heterogeneous catalysts were tested for the reduction of glycerol to 1,3-PD. Rh/SiO₂ catalyst with H₂WO₄ as co-catalyst gave 1,3-PD in 4 % yield at 473 K and 8.0 MPa of hydrogen pressure (Chaminand et al., 2004). Kurosaka et al., (2008) carried out the reduction of glycerol at 453 K, 8 MPa of hydrogen pressure and in 1,3-dimethyl-2-imidazolidone using a Pt/WO₃/ZrO₂ catalyst. This catalyst led to 24 % of yield in 1,3-PD. Recently, Tomishige group

CHAPTER 5

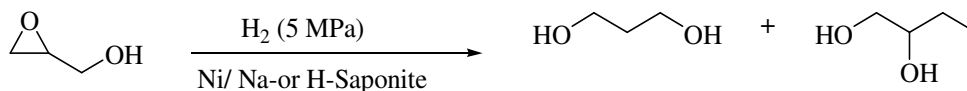
reported a series of supported Rh and Ir catalysts modified with ReO_x and co-catalyzed by various mineral and solid acids (Nakagawa et al.; 2010, 2012; Amada et al., 2011). The authors claimed that in the best case, 1,3-PD was obtained with 38 % of yield, which is the highest reported in the literature. Huang et al. described the vapor phase reduction of glycerol using Cu/SiO_2 in the presence of $\text{H}_4\text{SiW}_{12}\text{O}_{40}$ as an acid co-catalyst (Huang et al., 2009). The reaction, performed at 483 K and 0.54 MPa hydrogen pressure, gave 83 % of conversion with 31.2 % and 22.2 % of selectivity to 1,3-PD and 1,2-PD, respectively.

In general, many of the heterogeneous and homogeneous catalytic systems reported in the literature for the hydrogenolysis of glycerol to 1,3-propanediol involve expensive noble metals, such as Pt, Ir, Rh and Pd (Montassier et al., 1988; Kurosaka et al., 2008; Nakagawa et al., 2010; Huang et al., 2009). Moreover, the reaction with heterogeneous catalysts involves high temperature and/or hydrogen pressure together with long reaction times (Che et al., 1987; Qin et al., 2010). Additionally, the selectivity and yield to 1,3-PD in most cases were low. In order to enhance the 1,3-PD selectivity and yield, other approaches involving non-direct reactions based on protective group chemistry (Zhu et al., 2012) and toxic acrolein intermediates were proposed (Wang et al., 2003). These reactions resulted in 1,3-PD yields of 72 and 60 %, respectively.

Glycidol is an important intermediate in the production of functional epoxides, such as glycidyl urethanes and 2,3-epoxypropyl chloroformate (Girke et al., 1998). Industrially, it is prepared by epoxidation of allyl alcohol by hydrogen peroxide in the presence of vanadium or tungsten catalyst (Grigor'ev et al., 1979; Sienel et al., 1987), or by the reaction of epichlorohydrin with a base (Hutchings et al., 1995; Richey, 1993). Glycidol has been catalytically synthesized from glycerol and cyclic carbonates in high yields (63-83 %), under low pressure and at 413-548 K (Malkemus et al., 1958; Yoo et al., 2001; Gade et al., 2012). Direct synthesis of glycidol from glycerol and dimethyl carbonate was possible by using tetramethylammonium hydroxide ionic liquid ($[\text{TMA}][\text{OH}]$) (Bolívar-Díaz et al., 2013) or a NaAlO_2 solid base catalyst (Bai et al., 2013) at 353–365 K. After 90 min of reaction, the former yielded 78 % and the latter 76 % of glycidol.

Application of Acid Saponite in Glycidol Hydrogenolysis

Whilst there are no literature records for the direct reduction of glycidol to 1,3-PD, hydrogenolysis of structurally similar cyclic ethers has been reported (Koso et al., 2011; Chen et al.; 2012). Acid catalyzed ring opening reaction followed by metal catalyzed hydrogenation of tetrahydrofurfuryl alcohol was proposed using ReO_x -promoted Rh/C (Koso et al., 2011) and Ir– $\text{ReO}_x/\text{SiO}_2$ (Chen et al.; 2012) with good activity ($\geq 47\%$ conversion) and high selectivity to 1,3-PD (97%). In this study, we propose glycidol as an alternative to glycerol to produce 1,3-PD by hydrogenolysis (Scheme 1), using promising catalytic systems based on Ni, a cheap non-noble metal, supported on several saponites. The role of the acidity and surface area of the support was investigated. In addition, the effect of the reaction temperature, Ni loading and the reaction time were studied and optimized.



Scheme 5.2-1: Proposed reaction pathway for the hydrogenolysis of glycidol to propanediols.

Experimental

Preparation of nickel catalysts supported on saponites

Supported Ni catalysts were prepared by incipient wetness impregnation method using 6 H-saponites (labeled as S1-S6) and 2 Na-saponites (labeled as S4[#] and S5[#]) as supports. The saponites were synthesised following a method previously reported by our research group (Gebretsadik et al., 2014; 2015). The synthetic conditions were modified with the aim of preparing saponite supports with a wide range BET areas, porosities and acidities. Two samples, namely S1 and S2, were prepared at pH 8 without template and using microwaves during aging from slurries dilution of 125 and 50, respectively, expressed as $\text{H}_2\text{O}/\text{Si}$ molar ratio. Two other samples were prepared at pH 13, without template and using microwaves (labeled as S3) and conventional oven (labelled as S4) during the aging treatment. Sample S5 was prepared at pH 13 in the presence of surfactant (i.e., dodecyltrimethylammonium chloride) and using microwaves during aging. Sample S6 was synthesized at pH 8, in the presence of surfactant and at 125 of

CHAPTER 5

slurry dilution. Samples, S5[#] and S6[#], which were the Na-form of S4 and S5, respectively, were used for comparison. The samples gave a wide range of properties with respect to their specific BET areas, average pore radius and acidity, as shown between parentheses in Table 5.2-1. This was a result of the different synthesis conditions.

For the catalyst synthesis, 1 g of support (saponite) was kept in a round bottom flask. A 0.5 M nickel nitrate solution in ethanol was used to prepare catalysts with 15, 30 and 40 wt % Ni loading uniformly dispersed on the support. The solvent was removed by rotary evaporation and the resulting samples were dried in an oven at 363 K overnight and calcined at 723 K for 5 h. The resulting solid was reduced in a tubular reactor under hydrogen flow (75 ml/min) at 623 K for 6 h. The catalysts were labelled as Ni(x) support name (S1-S6, S4[#], S5[#]), where the number x represented the wt % of Ni loading. The letter P before the name of the samples stands for the catalyst precursors, which are the calcined samples before reduction.

Catalyst characterization

X-ray diffractogram (XRD) patterns of the powdered catalysts precursors (NiO/saponite) and catalysts were recorded on a Siemens D5000 diffractometer equipped with a CuK α radiation ($\lambda = 1.54 \text{ \AA}$) source. Measurements were done in the 2 θ diffraction range of 5- 70° with an angular step of 0.05° and at rate of 3s per step. Crystalline phases were identified by cross comparison of the diffractogram of the sample with a reference data from international centre for diffraction data (JCPDS files). Integral breadth, estimated by fitting the characteristic reflection of each phase using TOPAS 4.1, was used to calculate the crystallite sizes. In-situ XRD was conducted for the Ni(15)/S4 and Ni(15)/S5 samples to confirm the formation of metallic Ni. The samples were heated in an Anton Paar XRK900 X-ray reactor chamber mounted on the diffractometer, from room temperature to 573 K at a heating rate of 50 K/ min under a flow of 25% H₂ in He. Subsequently, the catalyst was heated in 30 K steps until reaching 773 K. At each step, the sample was kept for 30 min and

Application of Acid Saponite in Glycidol Hydrogenolysis

the XRD pattern was recorded in the 2θ range of $40\text{-}60^\circ$, where the most intense reflections of Ni and NiO appear. The measurements were done at a step size of $0,05^\circ$ and a rate of 2 s per scan using a Bruker-AXS D8 Advance powder X-ray diffractometer equipped with a $\text{CoK}\alpha$ radiation ($\lambda = 1.79 \text{ \AA}$) source.

N_2 adsorption-desorption measurements were performed on an ASAP 2000 at 77 K to determine the specific area and average pore size of the samples. Before measurement, the samples were degassed overnight at 383 K. Specific surface area was determined by applying the BET method and the pore size distribution was estimated from the BJH method.

TEM characterization was done using a JEOL 1011 transmission electron microscope operating at an accelerating voltage of 100 kV and magnification of 200 k. Sample (0.1 mg) was dispersed in ethanol (50 μL) with the aid of an ultrasound, then it was deposited on a carbon coated copper grid and air dried.

Metallic area was determined from H_2 chemisorption experiment using an Autochem AC2920 Micrometric apparatus. In a typical experiment, 0.3 g of pre-reduced sample was re-activated by reduction under hydrogen flow at 623 K for 1 h and flushed with helium (40 ml/ min) for 30 min and cooled down to 313 K. Pulses of hydrogen were injected until saturation. The sample was purged with helium to remove the excess hydrogen. The number of metal active sites was proportional to the number of hydrogen atoms irreversibly chemisorbed and were obtained by the linear portion of the isotherm to zero pressure. The number of surface nickel atoms was calculated by assuming a spherical particles and a stoichiometric factor of 1 corresponding to 1 hydrogen atom per each exposed Ni atom. The Ni surface area and density per atom used in the calculation were, 0.065 nm^2 and 8.9 g/cm^3 , respectively.

An Autochem AC2920 Micrometric apparatus was used to measure the temperature-programmed reduction of the samples. The sample, previously calcined (100 mg), was placed into a tubular reactor and heated from room temperature to 1173 K at a rate of 10 K/min under a flow of 5 vol. % H_2 in argon (50 mL/ min). A TCD detector monitored the amount of hydrogen consumed.

CHAPTER 5

The surface acidity of the catalyst precursors was determined from thermogravimetric analysis (TGA) of the samples treated with cyclohexyl amine (CHA) following the protocol described by Mokaya *et al.* (1997). The total acidity was equivalent to the amount of CHA desorbed in the temperature range of 473-923 K where the sample without CHA treatment did not show any significant mass loss (Gebretsadik *et al.*, 2015). The analysis was conducted in a Labsys Setaram TGA microbalance equipped with a temperature programmable furnace. Each sample was heated under N₂ flow (80 cm³/ min) from 303 to 1173 K at a rate of 10 K/ min. In all experiments, around 100 mg of the catalyst precursors were used.

Catalytic activity test

Hydrogenolysis of glycidol was tested in a 50 ml stainless steel autoclave equipped with an electronic temperature controller and a mechanical stirrer. Glycidol (3.77 mL) was dissolved in sulfolane (30 mL) and purged with nitrogen. A freshly reduced catalyst (1 g) was carefully transferred to the reactor under a positive nitrogen pressure to avoid contact with atmosphere. The reactor was sealed and purged three times with 2 MPa N₂ pressure and three times with 1 MPa H₂ pressure. After performing a leakage test, the temperature of the reaction was set at 393 K and the mixture was stirred at high rpm (600 rpm), which along with the use of powdered catalysts ensured easy mass and heat transfer and avoids internal and external diffusion problems.

The influence of the reaction temperature (333, 423, 453 K) was studied for the Ni(40)S5 catalyst. When the temperature in the electronic control reached the reaction temperature, the hydrogen pressure was adjusted at 5 MPa and the reaction time was started (t_0). The reaction was run for 1, 2 or 4 h, while feeding hydrogen on demand. At the end of the reaction, the mixture was cooled down and gaseous reaction products were collected in a gas sample bag. The reaction products were separated from the catalyst by centrifugation and liquid products were analysed on a Shimadzu GC-2010 chromatograph using SupraWAX-280 capillary column, 1-butanol as internal standard and a FID detector. Some of the liquid samples were submitted for GC-MS

Application of Acid Saponite in Glycidol Hydrogenolysis

analysis to identify unknown products. Conversion and selectivity of the reactions were calculated according to the following equations:

$$\text{Conversion} = \frac{(\text{moles of glycidol } t_o - \text{moles of glycidol } t_f)}{\text{moles of glycidol } t_o} * 100\%$$

$$\% \text{ selectivity }_x = \frac{\text{moles of analyte } x}{\text{moles of glycidol converted}} * 100\%$$

Results and discussion

Characterization of the precursors and catalysts

XRD patterns of the catalyst precursors showed peaks at 2θ of 37.1, 43.3° and 62.9, which were due to the NiO crystalline phase (Figure 5.2-1A). Peaks at 2θ of 19.4, 35.6, 60.5°, observed for all samples, are related to the (110, 020), (201) and (060) reflections, respectively, corresponding to the saponite support. The average NiO crystallite sizes, reported in Table 5.2-1, were calculated from the peak width obtained by fitting the characteristic reflections of NiO using TOPAS 4.1 and applying the Scherrer equation. Accordingly, the catalyst precursors, PNi(15)/S1, PNi(15)/S2, PNi(15)/S5 and PNi(15)/S6 had NiO crystallite sizes of 10, 9, 8 and 7 nm, respectively. Higher NiO crystallite sizes were obtained for the catalyst precursors PNi(15)/S3 (14 nm) and PNi(15)/S4 (15 nm). The NiO crystallite size was higher when increasing the amount of metal loading (30 and 40 wt %) for both S5 and S4 supports (Table 5.2-1). The NiO crystallite size was also larger for the precursors supported on the Na-form of the saponites, PNi(30)/S4[#] (50 nm) and PNi(40)/S5[#] (33 nm), when compared to those supported on the acid forms, PNi(30)/S4 (36 nm) and PNi(40)/S5 (25 nm). As a consequence, the acidity of H-saponites seems to favour the dispersion of the NiO.

After reduction at 623 K for 6 h, the XRD patterns of the catalysts prepared at 15 wt % Ni loading did not show the presence of metallic nickel, except for the Ni(15)S4 catalyst (Figure 5.2-1B). This could be explained by the low reducibility of the metal centers on these catalysts although some re-oxidation during catalyst handling during characterization could not be discarded. In contrast, the pattern of

CHAPTER 5

the Ni(15)/S4 catalyst (Figure 5.2-1B, (a)) exhibited, under the same reduction conditions, peaks at 2θ values of 44.5° and 51.8° corresponding to metallic nickel phase. The catalysts with higher Ni loading (30 and 40 wt %) supported on the H- and Na-form of the S4 and S5 supports showed XRD patterns (Figure 5.2-1C, (b)-(e)) with less intense NiO diffraction peaks with respect to their precursors. Additionally, the reflection of the Ni metallic phase appeared in the diffractograms. The Ni crystallite size in the reduced samples was slightly lower than the size of their NiO precursors. Catalysts prepared with the S4 support had high amount of metallic Ni while the amount of NiO phase was slightly higher and when the Na-form was used as support. For the catalysts with the S5 support (Fig 5.2-1B, (b)-(d)), high amount of metallic nickel was detected in Ni(40)/S5 and Ni(40)/S5#. In contrast, an important amount of NiO remained in Ni(30)/S5. This behaviour will be explained later with the TPR profiles of their precursors.

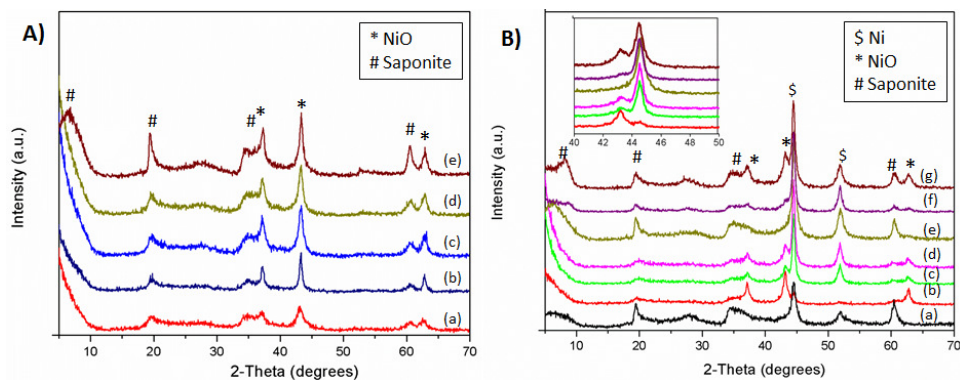


Figure 5.2-1: XRD patterns of A) the catalyst precursors (a) PNi(15)/S3 (b) PNi(15)/S5 (c) PNi(15)/S2 (d) PNi(15)/S1 (e) PNi(15)/S4 and B) the catalysts (a) Ni(15)/S4 (b) Ni(30)/S5 (c) Ni(40)/S5 (d) Ni(40)/S5# (e) Ni(30)/S4 (f) Ni(40)/S4 (g) Ni(30)/S4#.

The N_2 adsorption-desorption isotherms of some characteristic catalyst precursors (i.e., PNi-saponites) are displayed in Figure 5.2-2A-D. All catalyst precursors showed a type IV isotherm according to de Boer's classification and a similar type of hysteresis loop, similar to their corresponding supports, as previously reported (Gebretsadik et al., 2014; 2015). The average pore radius was in the mesoporous range for all the catalyst precursors with values slightly lower than those corresponding to the supports, due to the deposition of the NiO particles

(Table 5.2-1). Catalyst precursors supported on both H- and Na-form of S5 mainly had type D hysteresis loop while catalyst precursors supported on S4 (Figure 5.2-2C) mostly showed type B hysteresis loop, independent of the wt % of Ni loading. Type B hysteresis loop is due to mesoporosity with the presence of oriented lamella particles and D type hysteresis is the result of the presence of disordered lamella particles, which can be correlated with a higher degree of delamination.

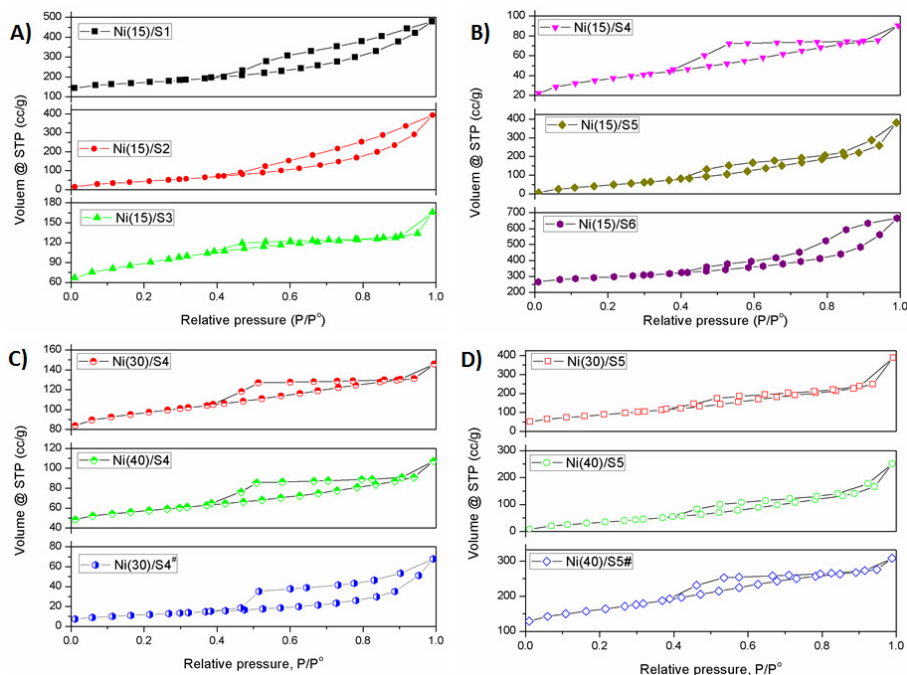


Figure 5.2-2: N₂ adsorption-desorption isotherms of the supported Ni catalysts A) 15 wt % Ni on, S1, S2 and S3; B) 15 wt % Ni on S4, S5 and S6; C) 30 and 40 wt % Ni on H- and Na-S4; and D) at 30 and 40 wt % Ni on H- and Na-S5.

The specific BET areas of the catalyst precursors are presented in Table 5.2-1. All the catalyst precursors had lower area than their corresponding supports, which are shown in parentheses in Table 5.2-1. This surface area decrease can be explained by the occupation of part of the pore volume by NiO. The highest BET area, among samples of 15 wt % Ni loading, was obtained for the catalyst precursor of Ni(15)/S5 (i.e., 376 m²/g) and the lowest for the PNi(15)/S4 (i.e., 137 m²/g). The other catalyst precursors of PNi(15)/S1, PNi(15)/S2, PNi(15)/S3

CHAPTER 5

and PNi(15)/S6 had comparable BET areas (i.e., 211-274 m²/g). The BET areas of the catalyst precursors decreased when increasing the Ni loading. The BET areas of the catalyst precursors PNi(30)/S4[#] (i.e., 87 m²/g) and PNi(40)/S5[#] (i.e., 203 m²/g) were lower than those supported on the H-forms, PNi(30)/S4 (i.e., 126 m²/g) and PNi(40)/S5 (i.e., 229 m²/g). This could be explained by the assisted dispersion of the NiO by the acid centres of the support. More details about this effect will be discussed later.

TEM images of catalyst precursors and catalysts were obtained for all samples prepared with S4 and S5 supports. Typical TEM images of several catalysts are displayed in Figure 5.2-3A-F. These micrographs showed the lamellar structure of the supports and dark spots that can be assigned to Ni or NiO nanoparticles. The average particle size is indicated in Table 5.2-1. The NiO particles size observed by TEM in the catalyst precursors are also shown in Table 1. The average particle size calculated from TEM analysis was in good agreement with the average crystallite size calculated from XRD measurements for the NiO and Ni particles.

The surface acidity of the different catalyst precursors, in mEq. CHA/ g, is shown in Table 5.2-1. The lowest value was obtained for the catalyst precursor PNi(15)/S2 (i.e., 0.46) among those containing 15 wt % Ni loading. The acidity value of PNi(15)/S6 was intermediate (i.e., 0.66). The other catalyst precursors, PNi(15)/S1, PNi(15)/S3, PNi(15)/S4 and PNi(15)/S5 had comparatively higher acidity values (i.e., 0.82-0.96), the highest being for PNi(15)/S5 and the lowest for PNi(15)/S4. The surface acidity decreased when the Ni content increased, the PNi(30)/S5 and PNi(40)/S5 decreased to 0.67 and 0.59 mEq. CHA/ g sample. A similar drop in acidity was observed for the PNi(30)/S4 (0.63) and PNi(40)/S4 (0.56) catalyst precursors. PNi(30)/S4[#] and PNi(40)/S5[#] catalyst precursors had acidity values of 0.43 and 0.37 mEq. CHA/g, respectively. These lower values are in agreement with the fact that S5[#] and S4[#] supports are in the Na-forms.

The TPR profiles of the catalyst precursors at 15 % metal loading showed the presence of two or three reduction peaks for each sample (Figures 5.2-4A-B) corresponding to different degrees of interaction between NiO and the support. The higher reducibility was observed for the NiO in the PNi(15)/S4 catalyst

Application of Acid Saponite in Glycidol Hydrogenolysis

precursor, with the presence of the main peak at comparatively lower temperature (673 K). In contrast, lower reducibility was observed for the PNi(15)/S1, PNi(15)/S2, PNi(15)/S3 and PNi(15)/S5 catalyst precursors with an important contribution of the reduction peaks between 900 and 1073 K. However, these catalyst precursors presented also reduction peaks between 616 and 748 K associated to NiO particles with higher reducibility. An intermediate reducibility can be assigned to NiO in the Ni(15)/S6 catalyst with an intense peak at 823 K and a shoulder at 701 K.

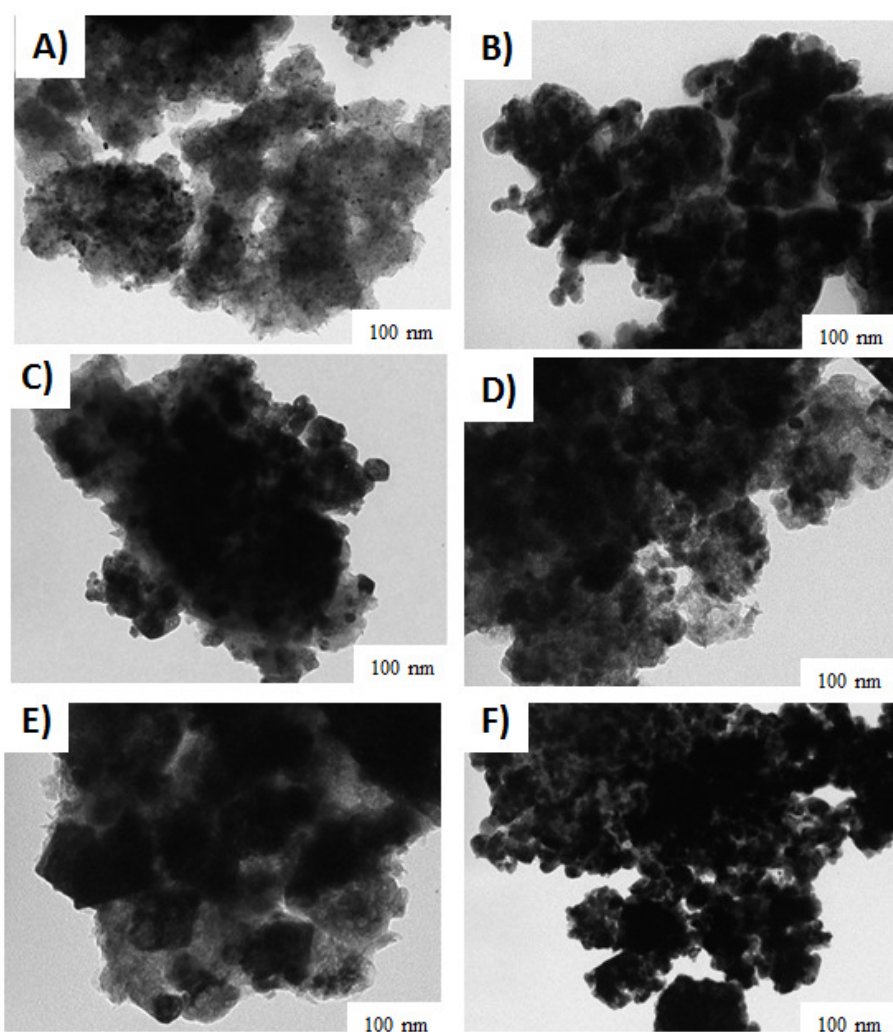


Figure 5.2-3: TEM micrographs of the catalysts A) Ni(15)S5 B) Ni(15)S4 C) Ni(30)S5 D) Ni(40)S5 E) Ni(40)S5# F) Ni(40)S4.

CHAPTER 5

Table 5.2-1: Characterization of the catalyst precursors and catalysts.

Catalyst Precursors	BET (m ² /g)	Average pore radius (Å)	Acidity ^a (mEq./g)	NiO ^b size (nm)	NiO ^c size (nm)	Catalysts	Ni (NiO) ^b size (nm)	Ni (NiO) ^c size (nm)	MSA ^d (m ² / g)
PNi(15)S1	274 (461)	43 (26)	0.85 (0.87)	—	10	Ni(15)S1	—	—	—
PNi(15)S2	265 (394)	49 (39)	0.46 (0.53)	—	9	Ni(15)S2	—	—	—
PNi(15)S3	211 (384)	20 (18)	0.91 (1.03)	—	14	Ni(15)S3	—	—	—
PNi(15)S4	137 (196)	21 (26)	0.82 (1.07)	—	15	Ni(15)S4	13	12	4.0
PNi(15)S5	376 (603)	36 (35)	0.96 (1.02)	9	10	Ni(15)S5	(7)	8	0.9
PNi(15)S6	274 (339)	50 (58)	0.62 (0.66)	—	7	Ni(15)S6	—	—	—
PNi(30)S5	318	38	0.67	18	19	Ni(30)S5	16	17	2.8
PNi(40)S5	229	38	0.59	26	27	Ni(40)S5	23	22	7.5
PNi(40)S5 [#]	203	35	0.37	37	39	Ni(40)S5 [#]	35	33	3.5
PNi(30)S4	126	21	0.63	44	45	Ni(30)S4	40	36	4.1
PNi(40)S4	93	26	0.56	50	51	Ni(40)S4	48	45	3.3
PNi(30)S4 [#]	—	27	0.43	63	65	Ni(30)S4 [#]	52	48	2.4

The values shown in parentheses correspond to the supports. ^a Acidity in mEq CHA/g of sample of the catalyst precursors from TGA of cyclohexylamine (CHA) treated samples. ^b XRD, ^c TEM, ^d Metallic area from H₂ chemisorption in m²/ g of catalyst.

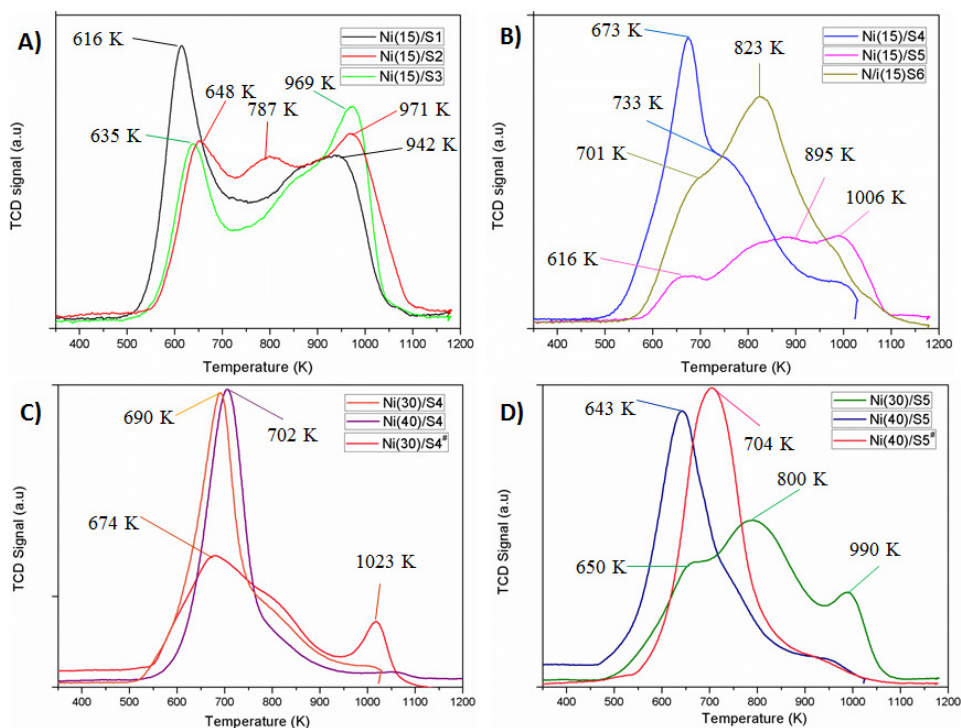


Figure 5.2-4: TPR profile of the catalyst precursors A) 15 wt % Ni loading on S1, S2 and S3; B) 15 wt % Ni on, S4, S5 and S6; C) 30 and 40 wt % Ni loading on the Na- and H-S4; and D) 30 and 40 wt % Ni loading on the Na- and H-S5.

In-situ XRD experiments, plotted on Figures 5.2-5A and 5.2-5B, were conducted for the PNi(15)/S4 and PNi(15)/S5 catalyst precursors in order to gain additional information about the NiO reduction temperature. The reduction of both catalyst precursors started at 623 K, then the amount of metallic nickel increased and the amount of NiO decreased when increasing the reduction temperature. However, the relative percentage of metallic nickel for the Ni(15)/S4 catalyst was higher at each step than for Ni(15)/S5. This agrees with the higher reducibility of the Ni(15)/S4 catalyst precursor, as previously discussed.

The TPR profiles of PNi(30)/S4 and PNi(40)/S4 catalyst precursors (Figure 5.2-4C) showed a symmetric peak with a maximum at 690 and 702 K, respectively. This slight difference could be related to the smaller NiO particle size of the former sample (Table 5.2-1). In contrast, the reducibility of the PNi(30)/S5 catalyst precursor was significantly lower than that of PNi(40)/S5, as confirmed

CHAPTER 5

by the shift of the main reduction peak from 643 K to 800 K (Figure 5.2-4D). Moreover, the TPR of Ni(30)/S5 presented peaks at 650 and 990 K corresponding to NiO particles with different degrees of interaction with the support. Catalyst precursors with 30 and 40 wt % of Ni loading, supported on S5, had in general higher reducibility than those supported on S4, with the exception of PNi(30)/S5. These results suggest that the highest BET area of the S5 support favours the dispersion of the Ni particles. The low reducibility of PNi(30)/S5 compared to PNi(30)/S4 might be a consequence of a strong NiO-support interaction in the former catalyst precursor. The metallic area of the catalysts can be correlated with the reducibility of their corresponding catalyst precursors and the resulting metal particle size. Thus, the catalyst with the highest metallic area was Ni(40)/S5 (7.5 m²/g). The metallic area of the Ni(30)/S5 catalyst was lower (2.8 m²/g) due to its low reducibility. Finally, the metallic areas of Ni(30)/S4 and Ni(40)/S4 were 4.1 and 3.3 m²/g, respectively. These values are in agreement with the increase of Ni particle size in the sample with higher Ni loading.

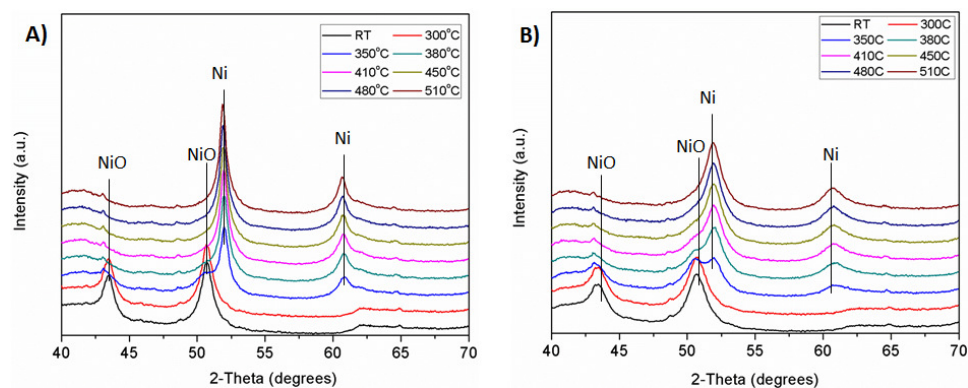


Figure 5.2-5: In-situ XRD profiles in dynamic conditions and under reducing atmosphere for the catalysts A) Ni(15)/S4 and B) Ni(15)/S5.

For the PNi(40)/S5[#] and PNi(30)/S4[#] catalyst precursors, the reducibility was lower than for the of PNi(40)/S5 and PNi(30)/S4 ones, respectively. This could be most likely related to the higher NiO particle size when supported on Na⁺-saponite (Table 5.2-1). We have discussed earlier that the acid centres on a protonated saponite had a higher dispersion capacity than Na⁺. The XRD corresponding to the Ni(30)/S4, Ni(30)/S4[#], Ni(40)/S5 and Ni(40)/S5[#] catalysts are shown in Figure

5.2-1B. The relative amounts of NiO and Ni phases observed by XRD were in agreement with the TPR results and the H₂ chemisorption measurements.

Catalytic activity: Effect of the support

The catalytic activities of all the catalysts studied in this work are presented in terms of conversion, 1,2- and 1,3-PD selectivity and 1,3-PD/1,2-PD ratios. It was not possible to report to activity in terms of TOF or other more informative activity parameters. This was because the reactions in one hand involves both acid and metal sites and on the other hand competitive reactions involving metal or acid sites were thought to be involved making reporting activity report in terms of TOF meaningless.

Table 5.2-2 summarizes the catalytic results for the hydrogenolysis of glycidol using catalysts with 15 wt % Ni loading supported on various acid saponites. All catalysts showed comparable moderate activities (conversion, 33-48 %) and low selectivity to propanediols (1,2-PD + 1,3-PD) (20-46%) except the Ni(15)/S4 catalyst, which presented high selectivity towards propanediols (97%). For this catalyst, the selectivity to 1,2-PD and 1,3-PD at 44% of conversion was 74% and 23%, respectively. For all catalysts, the selectivity to 1,2-PD was higher than for 1,3-PD. The highest 1,3-PD/1,2-PD ratios were obtained for the Ni(15)/S3, Ni(15)/S5 and Ni(15)/S6 catalysts with 0,78, 0,79 and 0,83, respectively. The selectivity to undesired products (named as others in Table 5.2-2) was, in general, high. These other products were propanol and those resulting from the condensation between glycidol and PDs, according to GC-MS analysis. In fact, the formation of similar condensation reaction products was reported between aldehydes or ketones and diols on solid acid catalysts (Schlaf, 2006). We cannot discard the contribution of other products resulting from C-C cleavage or polymerization that cannot be detected in the chromatogram.

Two different catalytic reactions compete in the glycidol transformation: the metal catalysed hydrogenolysis to propanediols and the acid and metal catalysed secondary reactions to side-products. The differences in conversion were not

CHAPTER 5

important and do not seem to be related to differences in the surface area. The catalyst with the lowest BET surface area, Ni(15)S4 (137 m²/g), showed 44% of conversion and Ni(15)/S5 catalyst, with the highest area (376 m²/g), showed 46% of conversion. Probably, the low conversion obtained for all catalysts (33-48%) was a result of the low activity of the metal and acid sites at 393 K. In these catalysts, the selectivity to propanediols can be directly linked to the reducibility of the catalyst precursor. In this way, the Ni(15)/S4 catalyst with the highest reducibility and metallic area (4.0 m²/g) was the most selective to propanediols (i.e., 97 %). The other four Ni(15)/S1, Ni(15)/S2, Ni(15)/S3 and Ni(15)/S6 catalysts presented propanediols selectivity between 30 and 46%.

Table 5.2-2: Catalytic activity test results about the effect of the support.

Catalyst	Conversion (%)	Selectivity (%)			1,3-PD/ 1,2-PD	1,3-PD yield (%)
		1,3-PD	1,2-PD	Others		
Ni(15)/S1	48	14	21	65	0.67	6.7
Ni(15)/S2	46	17	29	54	0.59	7.8
Ni(15)/S3	33	14	18	68	0.78	4.6
Ni(15)/S4	44	23	74	3	0.31	10.1
Ni(15)/S5	46	13	17	70	0.76	6.0
Ni(15)/S6	45	9	11	80	0.82	4.0

The precursors of these catalysts showed significant reduction peaks at low and high temperature. The 1,3-PD/1,2-PD ratio increased when the selectivity to propanediols decreased. Considering that the lower propanediols selectivity corresponded to the catalyst with the highest number of acid sites, some contribution of those in the hydrogenolysis of glycidol to 1,3-PD could be expected. We propose that the hydrogenolysis reaction can follow two different mechanisms. In the first one, a Brønsted acid activation of glycidol through the O in the cyclic ether takes place and is followed by metal catalysed hydrogenation in the C2 and C3 carbons of the glycidol (Chia et al., 2011). The other involves a direct hydrogenation on the C3 position, without acid activation. In the former

Application of Acid Saponite in Glycidol Hydrogenolysis

mechanism, the products are 1,2-PD and 1,3-PD whereas in the later case, 1,2-PD is the main product.

The highest selectivity of the Ni(15)/S6 catalyst to other side products suggests that the support acidity is not the only one factor to be considered, since S6 is not the support with the highest acidity. Low reducibility of NiO in the PNi(15)S6 precursor should have some contribution to the formation of undesired products.

Influence of metal loading and support acidity

The Ni(15)/S5 and Ni(15)/S4 catalysts were identified as promising as they had a high 1,3-PD/ 1,2-PD ratio (i.e., 0.76) and a high 1,3-PD selectivity (i.e., 23%), respectively. Additionally, the BET areas were the highest (i.e., 603 m²/g) for the S5 support and lowest (i.e., 196 m²/g) for the S4, with comparable acidity values (~ 1.0 mEq/g). Hence, we did further studies on these supports to establish the effect of surface area and acidity of the support at higher Ni loading (30 and 40 wt %). Some catalysts were also prepared with the supports in the Na-form and their catalytic activities were evaluated.

The catalytic activities of the catalysts supported on S4 and S5 at 30 and 40 wt. % Ni loading were higher than those obtained for the catalysts with 15 wt % Ni loading (Table 5.2-3). Almost total conversion was obtained for the catalyst supported on the H-form of the S4 and S5 supports at 30 and 40% Ni loading (Table 3). However, lower conversion (i.e., 73%) was obtained for the catalyst supported on the Na-form of S5. The selectivities towards propanediols (1,3-PD + 1,2-PD) were higher than those obtained for the corresponding catalysts with 15 wt % Ni loading. The diol selectivities increased with the Ni loading on the catalysts supported on S4 (78% for Ni(30)/S4 and 95% for Ni(40)/S4). In contrast, for S5 the opposite effect was observed (84% for Ni(30)/S5 and 78% for Ni(40)/S5). The catalysts with the Na-form of the supports increased the selectivity towards propanediols. The selectivity to 1,3-PD was higher for the catalysts prepared at higher Ni loading supported in S5 (20-25%). The 1,3-PD/

CHAPTER 5

1,2-PD ratios were lower at 30 and 40 wt % Ni loading than at 15 wt % Ni loading. Clearly, the catalysts supported on S5 gave higher 1,3-PD/1,2-PD ratios than that supported on S4. Additionally, the Ni(40)/S5 catalyst presented the highest yield to 1,3-PD among all the catalysts investigated in this work (i.e., 26%).

With respect to the selectivity to propanediols (1,2-PD + 1,3-PD), the most important differences were observed between Ni(40)/S4 with the 95% of diol selectivity and Ni(30)/S4 and Ni(40)/S5 with around 78% selectivity. These differences could be explained considering the metallic area of the three catalysts, 3.3, 4.1 and 7.5 m²/g, for Ni(40)/S4, Ni(30)/S4 and Ni(40)/S5, respectively. Higher nickel metallic area should involve higher metallic activity, increasing the hydrogenolysis capacity of Ni, but also its hydrogenating capacity (Jiménez-Morales et al., 2012), and consequently, favouring the C-C cracking. This will be more important in catalyst Ni(40)/S5 with the highest metal area. For catalyst Ni(30)/S4 the presence of higher amount of acid sites should be also taken into account (Table 5.2-1) to explain the increase in the % selectivity to others. In consequence, the presence of more active catalysts could suppose a negative effect on the propanediols selectivity.

Table 5.2-3: Catalytic activity results on the influence of metal loading and support acidity.

Catalyst	Conversion (%)	Selectivity (%)			1,3-PD/1,2-PD	1,3-PD yield (%)
		1,3-PD	1,2-PD	Others		
Ni(30)/S4	100	11	67	22	0.16	11
Ni(40)/S4	100	13	82	5	0.16	13.0
Ni(30)/S4 [#]	99	10	74	16	0.13	9.9
Ni(30)/S5	93	23	61	16	0.38	21.4
Ni(40)/S5	100	26	53	21	0.49	26
Ni(40)/S5 [#]	73	20	64	16	0.31	14.6

Ni(30)/S5 catalyst with metallic area of 2.8 m²/g presented 84% of selectivity to propanediols with lower selectivity to undesired products, and hence it had lower cracking capacity than the Ni(40)/S5 catalyst. The results of 1,3-PD selectivity and 1,3-PD/1,2-PD ratio suggest again that the differences can be

Application of Acid Saponite in Glycidol Hydrogenolysis

related to an acid activation of glycidol in the hydrogenolysis process as commented in the previous section. Considering the loss of acid sites when increasing the wt % of Ni, the acid activation should be lower. This could explain the lower 1,3-PD/1,2-PD selectivity ratio observed for catalysts with the 30 and 40 wt % Ni loading with respect to those with 15 wt % Ni. This decrease was more important for the catalysts prepared with the support with lower area (S4). Probably, the access of glycidol to the acid activation was more hindered. From this analysis we can suggest that 1,3-PD formation can be related to a balanced interplay between the acid and metal function of the catalysts.

The beneficial effect of the acid sites was observed by analysing the catalytic activity of the Na-form, Ni(30)/S4[#] and Ni(40)/S5[#] catalysts. These catalysts presented lower conversions and selectivities to 1,3-PD in comparison to their corresponding catalysts prepared with the H-form of the supports. This catalytic behaviour can be correlated with the lower acidity of these catalysts together with their lower metallic area due to their higher nickel particles size. This behaviour confirms again the contribution of acidity in the 1,3-PD formation.

Reaction was performed using Ni(40)/S5 as a catalyst, at 393 K and by keeping all the other conditions constant as in the previous reactions. After 4 h, the reaction was stopped, cooled down and filtered under N₂ atmosphere. The filtrate was put into a batch reactor along with the same amount of glycidol reactant as in the original catalysed reaction. The mixture was purged and heated to 393 K under the same H₂ pressure (5 MPa) and allowed to run for 2 h. At the end of the 2 h, the reaction was stopped cooled down and the mixture was analysed. The reaction did not show detectable conversion, proving that the reaction is catalysed by the solid catalyst and the contribution of homogeneous reaction by a leached catalyst material was not important.

Optimization of the reaction temperature and time

After screening the catalytic materials, the influence of the reaction temperature and time was studied with the most promising, Ni(40)/S5 catalyst.

CHAPTER 5

The effect of the reaction temperature on the hydrogenolysis of glycidol was investigated at 353, 393, 423 and 453 for 4 h. The results, in Figure 5.2-6, revealed that at 353 K, moderate conversion (46 %), high diol selectivity (84 %) and the lowest 1,3-PD/ 1,2-PD ratio (i.e., 0.21) was obtained. When the reaction temperature was increased to 393 K or higher, total conversion was obtained. The diol selectivity decreased to 78% with higher 1,3-PD/ 1,2-PD ratio (i.e., 0.49) at 393 K compared to the results obtained at 353 K. Further increase of the reaction temperature up to 423 and 453 K decreased the propanediol selectivity to 56 and 52%, respectively. This decrease of diol selectivity can be considered similar to that observed in the previous section when catalysts with higher metallic activity were used. However, the reaction temperature had a positive effect on the 1,3-PD/1,2-PD ratio and increased up to 0.88 at the highest reaction temperature.

As commented in previous sections, we proposed that the hydrogenolysis reaction follows two different mechanisms. One of them could be by the acid activation of glycidol, favoring the 1,3-PD formation. This mechanism is favored when the activity of the acid sites is higher. At higher reaction temperatures, the contribution of this mechanism is most likely higher, with a subsequent increase of the 1,3-PD/1,2-PD ratio. In order to explain the differences observed in diol formation, we studied the contribution of the acid catalyzed side reactions at high (453 K) and low (393 K) reaction temperatures. First, we performed the reaction with glycidol at 453 K using the PNi(40)S5 catalyst precursor as a sample without metal sites. The reaction led 52 % of conversion after 2 h. The products identified were propanal and different geometric and stereo-isomers of di(hydroxymethyl)-1,4-dioxane. Considering the low peak areas of the identified products, we assumed that some reaction products were not detected in the GC analysis. They should be mainly gaseous products due to cracking. However, we cannot discard the possible formation of some condensation or polymerization products that could be retained in the catalyst or that have not been detected by GC due to their higher retention time.

The importance of the acid catalyzed reaction at lower temperature was evaluated at 393 K using the PNi(15)/S5 catalyst precursor, a material with higher amounts of acid sites. The reaction gave only 18 % of conversion after 4 h suggesting that acid

catalyzed reactions (condensation, polymerization or C-C cracking) are less important at 393 K, in line with our thoughts. These experiments with the catalyst precursors support the contribution of acid sites in lowering the PD selectivity due to undesired cracking and polymerization reactions. Finally, we performed a blank test in the absence of catalyst using glycidol at 453 K for 2 h under 5 MPa hydrogen pressure. The conversion was very low (< 2%) and rule out an effect of the autoclave and thermal reaction on the experimental results.

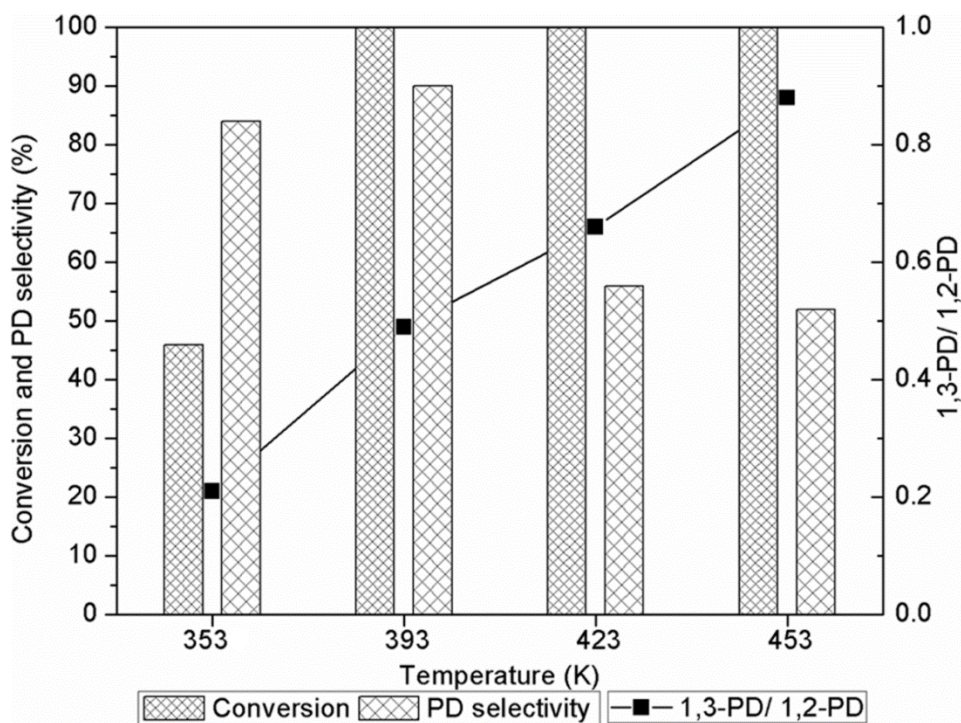


Figure 5.2-6: Influence of the reaction temperature on the hydrogenolysis of glycidol using the Ni(40)/S6 catalyst.

Considering the decrease of diol selectivity after 4 h of reaction at 453 K, we aim to understand the effect of the reaction time. For this reason, we performed the reaction at the same conditions but at shorter reaction time (1 and 2 h) using the Ni(40)/S5 catalyst. After the first hour, total conversion was already obtained with 30 and 29 % selectivities to 1,2-PD and 1,3-PD, respectively. After 2 and 4

CHAPTER 5

h, the 1,2-PD and 1,3-PD decreased slightly to 29 and 28 % and 26 and 24 %, respectively. This decrease in the diol selectivity values could be explained by some contribution of the acid sites, over hydrogenolysis or hydrogenation side reactions of propanediols. The reactivity of the PDs was evaluated in a stability test. In the experiment, an equimolar mixture of 1,2-PD and 1,3-PD with total concentration equivalent to the initial glycidol concentration was used at 453 K, 50 bar H₂ pressure and with Ni(40)/S5 as catalyst. The reaction led 13 % of conversion with respect to 1,2-PD and 10% of conversion with respect to 1,3-PD after 2 h of reaction. This study showed that shorter reaction times are beneficial to avoid the over hydrogenolysis of propanediols to undesired products.

At the optimum reaction condition, 453 K and after 1 h, the reaction gave 30 % and 29 % selectivity, respectively, for 1,2-PD and 1,3-PD yield with total conversion. The yield of 1,3-PD (i.e. 29%) is comparable or higher than the yield reported by other authors for the direct hydrogenolysis of glycerol using noble metal based catalysts and reactions performed at higher temperature (>453 K) and longer time (8-24 h) and high H₂ pressure (Che, 1987; Drent and Jager, 2000; Schlaf et al., 2001; Chaminand et al., 2004; Nakagawa et al., 2010; Amada et al., 2011; Nakagawa et al., 2012).

Conclusions

The selective hydrogenolysis of glycidol to propanediols was evaluated by using Ni catalyst supported on various mesoporous acid saponites. Acidity and BET area of the support played an important role in Ni dispersion. The presence of high acidity resulted in a strong NiO-acid sites interaction rendering NiO species less prone to reduction. The catalysts with 15% of Ni presented the lowest metallic area and the highest acidity. This favored side reactions leading to the formation of undesired products. The selectivity to propanediols (1,2-PD + 1,3-PD) was higher when increasing the metal area and when decreasing acidity. The 1,3-PD/1,2-PD ratio was, in general, opposite to the diols selectivity. The contribution of an acid activation of glycidol during the hydrogenolysis reaction

Application of Acid Saponite in Glycidol Hydrogenolysis

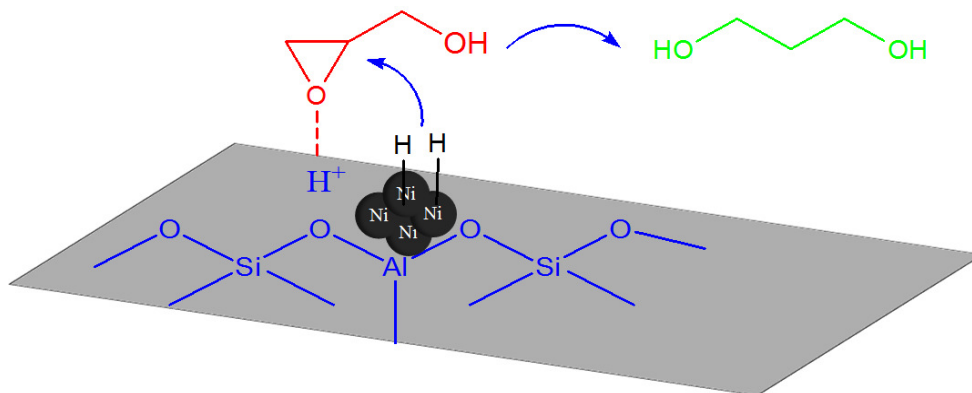
could favor the 1,3-PD formation. An optimum distribution of metal and acid centers was crucial to improve the 1,3-PD formation.

The increase in the amount of Ni loading to 30 and 40 wt % led to higher catalytic activity (93-100%) with higher diols selectivity values compared to those of the catalysts at 15 wt % Ni loading. In these catalysts, however, the 1,3-PD/1,2-PD ratio decreased. The catalysts within the Na-forms of the S4 and S5 supports gave even lower 1,3-PD/1,2-PD ratio corroborating the importance of the acid sites in the selective formation of 1,3-PD. High yield to 1,3-PD (26%), was obtained for Ni(40)/S5 catalyst after 4 h of reaction at 353 K. The catalytic activity of Ni(40)/S5 catalyst increased from 46 % at 353 K to total conversion at higher temperatures (393, 423 and 453 K). The 1,3-PD/1,2-PD ratio also increased with temperature, but the PDs selectivity decreased due to both Ni and acid catalyzed side reactions. Total conversion and higher yield to 1,3-PD (29%) was obtained when the reaction was performed at 453 K in 1 h. This yield was comparable to the result obtained for glycerol hydrogenolysis using noble metal catalysts at harder conditions.

Acknowledgments

The authors are grateful for the financial support of the Ministerio de Economía y Competividad of Spain and FEDER funds (CTQ2011-24610). The authors are indebted to Prof. Bert Weckhuysen for his fruitful scientific discussion on the catalytic results. The authors also appreciate the help of Ramon Oord and Arjan den Otter, from the Inorganic chemistry and catalysis group of Utrecht University, in performing H₂ chemisorption of samples.

5.3. Liquid phase hydrogenolysis of glycidol over Ni-Cu bimetallic catalysts supported on acid saponite



Abstract

The liquid phase hydrogenolysis of glycidol was evaluated on various acid saponite (S) supported Ni-Cu bimetallic catalysts. Characterization of the catalyst showed that Ni and Cu are in intimate contact. XRD measurements revealed the formation of an alloy. H_2 chemisorption results showed that the Ni metallic area progressively decreased with an increase in the wt % ratio of Cu. The catalytic performance of the reduced samples was tested on a batch reactor at 393 and 453 K. In the presence of high metal activity (higher Ni wt %), the formation of 1,2-PD outweighed, while high acid activity led to the formation of dimerization and oligomerization reaction products. The addition of Cu and the increase of the reaction temperature decreased the diol formation but boosted the 1,3-PD/1,2-PD ratio. We suggest that this is due to an improvement of the collaborative effect between metal Ni and H^+ .

Introduction

Biomass valorization is crucial for the sustainability of our society (Fernando et al., 2006 and Ragauskas et al., 2006) and aids to solve the environmental impact related to the use of fossil fuel (Corma et al., 2007 and ten Dam and Hanefeld, 2011). One of the most explored valorization processes at the academic and industrial level is the conversion of renewable oils into biodiesel. Additionally, this chemical process produces glycerol in 10 % yield. The rapid growth of the biodiesel industry results in a glycerol oversupply, which negatively impacts the market value of this product. (Huber et al., 2006; Pagliaro et al., 2007; Behr et al., 2008; Zhou et al., 2008; Ryneveld et al., 2011) In order to make the biodiesel industry more economically competitive, various innovative processes were developed to transform glycerol to other added value chemicals. (Zhou et al., 2008; Qin et al., 2010)

Selective hydrogenolysis of glycerol to 1,3-propanediol (1,3-PD) is a valorization route especially attractive due to the high cost of the current industrial processes. (Kraus, 2008) 1,3-PD is an important monomer in the synthesis of polypropylene terephthalate (PPT) (Julien et al., 2004), a polymer that displays excellent chemical resistance, light stability, elastic recovery and dyeability. (Caley and Everett, 1967 and Zimmerman and Isaacson, 1974) The hydrogenolysis of glycerol to 1,3-PD has been attempted by different research groups. (Chaminand et al., 2004; Akiyama et al., 2009; Gandarias et al., 2010; Gong et al., 2010; Nakagawa et al., 2010; 2014; Qin et al., 2010) The most interesting results in terms of 1,3-PD yield were obtained when expensive noble metal based catalysts were used at harsh reaction conditions and long reaction time. (Chaminand et al., 2004; Gong et al., 2010; Nakagawa et al., 2010; Qin et al., 2010).

Glycidol could be an alternative to glycerol for propanediol production since is a highly reactive molecule that could be readily obtained in one step from the reaction of glycerol and dimethyl carbonate. (Yoo et al., 2001; Bai et al., 2013) Epoxides can undergo ring opening reactions in the presence of solid acid (Fási et al., 1999; 2000; 2011) and supported metal catalysts. (Bartókl et al., 1998; Pálinkó et al., 2002a, b) Isomerization and hydrogenolysis of epoxides to aldehydes, ketones or alcohols using

CHAPTER 5

different supported metal catalysts has been described. (Bartókl et al., 1998; Pálincó et al., 2002a, b) Tetrahydrofurfuryl alcohol (THFA) was hydrogenolyzed to 1,5-pentanediol using Mo and Re modified Rh (Koso et al., 2008; 2009; Chen et al., 2010) and Re modified Ir (Chen et al., 2012) catalysts supported on SiO₂ or C. Dumesic et al. (2011) reported the hydrogenolysis of secondary C-O bonds of several cyclic ethers. The authors claimed that these reactions require a bifunctional catalyst. In this way, acidic O-H groups on ReOx associated Rh activates the cyclic ether.

Saponite, $M_{x-y/n}[(Mg_{6-y}Al_y)^T(i_{8-x}Al_x)^O.O_{20}(OH)_4].nH_2O$, is a trioctahedral clay of the smectite group containing an octahedral (O) sheet of MgO between tetrahedral (T) sheets of SiO₄. Isomorphous substitution of Si by Al generates a negative layer charge which should be compensated by interlayer hydrated cations (M^{n+}). When the interlayer cation is H⁺, the saponite has Brønsted acidity (Vogels et al., 2005) and can be an interesting support with acid properties.

The use of Ni as a cheaper alternative to noble metals in the hydrogenolysis of biomass-derived polyols has attracted a great attention. (Saxena et al., 2005; Zhou et al., 2012; Ye et al., 2012) Ni has high hydrogen activation capacity and could be used for the production of alcohols from epoxides. (Gandarias et al., 2012) The mechanism of the ring opening depends on several factors, such as the presence of Brønsted acidity and type of metal. (Chen et al., 2012) The control of the reaction pathway will be fundamental for the production of 1,3-PD or 1,2-PD from glycidol. The Ni activity is strongly dependent on Ni ensemble size. (Ponec, 2001) The addition of Cu, as a second metal, can be a good option to decrease the Ni particle size, since the Cu can reduce the ensemble size of Ni by formation of an alloy. (Gandarias et al., 2013) Cu is a less-active metal but can be an efficient catalyst for a selective C-O bond hydrogenolysis. (Sato et al., 2008; Li et al., 2009). The study of Ni-Cu bimetallic catalysts is of interest for understanding the effect of Cu on Ni catalysts on the selectivity to 1,2-PD and 1,3-PD from glycidol using an acid support.

The aim of this work was to investigate the catalytic activity of acid saponite-supported Ni-Cu bifunctional catalysts for the hydrogenolysis of glycidol. Catalysts with different wt % ratios of Ni and Cu were prepared and their catalytic activity was

tested. Some selected catalysts were tested at higher reaction temperature to see the effect of this parameter on the catalytic results.

Experimental

Preparation of supported catalysts

Supported Ni, Cu and Ni-Cu catalysts were prepared by the incipient wetness impregnation method using H-saponite (S), previously reported (Gebretsadik et al., 2015) by our research group, as support. For catalyst preparation, 1 g of support was introduced into a round bottom flask. A calculated volume of 0.5 M nickel or copper nitrate solution in ethanol to make supported catalysts at 30 wt % Ni or Cu loading was poured uniformly over the support. For the Ni-Cu bimetallic catalysts, calculated amounts of $\text{Ni}(\text{NO}_3)_2$ and $\text{Cu}(\text{NO}_3)_2$, to make a Ni-Cu catalyst at Ni:Cu wt % ratio (9:1), (6:1), (3:1), (1:1) and (1:3) were dissolved in ethanol to make a 0.5 M solution with respect to the total moles of the metal precursors. The solution was transferred uniformly into the round bottom flask with the support. The solvent was removed by rotary evaporation. The samples were dried in an oven at 363 K overnight, calcined at 723 K for 5 h and reduced in a tubular reactor under hydrogen flow (75 mL/ min) at 623 K for 6 h. The monometallic catalysts were labelled as Ni/S and Cu/S. In the case of the bimetallic catalysts, the nomenclature appeared as Ni-Cu(X:Y)/S where X, Y represented the relative wt % ratio of Ni and Cu, respectively. One more sample, Ni-Cu(6:1)**/S, was prepared at 40 wt % of total metal loading in a Ni:Cu wt % ratio of 6:1, for comparison. The catalysts precursors, i.e., the materials before reduction, were labeled with a P at the beginning of the name.

Catalyst characterization

X-ray diffraction (XRD) patterns of the powdered catalyst samples were recorded on a Siemens D5000 diffractometer equipped with a $\text{CuK}\alpha$ radiation ($\lambda \approx 1.5406 \text{ \AA}$) source. Measurements were done in $5\text{-}70^\circ$ 2θ diffraction angles, with an angular step of 0.05° and at a rate of 3s per step. Crystalline phases were identified by cross comparison of the diffractogram of the sample with a reference data from international

CHAPTER 5

center for diffraction data (ICDD, release 2004) files. TOPAS 4.1 software was used to fit the diffractograms with the Rietveld method and the crystal structure of each phase. The average crystallite size was calculated as a mean value from all the diffracted peaks once the instrumental contribution to the peaks width was removed. The cell parameters calculated from the refined diffractogram were used to examine the formation of Ni-Cu alloy and to determine the stoichiometry of constituent metals in the alloy.

N₂ adsorption-desorption analysis of the catalyst precursors and spent catalyst samples were performed on Quadrasorb SI surface analyser at liquid nitrogen temperature (77 K) to determine the BET area, pore volume and average pore size. Before measurement, fresh catalyst precursor samples were degassed overnight at 383 K. The spent catalysts were degassed at higher temperature (573 K) for 3 h in order to remove the high boiling point solvent, sulfolane (b.pt 558 K), used during the catalytic reaction that could not be removed by aqueous washing. Specific surface area was determined by applying the BET method and the pore size distribution was estimated from BJH method.

TEM characterization of the catalysts was done using a JEOL 1011 transmission electron microscope operating at an accelerating voltage of 100 kV and magnification of 200 k. The catalyst powder (0.1 mg) was dispersed in ethanol (50 µL) with the aid of ultrasounds. Then, the suspension was placed on a carbon coated copper grid and air dried.

The temperature-programmed reduction profile of the catalyst precursors was analyzed by an Autochem AC2920 Micrometric apparatus. A sample calcined beforehand (100 mg) was introduced into the sample tube equipped with thermal conductivity detector. The sample was heated from room temperature to 1173 K at a rate of 10 K/min under a flow of 5% H₂ in argon (50 mL/min). The amount of hydrogen consumed was monitored by a TCD detector.

Surface acidity of the catalyst precursors was determined from thermogravimetric analysis (TGA) of their cyclohexylamine (CHA) treated samples following the protocol described by Mokaya et al. (1997) The total acidity was equivalent to the amount of cyclohexylamine desorbed at the temperature range of 473-923 K in which

Application of Acid Saponite in Glycidol Hydrogenolysis

the sample without cyclohexylamine treatment did not show any significant mass loss. (Gebretsadik et al., 2015) The samples without cyclohexylamine treatment were analysed in the same way and used as a blank to account for potential mass loss unrelated to the basic probe molecule. The analysis was conducted in a Labsys Setaram TGA microbalance equipped with a programmable temperature furnace. Each sample was heated under N₂ flow (80 cm³/ min) from 303 to 1173 K at a rate of 10 K/ min. In all experiments, the amount of sample used was around 100 mg.

The amount of organic material deposited on the spent catalyst was determined by TG analysis. In the analysis, the spent catalyst was dried at 573 K under vacuum for 3 h in order to remove the adsorbed sulfolane solvent used in the catalytic reaction. About 100 mg of the dried samples was put in the sample holder and heated from 303 to 1173 K under air flow (80 cm³/ min) at a heating rate of 10 K/ min. The same temperature range, as in the acidity determination (523-923 K), was used to determine the percentage of organic product.

Catalytic activity test

Hydrogenolysis of glycidol was tested in a 50 mL stainless steel autoclave equipped with an electronic temperature controller and a mechanical stirrer. Glycidol (3.77 mL) was dissolved in sulfolane (30 mL) and purged with nitrogen. A freshly reduced catalyst (1 g) was carefully transferred to the reactor under a positive nitrogen pressure to avoid contact with the atmosphere. The reactor was sealed and purged three times with 4 MPa N₂ pressure and three times with 1 MPa H₂ pressure. After performing a leakage test, the temperature of the reaction was set at 393 or 453 K, the stirring at 600 rpm and 1 MPa H₂ was fed. When the temperature in the electronic control reached the final temperature of the reaction, the hydrogen pressure was adjusted at 5 MPa and the reaction time was started (t₀). The reaction was allowed to run for 1 or 4 h while feeding hydrogen on demand. At the end of the reaction (t_f), the reaction mixture was cooled and gaseous reaction products were collected in a gas bag. The reaction products were separated from the catalyst by centrifugation and liquid products were analysed on a Shimadzu GC-2010 chromatograph using a

CHAPTER 5

SupraWAX-280 capillary column, 1-butanol as internal standard and a FID detector. Some liquid samples were submitted for GC-MS analysis to identify the unknown products. Conversion and selectivity of the reactions were calculated according to the following equations:

$$\text{Conversion} = \frac{(\text{moles of glycidol } t_o - \text{moles of glycidol } t_f)}{\text{moles of glycidol } t_o} * 100\%$$

$$\text{Selectivity to } x (\%) = \frac{\text{moles } x * \text{carbon in } x}{\text{moles of glycidol converted} * \text{carbon in glycidol}} * 100\%$$

Results and discussion

Catalytic Precursors characterization

The reducibility of the supported metal oxides was assessed by temperature-programmed reduction. Figure 5.3-1 shows the reduction profiles of the catalyst precursors. The reducibility of a metal oxide depends on many factors, such as the nature of the supported metal, its particle size and its interaction with the support (Carrero et al., 2010). The monometallic Ni catalyst precursor (PNi/S) displayed two reduction peaks: one well-defined peak centered at 770 K and a broad shoulder between 820-1000 K. The lower temperature peak was due to smaller NiO particles whereas the broad peak was assigned to either more aggregated NiO or NiO particles, which had strong interaction with the support. Similarly, PCu/S (Figure 5.3-1 (g)) showed the main reduction peak at 520 K with shoulders at 390-470 and 557 K. The different contributions can be attributed to CuO particles with different size and support interaction. The presence of Cu and an increase in its wt % ratio progressively shifted the main reduction peak to lower reduction temperatures. For PNi-Cu(3:1)/S, another small peak, which was shifted even to lower reduction temperature with respect to the monometallic Cu catalyst, appeared at 490 K. This peak was the main reduction peak for PNi-Cu(1:1)/S and PNi-Cu(1:3)/S. As we will discuss later, this peak could be related to the formation of an alloy. The PNi-Cu(1:1)/S and PNi-Cu(1:3)/S samples also showed peaks that shifted to lower reduction temperatures compared to the monometallic PCu/S catalyst precursor. This could be attributed to

Application of Acid Saponite in Glycidol Hydrogenolysis

the higher reducibility of the smaller copper oxide particles obtained in the bimetallic catalysts. (Shen and Song, 2002; López-Suárez et al., 2008)

The N₂-adsorption results of the support and the catalyst precursors are presented in table 5.3-1. The support (S) had specific BET area of 196 m²/g and pore volume of 0.21 cc/ g. The values of specific BET area and pore volume decreased to 122-112 m²/g and 0.17-0.12 cc/g, respectively, for the supported catalysts precursors prepared at 30 wt % total metal loading. The value of the specific BET area decreased further to 77 m²/g for the catalyst prepared at 40 wt % total metal loading for comparison. This could be attributed to the occupation of part of the pore volume of the support by the metal oxide particles. The decrease of the pore volume was more significant when the wt % of the Ni loading increased. A similar result was reported by Obregón and coworkers (Obregón et al., 2014). They claimed that Ni is preferentially deposited in bigger pores while Cu takes up the external surface.

CHAPTER 5

Table 5.3-1: Characterization results of the catalyst precursors and fresh catalysts.

Support and catalyst precursors	BET (m ² /g)	Average pore radius (Å)	Pore volume (cc/g)	Acidity (mEq. CHA/g)	Catalysts	Metal crystallite size XRD (nm)	Particle size TEM (nm)	Metallic area (m ² /g sample)
S	196	21	0.21	1.33	S	—	—	—
PNi/S	126	21	0.13	1.21	Ni/S	8	15	7.5
PNi-Cu(9:1)/S	129	25	0.13	1.22	Ni-Cu(9:1)/S	12	—	3.4
PNi-Cu(6:1)/S	127	23	0.14	1.22	Ni-Cu(6:1)/S	11	—	2.8
PNi-Cu(3:1)/S	116	29	0.17	1.19	Ni-Cu(3:1)/S	9	14*	2.4
PNi-Cu(1:1)/S	116	27	0.17	1.07	Ni-Cu(1:1)/S	11 (18)	13*	0.4
PNi-Cu(1:3)/S	114	30	0.17	1.03	Ni-Cu(1:3)/S	7 (41)	18*	0.2
PCu/S	112	29	0.18	1.05	Cu/S	62	95	0.1
PNi-Cu(6:1)**/S	77	30	0.15	0.81	Ni-Cu(6:1)**/S	—	—	4.3

* Particle size of the Ni-Cu alloy, ** catalyst at 40 wt % metal loading (other catalysts were prepared with 30 wt % total metal loading) and the values in parenthesis correspond to the Ni-Cu alloys while the other values stand for the Ni or Cu crystallite size.

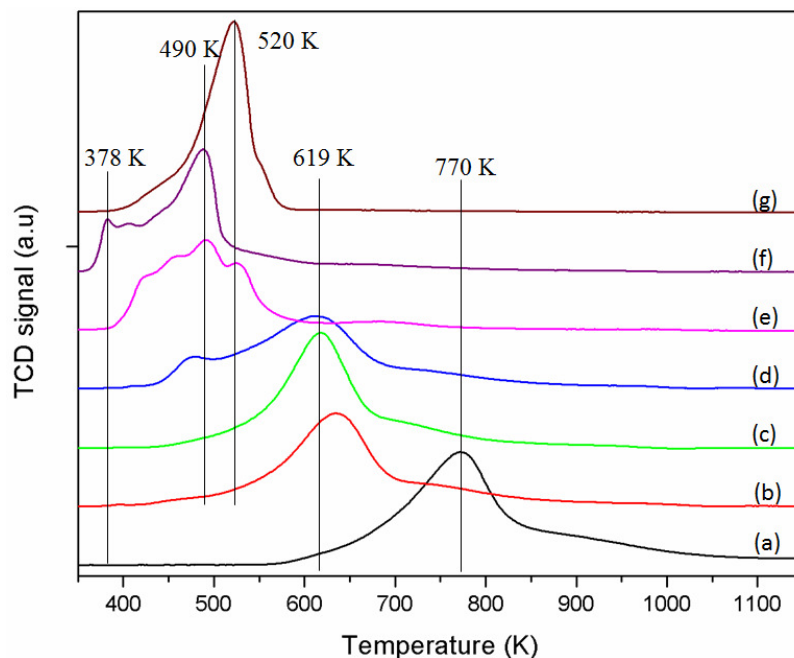


Figure 5.3-1: TPR profiles of all the catalyst precursors (a) Ni/S (b) Ni-Cu(9:1)/S (c) Ni-Cu(6:1)/S (d) Ni-Cu(3:1)/S (e) Ni-Cu(1:1)/S (f) Ni-Cu(1:3)/S (g) Cu/S.

The total surface acidity of all the catalyst precursors (1.03-1.21 mEq CHA/g) was lower than the acidity of the support alone (1.33 mEq CHA/g), as shown in table 5.3-1. The decrease in the acidity of the catalyst precursors could be explained by the coverage of part of the acid sites with the impregnated metal, as confirmed by the lower surface area of the catalyst precursors compared to the support. It was also observed that the surface acidity of the catalyst precursor decreased at higher wt % Cu loading. This could be related to a higher presence of CuO on the external surface. (Obregón et al., 2014)

Characterization of fresh catalysts

The XRD patterns of the catalysts, reduced at 623 K under H₂ flow for 6 h, are displayed in figure 5.3-2. All patterns presented the characteristic saponite reflections at 19.4, 35.6, 60.5°, 2θ, due to (110, 020), (201) and (060) planes, respectively, together with metallic phases. For the monometallic Ni catalyst, Ni/S, reflections appeared at 44.5° and 51.9°, 2θ, corresponding to (111) and (200) planes of metallic

CHAPTER 5

nickel without observing significant amounts of the NiO phase. Cu/S showed reflections at 43.3 and 50.4°, 2 θ , which are assigned to (111) and (200) planes of metallic Cu.

In the case of Ni-Cu bimetallic catalysts, illustrated in Figure 5.3-2 b-f, the position of the reflection peaks were shifted, depending on the wt % ratios of Ni and Cu, to lower 2 θ angles with respect to the peaks of the supported monometallic Ni catalyst. Accordingly, slight comparable shift in the position of the Ni peak at 44.5°, 2 θ was observed for Ni-Cu(9:1)/S and Ni-Cu/(6:1) samples. Catalyst Ni-Cu(3:1)/S showed further shift and the reflection appeared broader. This shift in the position of the peak could be related to the formation of a Ni-Cu alloy, as previously reported. (Gandarias et al., 2013) For the Ni-Cu(1:1)/S and Ni-Cu(1:3)/S catalysts, the peak shift was even more pronounced. Unlike in previous reports (Li et al., 2009; Gandarias et al., 2013) where the Ni-Cu alloy was more enriched with Cu irrespective of the initial metal ratio, in our case, the stoichiometry of the alloy formation was governed by the atomic ratios of Ni and Cu in the samples. This might be the result of the calcination procedure at 723 K for 5 h that favored good mixing of the metals. In catalysts Ni-Cu(1:1)/S and Ni-Cu(1:3)/S, especially in the later sample, some amount of metallic Cu, which did not form an alloy, was also present.

The cell parameters of the samples were plotted against the atomic ratios of Ni, as shown in figure 5.3-2. The cell parameter clearly showed a tendency to decrease as the Ni content of the alloy increased, as expected from the Vegard's law. (West, 1985) As Ni and Cu have the same crystal structure, a continuous solid solution between the two metals can be expected. For catalysts Ni-Cu(9:1)/S, Ni-Cu(6:1)/S, Ni-Cu(3:1)/S and Ni-Cu(1:1)/S, there was a good agreement between the Vegard's law and the cell parameter values determined. This could suggest that the atomic ratios of Ni and Cu in the sample and the stoichiometry of the alloy were almost identical. In sample Ni-Cu(1:3)/S, probably the surface was enriched with Cu, as confirmed by the deviation of its cell parameter to that would be expected from Vegard's law. This might be due to thermodynamic reasons whereby the lower surface free energy of Cu, when compared to Ni, led to an enrichment of Cu in the external surface of the bimetallic catalyst. (Kitla et al., 2013)

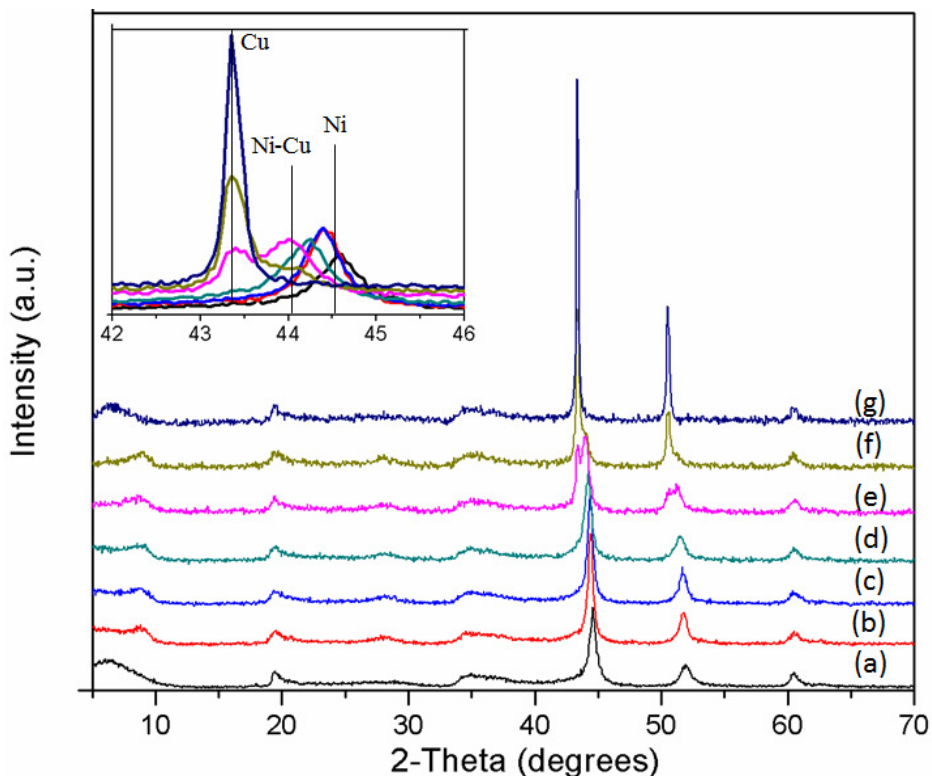


Figure 5.3-2: XRD patterns of a) Ni/S b) Ni-Cu(9:1)/S c) Ni-Cu(6:1)/S d) Ni-Cu(3:1)/S e) Ni-Cu(1:1)/S f) Ni-Cu(1:3)/S g) Cu/S catalysts.

The average crystallite sizes of Ni, Cu or Ni-Cu alloy of the catalysts was determined from their XRD pattern by applying the Scherrer equation (Table 5.3-1). Monometallic Ni and Cu catalysts showed particle sizes of 8 and 62 nm, respectively. Ni-Cu(9:1)/S, Ni-Cu(6:1)/S and Ni-Cu(3:1)/S samples had Ni-Cu alloy particle sizes of 12, 11 and 9 nm, in this order. For the other two samples, Ni-Cu(1:1)/S and Ni-Cu(1:3)/S, two types of particles namely, metallic Cu and Ni-Cu alloy were observed. The average crystallite size of the alloy particles was 11 and 7 and the Cu crystallite size was 18 and 41 nm, correspondingly for Ni-Cu(1:1)/S and Ni-Cu(1:3)/S. These results suggest that the formation of a Ni-Cu alloy helps to the dispersion of Cu.

Representative TEM images of some of the catalysts are displayed in figure 5.2-4. TEM micrographies give direct evidence on the degree of dispersion and homogeneity of the metal particles. The monometallics Ni/S and Cu/S, in figure 5.2-4A and 5.2-4E, respectively, showed particles with a good size homogeneity. The

CHAPTER 5

average particle size of Ni/S (15 nm) was much smaller than Cu/S (95 nm). This is in agreement with the crystallite size calculated from the XRD patterns.

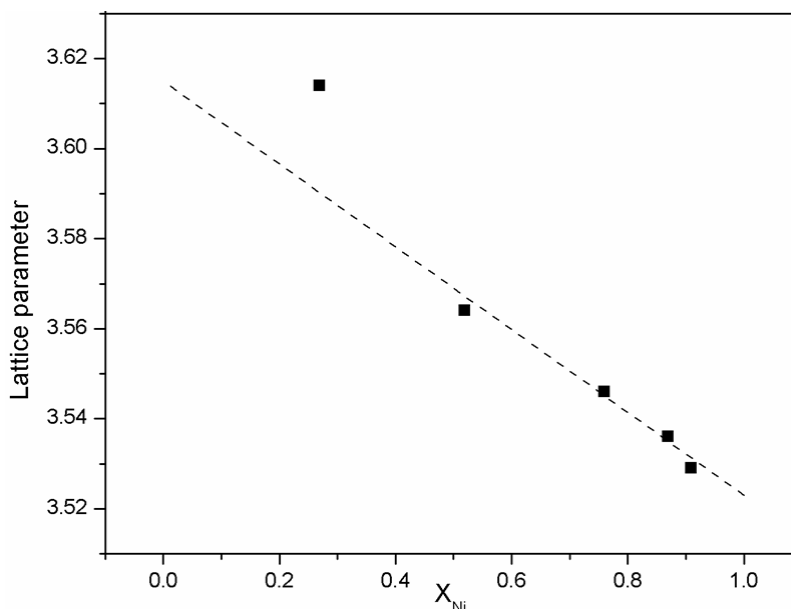


Figure 5.3-3: Cell parameter and atomic ratio relationship of the sample and Vegard's curve.

The metallic area of Ni in the fresh catalyst samples, determined from hydrogen chemisorption analysis, is presented in table 5.2-1. Ni/S showed the highest Ni metallic area (7.5 m²/g) among all the catalyst samples studied. The Ni metallic area decreased for the bimetallic catalysts when increasing the wt % of Cu loading. Ni-Cu(1:1)/S and Ni-Cu(1:3)/S catalysts had a metallic area of 0.4 and 0.1 m²/g, respectively. The Cu/S catalyst did not show appreciable amount of hydrogen strongly chemisorbed. These results were in agreement with the low chemisorption capacity of Cu. (Batista et al., 2001)

Characterization of spent catalysts

The N₂-adsorption results of the spent catalysts are presented in table 5.3-2. Comparing these results with the corresponding values obtained for the catalyst precursors (Table 5.4-1), the spent catalysts, in general, had higher BET area and pore volume than their corresponding catalyst precursors. This could be due to a higher

Application of Acid Saponite in Glycidol Hydrogenolysis

metal dispersion of the spent catalyst, which was also reported for a spent Cu catalyst supported on hectorite. (Sánchez et al., 2012) However, the spent catalysts with higher Cu wt % and tested at higher reaction temperature (453 K) exhibited lower BET area and pore volume. These results could be explained considering differences in the residual carbon compounds deposited on the catalyst surface during reaction. These differences were supported by the quantification of the coke formation by temperature programmed oxidation-thermogravimetric analysis (Table 5.3-2) of the spent catalysts. The results showed lower percentage of deposited organic compounds for the samples with lower Cu wt % and for all catalysts used at lower reaction temperature.

Table 5.3-2: N₂ physisorption and temperature programmed oxidation results of the spent catalysts.

Sample	BET (m ² /g)	Pore volume (cc/g)	% organic deposition
Ni/S-U	157 [#]	0.20 [#]	n.d
Ni-Cu(9:1)/S-U	155	0.20	1
	156 [#]	0.20 [#]	1 [#]
Ni-Cu(6:1)/S-U	155	0.19	1
	153 [#]	0.20 [#]	3 [#]
Ni-Cu(3:1)/S-U	134 [#]	0.17 [#]	4 [#]
Ni-Cu(1:1)/S-U	131	0.17	2
	110 [#]	0.15 [#]	7 [#]
Cu/S-U	130	0.14,	2
	118 [#]	0.16 [#]	9 [#]
Ni-Cu(6:1)*S-U	101 [#]	0.15 [#]	1

[#] The results corresponds to the catalysts used at 453 K for 1 h, whereas, other results are for catalysts used at 393 K for 4 h.

CHAPTER 5

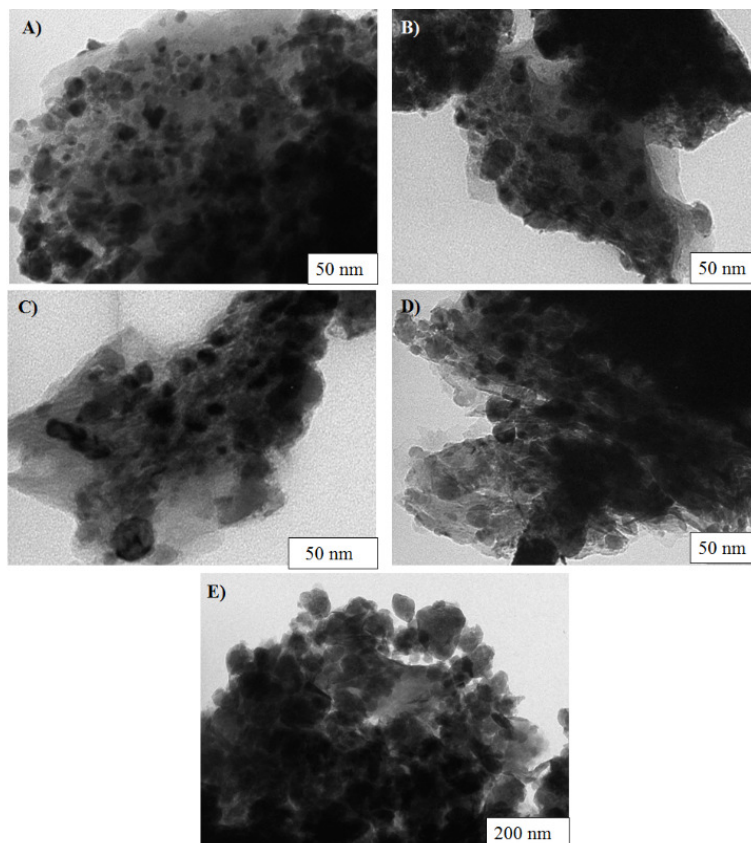


Figure 5.3-4: TEM images of A) Ni/S (300 k) B) Ni-Cu(3:1)/S (300 k) C) Ni-Cu(1:1)/S (500 k) D) Ni-Cu(1:3)/S (300 k) E) Cu/S (80 k) catalysts.

Catalytic Activity: Effect of metal composition

The effect of the type of metal (Ni or Cu) and the relative composition of the two metals in the Ni-Cu bimetallic catalysts on the product distribution of glycidol hydrogenolysis was studied by testing them at 393 K for 4 h. The catalytic results are shown in Table 5.3-3. The major products of the reaction identified from GC-MC analysis include 1,3-PD, 1,2-PD, propanol and cyclic dimerization products such as dioxane and dioxolane derivatives. The proposed acid, metal, and acid/metal catalyzed reaction pathways leading to each of the products identified from GC-MS analysis are illustrated in scheme 5.4-1. Metal and acid sites promote the formation of 1,3-PD, therefore, we foresee that collaboration between both active sites will be

Application of Acid Saponite in Glycidol Hydrogenolysis

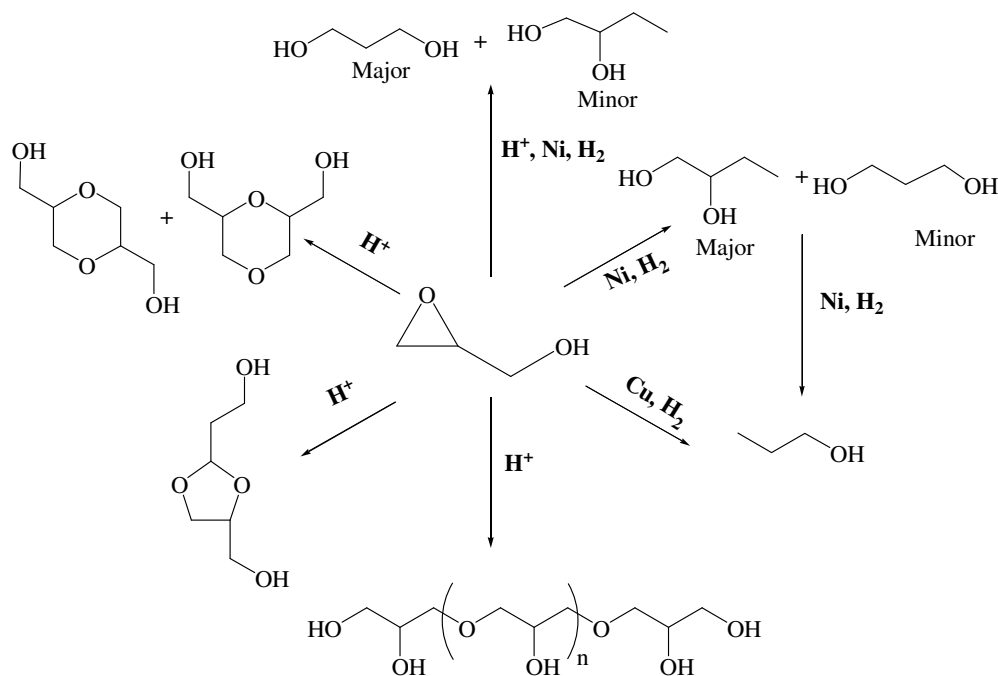
crucial. The acid catalyzed isomerization reaction products, reported by other authors on differently substituted oxiranes (Fási et al., 1999; 2000; 2001), were not detected. This might be because acid catalyzed isomerization reaction products of glycidol, the bifunctional, 3-hydroxypropionaldehyde or acetol, were unstable under our reaction conditions and could undergo hydrogenation, condensation or oligomerization reactions. The formation of high molecular weight oligomerization reaction products, deposited on the spent catalysts, was confirmed in some catalysts by temperature programmed oxidation-thermogravimetric analysis as commented in the previous section.

The catalytic activity results of the catalysts tested at 393 K for 4 h showed full conversion for Ni/S catalyst. However, the conversion values decreased when increasing the wt % of Cu loading in the catalysts. Thus, catalysts, Ni-Cu(9:1)/S, Ni-Cu(6:1)/S and Ni-Cu(3:1)/S exhibited comparable conversion, (78-73 %) whereas conversion decreased further to 56-34 % for catalysts Ni-Cu(1:1)/S, Ni-Cu(1:3)/S and Cu/S as the wt % ratio of Cu increased. These conversion values are in good agreement with the Ni metallic area and could be explained by the higher hydrogenating capacity of Ni compared to Cu at this comparatively lower reaction temperature.

Regarding the product distribution of the catalysts for the reactions carried out at 393 K for 4 h, it was observed that the total diol selectivity decreased and the propanol and dioxane and dioxolane selectivity values increased when increasing the wt % ratio of Cu in the catalysts (Table 5.3-3). We propose that diols might be formed mainly by nickel catalyzed hydrogenation, favoring the 1,2-PD formation. However, the 1,3-PD/1,2-PD ratio increased with the increase of Cu. This suggests that it is necessary to modify the activity of Ni in order to promote the collaborative effect between acid and metal sites. The acid activated oxirane ring of the glycidol could favor the cycle opening by the cleavage of the more hindered C2, as has been commented in the literature for other cyclic ethers (Fási et al., 1999), favoring the formation of 1,3-PD. The high total diol selectivity of the catalysts with high Ni wt % ratio confirmed higher hydrogenating capacity of Ni and was in agreement with their higher Ni metallic area. In the case of Ni/S catalyst, the lowest, 1,3-PD/ 1,2-PD ratio (0.17) could indicate that

CHAPTER 5

its high Ni metallic area ($7.5 \text{ m}^2/\text{g}$ of catalyst) could favor direct hydrogenation without the involvement of acid sites. This could favor hydrogenolysis of the less sterically hindered primary C-O bond leading to the formation of 1,2-PD. In the other catalysts, in which the Ni metallic area was moderate or low, the contribution of such direct reactions could be lower and hydrogenolysis, through acid activation, favored 1,3-PD formation.



Scheme 5.3-4: A simplified reaction pathways for acid, Ni/Cu and Ni/Cu and acid catalyzed reaction of glycidol under H_2 atmosphere.

Table 5.3-3: Catalytic activity of all the catalysts at 393 K.

Catalyst	Temperature (K)	Time (h)	Conversion (%)	Selectivity (%)							1,3-PD/ 1,2-PD	1,3-PD yield (%)
				1,2-PD	1,3-PD	1,2-PD + 1,3-PD	Propanol	Dioxane/ dioxolane	Others			
Ni/S	393	4	100	78	13	91	3	—	6	0.17	13	
Ni/S	453	1	99	57	23	80	14	—	6	0.40	23	
Ni-Cu(9:1)/S	393	4	78	55	23	78	6	8	8	0.42	18	
Ni-Cu(9:1)/S	453	1	96	41	22	63	16	15	6	0.54	21	
Ni-Cu(6:1)/S	393	4	77	48	22	70	12	11	7	0.46	17	
Ni-Cu(6:1)/S	453	1	94	37	21	58	21	15	6	0.57	20	
Ni-Cu(3:1)/S	393	4	73	43	20	63	13	18	5	0.47	15	
Ni-Cu(3:1)/S	453	1	92	32	19	50	22	18	10	0.59	17	
Ni-Cu(1:1)/S	393	4	56	35	17	52	19	21	7	0.49	10	
Ni-Cu(1:3)/S	393	4	37	28	15	42	23	28	7	0.53	6	
Ni-Cu(1:3)/S	453	1	82	18	13	31	32	26	11	0.72	11	
Cu/S	393	4	34	9	5	14	34	47	5	0.56	2	
Cu/S	453	1	75	5	4	9	45	31	15	0.80	3	
Ni-Cu(6:1)**/S	393	4	70	69	13	82	9	5	4	0.19	9	
Ni-Cu(6:1)**/S	453	1	95	48	21	70	21	4	5	0.44	20	

*The total metal loading of this sample was 40 wt % while for the other samples it was 30 wt %.

CHAPTER 5

In the case of propanol, for Ni/S catalyst the selectivity was 3 % and for other catalysts, the selectivity increased progressively when the Ni metallic areas decreased and the wt % of Cu in the catalysts increased. This might indicate that the main route for propanol formation was not over hydrogenolysis, as could be expected from the lower activity of Cu and the lower degree of over hydrogenolysis expected at such lower reaction temperature (393 K) for Ni/S (Scheme 5.3-1). In the literature, it was suggested that Cu has deoxygenation capacity on epoxide rings (Bartók1 et al., 1998) at similar reaction conditions as those used in our experiments. Hence, the propanol could be the product of deoxygenation of glycidol to 3-propen-1-ol followed by hydrogenation.

The dioxane or dioxolane selectivity increased with a decrease in the Ni metallic area. This suggests that when hydrogenolysis activity is lower, the contribution of acid catalyzed reaction is higher and favors the intermolecular oligomerization and dimerization of the reactions products.

In order to establish the role of acidity in the selective formation of 1,3-PD, the catalytic activity of Ni-Cu(6:1)*S catalyst with higher total metal loading (40 wt %), was tested at 393 K for 4 h. This catalyst showed the lowest surface acidity (0.81 mEq CHA/ g) among all the catalysts tested probably due to coverage of the acid sites by metal sites and its higher Ni metallic area (4.3 m²/g of catalyst) compared to Ni-Cu(6:1)/S (2.8 m²/ g of catalyst). This catalyst showed higher total diol selectivity and lower propanol and dioxane or dioxolane selectivity compared to the other bimetallic catalysts. In addition, the 1,3-PD/ 1,2-PD ratio was the lowest (0.19) of all the bimetallic catalysts. This might suggest that the low acidity of the catalyst might decrease the probability of acid activation necessary to the formation of 1,3-PD. The reaction could be dominated by direct hydrogenolysis leading to the cleavage of the less sterically hindered 1 C-O bond and, therefore, to the formation of 1,2-PD.

Effect of reaction temperature

This study was performed by increasing the reaction temperature to 453 K (Table 5.3-3) and using several Ni-Cu bimetallic catalysts at different relative wt % of Ni and

Application of Acid Saponite in Glycidol Hydrogenolysis

Cu. The study was carried out in order to evaluate the effect of Cu, less active metal, in controlling the formation of the cracking gaseous products and the deep hydrogenation to carbonaceous materials that can be produced at higher reaction temperature. The catalytic activities obtained at 453 K were compared with to the corresponding results obtained at 393 K to see the effect of temperature on the selectivity to 1,3-PD and 1,2-PD. The types of products that were formed at 453 K were similar to those obtained at 393 K. The most important difference was observed on the product distribution. The diol selectivity decreased and the selectivity to propanol and dioxane or dioxolane increased for all catalysts when the reaction temperature was raised from 393 to 453 K (Table 5.3-3). However, an increase in the 1,3-PD/1,2-PD ratio was also observed for the catalysts used at 453 K compared to those used at 393 K. In general, the selectivity to “others” was more significant when the reactions were carried out at higher temperature and with catalysts of high Cu wt % ratio.

All catalysts displayed higher conversion at 453 K than at 393 K. The increase of activity was higher for the catalysts with higher wt % of Cu. The conversion values were comparable for Ni/S, Ni-Cu(9:1)/S, Ni-Cu(6:1)/S and Ni-Cu(3:1)/S catalysts (99-92 %). The activity dropped to 82 and 75%, respectively for Ni-Cu(1:3)/S and Cu/S. The diol selectivity decreased and the propanol selectivity increased at higher reaction temperature. This could be explained by over hydrogenolysis of the diols to propanol. Similar results were reported on diol over hydrogenolysis for supported Ni catalysts at comparable reaction temperature. (Gandarias et al., 2012) In contrast, for catalysts with lower Ni metallic area and higher Cu wt % ratio, the Cu catalyzed deoxygenation pathway (Bartók1 et al., 1998) resulted, initially, in the formation of acrolein, which upon hydrogenation gave propanol.

Dioxane and dioxolane were not observed for Ni/S catalyst both at 393 and 453 K suggesting that the acid catalyzed reactions were less important for the catalyst without copper, due to the higher activity of Ni. In contrast, the dioxane and dioxolane amounts were higher for the catalysts with lower Ni metallic area (Table 5.3-3). Thermogravimetric-temperature programmed oxidation analysis (TG-TPO) of the

CHAPTER 5

spent catalysts revealed higher percentage of carbon deposition materials when the reaction was performed at 453 K and when the catalysts of higher amount of Cu were used (Table 5.3-3). This might suggest that the “others” products in this reaction were high molecular weight oligomerization products that could not be identified in the GC-MS analysis.

The 1,3-PD/1,2-PD ratio increased when increasing the reaction temperature for all catalysts (Table 5.3-4). For example, the 1,3-PD/1,2-PD ratio drastically increased from 0.17 at 393 K to 0.40 at 453 K for Ni/S. This might suggest that there was a shift in the mechanism leading to the formation of diols when the reaction temperature was increased. As we proposed earlier, the higher acid activity at 453 K could favor hydrogenolysis through a collaborative action between H⁺ and metal sites favoring the formation of 1,3-PD. This ratio increased further when the wt % ratio of Cu increased suggesting that the acid catalyzed route is even more important at lower Ni metallic area, which is responsible for the direct hydrogenolysis route.

A similar trend in conversion and selectivity was observed at higher reaction temperature when Ni-Cu(6:1)*S, with lower surface acidity and higher metallic area, was used as catalyst for comparison (Table 5.3-3). However, the diol selectivity was higher and the dioxane/ dioxolane selectivity was lower for this catalyst compared to Ni-Cu(6:1)/S. This was in agreement with the higher Ni metallic area and lower surface acidity of the former sample. Although the 1,3-PD/1,2-PD ratio increased for Ni-Cu(6:1)**S at higher reaction temperature, the value was lower than that of Ni-Cu(6:1)/S signifying that the collaborative mechanism was less important for the former catalyst. This could be due to the combined effect of higher Ni metallic area and lower surface acidity of this catalyst.

Conclusions

Acid saponite supported Ni-Cu bifunctional catalysts were active for the hydrogenolysis of glycidol at 393 K, 5 MPa H₂ pressure and after 4 h of reaction, the catalysts gave conversions between 34-100%. We investigated the activity of the materials with different Ni-Cu ratios and reaction temperature. Characterization of the catalysts revealed formation of Ni-Cu alloy and a decrease in the Ni area with the

Application of Acid Saponite in Glycidol Hydrogenolysis

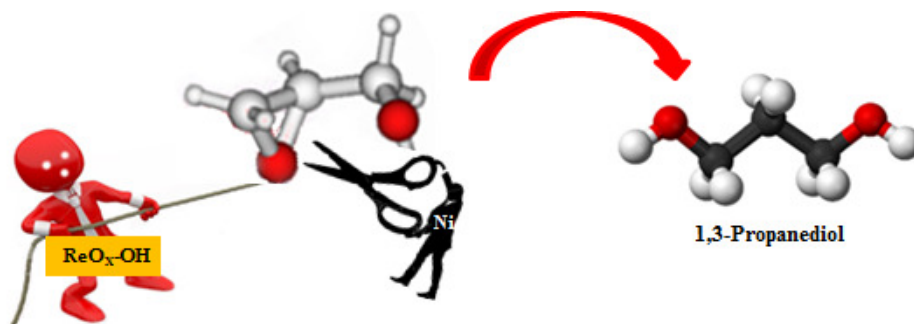
addition of Cu. This indicates that Ni and Cu are in intimate contact. The presence of Cu moderates the hydrogenation activity of Ni, decreasing the yield to diols, but increasing the selectivity towards 1,3 PD. These results suggest that Cu is required to modulate Ni activity and promote the H⁺-metal collaborative mechanism. At higher reaction temperature, the acid activation is improved and, thus, the 1,3-PD/ 1,2-PD ratio increased. However, the increase in the reaction temperature with high Cu loading decreased the diol selectivity significantly and the selectivity of Cu catalyzed deoxygenation and acid catalyzed oligomerization and polymerization reaction products increased.

Acknowledgements

The authors are grateful for the financial support of the Ministerio de Economía y Competitividad of Spain and FEDER funds (CTQ2011-24610).

5.4. Hydrogenolysis of glycidol to 1,3-propanediol using MO_x modified Ni, Cu mono and bimetallic catalysts supported on acid mesoporous saponite.

Abstract



Ni and Cu monometallic and bimetallic catalysts modified with various types of acid oxides MO_x (Mo, V, W and Re) were tested for the hydrogenolysis of glycidol. Characterization results revealed that the presence of modifiers affected dispersion and reducibility of the NiO particles, and the strength and amount of the acid sites. Among the modifiers tested, Re showed the highest activity, high propanediols selectivity and the highest 1,3-PD/1,2-PD ratio. Subsequent Ni-Cu/Re ratio modification gave even a better composition when monometallic Ni was used as active metal at 40 % wt loading with 7 wt % Re. With this catalyst, the best yield of 1,3-PD (46.1 %) with a 1,3-PD/1,2-PD ratio of 1.24 was obtained at moderate reaction temperature (393 K), 5 MPa H_2 pressure after 4 h of reaction.

Introduction

Biomass is a renewable source of organic carbon that is becoming important for the production of sustainable fuels and chemicals (Schlaf, 2006; Corma et al., 2007; Bruijninx and Román-Leshkov, 2014). One of the most abundant biomass-related renewable materials is glycerol, which is generated during biodiesel production by transesterification of vegetable oils (Zhou et al., 2008). Biomass has higher O/C ratio than most valuable chemicals (West et al., 2009; Yamaguchi et al., 2009). Then, it is desirable to develop catalytic hydrogenolysis reactions to transform it into useful chemicals (Nakagawa and Tomishige, 2011; Sitthisa et al., 2011; Deutsch and Shanks, 2012). Catalysts should have the ability to activate hydrogen, in hydrogenolysis reactions. Hydrogen can be activated on a metal surface. Typical metals used in hydrogenolysis include, nickel, copper and noble metals (Mäki-Arvela et al., 2005; Deutsch and Shanks, 2012).

Hydrogenolysis of glycerol has been widely studied. With most of the catalytic systems, the main product was 1,2-propanediol (PD) (Dasari et al., 2005). However, the hydrogenolysis of glycerol to 1,3-PD is economically more attractive because 1,3-PD is an important monomer in the synthesis of polypropylene terephthalate (PPT), a polymer that displays excellent properties (Julien et al., 2004). Additionally, the current industrial production of 1,3-PD is costly and involves the use of petrochemical based hazardous chemicals (Kraus, 2008) The addition of acid ion exchangers (Kusunoki et al., 2005; Miyazawa et al., 2007) or the presence of a solid base co-catalyst (Feng et al., 2007), increased activity and 1,2-PD selectivity. In order to favor the formation of 1,3-PD, tungsten-based materials or acid oxides, such as ReO_x or MoO_x , which are capable of activating glycerol, have been proposed as co-catalysts of several supported-metal catalysts. This information has been published in a recent review by Nakagawa et al., 2014.

The hydrogenolysis of glycerol with Ru/C catalyst using H_2WO_4 as co-catalyst at 453 K in sulfolane yielded 12% of selectivity to 1,3-PD and 1,3-PD/1,2-PD ratio of 2 (Chaminand et al., 2004). Commercial Pt/SiO₂ and Pt/Al₂O₃ catalysts modified with H_2WO_4 , phosphotungstic acid ($\text{H}_3\text{PW}_{12}\text{O}_{40}$) or silicotungstic acid ($\text{H}_4\text{SiW}_{12}\text{O}_{40}$) gave

CHAPTER 5

higher selectivity to 1,3-PD (20-40%) at 473 K (ten Dam et al., 2013). This has been related to the presence of W compounds, which increased the amount of Brønsted acid sites (Gong et al., 2010). Several tungsten oxides co-supported with an active metal catalysts showed high selectivity to 1,3-PD (Kurosaka et al., 2008). For example, Pt/WO₃/ZrO₂ catalyst afforded 1,3-PD in 32% yield (Ross-Medgaarden et al., 2008). The use of alumina as support was also tested (Suzuki et al., 2007; Arundhathi et al., 2013). Pt(5 wt%)-W(5 wt%)/Al₂O₃ catalyst patented by KAO Corporation (Suzuki et al., 2007) gave 67% selectivity to 1,3-PD at 23% glycerol conversion. Highly dispersed Pt particles were obtained by using mesoporous WO₃ as support resulting in selectivity to 1,3-PD of 39.3% for a 18% of conversion (Liu et al., 2012).

Protons on ReO_x associated hydroxyl groups are acidic and capable of activating glycerol (Chia et al., 2011). Ir-ReO_x/SiO₂ (Nakagawa et al., 2010; 2012) and Rh-ReO_x/SiO₂ (Chen et al., 2010) catalysts were tested for the hydrogenolysis of glycerol at 393 K in the presence of small amounts of mineral or solid acid additives. In the former catalyst, 1,3-PD was obtained with 46% selectivity for a 81% of conversion while the later was equally active, but its selectivity to 1,3-PD was much lower (14%).

In general, the selective hydrogenolysis of glycerol to 1,3-PD requires expensive noble-metal based catalysts, high temperature and/ or pressure and longer reaction time. Even at these reaction conditions, the yield of 1,3-PD was low or moderate. In a previous work (Gebretsadik et al., 2015), we showed that glycidol, a more reactive molecule which could be readily obtained from glycerol (Yoo et al., 2001; Bai et al., 2013), could be an alternative to glycerol to obtain propanediols by catalytic hydrogenolysis, using mesoporous acid saponite supported Ni catalysts.

In the literature, the hydrogenolysis of tetrahydrofurfuryl alcohol (THFA), a cyclic ether with similar substitution pattern as glycidol, has been reported, using Ir-ReO_x/SiO₂ (Chen et al., 2012), Rh-ReO_x/SiO₂ (Liu et al., 2014; Chia et al., 2011), and Rh-MoO_x/SiO₂ (Koso et al., 2009; 2012) catalysts. All these catalysts led to 1,5-pentanediol with very high selectivity (> 90 %). The mechanism of THFA hydrogenolysis involved adsorption of THFA, at the -CH₂OH group, on the protonated ReO_x or MoO_x surface, to form alkoxide species. Hydride activated on the

metal attack C–O bond neighboring $-\text{CH}_2\text{ORe}/\text{MoO}_x$ and hydrolysis releases 1,5-PD (Koso et al., 2009; Chen et al., 2012).

In this work, we proposed to use glycidol as an alternative substrate to glycerol for the synthesis of 1,3-PD by catalytic hydrogenolysis. The hydrogenolysis capacity of Ni, Cu and Ni-Cu catalysts in the presence of various modifiers, MO_x (Mo, V, W and Re) using a mesoporous acid saponite as support and source of Brønsted acidity, was investigated. The effect of metal to modifier ratio was studied for ReO_x .

Experimental

Preparation of supported catalysts

Mesoporous acid saponite (MS) (BET surface area, 600 m^2/g), previously reported in our group (Gebretsadik et al., 2015) was used as support for catalyst preparation. Ni-Cu/MS catalysts with 20, 30 and 40 wt % total metal loading, and Ni: Cu wt % ratio 6:1 were prepared by impregnation of 1 g of the support with a calculated volume of 0.5 M Ni-Cu in ethanol solution containing appropriate amounts of $\text{Ni}(\text{NO}_3)_2$ and $\text{Cu}(\text{NO}_3)_2$ salts. After removing the solvent by rotary evaporation and drying at 383 K overnight, the samples were calcined at 723 K for 5 h.

Several Ni-Cu- MO_x/MS (M = W, Mo, V and Re) catalysts were prepared by impregnating the Ni-Cu/MS (prepared at 40 wt % Ni-Cu loading) with an aqueous solution of the modifier metal precursors, $(\text{NH}_4)_{10}\text{W}_{12}\text{O}_{41}\cdot 4\text{H}_2\text{O}$, $(\text{NH}_4)_6\text{Mo}_7\text{O}_{24}\cdot 4\text{H}_2\text{O}$, NH_4VO_3 and NH_4ReO_4 . The amount of MO_x modifier expressed per mass of W, Mo and V respect to unmodified catalyst, was 7 wt %. The amount of Re loading was varied at 3, 7 and 15 wt %, resulting in catalysts Ni-CuRe(3)/MS; Ni-CuRe(7)/MS and Ni-CuRe(15)/MS, respectively.

The effect of the Ni-Cu/Re wt % ratio was also studied by preparing two catalysts, Ni-Cu*Re(7)/MS and Ni-Cu**Re(7)/MS, modifying the wt % of metal loading at 30 and 20 wt % Ni-Cu, respectively, maintaining the amount of Re loading as in the Ni-CuRe(7)/MS catalyst. Monometallic Ni and Cu catalysts were prepared at 40 wt % metal loading and modified with 7 wt % Re, for comparison.

CHAPTER 5

All catalysts were reduced in a tubular reactor under hydrogen flow (75 mL/ min) at 623 K for 6 h.

The preparation conditions and nomenclature of the catalysts are summarized in table 5.4-1. The catalyst precursors were labelled with P at the beginning of the name.

Table 5.4-1: Nomenclature, type of modifier, amount of metal and modifier loading of the catalysts.

Catalysts	Ni-Cu wt % loading	Modifier M (MO _x)	Modifier wt %
Ni-Cu/MS	40	—	—
Ni-CuV(7)/MS	40	V	7
Ni-CuMo(7)/MS	40	Mo	7
Ni-CuW(7)/MS	40	W	7
Ni-CuRe(7)/MS	40	Re	7
Ni-CuRe(3)MS	40	Re	3
Ni-CuRe(15)/MS	40	Re	15
Ni-Cu*Re(7)/MS	30	Re	7
Ni-Cu**Re(7)/MS	20	Re	7
NiRe(7)/MS	40	Re	7
CuRe(7)/MS	40	Re	7

The amount of metal loading was * 30 wt % ** 20 wt %. In the other samples, the metal loading was 40 wt %.

Catalyst characterization

X-ray diffractogram (XRD) patterns of powdered catalyst samples were recorded on a Siemens D5000 diffractometer equipped with a CuK α radiation ($\lambda = 1.54 \text{ \AA}$) source. Measurements were done in the 2θ diffraction angle 5 and 70° with an angular step of 0.05° and at rate of 3 s per step. Crystalline phases were identified by cross comparison of the diffractogram of the sample with a reference data from international centre for diffraction data (JCPDS files). Integral breadth estimated by fitting intense reflection peaks of Ni or NiO and by applying TOPAS 4.1, was used to calculate the crystallite sizes using the Scherrer equation.

N₂ adsorption-desorption analysis was performed on Quadrasorb sorptometer at liquid nitrogen temperature (77 K) to determine the specific BET area and porosity. Before measurement, samples were degassed overnight at 383 K. Specific surface area was determined by applying the BET method and the pore size distribution was estimated by BJH method.

Temperature-programmed reduction of the samples was measured by an Autochem AC2920 Micrometric apparatus. The catalyst precursor sample, calcined beforehand (100 mg), was placed into a tubular reactor and heated between room temperature and 1173 K at rate of 10 K/min under a flow of 5 vol.% H₂ in argon (50 mL/min). The final temperature was maintained for 1 h and a TCD detector monitored the amount of hydrogen consumed.

The surface acidity of the catalyst precursors was determined by thermogravimetric analysis (TGA) of the cyclohexylamine treated samples following the protocol described by Mokaya *et al.* (1997). The total acidity was equivalent to the amount of cyclohexylamine (CHA) desorbed at the temperature range of 523-923 K in which the sample without cyclohexylamine treatment did not show any significant mass loss (Gebretsadik *et al.*, 2014). The analysis was conducted in a Labsys Setaram TGA microbalance equipped with a programmable temperature furnace. Each sample was heated under an N₂ or air flow (80 cm³/min) from 303 to 1173 K at a rate of 5 K/min. The amount of sample used was about 100 mg in all experiments.

Surface characterization of some fresh, spent and H₂ reactivated fresh catalysts was performed by X-ray photoelectron spectroscopy (XPS) on a SPECS system equipped with an Al anode XR50 source operating at 150 mW and a Phoibos MCD-9 detector. The pressure in the analysis chamber was always kept below 10⁻⁷ Pa. The area analyzed was about 2 mm x 2 mm. The pass energy of the hemispherical analyzer was set at 25 eV and the energy step was fixed at 0.1 eV. The sample powders were pressed to self-supported pellets. In situ experiments were performed under dynamic conditions in an adjacent chamber at atmospheric pressure equipped with a mass spectrometer and an IR lamp to heat the sample. The sample was transferred under ultra-high vacuum between the in situ chamber and the analysis chamber. Gases were

CHAPTER 5

accurately dosed into the in situ chamber by using mass flow controllers, and the temperature was measured by using a K-type thermocouple in contact with the sample holder. Data processing was performed with the CasaXPS program (Casa Software Ltd., UK). The binding energy (BE) values were referred to the C 1s peak at 284.8 eV. Atomic fractions were calculated using peak areas normalized on the basis of acquisition parameters after background subtraction, experimental sensitivity factors and transmission factors provided by the manufacturer.

Catalytic activity test

The activity test was performed on the hydrogenolysis of glycidol in a 50 mL stainless steel autoclave equipped with an electronic temperature controller and a mechanical stirrer. Glycidol (3.77 mL) was dissolved in sulfolane (30 mL) and purged with nitrogen and 1 g of freshly reduced catalyst was carefully transferred to the reactor under a positive nitrogen pressure to avoid contact with atmosphere. The reactor was sealed, purged three times with 4 MPa N₂ pressure and three times with 1 MPa H₂ pressure. After performing a leakage test, the temperature of the reaction was set at 393 K and the mixture was stirred at 600 rpm and 1 MPa H₂ was fed. When the temperature in the electronic control reached the final temperature of the reaction, the hydrogen pressure was adjusted at 5 MPa and the reaction time was started (*t*₀). The reaction was run for 4 h while feeding hydrogen on demand. At the end of the reaction time (*t*_f), the mixture was cooled down and the reaction products were separated from the catalyst by filtration. Liquid products were analysed on Shimadzu GC-2010 chromatography using SupraWAX-280 capillary column, 1-butanol as internal standard and a FID detector. Some liquid samples were submitted for GC-MS analysis to identify unknown products. Conversion and selectivity were calculated according to the following equations:

$$\text{Conversion} = \frac{(\text{moles of glycidol } t_0 - \text{moles of glycidol } t_f)}{\text{moles of glycidol } t_0} * 100\%$$

$$\text{Selectivity to } x \text{ (\%)} = \frac{\text{moles } x * \text{carbon in } x}{\text{moles of glycidol converted} * \text{carbon in glycidol}} * 100\%$$

Results and discussion

Characterization of the catalyst precursors and catalysts

XRD patterns of the Ni-Cu catalysts and modified Ni-Cu catalyst samples, after reduction at 623 K for 6 h, are displayed in Figure 5.4-1A. All catalysts presented peaks at 19.4, 35.6 and 60.5°, 2 θ , corresponding to the (110, 020), (201) and (060) reflections of the saponite support and peaks at 44.5 and 51.9°, 2 θ , related to the presence of metallic nickel. A small peak for Ni-CuMo(7)/MS (figure 5.4-1A, (c) and a shoulder for Ni-CuV(7)/MS (figure 5.4-1A, (b)) and Ni-CuW(7)/MS (figure 5.4-1A, (d)), observed at 43.2 and 62.8°, 2 θ , were due to the presence of some amount of unreduced NiO or oxidized Ni. Peaks corresponding to the modifiers and Cu were not observed in any sample, suggesting its small particle size or low crystallinity. In addition, there was no appreciable shift in the cell parameter of Ni in bimetallic catalysts and the formation of a Ni-Cu alloy was not clear from the XRD pattern. The presence of modifier favoured the dispersion of Ni, since the Ni crystallite size decreased from 27 nm to 11-21 nm in the presence of the modifiers (Table 5.4-2).

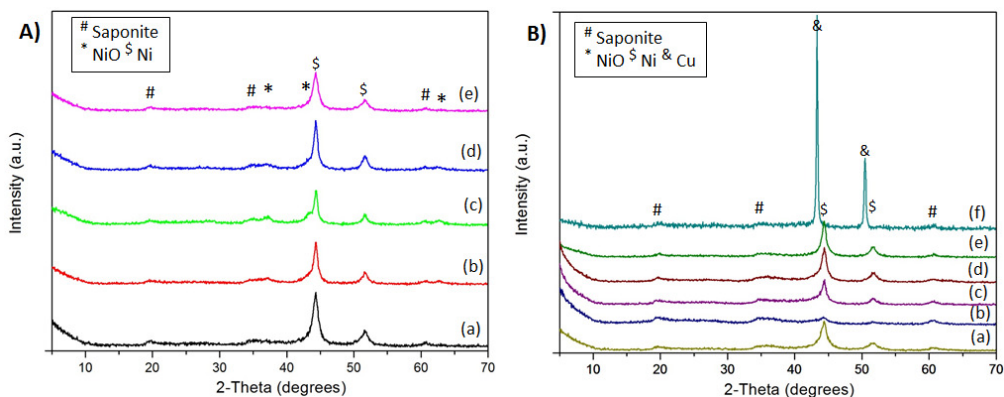


Figure 5.4-1: XRD patterns of (A) Ni-Cu/MS samples with 40 wt % Ni-Cu loading (a) without modifier (b) Mo (c) V (d) W (e) Re modifier at 7 wt % loading and (B) (a) NiRe(7)/MS (b) Ni-CuRe**(7)/MS (c) Ni-Cu*Re(7)/MS (d) Ni-CuRe(3)/MS (e) Ni-CuRe(15)/MS (f) CuRe(7)/MS.

Figure 5.4-1B shows the XRD patterns of supported monometallic Ni and Cu catalysts modified with Re, and Ni-Cu bimetallic catalysts with different wt % of Ni-Cu loading

CHAPTER 5

and modifier amount. For the monometallic modified Cu catalyst, sharp peaks were observed at 43.3 and 50.4°, 2 θ , which were attributed to metallic copper crystalline phase. In the other samples, Ni phase was mainly observed and the Ni crystallite size increased when increasing the Ni-Cu wt % loading. Residual amounts of NiO were detected in Ni-Cu*Re(7)/MS. For Ni-Cu**Re(7)/MS, the peaks were very broad and the presence of residual amounts of NiO cannot be discarded. The Ni crystallite sizes of these two samples were 6 and 3 nm, respectively, in agreement with their lower metal loading. The value increased to 11 nm for Ni-CuRe(7)/MS. The other samples had comparable crystallite sizes (12-14 nm).

Table 5.4-2: Characterization results of the catalyst precursors and catalysts.

Catalyst Precursors	BET (m ² /g)	Av. pore radius (Å)	Acidity ^a (mEq./g)	Catalyst	XRD Ni/ (NiO) (nm)
PNi-Cu/MS	220	27	0.86	Ni-Cu/MS	27
PNi-CuV(7)/MS	179	25	1.82	Ni-CuV(7)/MS	21 (3)
PNi-CuMo(7)/MS	156	26	1.69	Ni-CuMo(7)/MS	21 (6)
PNi-CuW(7)/MS	157	23	1.74	Ni-CuW(7)/MS	16 (4)
PNi-CuRe(7)/MS	340	31	1.88	Ni-CuRe(7)/MS	11
PNi-CuRe(3)/MS	347	31	1.45	Ni-CuRe(3)/MS	12
PNi-CuRe(15)/MS	268	34	1.92	Ni-CuRe(15)/MS	14
PNi-Cu*Re(7)/MS	362	30	1.95	Ni-Cu*Re(7)/MS	6
PNi-Cu**Re(7)/MS	429	33	2.03	Ni-Cu**Re(7)/MS	3
PNiRe(7)/MS	331	33	1.71	NiRe(7)/MS	13

^a Acidity in mEq.CHA/ g of sample of the catalyst precursors from TGA of cyclohexylamine (CHA) treated samples. The values in bracket correspond to the NiO crystallite size.

In order to explain the XRD results, it was necessary to have information about the interactions between NiO and CuO phases with the support and the modifiers, present in the precursors. For this reason, the acidity and reducibility study of the catalyst precursors were performed. The acidity values of precursors could give important information about the differences in catalysts that might be used to justify their catalytic behaviour.

The N₂-physisorption analysis results of the catalyst precursors are presented in table 5.4-2. The specific BET areas of all the catalysts precursors were lower than the BET area of the support (600 m²/g) (Gebretsadik et al., 2015a) indicating that some of the pore volume was occupied by the metal oxide particles. Comparing the BET areas of the unmodified catalysts precursor with the modified ones, they were lower for the V, Mo and W modified catalyst precursors. In contrast, for those modified with Re, the BET area was much higher (340 m²/g). This result suggested that Re favored the dispersion of the metal oxide particles to a greater extent than the other modifiers. This was supported by the XRD results, which showed smaller metal particles for the corresponding reduced catalysts.

At 3 wt % Re loading, the BET area was slightly higher (347 m²/g). However, when the Re loading was increased to 15 %, the BET area decreased to 268 m²/g. The BET area of the modified monometallic catalyst precursor, PNiRe(7)/MS (331 m²/g) was slightly lower than that of bimetallic modified catalyst precursor (PNiCuRe(7)/MS). This might indicate that the presence of Cu could assist the dispersion of Ni. The BET area values increased to 362 m²/g and 429 m²/g, respectively, when decreasing the amount of Ni-Cu loading to 30 and 20 %. The average pore radius of all the catalyst precursors was in the mesoporous range.

Figure 5.4-2A displays the thermogravimetric analysis results of cyclohexylamine treated modified Ni-Cu catalyst precursors, used for the determination of the total surface acidity of the samples. The minima corresponding to the first derivative of the mass loss curve can be associated to different processes related to the mass loss. Thus, those centred at about 350 and 1100 K, can be attributed to the water loss due to the dehydration of interlayer cations and dehydroxylation of the saponite structure, respectively. The other minima correspond to the mass loss associated with cyclohexylamine desorption. The number of these minima can be attributed to different acid sites while their temperature can be related to the acidity strength. Thus, the minima appeared at higher temperature correspond to stronger acid sites.

CHAPTER 5

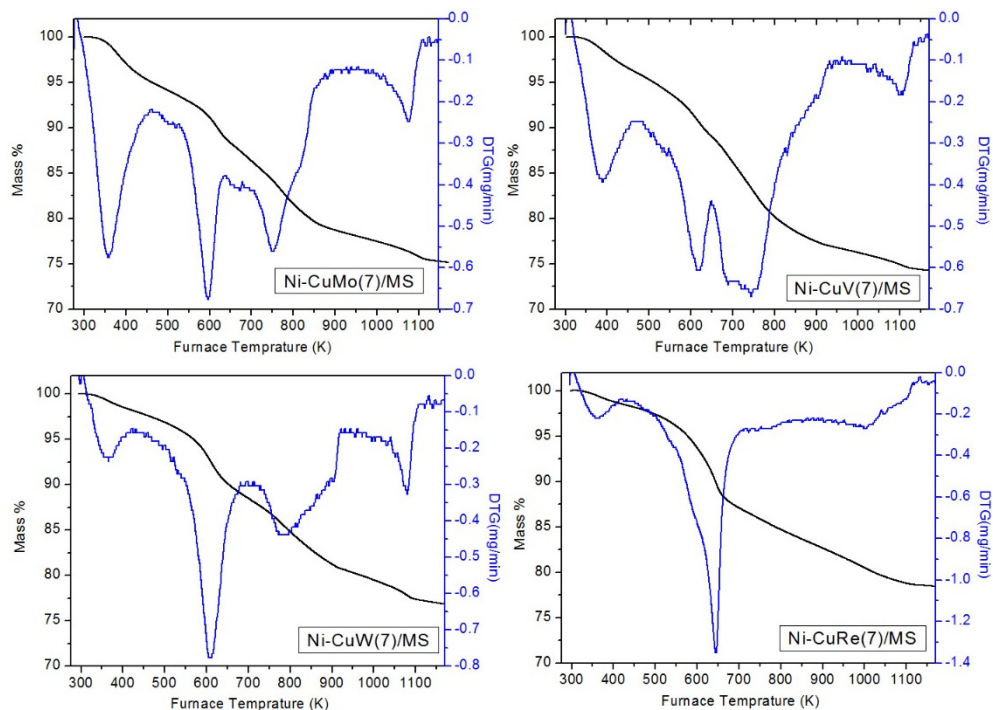


Figure 5-4-2: TGA results of cyclohexylamine treated samples of the modified catalyst precursors.

For PNi-CuMo(7)/MS, PNi-CuV(7)/MS and PNi-CuW(7)/MS catalyst precursors, two types of acid sites were observed. The minimum observed for all samples at about 600 K was similar to that of the unmodified catalyst precursor. This can be related to the acid sites of the support not influenced by the modifiers. Another broader minimum, which appeared at an inflection point of about 750 K in all the modified catalyst precursors could be due to additional stronger acid sites associated to the presence of the modifiers. For PNi-CuRe(7)/MS, mainly one minimum at 650 K was observed with only a small shoulder at around 600 K, that can be assigned to the acidity of the unmodified acid sites of the support.

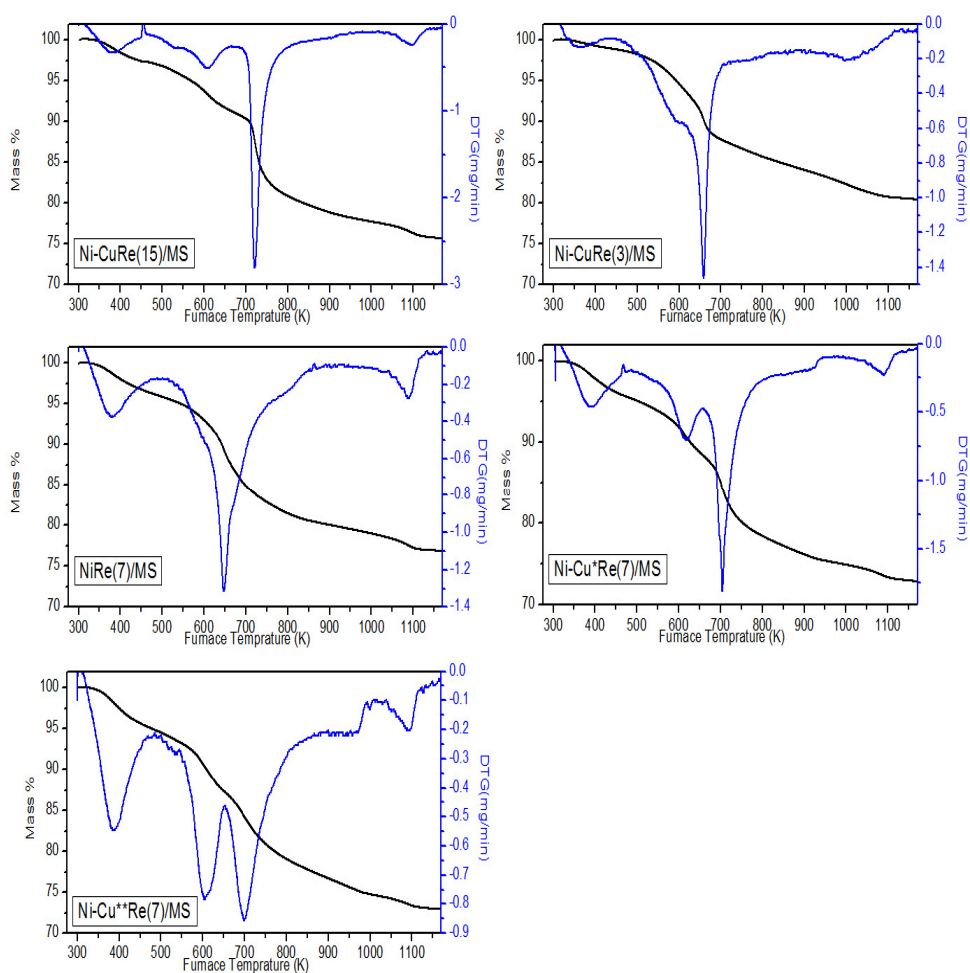


Figure 5.4-3: The TGA of cyclohexylamine treated catalysts precursor samples with different Re/Ni+Cu ratio.

It can be argued that Re, Ni and Cu oxides in PNi-CuRe(7)/MS are well dispersed, covering the main part of the support external surface, and the accessibility of the acid sites of the support for the CHA probe molecule was restricted. The stronger acid sites detected in the catalyst precursors in the presence of modifiers could be related to the H^+ of the modifier, associated with –OH groups (Chen et al., 2012), or with Lewis acid sites of the modifiers. The TGA analysis results of cyclohexylamine treated Ni-Cu catalysts precursors at different wt % Ni-Cu loading and modified with different amounts of Re are displayed in figure 5.4-3. For catalyst precursors with 40 wt % Ni-Cu loading, the small

CHAPTER 5

minimum corresponding to the loss of CHA adsorbed on the acid sites of the support of the unmodified sample, appeared more defined at 3 and 15 wt % Re loading than at 7 wt %. When the Re loading was increased to 15 wt %, the position of the minimum related to the CHA adsorbed on the acid sites generated by the presence of modifiers shifted to higher temperature (700 K). This minimum also appeared at about 700 K for PNi-Cu*Re(7)/MS and PNi-Cu**Re(7)/MS. However, for these two samples, the mass loss due to the desorption of CHA adsorbed on the acid sites corresponding to the support increased when decreasing the Ni-Cu loading. These results are consistent with the lower coverage of the support, when the Ni-Cu loading was lower.

The total surface acidity of all the modified catalyst precursors was much higher (1.45-2.03 mEq. CHA/g) than that of the unmodified Ni-Cu catalyst precursor (0.85 mEq. CHA/g) (Table 5.4-2). This confirms that modifiers provide an additional acidity, as previously commented. The total surface acidity values were higher for Re modified catalyst precursors following, in general, a similar trend to the BET area. The values of total surface acidity increased with an increase in the amount of modifier or a decrease in the wt % of Ni-Cu loading.

The temperature-programmed reduction profiles of the unmodified Ni-Cu catalyst precursors and those modified with Mo, V, W and Re are displayed in figure 5.4-4A. The interval of temperature registered corresponds to the NiO reduction. However, the contribution of some modifier reduction cannot be discarded. The reduction peaks of NiO should be consequence of its interaction with the support and with the modifiers, considering that NiO should be located between the support and modifiers taking into account the order of impregnation. For all the modified catalyst precursors, except for PNi-CuW(7)/MS, the main reduction peaks shifted to higher temperature with respect to the unmodified one. This shift in the reduction temperature could be related to smaller NiO particles interacting with the other phases. This makes the reduction of the NiO more difficult. The shift for the sample with Re was very small (12 K). This lower shift is difficult to explain, but in this sample a higher dispersion of Re₂O₇ phase on the smaller NiO particle size could favor interactions of Re(VII) with the O of the

NiO structure, decreasing the electronic density on the Ni(II), and consequently, favoring its reduction. This interaction can partially compensate the interaction with the support. In this sample, a well-defined peak was observed at lower reduction temperature (530 K) that could be related to more effective NiO-Re₂O₇ interactions in some particles.

For Ni-CuW(7)/MS, the main reduction peak shifted to lower temperature by about 20 K with respect to the peak of the unmodified catalyst. This can be probably more related to a decrease of the NiO particle size than to differences in interactions, since the degree of dispersion of this modifier (WO₃) was not so good as for Re₂O₇.

Figure 5.4-4B shows the reduction profiles of some Ni-Cu bimetallic catalyst precursors with different metal to Re modifier ratio. The reduction of the modified monometallic Ni catalyst precursor, PNiRe(7)/MS, occurred in a broad interval (550-750 K) with two maxima, one more intense at 639 K and other at 703 K. Regarding the modified bimetallic catalyst, some part of NiO was easily reduced but other was more difficult. The differences of reducibility could be related to differences in NiO and Re₂O₇ dispersions.

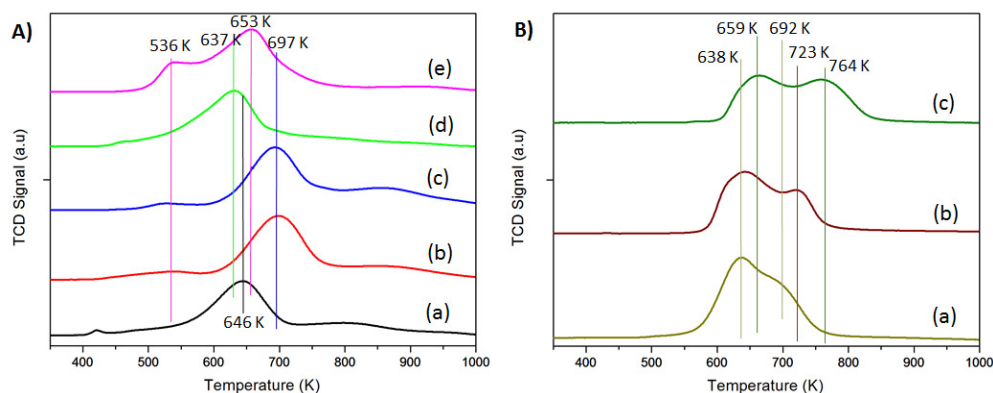


Figure 5.4-4: TPR profiles of (A) Ni-Cu/MS catalysts with 40 wt % of Ni-Cu loading (a) without modifier (b) Mo (c) V (d) W and (e) Re modifier at 7 wt % loading (B) (a) Ni(40)Re(7)/MS (b) Ni-Cu*Re(7)/MS (c) Ni-Cu**Re(7)/MS.

In the other Ni-Cu catalysts prepared with 20 and 30 wt % total metal loading, the reduction peaks shifted to slightly higher temperatures. Two different

CHAPTER 5

reduction peaks were observed for both samples, which might stand for NiO particles with different interactions. The reducibility was more difficult for the precursor that after reduction presented the smallest Ni particles (3 nm), probably due to stronger interaction with the support. The reduction peaks at lower temperature, at 642 and 659 K for PNi-Cu*Re(7)/MS and PNi-Cu**Re(7)/MS, respectively, could be related to efficient NiO interactions with Re_2O_7 that can favor its reduction. The lower reducibility of these samples could justify the presence of the residual amounts of NiO observed by XRD for these catalysts (Fig. 5.4-1B, (b) and (c)).

Catalytic Activity

Influence of the type of modifier

Table 5.4-3 shows the catalytic activity results of Ni-Cu catalysts modified with various types of metal oxides. The activity should be a result of the metal and acid sites contribution, responsible for hydrogenolysis and condensation reactions, respectively. These are competitive reactions. However, a cooperative effect of metal and acid sites could be expected in the hydrogenolysis reaction to increase the selectivity to 1,3-PD. This can take place by activation of glycidol, by H^+ interacting with the oxirane group (Chia et al., 2011) or by interactions of acid metal oxides MO_x with the alcohol of the glycidol (Chen et al., 2012). All the modified samples showed comparable or higher activity compared to that of the unmodified catalyst. This might indicate that the modifiers could have glycidol activation role. The diol selectivity of these catalysts increased when using W and Re modifiers. This could be explained by the higher amount of metal phase, as a consequence of the higher reducibility of the corresponding catalyst precursors. For Mo and V modified catalysts, the propanediols selectivity was lower, in agreement with their lower NiO reducibility and the presence of residual amounts of NiO in the fresh catalysts.

All catalysts displayed comparable propanol selectivity suggesting that the formation of propanol was not related to high metal activity and was not the result of

overhydrogenolysis of propanediols. The presence of propanol can be justified by the capacity of Cu to deoxygenate oxirane rings, as previously reported in the literature (Bartók1 et al., 1998). Regarding the condensation products selectivity (dioxane/dioxolane), the unmodified catalyst and those modified with Mo and V gave comparable selectivity (21-28%). The selectivity towards these products was lower for Re and W modified catalysts. These results agree with the higher metal activity of the later samples.

Regarding the 1,3-PD/1,2-PD ratio, the unmodified catalyst, Ni-Cu/MS, showed a value of 0.33, which decreased in the case of W modified catalyst, was comparable to Mo modified catalyst, slightly higher for the V modified catalyst and higher for the catalyst with Re as modifier. The low 1,3-PD/1,2-PD ratio of Ni-CuW(7)/MS (0.24), could be associated to Ni activity without acid collaboration, due to, probably a worse dispersion of WO₃ on the metal particles. For V and Re modified catalysts, the improved 1,3-PD/1,2-PD ratio might reflect the cooperation between acid and metal sites. This was especially the case for Re modified catalyst. The highest dispersion of the metal and the O-H groups of the ReO_x phase makes possible this collaborative action. In general, among all the modified catalysts tested, the highest 1,3-PD yield (31.6%) was obtained for Ni-Cu-Re (7)/MS catalyst.

Effect of Re to metal loading ratio

The effect of the amount of Re loading was studied by varying the amount of Re (3, 7, 15 %) at constant Ni-Cu loading (40 %) and changing the Ni-Cu wt % loading (20, 30 and 40 %) at constant Re amount (7 wt %).

The conversion was similar for all catalysts and was not affected significantly by the Re to metal ratio. The selectivity to each of the products varied depending on the Re/Ni-Cu ratio. When the amount of Re loading increased at constant Ni-Cu loading, the 1,2-PD selectivity decreased, the 1,3-PD selectivity slightly increased, and hence the 1,3-PD/1,2-PD ratio increased. This might confirm that ReO_x could be involved in the activation of glycidol leading to the formation of 1,3-PD. All the catalysts gave comparable propanol selectivity (6-8%) suggesting

CHAPTER 5

that its formation was not related to the acid sites or to the metal activity. The selectivity to condensation products was higher at higher and lower Re loading. At higher Re/M molar ratio, this can be related to the higher and stronger acidity (Fig. 5.4-2) while at lower Re loading, it could be associated with lower hydrogenolysis metal activity due to its lower reducibility, as discussed earlier.

Application of Acid Saponite in Glycidol Hydrogenolysis

Table 5.4-3: Catalytic activity test result.

Catalyst	Conversion	Selectivity (%)				1,3-PD/ 1,2-PD	1,3-PD yield (%)
		1,2-PD	1,3-PD	Propanol	Condensation products (dioxane/ dioxolane)		
CuRe(7)/MS	40	9	8	9	59	0.89	3.2
Ni-Cu/MS	73	47	15	5	21	0.33	11.0
Ni-CuMo(7)/MS	73	48	16	7	28	0.33	11.7
Ni-CuV(7)/MS	88	43	19	5	22	0.45	16.7
Ni-CuW(7)/MS	95	66	16	5	2	0.24	15.2
Ni-CuRe(7)/MS	98	45	34	8	8	0.76	31.6
Ni-CuRe(3)/MS	98	49	29	8	14	0.59	28.4
Ni-CuRe(15)/MS	98	42	35	6	13	0.83	34.3
Ni-Cu*Re(7)/MS	96	38	31	8	11	0.82	31.7
Ni-Cu**Re(7)/MS	98	35	31	7	13	0.89	33.3
NiRe(7)/MS	98	38	47	7	6	1.24	46.1
Re(7)/MS	47	n.d	n.d	—	59	—	—

CHAPTER 5

When Ni-Cu loading decreased (40, 30 and 20%), the molar ratio Re/Ni-Cu increased, resulting in different catalytic behaviour. The propanediols selectivity slightly decreased and the 1,3-PD/1,2-PD ratio increased. The selectivity to condensation products increased when the Ni-Cu loading was lower. The reducibility of NiO was difficult and acidity was higher for samples with lower metal loading. Hence, the lower diol selectivity and higher condensation products selectivity could be explained by lower metal and higher acid activity, respectively. On the other hand, this increase of acidity had a positive effect to improve the formation of 1,3-PD.

Several Re modified monometallic Ni and Cu and one Re modified support without metal phase catalysts were prepared and their catalytic activity was tested for comparison. Re modified Ni catalyst showed the highest selectivity to propanediols (85%) and 1,3-PD selectivity with the highest 1,3-PD/1,2-PD ratio (1.24) and low condensation products selectivity. The high 1,3-PD selectivity could be related to an effective collaborative action between metal and acid sites. On the other hand, the modified Cu catalyst afforded the lowest propanediol selectivity, higher propanol selectivity and the highest condensation products selectivity. This might reflect the poor hydrogenolysis activity of Cu at the conditions used, and the high activity of the acid sites. The propanol, as discussed earlier, is the result of Cu catalysed deoxygenation reaction of the epoxide ring followed by hydrogenation of the resulting double bond. Re modified support showed comparable moderate activity as that of the modified Cu catalyst with identical condensation products selectivity. This confirms the previous argument that condensation products can be related to acid sites.

In summary, among all the modified catalysts tested, Re modified catalysts showed higher activity, propanediols selectivity and 1,3-PD/1,2-PD ratio. The experiments about Re/M ratio revealed that for the monometallic Ni catalyst at 40 wt % loading, the best content of Re was 7 wt %. The activity test at this optimum composition, catalyst NiRe(7)/MS, at 393 K gave 46.1 % of 1,3-PD yield with a 1,3-PD/1,2-PD ratio of 1.24 for a 98 % of conversion after 4 h of reaction.

XPS study: Ni-CuRe(7)/MS vs NiRe(7)/MS catalysts.

In order to better understand the differences in the catalytic behaviour of NiRe(7)/MS and Ni-CuRe(7)/MS catalysts, three XPS experiments were designed. In the 3 experiments, the sample was prepared as described in the experimental section. The first group of samples were named as fresh catalysts since they were the catalysts used after reduction in the quartz tube reactors. However, in these samples some degree of oxidation could be expected during catalyst handling for the XPS analysis. The second group of samples were the catalysts which were reductively activated in-situ at 623 K for 30 min and the third group of samples were the spent catalyst samples after being used in the catalytic test and without any treatment. The fresh, H₂ activated and spent samples of the supported ReO_x without metal, Re/MS were also performed to serve as a reference and for comparison.

The surface composition of the fresh and spent samples was compared to that of the theoretical composition of the catalysts (Table 5.4-4). Regarding the ratio between Ni and Cu, the nominal bulk values of the catalyst is Ni:Cu=6:1 by weight, which corresponds to an atomic ratio of Cu/Ni=0.16. The fresh sample Ni-CuRe(7)/MS exhibited a surface atomic ratio of Cu/Ni close to this value, 0.15, which means that Ni and Cu are both equally dispersed on the surface. The spent sample showed a slightly higher Cu/Ni ratio of 0.19, indicating a slight enrichment of Cu at the surface. In the H₂ activated sample, the Cu/Ni surface atomic ratio increased considerably up to 0.28, indicating segregation of Cu towards the surface. The theoretical Re/(Ni+Cu) atomic ratio was approximately 0.052 for samples NiRe(7)/MS and Ni-CuRe(7)/MS. The values of the Re/(Ni+Cu) atomic ratios at the surface measured by XPS were not very different, 0.031 (NiRe(7)/MS) and 0.047 (Ni-CuRe(7)/MS) in the fresh samples. This means that the dispersion of Re was good especially when Cu was present in the catalyst. For NiRe(7)/MS catalyst, it could be possible that Re was decorated by Ni. Interestingly, the spent samples showed comparable Re/(Ni+Cu) atomic ratios than the fresh ones, 0.039 and 0.045. In contrast, the in situ reduced samples at 623 K had lower Re/metal atomic ratios, 0.020 Re/ Ni and 0.029 Re/(Ni+Cu). The decoration of ReO_x

CHAPTER 5

by the Ni particles could explain the collaborative effect between Ni and ReO_x , which is considered responsible for the observed 1,3-PD production with NiRe(7)/MS.

Application of Acid Saponite in Glycidol Hydrogenolysis

Table 5.4-4: XPS analysis results of selected fresh, H₂ activated and used catalysts.

Catalyst	Binding energies (eV) of characteristic peaks			Re/	Ni/Cu	Ni(R)/	Cu(R)/
	Ni	Cu	Re	Ni-Cu		Ni (O)	Cu(O)
Re/MS-fresh	—	—	Ox 4d _{5/2} -265.1 Red 4d _{5/2} -260.8	—	—	—	—
Re/MS-red	—	—	Ox 4d _{5/2} -264.8 Red 4d _{5/2} -260.6	—	—	—	—
Ni-CuRe(7)/MS	Ni ⁰ 2p _{3/2} -852.4	Cu ²⁺ 2p _{3/2} -933.1	Ox 4d _{5/2} -263.9	0.047	0.15	0.14	1.14
-fresh	Ni ²⁺ 2p _{3/2} -854.4	Cu ^{0,+} 2p _{3/2} -931.1	Red 4d _{5/2} -260.6				
Ni-CuRe(7)/MS	Ni ⁰ 2p _{3/2} -852.5	Cu ²⁺ 2p _{3/2} -928.5	Ox 4d _{5/2} -263.5	0.029	0.28	0.15	1.76
-red	Ni ²⁺ 2p _{3/2} -855.8	Cu ^{0,+} 2p _{3/2} -931.7	Red 4d _{5/2} -260.6				
Ni-CuRe(7)/MS	Ni ⁰ 2p _{3/2} -852.5	Cu ²⁺ 2p _{3/2} -932.7	Ox 4d _{5/2} -263.8	0.045	0.19	0.45	3.60
-used	Ni ²⁺ 2p _{3/2} -854.5	Cu ^{0,+} 2p _{3/2} -932.2	Red 4d _{5/2} -259.5				
NiRe(7)/MS	Ni ⁰ 2p _{3/2} -852.6	—	Ox 4d _{5/2} -263.4	0.031	—	0.15	—
-fresh	Ni ²⁺ 2p _{3/2} -854.7		Red 4d _{5/2} -260.0				
NiRe(7)/MS	Ni ⁰ 2p _{3/2} -852.4	—	Ox 4d _{5/2} -263.9	0.020	—	0.13	—
-red	Ni ²⁺ 2p _{3/2} -855.9		Red 4d _{5/2} -261.3				
NiRe(7)/MS	Ni ⁰ 2p _{3/2} -852.3	—	Ox 4d _{5/2} -265.0	0.039	—	0.96	—
-used	Ni ²⁺ 2p _{3/2} -854.6		Red 4d _{5/2} -261.0				

The Re 4d spectra of the different catalysts as prepared (fresh), after H₂ activation in situ at 623 K, and after reaction (spent) are displayed in figure 5.4-5. All the spectra showed two components corresponding to two different oxidation states for Re. The red line indicates the position of the Re 4d_{5/2} photoelectrons corresponding to the lower oxidation state whereas the blue one indicates the position of the Re 4d_{5/2} photoelectrons corresponding to the higher oxidation state. The 4d_{3/2} peaks are superposed to the C 1s photoelectrons. In the fresh samples, Re was mainly in the higher oxidation state for NiRe(7)/MS and Ni-CuRe(7)/MS catalysts, whereas in the Re(10)/MS sample the contribution of the less oxidized form was more important. After in situ H₂ activation at 623 K, Re became less oxidized, but there was always a component of highly oxidized Re (probably VII or VI). It is interesting to note that the reduction degree of Re was similar for samples Re and NiRe(7)/MS (88-93%), but in the sample Ni-CuRe(7)/MS, Re was much more difficult to reduce (after reduction there was about 75% Re reduced to lower oxidation state). Probably, the Cu-Re interaction favors the electronic transfer from Re to Cu, increasing the oxidation state of Re. The spent samples exhibited both Re species, in similar amounts as in the corresponding fresh samples.

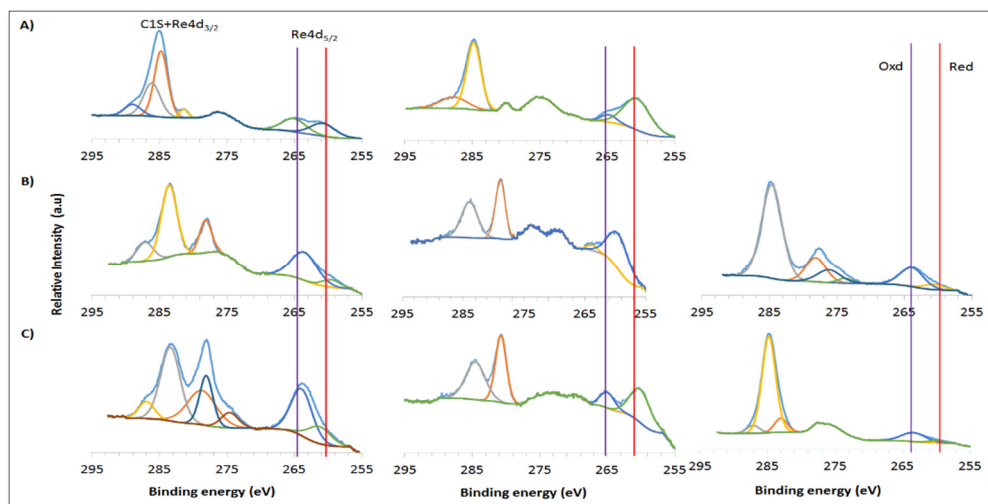


Figure 5.4-5: Re 4d spectra of A) fresh and reduced Re(7)/MS and fresh, reduced and spent catalysts, from left to right, of B) NiRe(7)/MS and C) Ni-CuRe(7)/MS. The red line indicates the position of Re in a low oxidation state whereas the blue one indicates the position of oxidized Re, both corresponding to 4d_{5/2} photoelectrons. The 4d_{3/2} peaks are superposed to the C 1s photoelectrons.

Considering the real catalysts, from the commented XPS results, it is possible to argue that there is a higher amount of Re with higher oxidation state in Ni-CuRe(7)/MS catalyst compared to NiRe(7)/MS catalyst. This might result in a higher acid activity of the catalyst, Ni-CuRe(7)/MS, according to the observed products distribution.

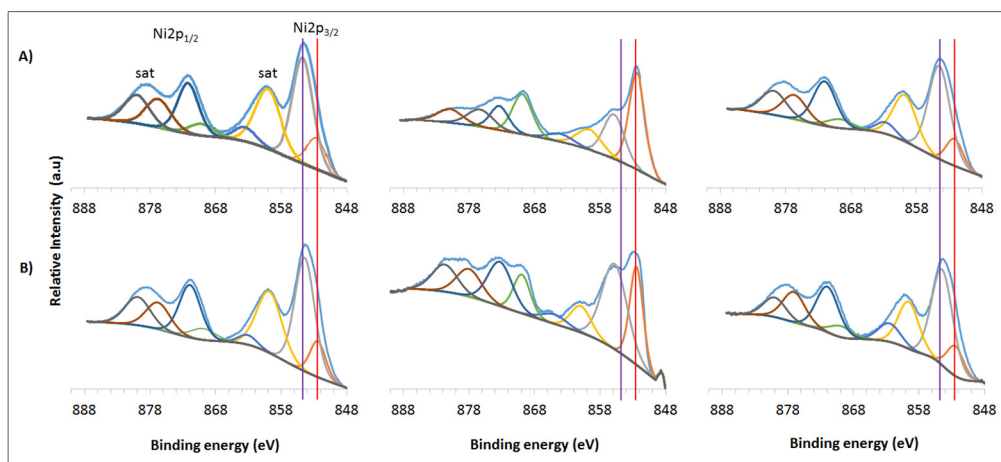


Figure 5.4-6: Ni 2p spectra of the fresh, reduced and spent catalysts, from left to right of A) NiRe(7)/MS and B) Ni-CuRe(7)/MS. The red line indicates the position of reduced Ni whereas the blue one indicates the position of oxidized Ni ($2p_{3/2}$ photoelectrons).

Figure 5.4-6 shows the Ni 2p spectra for several samples containing Ni (NiRe(7)/MS and Ni-CuRe(7)/MS). The fresh samples exhibited similar Ni spectra, with Ni mainly oxidized, but with the presence of a minor component of reduced Ni as well. After in situ H_2 activation at 623 K Ni was reduced considerably, but not totally. It is interesting to highlight that a significant fraction of Ni was still oxidized after the in situ reduction in the Ni-CuRe(7)/MS sample (about 75% of oxidized Ni). In contrast, the degree of Ni reduction was much higher in the sample without Cu, the NiRe(7)/MS sample (about 57% of oxidized Ni). This fact, together with the difficulty of reducing Re in the Ni-CuRe(7)/MS sample during the in situ reduction treatment as pointed out above, suggests that the presence of Cu strongly interacts with both Re and Ni and that Cu prevents both Re and Ni reduction. This is likely an electronic donation from Re and Ni towards Cu. Finally, the Ni spectra of NiRe(7)/MS and Ni-CuRe(7)/MS spent samples were virtually identical and similar to the corresponding

fresh samples. These experiments showed that in the catalyst without Cu, NiRe(7)/MS, there was a higher amount of reduced Ni, which in turn can be correlated with the higher propanediol selectivity.

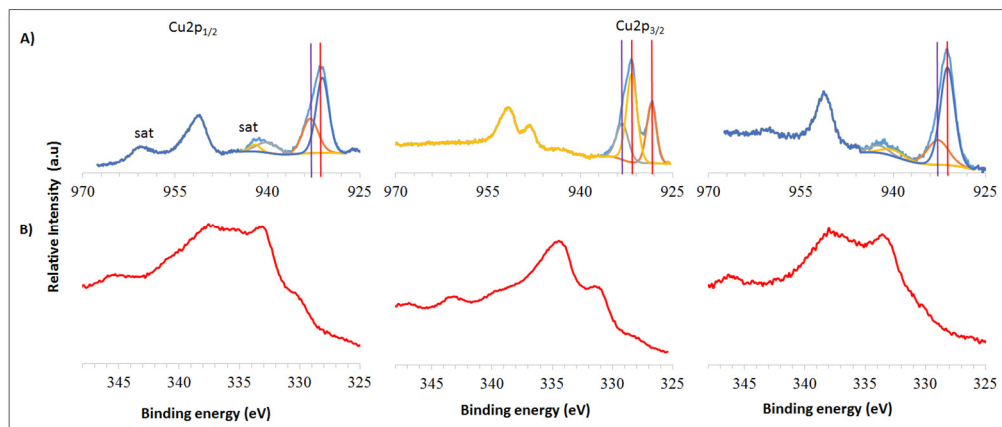


Figure 5.4-7: Cu 2p (A) and Auger Cu LMM (B) spectra of fresh, reduced and spent Ni-CuRe(7)/MS catalyst. The red line indicates the position of reduced Cu whereas the blue one indicates the position of oxidized Cu ($2p_{3/2}$ photoelectrons). In addition, Cu(II) species are accompanied by satellite lines (sat).

Figure 5.4-7 shows the Cu 2p spectra for the sample Ni-CuRe(7)/MS) as well as the Cu LMM Auger lines. In the fresh sample both reduced and oxidized Cu can be observed. However, after in situ H_2 activation at 623 K the spectrum changed dramatically and Cu was strongly reduced (about 78%). This was also clearly observed in the Auger lines, where the peaks at 334.9 and 332.0 eV clearly showed the presence of metallic Cu. It is outstanding the absence of satellite lines and the appearance of two different reduced Cu species after the in situ reduction treatment in the Cu 2p spectra. At this point it is difficult to unambiguously identify the nature of these two species. One of the components may correspond to metallic Cu and the other one can be assigned to a Cu-M interaction. In fact, the electron donation from Re and Ni towards Cu in the Ni-CuRe(7)/MS) sample, discussed above, agrees with the observed strongly reduced component in the Cu 2p spectrum, which is compatible with the existence of a type of Cu that acts as an electron acceptor. Finally, for the spent sample the spectrum was similar to that of the fresh one, although the lower

intensity of the satellite lines in the 2p spectrum indicates a slightly higher reduction character in the spent sample.

Conclusions

Ni-Cu catalysts prepared at 40 wt % total metal loading were modified with 7 wt % Mo, V, W and Re loading with respect to the unmodified catalyst. Some catalysts at different Ni-Cu/Re ratio and Re modified monometallic Ni and Cu catalysts, were prepared for comparison. The characterization results revealed that the presence of all modifiers except tungsten made the reduction of NiO more difficult. The reducibility of NiO got harder when the amount of metal loading was lower and the wt % of Re loading increased. Total surface acidity and acidity strength increased in the presence of modifiers, with an increase in the amount of modifier and with a decrease in the amount of metal loading. BET area and XRD analysis revealed that the dispersion of the NiO and the Ni in precursors and catalysts, respectively, increased in the presence of modifiers and with a decrease in the amount of Ni-Cu loading; the dispersive effect was higher in the presence of Re modifier.

The catalytic activity of all the modified catalysts was comparable or higher than the unmodified catalysts. The presence of V and Re modifier increased the 1,3-PD and 1,2-PD ratio to 0.45 and 0.7, respectively compared to the unmodified catalyst (0.33) or those modified with W (0.24) or Mo (0.33). The results confirmed that Re plays an important role in improving the 1,3 production. The W modified catalyst gave the highest selectivity to propanediol (82%), the lowest selectivity to condensation products (2%) and the lowest 1,3-PD/1,2-PD ratio, in agreement with its high NiO reducibility and hence metal activity.

The important role of Re modifier was confirmed by the increase of 1,3-PD/1,2-PD ratio when Re/ Ni + Cu ratio increased by increasing the Re content or decreasing the Ni-Cu loading. However, at lower metal loading the diol selectivity was lower and the selectivity to the condensation products was higher as would be expected from the low NiO reducibility and high acidity of these samples. The monometallic Cu catalysts gave the lowest propanediol and the highest condensation products selectivity comparable to that of the Re modified support without an active metal. This

confirmed the lower hydrogenolysis capacity of Cu in the catalytic system. The modified Ni catalysts showed high 1,3-PD/1,2-PD ratio (1.24), high propanediol selectivity and the highest 1,3-PD yield (46.1%) of all the catalysts studied. The results can be explained by some decoration of the Ni particles by the ReO_x that favour the collaborative action between the metal sites and ReO_x responsible for the 1,3-PD production. The yield of 1,3-PD obtained in this work was comparable or higher than those previously reported in literature with glycerol, using noble metal catalysts, at harsh reaction conditions and longer reaction times.

Acknowledgments

The authors are grateful for the financial support of the Ministerio de Economía y Competitividad of Spain and FEDER funds (CTQ2011-24610).

6. General conclusions



In this chapter, the main findings of the thesis are highlighted and important conclusions are drawn.

Study of parameters of influence in mesoporous saponite synthesis

Several saponites were prepared at pH 8 and 13, using microwaves or conventional oven during the aging treatment, without and with template (polymer or surfactant) and from slurries of different degrees of dilution for samples prepared a pH 8. The effect of surfactant in the in-situ hydrothermal crystallization and post-synthesis modification was studied.

- The use of conventional oven in the aging treatment, at both pH (8 and 13), reduced the amount of amorphous silica content and improved the O-Si-O ordering. On the other hand, the use of microwaves increased the Al^T/Al^O ratio and delamination, with an increase of specific BET area, C.E.C and acidity.
- The presence of polymer, at pH 8, showed a dilution dependent effect and improved stacking at lower dilution and assisted delamination at medium dilution. At both pH (8 and 13) and aging conditions (microwaves or conventional oven) and independent of degree of slurry dilution, the presence of polymer helped to decrease the amount of amorphous silica, improved the O-Si-O ordering, but a lower Al^T/Al^O ratio was obtained. At pH 13, surfactant resulted in the presence of amorphous silica, lower Al^T/Al^O ratio and lower C.E.C value.
- Both polymer and surfactant improved delamination of the saponite both at pH 8 and 13. However, the surface area and porosity of the samples prepared with surfactant was higher due to the easier in the removal of the surfactant than the polymer by calcination.
- The amount of amorphous silica, Al^T/Al^O ratio, specific BET area and C.E.C decreased and the ordering of the O-Si-O bond increased with a decrease in the synthesis gel dilution, in both conventional and microwaves synthesis. Sample synthesized at medium dilution, SM8(125) showed the highest surface area, C.E.C value and Al^T/Al^O ratio.

- At pH 13, the use of surfactant in both in-situ hydrothermal crystallization and in post-synthesis modification gave delaminated samples. However, the degree of delamination was higher in the in situ synthesis than by post synthesis modification.

Among all the synthesized samples, the highest specific BET area ($600 \text{ m}^2/\text{g}$) was obtained using surfactant as a template, at pH 13 and using microwaves during the aging treatment. The highest surface acidity (1.02-1.07) was obtained for samples prepared at pH 13, with conventional oven or microwaves.

Study of Ni supported on acid mesoporous saponite catalysts for the hydrogenolysis of glycidol

Several Ni supported on various acid mesoporous saponite catalysts were tested for the hydrogenolysis of glycidol. The factors studied were, use of saponites with different properties, wt % of Ni loading, temperature and time of the reaction.

- The acidity and specific BET area of the support played an important role on the dispersion and reducibility of the NiO particles.
- Catalysts prepared at lower Ni loading (15 wt %) showed lower reducibility, higher dispersion, and higher surface acidity and gave lower conversion and lower propanediol selectivity, but higher 1,3-PD/ 1,2-PD ratio than the corresponding samples prepared at higher Ni loading (30 and 40 wt %).
- Catalysts prepared with the Na-form of the saponite or at higher Ni loading gave lower 1,3-PD/1,2-PD ratio. This confirmed the important role of acid sites in the selective formation of 1,3-PD by the activation of the oxirane ring.
- The conversion and 1,3-PD/ 1,2-PD ratio increased and the propanediol selectivity decreased with an increase in the reaction temperature. The best catalytic results, with 29% yield to 1,3-PD, a 1,3-PD/ 1,2-PD ratio of 0.49 at total conversion, was obtained at 453 K, 5 MPa H_2 pressure and after 1 h of reaction, using Ni(40)/S5 as catalyst.

Effect of the presence of Cu on acid saponite supported Ni catalysts in glycidol hydrogenolysis.

The effect of the presence of Cu in Ni catalysts was investigated by preparing Ni-Cu catalysts at different Ni and Cu wt % ratio, using a saponite (S) synthesized with conventional oven at pH 13, as support. The effect of the reaction temperature was studied on some selected catalysts by performing the reaction at 393 and 453 K.

- Characterization results revealed the formation of Ni-Cu alloy in Ni-Cu bimetallic catalysts.
- The presence of Cu in the Ni-Cu catalysts and the increase in its wt % resulted in lower conversion, lower propanediol selectivity but the 1,3-PD/ 1,2-PD ratio increased slightly.
- At higher reaction temperature (453 K), the conversion and 1,3-PD/ 1,2-PD ratio increased and the selectivity to propanediols decreased. The decrease in propanediol selectivity was especially important in catalysts with high Cu wt %.
- The presence of small amount of Cu was desirable to moderate the Ni activity and favour the metal-acid cooperative mechanism. The better Ni-Cu wt % ratio was (6:1) and with this catalyst and at 453 K, 20% of 1,3-PD yield was obtained at 94% conversion, 1,3-PD/ 1,2-PD ratio of 0.57 and after 1 h of reaction.

Role of modifiers on the activity of Ni, Cu and Ni-Cu bimetallic catalysts supported on mesoporous acid saponite in the hydrogenolysis glycidol.

The effect of the presence of various metal oxide (Mo, V, W and Re) modifiers in Ni, Cu and Ni-Cu catalysts supported on mesoporous acid saponite, on the hydrogenolysis of glycidol was investigated. The effect of metal to modifier weight percentage ratio on the catalytic activity was studied.

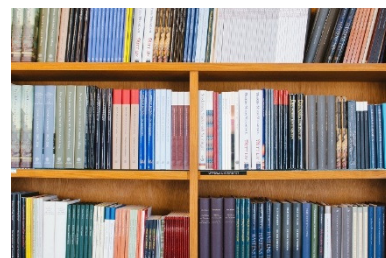
- The NiO reducibility was lower in the presence of modifiers except W while the surface acidity and acidity strength was higher.
- The dispersion of NiO increased in the presence of modifiers and with a decrease in the amount of metal loading. The dispersive effect was higher in

the case of ReOx modifier. The presence of Cu assisted the dispersion of ReOx and Ni. For ReOx modified monometallic Ni catalyst, Ni decorated with ReOx was observed.

- The 1,3-PD/ 1,2-PD ratio increased for V and Re modified catalysts with respect to unmodified catalyst. ReOx modified monometallic Ni catalyst gave the highest 1,3-PD/ 1,2-PD ratio (1.24) and 1,3-PD yield (46 %) at 393 K, 5 MPa H₂ pressure after 4 h. This was the highest yield of 1,3-PD obtained in this work. The high 1,3-PD yield was justified by metal-modifier collaborative mechanism.
- The 1,3-PD yield, obtained in this thesis, by catalytic hydrogenolysis of glycidol using cheap modified Ni-Cu catalysts at short time (1-4 h), at moderate reaction conditions (393 K and 5MPa H₂) was comparable or higher than many noble metal based catalytic systems that require harsh reaction conditions and longer reaction times to hydrogenolyze glycerol.

In the thesis, it was confirmed that glycidol could be an alternative substrate to glycerol for the catalytic production of 1,3-PD. Saponite served as an efficient acid support for the hydrogenolysis of glycidol to favor the formation of 1,3-PD.

7. References



- Adoor, S.G., Sairam, M., Manjeshwar, L.S., Raju, K.V.S.N., Aminabhavi, T.M. (2006). Sodium montmorillonite clay loaded novel mixed matrix membranes of poly(vinyl alcohol) for pervaporation dehydration of aqueous mixtures of isopropanol and 1,4-dioxane. *J. Membr. Sci.*, 285 (1-2), 182-195.
- Akiyama, M., Sato, S., Takahashi, R., Inui, K., Yokota, M. (2009). Dehydration-hydrogenation of glycerol into 1,2-propanediol at ambient hydrogen pressure. *Appl. Catal. A: Gen.*, 371, 60-66.
- Alther, G. R. (2003). The organo-clay/carbon combination for efficient PCB removal. *Contam. Soils*, 8, 189-200.
- Amada, Y., Shinmi, Y., Koso, S., Kubota, T., Nakagawa, Y., Tomishige, K. (2011). Reaction mechanism of the glycerol hydrogenolysis to 1,3-propanediol over Ir-ReOx/SiO₂ catalyst, *Appl. Catal. B: Environ.*, 105, 117-127.
- Ames, L.L., Sand, L.B. (1958). Factors effecting maximum hydrothermal stability in montmorillonites. *Am. Miner.*, 43, 641-648.
- Anastas, P.T., Warner, J.C. (1998). *Green Chemistry: Theory and Practice*, Oxford University Press: New York, 30.
- Andrew, E. R., Bradbury, A., Eades, R. G. (1959). Removal of Dipolar Broadening of Nuclear Magnetic Resonance Spectra of Solids by Specimen Rotation. *Nature*, 183, 1802-1803.
- Andrieux, P., Petit, S. (2010). Hydrothermal synthesis of dioctahedral smectites: The Al-Fe³⁺ chemical series: Part I: Influence of experimental conditions. *Appl. Clay Sci.*, 48 (1-2), 5-17.
- Arhancet J. P., Carrick W. J., Himelfarb P., Kazi M. S., Plundo, R. A., Powell J. B. (2000). Catalyst and process for preparing 1,3-propanediol. WO 2000025914 A1, to Shell.
- Arntz, D., Wiegand, N. (1991). Preparation of 1,3-propanediol by hydration of acrolein over phosphonate or aminophosphonate group containing ion exchange resins and subsequent catalytic hydrogenation. *Eur. Pat.* 412337, to Degussa AG.
- Arundhathi R., Mizugaki T., Mitsudome T., Jitsukawa K., Kaneda K. (2013). Highly Selective Hydrogenolysis of Glycerol to 1,3-Propanediol over a Boehmite-Supported Platinum/Tungsten Catalyst. *ChemSusChem*, 6, 1345-1347.

- Auerbach, M., Carrado, Kathleen A., Dutta, Prabir K. (Eds.). (2004). *Hand Book of Layered Materials*. Marcel Dekker, New York, Basel, 91–124.
- Babel, S., Kurniawan, T.A., 2003. Low-cost adsorbents for heavy metals uptake from contaminated water: a review. *J. Hazard. Mater.* 97 (1–3), 219–243.
- Bai, R., Zhang, H., Mei, F., Wang, S., Li, T., Gu, Y., Li, G. (2013). One-pot synthesis of glycidol from glycerol and dimethyl carbonate over a highly efficient and easily available solid catalyst NaAlO_2 . *Green Chem.*, 15, 2929–2934.
- Baños, R, Manzano-Agugliaro, F, Montoya, F. G., Gil, C., Alcayde, A., Gómez, J. (2011). Optimization methods applied to renewable and sustainable energy: A review. *Renew. Sust. Energ. Rev.*, 15 (4), 1753–1766.
- Bartók1, M., Fási, A., Notheisz, F. (1998a). The mechanism of hydrogenolysis and isomerization of oxacycloalkanes on metals XV. Transformation of ethyl- and vinyloxirane on Cu-SiO_2 . *J. Mol. Catal. A: Chem.*, 135, 307–316.
- Bartók1, M., Fási, A., Notheisz, F. (1998b). Transformation of vinyloxirane on Pt/SiO_2 and Pd/SiO_2 . *J. Catal.*, 175, 40–47.
- Barton, D. G., Soled, S. K., Meitzner, G. D., Fuentes, G. A., Iglesia, E. (1999). Structural and Catalytic Characterization of Solid Acids Based on Zirconia Modified by Tungsten Oxide. *J. Catal.*, 181, 57–72.
- Barwood, M. J., Breen, C., Clegg F., Hammond, C. L. (2014). The effect of organoclay addition on the properties of an acrylate based, thermally activated shape memory polymer. *Appl. Clay Sci.*, 102, 41–50.
- Batista, J., Pinar, A., Gomilšek, J.P., Kodre, A., Bornette, F. (2001). On the structural characteristics of gamma-alumina-supported Pd-Cu bimetallic catalysts. *Appl. Catal., A: Gen.*, 217, 55–68.
- Bech, J., 1987. *Les Terres Medicinales*. Discurs per Reial Academia de Farma`cia de Barcelona. Ed. Reial Acade`mia de Farma`cia de Barcelona-CIRIT (Generalitat de Catalunya), Barcelona, 105 pp.
- Beck, J. S., Vartuli, J. C., Roth, W. J., Leonowicz, M. E., Kresge, C. T., Schmitt, K. D, Chu, C. T., Olsen, D. H., Sheppard, E. W., McCullen, S. B., Higgins, J. B., Schlenkar, J. L. (1992). A new family of mesoporous molecular sieves prepared with liquid crystal templates. *J. Am. Chem. Soc.* 114, 10834–10843.

- Behr, A., Lilting J., Irawadi, K., Leschinski, J., Lindner, F. (2008). Improved utilization of renewable resources: New important derivatives of glycerol. *Green Chem.*, 10, 13-30.
- Bergadà, O., Vicente, I., Salagre, P., Cesteros, Y., Medina, F., Sueiras, J. E. (2007). Microwave effect during aging on the porosity and basic properties of hydrotalcites. *Microporous and Mesoporous Mater.*, 101, 363-373.
- Bergaoui, L., Lambert, J-F., Franck, R., Suquet, H., Robert, J-L. (1995). Al-pillared saponites. Part 3. Effect of parent clay layer charge on the intercalation-pillaring mechanism and structural properties. *J. Chem. Soc. Faraday Trans.*, 91, 2229-2139.
- Bergaya, F., Lagaly, G. (2006). General Introduction: Clays, Clay Minerals, and Clay Science. In: Bergaya, F., Theng, B.K.G., Lagaly, G. (Eds.), *Handbook of Clay Science: Developments in Clay Science*, vol. 1. Amsterdam, Elsevier, 1-18.
- Bergaya, F., Vayer, M. (1997). C.E.C of clays: Measurement by adsorption of a copper ethylenediamine complex, *Appl. Clay Sci.*, 12, 275-280.
- Bernardo, C.A., Alstrup, I., Rostrup-Nielsen, J.R. (1985). Carbon deposition and methane steam reforming on silica-supported Ni-Cu catalysts. *J. Catal.*, 96, 517-534.
- Bisio, C., Gatti, G., Boccaleri, E., Marchese, L., Superti, G.B., Pastore, H.O., Thommes, M. (2008). Understanding physico-chemical properties of saponite synthetic clays. *Microporous Mesoporous Mater.* 107 (1-2), 90-101.
- Bisio, C., Carniato, F., Paul, G., Gatti, G., Boccaleri, E., Marchese, L., Avogadro, A. (2011). One-pot synthesis and physicochemical properties of an organo-modified saponite clay. *Langmuir*, 27, 7250-7257.
- Bolívar-Díaz, C. L., Calvino-Casilda, V., Rubio-Marcos, F., Fernández, J. F., Bañares, M. A. (2013). New concepts for process intensification in the conversion of glycerol carbonate to glycidol, *Appl. Catal. B: Environ.*, 129, 575-579.
- Boyd, S. A., Shaobai, S., Lee, J-F., Mortland, M. M. (1988). Pentachlorophenol sorption by organo-clays. *Clays Clay Miner.*, 36, 125-130.

- Bozell J.J., Petersen G.R. (2010). Technology development for the production of biobased products from biorefinery carbohydrates-the US Department of Energy's "Top 10" revisited. *Green Chem.*, 12, 539-554.
- Bradley, S.M., Howe, R.F., Kydd, R.A. (1993). Correlation between aluminum-27 and gallium-71 NMR chemical shifts. *Magn Reson Chem* 31:883-886.
- Bradley, S.M., Kydd, R.A., Fyfe, C.A. (1992). Characterization of the galloaluminate $\text{GaO}_4\text{Al}_{12}(\text{OH})_{24}(\text{H}_2\text{O})_{12}^{7+}$ polyoxocation by MAS NMR and infrared spectroscopies and powder X-ray diffraction. *Inorg. Chem.*, 31, 1181-1185.
- Breen, C., Watson, R., Madejova, J., Komadel, P., Klapyta, Z. (1997). Acid-activated organoclays: Preparation, characterization and catalytic activity of acid-treated tetraalkylammonium-exchanged smectites. *Langmuir*, 13, 6473-6479.
- Brigatti, M.F., Galan, E., Theng, B.K.G. (2006). Structures and Mineralogy of Clay Minerals. In: Bergaya, F., Theng, B.K.G., Lagaly, G. (Eds.), *Handbook of Clay Science: Developments in Clay Science*, vol. 1. Elsevier, Amsterdam, 19-86.
- Bruijninx, P. C. A., Ramân-Leshkov. (2014). Sustainable catalytic conversions of renewable substrates. *Catal. Sci. Technol.*, 4, 2180-2181.
- Bull, T.E. (1999). Biomass in the Energy Picture. *Science*, 285, 1209-1209.
- Burch R. (ed.) *Pillared Clays*. (1988). *Catal. Today*, 2, 185-366.
- Busca, G. (2007). Acid catalysts in industrial hydrocarbon chemistry. *Chem. Rev.* 107, 5366-5410.
- Butruille J.R., T.J. Pinnavaia, in: J.L. Atwood et al. (Eds.), *Comprehensive Supramolecular Chemistry*, vol. 7, Pergamon Press, Oxford, 1996, p.219.
- Caley, P. N., Everett, R. C. (1967). Thermochemical Conversion of Biomass to Liquid Fuels and Chemicals. Patent US 3350871, to DuPont.
- Carniato, F., Bisio, C., Gatti, G., Guidotti, M., Sordelli, L., Marchese, L. (2011). Organic-inorganic hybrid saponites obtained by intercalation of titanosilsesquioxane. *Chem. Asian. J.*, 6 (3), 914-921.
- Carrado, K. A., Xu, L. (1998). In Situ Synthesis of Polymer-Clay Nanocomposites from Silicate Gels. *Chem. Mater.*, 10, 1440-1445.

- Carrado, K. A., Xu, L. (1999). Materials with controlled mesoporosity derived from synthetic polyvinylpyrrolidone–clay composites. *Microporous and Mesoporous Mater.*, 27(1), 87-94.
- Carrero, A., Calles, J.A., Vizcaíno, A.J. (2010). Effect of Mg and Ca addition on coke deposition over Cu-Ni/SiO₂ catalysts for ethanol steam reforming. *Chem. Eng. J.*, 163, 395–402.
- Carretero, M.I. (2002). Clay minerals and their beneficial effects upon human health. A review. *Appl. Clay Sci.*, 21 (3–4), 155–163.
- Casagrande, M., Storaro, L., Lenarda, M., Rossini, S. (2005). Solid acid catalysts from clays: oligomerization of 1-pentene on Al-pillared smectites. *Catal. Commun.*, 6, 568–572.
- Chaminand, J., Djakovitch, L., Gallezot, P., Marion, P., Pinel, C., Rosier, C. (2004). Glycerol hydrogenolysis on heterogeneous catalysts. *Green Chem.*, 6, 359-361.
- Che, T. M. (1987). Production of propanediols. US 4642394, to Celanese Corp.
- Cheeke, J. (2002). *Fundamentals and Applications of Ultrasonic Waves* (CRC Press, Boca Raton).
- Chen, K., Koso, S., Kubota, T., Nakagawa, Y., Tomishige, K. (2010). Chemoselective Hydrogenolysis of Tetrahydropyran-2-methanol to 1,6-Hexanediol over Rhenium-Modified Carbon-Supported Rhodium Catalysts. *ChemCatChem*, 2, 547-555.
- Chen, K., Mori, K., Watanabe, H., Nakagawa, Y., Tomishige, K. (2012). C-O bond hydrogenolysis of cyclic ethers with OH groups over rhenium-modified supported iridium catalysts. *J. Catal.*, 294, 171–183.
- Chevalier, S., Franck, R., Suquet, H., Lambert, J-F., Barthomeuf, D. (1994). Al-Pillared saponites. Part 1.-IR studies. *J. Chem. Soc. Faraday Trans.*, 90, 667-674.
- Chia, M., Pagán-Torres, Y.J., Hibbitts, D.D., Tan, Q., Pham, H.N., Datye, A.K., Neurock, M., Davis, R.J., Dumesic, J.A. (2011). Selective hydrogenolysis of polyols and cyclic ethers over bifunctional surface sites on rhodium-rhenium catalysts. *J. Am. Chem. Soc.*, 133, 12675-12689.
- Choy, J.-H., Choi, S.-J., Oh, J.-M., Park, T. (2007). Clay minerals and layered double hydroxides for novel biological applications. *Appl. Clay Sci.* 36 (1-3), 122-132.

- Christidis, G.E., Scott, P.W., Dunham, A.C. (1997). Acid activation and bleaching capacity of bentonites from the islands of Milos and Chios, Aegean, Greece. *Appl. Clay Sci.*, 12, 329-347.
- Cohen, J. B.; Schwartz, L. H. (1977). *Diffraction from Materials*, Academic Press, New York.
- Collins, M. J., Jr. (2010). Future trends in microwave synthesis *Future Med. Chem.*, 2, 151-155.
- Corma, A. (1997). From microporous to mesoporous molecular sieve materials and their use in catalysis *Chem. Rev.*, 97, 2373-2420.
- Corma, A., Iborra, S., Velty, A. (2007). Chemical Routes for the Transformation of Biomass into Chemicals. *Chem. Rev.*, 107, 2411-2502.
- Costenaro, D., Gatti, G., Carniato, F., Paul, G., Bisio, C., Marchese, L. (2012). The effect of synthesis gel dilution on the physico-chemical properties of acid saponite clays. *Microporous and Mesoporous Mater.*, 162, 159-167.
- Crum, L.A., Mason, T.J, Reisse, J., Suslick K.S. (Eds.) (1999). *Sonochemistry and sonoluminescence*, NATO ASI Series C, Vol. 524, Kluwer, Dordrecht, p.424.
- da Silva G. P., Mack M., Contiero J. (2009). Glycerol: a promising and abundant carbon source for industrial microbiology. *Biotechnol. Adv.*, 27, 30-39.
- Dahl, J.A.; Maddux, B.L.S.; Hutchison, J.E. (2007). Toward greener nanosynthesis. *Chem. Rev.*, 107, 2228-2269.
- Dam, J., Hanefeld, U. (2011). Renewable Chemicals: Dehydroxylation of Glycerol and Polyols, *ChemSusChem*, 4, 1017–1034.
- Dasari, M. A., Kiatsimkul, P.-P., Sutterlin, W. R., Suppes, G. J. (2005). Low-pressure hydrogenolysis of glycerol to propylene glycol. *Appl. Catal., A: Gen.*, 281, 225-231.
- Davidson, R.S.; Safdar, A., Spencer, J.D., Robinson, B. (1987). Applications of Ultrasound to Organic Chemistry. *Ultrasonics*, 25, 35-39.
- de Boer, J.H. (1958) *The Structure and Properties of Porous Materials*, Everett, D.H., Stone, F.S., Eds, Butterworths, London, p. 68.
- Decarreau, A. (1981). Cristallo-gène-se à basse température de smectites trioctae-driques par vieillissement de coprecipites silicome talliques de formule (Si(4-

$x)Al_x)M_3^{2+}O_{11}.nH_2O$, où x varie de 0 à 1 et où $M^{2+}=Mg-Ni-Co-Zn-Fe-Cu-Mn$.
Compt. Rend. Acad. Sci. Ser., II 292, 61-64.

- Dentel, S. K., Bottero, J. Y., Khatib, K., Demougeot, H., Duguet, J. P., Anselme, C. (1995). Sorption of tannic acid, phenol and 2,4,5-trichlorophenol on organoclays. *Water Res.*, 29, 1273-1280.
- Deutsch, K. L., Shanks, B. H. (2012). Active species of copper chromite catalyst in C–O hydrogenolysis of 5-methylfurfuryl alcohol. *J. Catal.*, 285, 235-241.
- Didi, M.A., Makhoukhi, B., Azzouz, A., Villemin, D. (2009). Colza oil bleaching through optimized acid activation of bentonite. A comparative study. *Appl. Clay Sci.*, 42, 336-344.
- Ding, Z., Kloprogge, J.T., Frost, R.L., Lu, G.Q., Zhu, H.Y. (2001). Porous clays and pillared clays-based catalysts. Part 2: A review of the catalytic and molecular sieve applications. *J. Porous Mater.*, 8 (4), 273-293.
- Drent, E., Jager, W. W. (2000). Hydrogenolysis of glycerol. US Patent 6080898, to Shell Oil Co.
- Farmer, V.C., Krishnamurti, G.S.R., Huang, P.M. (1991). Synthetic allophane and layersilicate formation in $SiO_2-Al_2O_3-FeO-Fe_2O_3-MgO-H_2O$ systems at 23°C and 89°C in a calcareous environment. *Clays Clay Miner.*, 39 (6), 561-570.
- Farmer, V.C., McHardy, W.J., Elsass, F., Robert, M. (1994). hkl-ordering in aluminous nontronite and saponite synthesized near 90 °C: effects of synthesis conditions on nontronite composition and ordering. *Clays Clay Miner.*, 42 (2), 180-186.
- Fási, A., Pálinkó, I., Kiricsi, I. (1999). Ring-opening and dimerization reactions of methyl- and dimethyloxiranes on HZSM-5 and CuZSM-5 zeolites. *J. Catal.*, 188, 385-392.
- Fási, A., Pálinkó, I., Kiricsi, I. (2000). Ring-opening reactions of ethyl- and vinyl-oxirane on HZSM-5 and CuZSM-5 catalysts. *Stud. Surf. Sci. Catal.*, 130, 839-844.
- Fási, A., Gömöry, Á., Pálinkó, I., Kiricsi, I. (2001). Isomerization and dimerization reactions of methyloxirane over various types of zeolite and zeotype. *J. Catal.*, 200, 340-344.

- Fási, A., Pálincó, I., Hernadi, K., Kiricsi, I. (2002). Ring-opening reactions of propylene oxide (methyloxirane) over Au/MgO and unsupported Au catalysts. *Catal. Lett.*, 81, 237-240.
- Fási A., Pálincó I., Gömöry Á., Kiricsi I. (2004). Ring-opening, dimerization and oligomerization reactions of methyloxirane on solid acid and base catalysts. *J. Mol. Catal. A: Chem.*, 208, 307-311.
- Feng J., Wang J., Zhou Y., Fu H., Chen H. and Li X. (2007). Effect of Base Additives on the Selective Hydrogenolysis of Glycerol over Ru/TiO₂ Catalyst. *Chem. Lett.*, 36, 1274–1275.
- Fernando, S., Adhikari, S., Chandrapal, C., Murali, N. (2006). Biorefineries: current status, challenges and future direction. *Energy Fuels*, 20, 1727-1737.
- Fetter, G., Tichit, D., de Menorval, L.C., Figueras, F. (1995) Synthesis and characterization of pillared clays containing both Si and Al pillars. *Appl. Catal. A: Gen.*, 126, 165–176.
- Figueras F. (1988). Pillared Clays as Catalysts. *Catal. Rev.-Sci. Eng.*, 30 (3). 457-499.
- Folleteo E.L., Morgado A.F., Porto L.M. (2001). Influência do tipo de ácido usado e da sua concentração na ativação de uma argila bentonítica. *Cerâmica*, 47, 208-211.
- Frost, RL, Kristof, J, Paroz, G.N., Klopogge, J.T. (1998). Raman spectroscopy o intercalated kaolinites. In: 16th international conference on raman spectroscopy, Cape Town, South Africa, 686–887.
- Furikado I., Miyazawa T., Koso S., Shimao A., Kunimori K. and Tomishige K. (2007). Catalytic performance of Rh/SiO₂ in glycerol reaction under hydrogen. *Green Chem.*, 9, 582–588.
- Gade, S.M., Munshi, M.K., Chherawalla, B.M., Rane, V.H., Kelkar, A.A. (2012). Synthesis of glycidol from glycerol and dimethyl carbonate using ionic liquid as a catalyst. *Catal. Commun.*, 27, 184-188.
- Gandarias, I., Arias, P.L., Requies, J., Guemez, M.B., Fierro, J.L.G. (2010). Hydrogenolysis of glycerol to propanediols over a Pt/ASA catalyst: The role of acid and metal sites on product selectivity and the reaction mechanism. *Appl. Catal. B: Environ.*, 97, 248-256.

- Gandarias, I., Fernández, S.G., Doukkali, M.E., Reques, J., Arias, P. L. (2013). Physicochemical study of glycerol hydrogenolysis over a Ni–Cu/Al₂O₃ catalyst using formic acid as the hydrogen source. *Top. Catal.*, 56, 995-1007.
- Gandarias, I., Reques J., Arias P. L., Armbruster U., Martin A. (2012). Liquid phase glycerol hydrogenolysis by formic acid over Ni-Cu/Al₂O₃ catalysts. *J. Catal.*, 290, 79-89.
- Gandía, L.M., Gil, A., Vicente, M.A., Belver, C. (2005). Dehydrogenation of ethylbenzene on alumina-pillared Fe-rich saponites. *Catal. Lett.*, 101 (3-4), 229-234.
- Garade, A.C., Biradar, N.S., Joshi, S.M., Kshirsagar, V.S., Jha, R.K., Rode, C.V. (2011). Liquid phase oxidation of p-vanillyl alcohol over synthetic Co-saponite catalyst, *Appl. Clay Sci.*, 53, 157-163.
- Gebretsadik, F. B., Salagre, P., Cesteros, Y. (2014). Use of polymer as template in microwave synthesis of saponite. Study of several factors of influence. *Appl. Clay Sci.*, 87, 170-178.
- Gebretsadik, F. B., Mance, D., Baldus, M., Salagre, P., Cesteros, Y. (2015a) Microwave synthesis of delaminated acid saponites using quaternary ammonium salt or polymer as template. Study of pH influence. *Appl. Clay Sci.*, DOI: 10.1016/j.clay.2015.05.004.
- Gebretsadik, F. B., Ruiz-Marinez, J., Salagre, P., Cesteros, Y. (2015b). Selective hydrogenolysis of glycidol to propanediols using Ni supported on various mesoporous acid saponites as bi-functional catalysts. *Chem. Eng. J.*, Submitted.
- Gedanken A. (2007). Using Sonochemistry for the fabrication of nanomaterials. *Ultrason. Sonochem.*, 14, 418–430.
- Gedanken A., Mastai Y., In *Chemistry of Nanomaterials*, Vol. 1: C. N. R. Rao, A. Müller, A. K. Cheetham (Eds.) (2005). Wiley-VCH, 3rd reprint, 113-169.
- Girke, W., Klenk, H., Arntz, D., Neher, A., Hass, T. (1998). Process for the preparation of 1,2- and 1,3-propanediol. DE 4238492 A1, to Degussa.
- Gladysz, J. A. (2002). Introduction: Recoverable catalysts and reagents-Perspective and prospective. *Chem. Rev.*, 102, 3215-3216.

- Gong, L., Lu, Y., Ding, Y., Lin, R., Li, J., Dong, W., Wang, T., Chen, W. (2010). Selective hydrogenolysis of glycerol to 1,3-propanediol over a Pt/WO₃/TiO₂/SiO₂ catalyst in aqueous media. *App. Catal. A: Gen.*, 390, 119-126.
- González, M. D., Cesteros, Y., Salagre, P., Medina, F., Sueiras, J. E. (2009). Effect of microwaves in the dealumination of mordenite on its surface and acidic properties. *Micropor. Mesopor. Mater.*, 118, 341-347.
- Gottschalk, G., Averhoff, B. (1992). Process for the microbiological preparation of 1,3-propane-diol from glycerol by citrobacter. US Patent 5164309, to Unilever Patent Holdings.
- Gregg, S.J. and Sing, K.S.W. (1982) Adsorption, Surface Area and Porosity, 2nd Edn, Academic Press, London.
- Griffen, D. T. (1992). Silicate Crystal Chemistry. Oxford University Press: Oxford, U.K.
- Grigorév, A. A., Markina, N. G., Katsman, L. A., Malnykina, M. I., Zavorotov, V. I., Pozin, L. S. (1979) Preparation of glycidol by a chlorine-free method, *Neftekhimiya*, 19, 803-808 (in Russian).
- Guggenheim, S. Martin, R. T. (1995). Definition of clay and clay mineral: joint report of the Aipea nomenclature and cms nomenclature committees. *Clays and Clay Minerals*, 43 (2), 255-256.
- Haas, T., Yu, D., Sauer, J., Arntz, D., Freund, A., Tacke, T. (1998). Process for the production of 1,3-propanediol by hydrogenating 3-hydroxypropionaldehyde. WO1998057913 A1.
- Haas, T., Jaeger, B., Weber, R., Mitchell, S.F., King C.F. (2005). New diol processes: 1,3-propanediol and 1,4-butanediol. *Appl. Catal. A: Gen.*, 280 83-88.
- Hanson, R. M. (1991). The synthetic methodology of non-racemic glycidol and related 2,3-epoxy alcohols. *Chem. Rev.*, 91, 437-476.
- He, H. P., Guo, J. G., Xie, X. D, Peng, J. L. (2001). Location and migration of cations in Cu²⁺-adsorbed montmorillonite. *Environ. Int.*, 26, 347-352.
- Herney-Ramirez J., Costa D.A., Madeira L.M., Mata G., Vicente M.A., Rojas-Cervantes M.L., Lopez-Peinado A.J., Martín-Aranda R.M. (2007). Fenton-like

- oxidation of orange II solutions using heterogeneous catalysts based on saponite clay. *Appl. Catal. B: Environ.*, 71, 44-56.
- Higashi, S., Miki, H., Komarneni, S. (2007). Mn-smectites: hydrothermal synthesis and characterization. *Appl. Clay Sci.*, 38 (1-2), 104-112.
- Himmi, E. H., Bories, A., Barbirato, F. (1999). Nutrient requirements for glycerol conversion to 1,3-propanediol by *Clostridium butyricum*, *Bioresour. Technol.*, 67, 123-128.
- Huang, L., Zhu, Y., Zheng, H., Ding, G., Li, Y. (2009). Direct conversion of glycerol into 1,3-propanediol over Cu-H₄SiW₁₂O₄₀/SiO₂ in vapor phase. *Catal. Lett.*, 131, 312-320.
- Huber, G.W., Iborra, S. Corma, A. (2006). Aqueous-phase reforming of ethylene glycol over supported Pt and Pd bimetallic catalysts. *Chem. Rev.*, 106, 4044-4098.
- Hutchings, G. J., Lee, D. F., Minihan, A. R. (1995). Epoxidation of allyl alcohol to glycidol using titanium silicalite TS-1: effect of the method of preparation. *Catal. Lett.*, 33, 369-385.
- Ishimaru, S., Yamauchi, M., Ikeda, R. (2003). A new semiconducting organic-inorganic nanocomposite, 1,5-diaminophthalene-saponite intercalation compound. *Solid State Commun.*, 127 (1), 57-59.
- Iwasaki, T., Onodera, Y., Torii, K. (1989). Rheological properties of organophilic synthetic hectorites and saponites. *Clays Clay Miner.*, 37, 248-257.
- Iwasaki, T., Reinikainen, M., Onodera, Y., Hayashi, H., Ebina, T., Nagase, T., Torii, K., Kataja, K., Chatterjee, A. (1998). Use of silicate crystallite mesoporous material as catalyst support for Fischer-Tropsch reaction. *Appl. Surf. Sci.*, 130-132, 845-850.
- Jaber, M., Miéché-Brendlé, J., (2005). Influence du milieu de synthèse sur la cristallisation de saponite: proposition de mécanisme réactionnel en milieu acide et basique. *C. R. Chim.*, 8, 229-234.
- Jaynes, W. F., Boyd, S. A. (1991). Hydrophobicity of siloxane surfaces in smectites as revealed by aromatic hydrocarbon adsorption from water. *Clays Clay Miner.*, 39, 428-436.

- Jérmôe, F., Pouilloux, Y., Barrault, J. (2008). Rational design of solid catalysts for the selective use of glycerol as a natural organic building block. *ChemSusChem.*, 7, 586-613.
- Jiménez-Morales, I., Vila, F., Mariscal, R., Jiménez-López, A. (2012). Hydrogenolysis of glycerol to obtain 1,2-propanediol on Ce-promoted Ni/SBA-15 catalysts. *Appl. Catal., B: Environ.*, 117-118, 253-259.
- Johnson, D. T., Taconi, K. A. (2007). The glycerin glut: options for the value-added conversion of crude glycerol resulting from biodiesel production. *Environ. Prog.*, 26, 338–348.
- Julien, C., Djakovitch, L., Gallezot, P., Marion, P., Pinel, C., Rosierb, C. (2004). Glycerol hydrogenolysis on heterogeneous catalysts. *Green Chem.*, 6, 359–361.
- Karge, J., Pfeifer, H. G, Holderich, H. W., Eds. (1994). *Studies in Surface Science and Catalysis*. Elsevier: Amsterdam.
- Katryniok, B., Paul, S., Bellière–Baca, V., Rey, P., Dumeignil, F. (2010). Glycerol dehydration to acrolein in the context of new uses of glycerol. *Green Chem.*, 12, 2079-2098.
- Kawi, S., Yao, Z.Y. (1999). Saponite catalysts with systematically varied Mg/Ni ratio: synthesis, characterization, and catalysis. *Microporous Mesoporous Mater.*, 33 (1-3), 49-59.
- Kim, Y., Lee, J.S., Rhee, C.H., Kim, H.K., Chang, H. (2006). Montmorillonite functionalized with perfluorinated sulfonic acid for proton-conducting organic–inorganic composite membranes. *J. Power Sources*, 162 (1), 180-185.
- Kitla, A., Safonova, O.V., Föttinger, K. (2013). Infrared Studies on Bimetallic Copper/Nickel Catalysts Supported on Zirconia and Ceria/Zirconia. *Catal. Lett.*, 143, 517-530.
- Klopprogge, J.T., Seykens, D., Geus, J.W., Jansen, J.B.H. (1992). A ^{27}Al nuclear magnetic resonance study on the optimization of the development of the Al_{13} polymer. *J. Non-Cryst. Solid*, 142, 94–102.
- Klopprogge, J.T., Breukelaar, J., Jansen, J.B.H., Geus, J.W. (1993). Development of ammonium-saponites from gels with variable ammonium concentration and water content at low temperatures. *Clays Clay Miner.*, 41 (1), 103-110.

- Kloprogge, J.T., Breukelaar, J., Geus, J.W., Jansen, J.B.H. (1994a). Characterization of Mgsaponites synthesized from gels containing amounts of Na⁺, K⁺, Rb⁺, Ca²⁺, Ba²⁺, or Ce⁴⁺ equivalent to the C.E.C of the saponite. *Clays Clay Miner.*, 42 (1), 18-22.
- Kloprogge, J.T., Breukelaar, J., Wilson, A.E., Geus, J.W., Jansen, J.B.H., (1994b). Solid-state nuclear magnetic resonance spectroscopy on synthetic ammonium/aluminum saponites. *Clays Clay Miner.*, 42 (4), 416-420.
- Kloprogge, J.T. (1998). Synthesis of smectites and porous pillared clay catalysts: review. *J. Porous Mater.*, 5, 5-42.
- Kloprogge, J.T., Frost, R.L. (1999a). Raman microscopy study of basic aluminum sulfate. Part II. Raman microscopy at 77 K. *J. Mater. Sci.*, 34, 4367-4374.
- Kloprogge, J.T., Komarneni, S., Amonette, J.E. (1999b). Synthesis of smectite clay minerals: a critical review. *Clays Clay Miner.*, 47(5), 529-554.
- Kloprogge, J.T., Frost, R.L. (2000). The effect of synthesis temperature on the FT-Raman and FT-IR spectra of saponites. *Vib. Spectrosc.*, 23, 119-127.
- Kloprogge, J.T., Duong, L.V., Frost, R.L. (2005). A review of the synthesis and characterization of pillared clays and related porous materials for cracking of vegetable oils to produce biofuels. *Environ. Geol.*, 47, 967-981.
- Komadel, P. (2003). Chemically modified smectites. *Clay Miner.*, 38, 127-138.
- Komarneni, S., Kozai, N., Paulus, W.J. (2001). Environment. Superselective clay for radium uptake. *Nature*, 410, 771-772.
- Konta, J. (1995). Clay and man: clay raw materials in the service of man. *Appl. Clay Sci.* 10 (4), 275-335.
- Koso, S., Furikado, I., Shima, A., Miyazawa, T., Kunimori, K., Tomishige, K. (2009). Chemoselective hydrogenolysis of tetrahydrofurfuryl alcohol to 1,5-pentanediol. *Chem. Commun.*, 15, 2035-2037.
- Koso, S., Ueda, N., Shinmi, Y., Okumura, K., Kizuka, T., Tomishige, K. (2009). Promoting effect of Mo on hydrogenolysis of tetrahydrofurfuryl alcohol to 1,5-pentanediol over Rh/SiO₂. *J. Catal.*, 267, 89-92.

- Koso, S., Nakagawa, Y., Tomishige, K. (2011). Mechanism of the hydrogenolysis of ethers over silica-supported rhodium catalyst modified with rhenium oxide. *J. Catal.*, 280, 221-229.
- Koso, S., Watanabe, H., Okumura, K., Nakagawa, Y., Tomishige, K. (2012). Comparative study of Rh–MoO_x and Rh–ReO_x supported on SiO₂ for the hydrogenolysis of ethers and polyols. *Appl. Catal., B: Environ.*, 111-112, 27-37.
- Kosuge, K., Shimada, K., Tsunashima, A. (1995). Micropore formation by acid treatment of antigorite. *Chem. Mater.*, 7, 2241-2246.
- Kraus, G.A. (2008). Synthetic Methods for the Preparation of 1,3-Propanediol. *Clean-Soil Air Water*, 36, 648–651.
- Kresge, C. T., Leonowicz, M. E., Roth, W. J., Vartuli, J. C., Beck, J. S. (1992). Ordered mesoporous molecular sieves synthesized by a liquid-crystal template mechanism. *Nature*, 359, 710-712.
- Kruus P., *Advances in Sonochemistry*, Vol. 2 (Ed.: T. J. Mason), JAI Press, London, 1991, 1-21.
- Kurokawa, H., Hayasaka, M., Yamamoto, K., Sakuragi, T., Ohshima, M., Miura, H. (2014). Self-assembled heterogeneous late transition–metal catalysts for ethylene polymerization; New approach to simple preparation of iron and nickel complexes immobilized in clay mineral interlayer. *Catal. Commun.*, 47, 13-17.
- Kurosaka, T., Maruyama, H., Naribayashi, I., Sasaki, Y. (2008). Production of 1,3-propanediol by hydrogenolysis of glycerol catalyzed by Pt/WO₃/ZrO₂, *Catal. Commun.*, 9, 1360-1363.
- Kusunoki, Y., Miyazawa, T., Kunimori, K., Tomishige, K. (2005). Highly active metal–acid bifunctional catalyst system for hydrogenolysis of glycerol under mild reaction conditions. *Catal. Commun.*, 6, 645-649.
- Lahr, D. G., Shanks, B. H. (2003). Kinetic analysis of the hydrogenolysis of lower polyhydric alcohols: Glycerol to glycols. *Ind. Eng. Chem. Res.*, 42, 5467-5472.
- Lahr, D. G., Shanks, B. H. (2005). Effect of sulfur and temperature on ruthenium-catalyzed glycerol hydrogenolysis to glycols. *J. Catal.*, 232, 386-394.
- Lam K. T., Powell J. B., Weider P. R. (1997). Process for preparing 1,3-propanediol. WO 1997016250 A1, to Shell.

- Lambert, J.F. Poncelet, G. (1997). Acidity in pillared clays-origin and catalytic manifestations. *Top. Catal.*, 4, 43-56.
- Li, P., Liu, J., Nag, N., Crozier, P.A. (2009). In situ preparation of Ni-Cu/TiO₂ bimetallic catalysts. *J. Catal.*, 262, 73–82.
- Lin, R.Y., Chen, B.S., Chen, G.L., Wu, J.Y., Chiu, H.C., Suen, S.Y., 2009. Preparation of porous PMMA/Na⁺-montmorillonite cation-exchange membranes for cationic dye adsorption. *J. Membr. Sci.* 326 (1), 117–129.
- Linssen, T., Cassiers, K., Cool P., Lebedev, O., Whittaker, A., Vansant, E.F. (2003). Physicochemical and structural characterization of mesoporous aluminosilicates synthesized from leached saponite with additional aluminum incorporation. *Chem. Mater.*, 15, 4863-4873.
- Liu, L., Zhang, Y., Wang, A., Zhang, T. (2012). Mesoporous WO₃ Supported Pt Catalyst for Hydrogenolysis of Glycerol to 1,3-Propanediol. *Chin. J. Catal.*, 33, 1257–1261.
- Liu, S., Amada, Y., Tamura, M., Nakagawa, Y. Tomishige, K. (2014). One-pot selective conversion of furfural into 1,5-pentanediol over Pd-added Ir-ReO_x/SiO₂ bifunctional catalyst. *Green Chem.*, 16, 617–626.
- Liu, X., Breen, C., (2005). High-Temperature Crystalline Phases in Nylon-6/Clay Nanocomposites. *Macromol. Rapid Commun.*, 26, 1081–1086.
- LMC International. (2013). *Feedstocks for Bio-Based Chemicals*. LMC International, Oxford, UK.
- Lopez-Galindo, A., Viseras, C. (2000). Pharmaceutical applications of fibrous clays (sepiolite and palygorskite) from some circummediterranean deposits. In: Gomes, C.S.F. (Ed.), 1st Latin American Clay Conference. *Associacao Portuguesa de Argilas (APA)*, vol. 1, pp. 258–270.
- López-Suárez, F.E., Bueno-López, A., Illán-Gómez, M.J. (2008). Cu/Al₂O₃ catalysts for soot oxidation: Copper loading effect *Appl. Catal. B: Environ.*, 84, 651-658.
- Lowe, I. J. (1959). Free induction decays of rotating solids. *Phys. Rev. Lett.*, 2, 285-287.

- Mäki-Arvela, P., Hájek, J., Salmi, T., Murzin, D. Y. (2005). Chemoselective hydrogenation of carbonyl compounds over heterogeneous catalysts. *Appl. Catal., A: Gen.*, 292, 1-49.
- Madejova, J., Komadel, P. (2001). Baseline studies of the clay minerals society source clays: Infrared Methods, *Clays Clay Miner.*, 49(5), 410-432.
- Malkemus, J.D., Currier, V. A., Bell, J. B. (1958). Method for preparing glycidol. USP 2856413, to Jefferson Chem Co Inc.
- Mane, R. B., Ghalwadkar, A. A., Hengne, A. M., Suryawanshi, Y. R., Rode, C. V. (2011). Role of promoters in copper chromite catalysts for hydrogenolysis of glycerol. *Catal. Today*, 164, 447-450.
- Manzano-Agugliaro, F., Sanchez-Muros, M. J., Barroso F. G, Martínez-Sánchez. A., Rojo, S., Pérez-Bañón, C. (2012). Insects for biodiesel production. *Renew. Sust. Energ. Rev.*, 16 (6), 3744-3753.
- Mata, G., Trujillano, R., Vicente, M.A., Belver, C., Fernández-García, M., Korili, S.A., Gil, A. (2007). Chromium–saponite clay catalysts: preparation, characterization and catalytic performance in propene oxidation. *Appl. Catal. A: Gen.*, 327 (1), 1-12.
- McKelvy, M.L., Britt, T.R., Davis, B.L., Gillie, J.K., Lentz, L.A., Leugers, A., Nyquist, R.A. and Putzig, C.L. (1996). Infrared spectroscopy. *Anal. Chem.*, 68, 93R-160R.
- McKeown, N.K., Bishop, J.L., Noe Dobrea, E.Z., Ehlmann, B.L., Parente, M., Mustard, J.F., Murchie, S.L., Swayze, G.A., Bibring, J.-P., Silver, E.A. (2009). Characterization of phyllosilicates observed in the central Mawrth Vallis region, Mars, their potential formational processes, and implications for past climate. *J. Geophys. Res.*, 114 (11), E00D10, 20 pp.
- Ming, Y. H., Zhonghui, L., Enze, M. (1988). Acidic and hydrocarbon catalytic properties of pillared clay. *Catal. Today*, 2, 321-338.
- Miyazawa, T., Kusunoki, Y., Kunimori, K., Tomishige, K. (2006). Glycerol conversion in the aqueous solution under hydrogen over Ru/C + an ion-exchange resin and its reaction mechanism. *J. Catal.*, 240, 213–221.

- Miyazawa, T., Koso, S., Kunimori, K., Tomishige, K. (2007). Glycerol hydrogenolysis to 1,2-propanediol catalyzed by a heat-resistant ion-exchange resin combined with Ru/C, *Appl. Catal. A: Gen.*, 318, 244-251.
- Miyazawa, T., Koso, S., Kunimori, K., Tomishige, K. (2007). Development of a Ru/C catalyst for glycerol hydrogenolysis in combination with an ion-exchange resin. *Appl. Catal. A: Gen.*, 329, 30-35.
- Mokaya, R., Jones, W., Moreno, S., Poncelet, G. (1997). n-heptane hydroconversion over aluminosilicate mesoporous molecular sieves. *Catal. Lett.*, 49, 87-94.
- Montassier, C., Giraud, D., Barbier, J. (1988) in: *Heterogeneous catalysis and fine chemicals*, Stud. Surf. Sci. Catal., ed. Montassier C. et al. Elsevier, Amsterdam, 165-170.
- Mortland, M. M., Shaobai, S., Boyd, S. A. (1986). Clay-organic complexes as adsorbents for phenol and chlorophenols. *Clays Clay Miner.*, 34, 581-585.
- Murray, H. H. (1988). Kaolin minerals; their genesis and occurrences. *Rev. Mineral. Geochem.*, 19 (1), 67-89.
- Nagarajan, V., Nakamura, C. E. (1998). Production of 1,3-propanediol from glycerol by recombinant bacteria expressing recombinant diol dehydratase. US 5821092, to Dupont.
- Nakagawa, Y., Shinmi, Y., Koso, S., Tomishige, K. (2010). Direct hydrogenolysis of glycerol into 1,3-propanediol over rhenium-modified iridium catalyst. *J. Catal.*, 272, 191-194.
- Nakagawa, Y., Tomishige, K. (2011). Heterogeneous catalysis of the glycerol hydrogenolysis. *Catal. Sci. Technol.*, 1, 179-190.
- Nakagawa, Y., Ning, X., Amada, Y., Tomishige, K. (2012). Solid acid co-catalyst for the hydrogenolysis of glycerol to 1,3-propanediol over Ir-ReO_x/SiO₂. *Appl. Catal. A: Gen.*, 433-434, 128-134.
- Nakagawa, Y., Tamura, M., Tomishige, K. (2014). Catalytic materials for the hydrogenolysis of glycerol to 1,3-propanediol. *J. Mater. Chem. A*, 2, 6688-6702.
- Obregón, I., Corro, E., Izquierdo, U., Requies, J., Arias, P.L. (2014). Levulinic acid hydrogenolysis on Al₂O₃-based Ni-Cu bimetallic catalysts. *Chinese J. Catal.*, 35, 656-662.

- Occelli, M. L., Olivier, J. P., Perdigon-Melon, J. A., Auroux, A. (2002). Surface area, pore volume distribution, and acidity in mesoporous expanded clay catalysts from hybrid density functional theory (DFT) and adsorption microcalorimetry methods. *Langmuir*, 18, 9816-9823.
- Oh, J., Dash, S., Lee, H. (2011). Selective Conversion of Glycerol to 1,3-Propanediol Using Pt-Sulfated Zirconia. *Green Chem.*, 13, 2004-2007.
- Okada, K.; MacKenzie, K.J.D. In *Nano Materials: From Research to Applications* (Hosono, H.; Mishima, Y.; Takezoe, H.; MacKenzie, K.J.D. Eds.) Elsevier: Oxford. 2006, pp. 349-382.
- Okada, K., Arimitsu, N., Kameshima, Y., Nakajima, A., MacKenzie, K.J.D. (2006). Solid acidity of 2:1 type clay minerals activated by selective leaching. *Appl. Clay Sci.*, 31, 185-193.
- Okada, K., Yoshizaki, H., Kameshima, Y., Nakajima, A., Madhusoodana, D. (2007). Synthesis and characterization of mesoporous silica from selectively acid-treated saponite as the precursors. *J. Colloid Interface Sci.*, 314 176–183.
- Pagliaro, M., Rossi, M. (2008). *The Future of Glycerol: New Usages for a Versatile Raw Material*, first ed., RSC Publishing, Cambridge, UK.
- Pagliaro, M., Ciriminna, R., Kimura, H., Rossi, M., Pina C. D. (2007). From glycerol to value-added products. *Angew. Chem. Int. Ed.*, 46, 4434-4440.
- Palomo, J. M., Segura, R. L., Mateo, C., Terreni, M., Guisan, J. M., Fernández-Lafuente, R. (2005). Synthesis of enantiomerically pure glycidol via a fully enantioselective lipase-catalyzed resolution. *Tetrahedron: Asymmetry*, 16, 869-874.
- Patete, J.M., Peng, X.H., Koenigsmann, C., Xu, Y., Karn, B., Wong, S.S. (2011). Viable methodologies for the synthesis of high-quality nanostructures. *Green Chem.*, 13, 482-519.
- Perosa, A., Tundo, P. (2005). Selective hydrolysis of glycerol with Raney nickel, *Ind. Eng. Chem. Res.*, 44, 8535-8537.
- Pinnavaia, T.J. (1983). Intercalated clay catalysts. *Science*, 220, 365-371.
- Polverejan, M., Liu, Y., Pinnavaia, T.J. (2002). Aluminated derivatives of porous heterostructures (PCH) assembled from synthetic saponite clay: properties as

- supermicroporous to small mesoporous acid catalysts. *Chem. Mater.*, 14, 2283-2288
- Ponec, V. (1997). On the role of promoters in hydrogenations on metals; α,β -unsaturated aldehydes and ketones. *Appl. Catal., A: Gen.*, 149, 27-48.
- Ponec, V. (2001). Alloy catalysts: the concepts. *Appl. Catal., A: Gen.*, 222, 31-45.
- Price, G.J. (1990). In *Advances in Sonochemistry*, Vol. 1 (Ed.: T. J. Mason), JAI Press, London, 231-287.
- Prieto, O., Vicente, M. A., Banares-Munoz, M. A. (1999). Study of the porous solids obtained by acid treatment of a high surface area saponite. *J. Porous Mater.*, 6, 335-344.
- Prihod'ko, R., Hensen, E. J. M., Sychev, M., Stolyarova, I., Shubina, T. E., Astrelin, I., van Santen, R. A. (2004). Physicochemical and catalytic characterization of non-hydrothermally synthesized Mg-, Ni- and Mg-Ni-saponite-like materials. *Microporous and Mesoporous Mater.*, 69, 49-63.
- Pruissen, D.J., Capkova, P., Driessen, R.A.J., Schenk, H. (1997). Molecular simulations of trioctahedral smectites intercalated with an aluminum complex cation. *Appl. Catal. A: Gen.*, 165, 481-488.
- Pushpletha, P., Rugmini, S., Lalithambika, M. (2005). Correlation between surface properties and catalytic activity. *Appl. Clay Sci.*, 30, 141-153.
- Qin, L. Z., Song, M. J., Chen, C. L. (2010). Aqueous-phase deoxygenation of glycerol to 1,3-propanediol over Pt/WO₃/ZrO₂ catalysts in a fixed-bed reactor. *Green Chem.*, 12, 1466-1472.
- Ragauskas, A.J., Williams, C.K., Davison, B.H., Britovsek, G., Cairney, J., Eckert, C.A., Frederick W.J. Jr., Hallett, J.P., Leak, D.J., Liotta, C.L., Mielenz, J.R., Murphy, R., Templer, R. Tschaplinski, T. (2006). The path forward for biofuels and biomaterials. *Science*, 311, 484-489.
- Ray, S. S., Okamoto, M. (2003). Polymer/layered silicate nanocomposites: A review from preparation to processing. *Prog. Polym. Sci.*, 28, 1539-1641.
- Richey, W. F. (1993). Chlorohydrins. In: Kroschwitz J. I., Howe-Grant M., eds., *Kirk-Othmer Encyclopedia of Chemical Technology*, 4th Ed., Vol. 6, New York, John Wiley, 140-155.

- Robertson, R.H.S. (1996). Cadavers, choleras and clays. *Br. Miner. Soc. Bull.*, 113, 3-7.
- Ross-Medgaarden, E. I., Knowles, W. V., Kim, T., Wong, M. S., Zhou, W., Kiely, C. J. Wachs, I. E. (2008). New Insights into the Nature of the Acidic Catalytic Active Sites Present in ZrO₂-supported Tungsten Oxide Catalysts. *J. Catal.*, 256, 108-125.
- Ruiz-Hitzky, E., Casal, B. (1985). Epoxide rearrangements on mineral and silico-alumina surfaces. *J. Catal.*, 92, 291-295.
- Ruppert, A.M., Weinberg, K., Palkovits, R. (2012). Hydrogenolysis Goes Bio: From Carbohydrates and Sugar Alcohols to Platform Chemicals, *Angew. Chem. Int. Ed.*, 51, 2564-2601.
- Rusell, J. D., Fraser, A. R. (1994). Infrared methods, in: Wilson, M. J. (Ed.), *Clay Mineralogy: Spectroscopic and Chemical Determinative Methods*. Chapman & Hall, London.
- Ryneveld, E., Mahomed, A., Heerden, P., Friedrich, H. (2011). Direct hydrogenolysis of highly concentrated glycerol solutions over supported Ru, Pd and Pt catalyst systems. *Catal Lett.*, 141, 958-967.
- Salla, I., Bergadà, O., Salagre, P., Cesteros, Y., Medina, F., Sueiras, J. E., Montanari, T. (2005). Isomerisation of styrene oxide to phenylacetaldehyde by fluorinated mordenites using microwaves. *J. Catal.*, 232, 239-245.
- Sánchez, T., Salagre, P., Cesteros, Y. (2013). Ultrasounds and microwave-assisted synthesis of mesoporous hectorites. *Microporous Mesoporous Mater.*, 171, 24-34.
- Sánchez, T., Salagre, P., Cesteros, Y., Bueno-López, A. (2012). Use of delaminated hectorites as supports of copper catalysts for the hydrogenolysis of glycerol to 1,2-propanediol. *Chem. Eng. J.*, 179, 302-311.
- Sanz, J. (2006). Nuclear Magnetic Resonance Spectroscopy. In: Bergaya, F., Theng, B. K. G., Lagaly, G. (Eds.), *Handbook of Clay Science*, vol.1. Elsevier, Amsterdam, 919-938.

- Sato, S., Akiyama, M., Takahashi, R., Hara, T., Inui, K., Yokota, M. (2008). Vapor-phase reaction of polyols over copper catalysts. *Appl. Catal., A: Gen.*, 347, 186-191.
- Saxena, U., Dwivedi, N. Vidyarthi, S.R. (2005). Effect of catalyst constituents on (Ni, Mo, and Cu)/ Kieselguhr-catalyzed sucrose hydrogenolysis. *Ind. Eng. Chem. Res.*, 44, 1466-1473.
- Schlaf, M., Ghosh, P., Fagan, P. J., Hauptman, E., Bullock, R. M. (2001). Metal-catalyzed selective deoxygenation of diols to alcohols. *Angew. Chem. Int. Ed.*, 40, 3887-3890.
- Schlaf, M. (2006). Selective deoxygenation of sugar polyols to α,ω -diols and other oxygen content reduced materials - A new challenge to homogeneous ionic hydrogenation and hydrogenolysis catalysis. *Dalton Trans.*, 394, 4645-4653.
- Schmidt, S. R., Tanielyan, S. K., Marin, N., Alvez, G., Augustine, R. L. (2010). Selective Conversion of Glycerol to Propylene Glycol Over Fixed Bed Raney Cu Catalysts. *Top. Catal.*, 53, 1214-1216.
- Selvam, P., Bhatia, S. K., Sonwane, C. G. (2001). Recent advances in processing and characterization of periodic mesoporous MCM-41 silicate molecular sieves. *Ind. Eng. Chem. Res.*, 40, 3237-3261.
- Shen, J., Song, C. (2002). Influence of preparation method on performance of Cu/Zn-based catalysts for low-temperature Steam reforming and Oxidative steam reforming of methanol for H₂ production for fuel cells. *Catal. Today*, 77, 89-98.
- Shinoda, T., Onaka, M., Izumi, Y. (1995). Proposed models of mesopore structures in sulfuric acid treated montmorillonites and K10. *Chem. Lett.*, 495-496.
- Sienel, G., Rieth, R., Rowbottom, K. T. (1987). Epoxides. In: Gerhartz W., Yamamoto Y. S., Kaudy L., Rounsaville J. F., Schulz G., eds., *Ullmann's Encyclopedia of Chemical Technology*, 5th Ed., Vol. A9, New York, Wiley-VCH Publishers, 541.
- Singla, R., Ashokkumar, M., Grieser, F. (2004). The mechanism of the sonochemical degradation of benzoic acid in aqueous solutions. *Res. Chem. Intermed.*, 30(7-8), 723-733.

- Sitthisa, S., Sooknoi, T., Ma, Y., Balbuena, P. B., Resasco D. E. Kinetics and mechanism of hydrogenation of furfural on Cu/SiO₂ catalysts. (2011). *J. Catal.*, 277, 1-13.
- Srodon, J. (2006). Identification and quantitative analysis of clay minerals, in: Bergaya, F., Theng, B.K.G., Lagaly, G. (Eds.), *Handbook of clay science*, vol.1, Elsevier, Amsterdam, 765-787.
- Sterte, J, Shabtai, J. (1987). Crosslinked smectites. V. Synthesis and properties of hydroxy-silicoaluminum montmorillonites and fluorhectorites. *Clays Clay Miner.*, 35, 429-439.
- Stokes, A.R., Wilson, A.J.C. (1942). A method of calculating the integral breadths of Debye–Scherrer lines. *Proc. Camb. Phil. Soc.*, 38, 313-322.
- Stuart, B. (1996) *Modern Infrared Spectroscopy*, John Wiley & Sons, New York and Chichester, UK, 180
- Suquet, H., Malard, C., Copin, E., Pezerat, H. (1981). Variation du parameter b et de la distance basale d(001) dans une serie de saponites a charge croissante. I. Etats hydrates. *Clays Clay Miner.*, 16, 53-67.
- Suslick, K. S., Price, G. J. (1999). Applications of ultrasound to materials chemistry. *Annu. Rev. Mater. Sci.*, 29, 295-326.
- Suslick, K.S. (Ed.) (1988). *Ultrasound: Its Chemical, Physical and Biological effects*, VCH, New York, 336pp.
- Suzuki, N., Yoshikawa, Y., Takahashi, M., Tamura, M. (2007). Process for producing product of hydrogenolysis of polyhydric alcohol. World Pat. 129560 to KAO Corporation.
- Taguchi, A., Schüth, F. (2005). Ordered mesoporous materials in catalysis. *Microporous and Mesoporous Mater.*, 77, 1-45.
- Tan, H.W., Abdul Aziz, A.R., Aroua, M.K. (2013). Glycerol production and its applications as a raw material: A review. *Renew. Sustainable Energy Rev.*, 27, 118-127.
- Tang, X., Shen, X.W.Q., Suib, S.L. (1995). Preparation and characterization of pillared gallium aluminum clays with enriched pillars. *Chem. Mater.*, 7, 102-110.

- Tarnacka, M., Flak, T., Dulski, M., Pawlus, S., Adrjanowicz, K., Swinarew, A., Kaminski, K., Paluch, M. (2014). High pressure polymerization of glycidol. Kinetics studies. *Polymer*, 55 1984-1990.
- ten Dam, J., Hanefeld, U. (2011). Renewable chemicals: dehydroxylation of glycerol and polyols. *ChemSusChem*, 4, 1017-1034.
- ten Dam J., Djanashvili K., Kapteijn F. and Hanefeld U. (2013). Pt/Al₂O₃ Catalyzed 1,3-Propanediol Formation from Glycerol using Tungsten Additives. *ChemCatChem*, 5, 497-505.
- Theocharis, C.R., Jacob, K.J., Gray, A.C. (1988). Enhancement of Lewis acidity in layer aluminosilicates. *J. Chem. Soc. Faraday Trans.*, 84, 1509-1516.
- Thompson, L.H.; Doraiswamy, L.K. (1999). Sonochemistry: Science and Engineering. *Ind. Eng. Chem. Res.*, 38, 1215-1249.
- Tong, D.S., Xia, H.S., Zhou, C.H. (2009). Designed preparation and catalysis of smectite clay-based catalytic materials. *Chin. J. Catal.*, 30 (11), 1170-1187.
- Torii, K., Iwasaki, T. (1988). Synthesis of novel Ni-hectorite inorganic complexes. *Chem. Lett.*, 17, 2045-2048.
- Trent D. L. (1996). Kirk-Othmer Encyclopedia of Chemical Technology (Ed.: J. I. Kroschwitz), Vol. 20, Wiley Interscience, New York, 271-302.
- Trujillano, R., Rico, E., Vicente, M.A., Herrero, M., Rives, V. (2010). Microwave radiation and mechanical grinding as new ways for preparation of saponite-like materials. *Appl. Clay Sci.*, 48, 32-38.
- Trujillano, R., Rico, E., Vicente, M. A., Rives, V., Ciuffi, K. J., Cestari, A., Gil, A., Korili S. A. (2011). Rapid microwave-assisted synthesis of saponites and their use as oxidation catalysts. *Appl. Clay Sci.*, 53(2), 326-330.
- Utracki, L.A., Sepehr, M., Boccaleri, E. (2007) Synthetic, layered nanoparticles for polymeric nanocomposites (PNCs), *Polym. Adv. Technol.*, 18, 1-37.
- Vaccari, A. (1998). Preparation and catalytic properties of cationic and anionic clays. *Catal. Today*, 41(1-3), 53-71.
- Vaccari, A. (1999). Clays and catalysis: A promising future. *Appl. Clay Sci.*, 14, 161-198.

- Valverde, J.L., Cañizares, P., Kou, M.R.S., Molina C.B. (2000). Enhanced thermal stability of Al-pillared smectites modified with Ce and La. *Clay Clay Miner.*, 48, 424-432.
- van Grieken, R., Serrano, D. P., Melero, J.A., García, A. (2004). Effect of the solvent in the liquid phase rearrangement of 1,2-epoxyoctane over Al-MCM-41 and Al-TS-1 catalysts. *J. Mol. Catal. A: Chem.*, 222, 167-174.
- van Santen, R. A., van Leeuwen, P. W. N. M., Moulyn, J. A., Averill, B. A. (2000). *Studies in Surface Science and Catalysis: Catalysis an integrated approach.* Elsevier, Amsterdam.
- Varma, R.S. (2002). Clay and clay-supported reagents in organic synthesis. *Tetrahedron Lett.*, 58, 1235-1255.
- Vartuli, J. C., Kresge C. T., Leonowicz M. E., Chu, A. S., McCullen, S. B., Johnson, I. D, Sheppard, E. W. (1994). Synthesis of mesoporous materials: Liquid-crystal templating versus intercalation of layered silicates. *Chem. Mater.*, 6, 2070-2077.
- Velasco, J., Pérez-Mayoral, E., Mata, G., Rojas-Cervantes, M.L., Vicente-Rodríguez, M.A. (2011). Cesium saponites as excellent environmental-friendly catalysts for the synthesis of N-alkyl pyrazoles. *Appl. Clay Sci.*, 54 (2), 125-131.
- Veniale, F. (1997). Applicazioni e utilizzazioni medico-sanitarie di materiali argillosi (naturali e modificati). In: Morandi, N., Dondi, M. (Eds.), *Argille e Minerali delle Argille. Guida alla Definizione di Caratteristiche e Proprieta` per gli Usi Industriali.* Corso di Formazione, Gruppo Ital. AIPEA. Rimini (Italy), 205-239.
- Vicente, I., Salagre, P., Cesteros, Y., Medina, F., Sueiras, J. E. (2010). Microwave-assisted synthesis of saponite. *Appl. Clay Sci.* 48(1-2), 26-31.
- Vicente, I., Salagre, P., Cesteros, Y. (2011). Ni nanoparticles supported on microwave-synthesised saponite for the hydrogenation of styrene oxide. *Appl. Clay Sci.*, 53, 212-219.
- Vicente-Rodriguez, M.A., Lopez-Gonzalez, D., Bañares-Muñoz, M.A. (1995). Preparation of microporous solids by acid treatment of a saponite. *Microporous Mater.*, 4, 251-264.

- Villaluenga, J.P.G., Khayet, M., Lopez-Manchado, M.A., Valentin, J.L., Seoane, B., Mengual, J.I. (2007). Gas transport properties of polypropylene/clay composite membranes. *Eur. Polym. J.*, 43 (4), 1132-1143.
- Viseras, C., López Galindo, A. (1999). Pharmaceutical applications of some Spanish clays (sepiolite, palygorskite, bentonite): some preformulation studies. *Appl. Clay Sci.*, 14, 69-82.
- Vogels, R.J.M.J., Breukelaar, J., Kloprogge, J.T., Jansen, J.B.H., Geus, J.W. (1997). Hydrothermal crystallization of ammonium-saponite at 200°C and autogenous water pressure. *Clays Clay Miner.*, 45 (1), 1-7.
- Wang, K., Hawley, M. C., DeAthos, S. J. (2003). Conversion of glycerol to 1,3-propanediol via selective dehydroxylation, *Ind. Eng. Chem. Res.*, 42, 2913-2924.
- West, A. (1985). *Solid State Chemistry and its Application*. John Wiley & Sons, New York, pp. 742.
- West, R. M., Kunkes, E. L., Simonetti, D. A., Dumesic, J. A. (2009). Catalytic conversion of Biomass-derived biomass to fuel and chemicals by formation and upgrading of mono-functional hydrocarbon intermediates. *Catal. Today* 147 115.
- Wu, P., Tatsumi, T. (2003). Novel titanosilicate with MWW structure: III. Highly efficient and selective production of glycidol through epoxidation of allyl alcohol with H₂O₂. *J. Catal.*, 214, 317-326.
- Xiao, Z., Li, C., Xiu, J., Wang, X., Williams, C. T., Liang, C. (2012). Insights into the reaction pathways of glycerol hydrogenolysis over Cu–Cr catalysts. *J. Mol. Catal. A: Chem.*, 365, 24-31.
- Xue, S., Pinnavaia, T.J. (2008). Porous synthetic smectite clay for the reinforcement of epoxy polymers. *Microporous Mesoporous Mater.*, 107, 134-140.
- Xue, S.Q., Pinnavaia, T.J. (2010). Methylene-functionalized saponite: a new type of organo-clay with CH₂ groups substituting for bridging oxygen centers in the tetrahedral sheet. *Appl. Clay Sci.*, 48 (1-2), 60-66.
- Yamaguchi, A., Hiyoshi N., Sato, O., Bando, K. K., Shirai, M. (2009). Enhancement of cyclic ether formation from polyalcohol compounds in high temperature liquid water by high pressure carbon dioxide *Green Chem.*, 11, 48-52.

- Yao, M., Liu, Z.-Y., Wang, K.-X., Li, C.-J., Zou, Y.-C., Sun, H.-J. (2004). Synthesis and characterization of pillared high layer charged synthetic saponite. *J. Porous Mater.*, 11 (4), 229-238.
- Yao, M., Liu, Z.Y., Wang, K.X., Zhu, M.Q., Sun, H.J. (2005). Application of FTIR technique in microwave-hydrothermal synthesis of saponite. *Spectrosc. Spectral Anal.*, 25 (6), 870-873.
- Yariv, S., Cross, H. (2002). *Organo-Clay Complexes and Interactions*. Maecel Dekker, Inc, New york.
- Ye, L., Duan, X., Lin, H., Yuan, Y. (2012). Improved performance of magnetically recoverable Ce-promoted Ni/Al₂O₃ catalysts for aqueous-phase hydrogenolysis of sorbitol to glycols. *Catal. Today*, 183, 65-71.
- Ying-Jie, Z., Feng, C. (2014). Microwave-Assisted Preparation of Inorganic Nanostructures in Liquid Phase. *Chem. Rev.*, 114, 6462-6555.
- Yoo, J. W., Mouloungui, Z., Gaset, A. (2001). Method for producing an epoxide, in particular of glycidol, and installation for implementation. USP 6316641, to Organisation Nationale Interprofessionnelle Des Oleagineux (O.N.I.D.O.L.).
- Yui, T., Yoshida, H., Tachibana, H., Tryk, D.A. (2002). Intercalation of polyfluorinated surfactants into clay minerals and the characterization of the hybrid compounds. *Langmuir*, 183 (14), 891-896.
- Zeng, A. P., Biebl, H. (2002). Bulk chemicals from biotechnology: the case of 1,3-propanediol production and the new trends. *Adv. Biochem. Eng. Biotechnol.*, 74, 239-259.
- Zhao, D, Yang, Y, Guo, X. (1992) Preparation and characterization of hydrosilicoaluminium pillared clays. *Inorg Chem.*, 31, 4727-4732.
- Zheng, Z., Wang, J., Lu, Z., Luo, M., Zhang, M., Xu, L. Ji, J. (2013). Hydrogenolysis of 2-Tosyloxy-1,3-propanediol into 1,3-Propanediol over Raney Ni Catalyst. *J. Braz. Chem. Soc.*, 24 (3), 385-391.
- Zhou, C.H., Li, X.N., Ge, Z.H., Li, Q.W., Tong, D.S. (2004). Synthesis and acid catalysis of nanoporous silica/alumina–clay composites. *Catal. Today*, 93(5), 607-613.

- Zhou, C.H., Tong, D.S., Bao, M.H., Du, Z.X., Ge, Z.H., Li, X.N. (2006). Generation and characterization of catalytic nanocomposite materials of highly isolated iron nanoparticles dispersed in clays. *Top. Catal.*, 39 (3-4), 213-219.
- Zhou, C. H., Zhao, H., Tong, D. S., Wu, L. M., Yu, W. H. (2013). Recent advances in catalytic conversion of glycerol. *Catal. Rev. Sci. Eng.*, 55, 369-453.
- Zhou, C. H., Beltramini, J. N., Fan, Y. X., Lu, G. Q. (2008). Chemoselective catalytic conversion of glycerol a biorenewable source as to valuable commodity chemicals. *Chem. Soc. Rev.*, 37, 527-549.
- Zhou, L., Wang, A., Li, C., Zheng, M., Zhang, T. (2012). Selective production of 1,2-propylene glycol from jerusalem artichoke tuber using Ni-W₂C/AC catalysts. *ChemSusChem*, 5, 932-938.
- Zhou, Y., Ouyang, F., Song, Z.-B., Yang, Z., Tao, D.-J. (2015). Facile one-pot synthesis of glycidol from glycerol and dimethyl carbonate catalyzed by tetraethylammonium amino acid ionic liquids. *Catal. Commun.*, 66, 25-29.
- Zhu, S., Zhu, Y., Hao, S., Chen, L., Zhang, B., Li, Y. (2012). Aqueous-Phase Hydrogenolysis of Glycerol to 1,3-propanediol Over Pt-H₄SiW₁₂O₄₀/SiO₂. *Catal. Lett.*, 142, 267-274.
- Zimmerman, D., Isaacson, R. B. (1974). Polyalkylene terephthalate molding resin. USP3814725, to Celanese Cor

